

NOISE INDUCED HEARING LOSS: CHANGES IN GENE EXPRESSION IN THE AUDITORY PATHWAY

Thesis Submitted for the degree of
Doctor of Philosophy
at the University of Leicester

by
Sherylanne Newton MSci
Department of Neuroscience, Psychology and Behaviour
University of Leicester

June 2017

i. Abstract

Noise-induced Hearing Loss: Changes in Gene Expression in the Auditory Pathway

Sherylanne Newton

Noise induced hearing loss is classically divided into permanent or temporary forms. Individuals with permanent threshold shifts (PTS) will permanently lose auditory sensitivity, whereas individuals with temporary threshold shifts (TTS) will experience elevated hearing thresholds immediately following noise exposure, which resolves over several weeks. TTS causes little lasting damage to the hair cell, stereocilia or supporting structures which form the organ of Corti within the inner ear, and was therefore considered “no harm, no foul”. However, recent evidence suggests that TTS and PTS also leads to, what has been termed, “silent damage”; neuropathic damage which causes the loss of synaptic innervation at the inner hair cell and a slowly developing neuronal death. This study investigates the gene expression changes which accompany this type of noise-induced damage in the spiral ganglion neuron (SGN). Previous studies of gene expression changes following noise insult have used whole cochlea preparations which do not differentiate between changes in different cochlear structures. Here we have used micro-dissection of the modiolus to focus on the SGNs and to minimise contribution from other cochlea structures. In order to maximise the amount of data collected from each experimental animal, cochlear nucleus (CN) samples were taken in parallel to look at noise-induced changes at this first region of the central auditory system. A 1.5hr noise exposure of 105 dB SPL broadband noise elicited a moderate form of PTS, characterized by an immediate threshold shift of up to 44 dB SPL, which partially recovers over 28 days. Tissue was collected at 1day, 7days and 28days following exposure and RNA-Sequencing was performed. Over the 28-day period 421 genes were significantly changed in the modiolus; these were suggestive of a chronic immune response and for the first time, fibrinogen and lipid dysregulation. In the cochlear nucleus, just 184 genes were altered over 28-days; changes to *Trpv4*, *Trpm3* and *TrkA* may contribute to increases in cell excitability in the CN following noise exposure.

ii. Acknowledgements

I would like to thank my supervisory team: first, Professor Blair Grubb for providing the knowledge, enthusiasm, skills, and encouragement whilst I was getting started on this project; and second Professor Ian Forsythe for “adopting me” and supporting me through the latter part of my PhD.

I would also like to thank Dr Mike Mulheran, who taught me everything I needed to know about the ABR; Dr Neil Ingham, for the use, set up, and calibration of the ABR equipment; Dr Miho Terunuma, for her crash course in western blotting, and Dr Nicolas Sylvius, for all of his help with the RNA-Sequencing. Much of this data would not exist without their expertise.

Thank to you the members of the laboratory who made my time there not only tolerable, but memorable: in particular Amy Richardson and Michelle Hammett, who kept me laughing.

Thank you to David: for your love and support, for always being interested about my day. Finally, thank you to my mother, who never told me a question was stupid, and always encouraged me to find out.

Table of Contents

i.	Abstract.....	i
ii.	Acknowledgements	ii
iii.	Table of Contents.....	iii
iv.	List of Tables	viii
v.	List of Figures	x
vi.	List of Abbreviations	xii
	Chapter 1: Introduction	13
	1.1 The Physics of Sound	14
	1.1.1 What is Sound?	14
	1.1.2 Nature of Sound Waves	14
	1.2 The Anatomy & Physiology of the Mammalian Ear	16
	1.2.1 The Outer & Middle Ear	17
	1.2.2 The Inner Ear	18
	1.2.3 Hair Cells Convert Sound into an Electrochemical Stimulus	19
	1.2.4 Synaptic Transmission within the Cochlea	20
	1.2.5 The Central Pathway	21
	1.2.6 Tonotopy in the Auditory System	23
	1.3 Hearing Loss & Dysfunction	29
	1.3.1 The Causes of Hearing Damage	29
	1.3.2 Permanent Threshold Shifts	29
	1.3.3 Temporary Threshold Shifts.....	30
	1.3.4 Neuronal Death.....	31
	1.3.5 Noise Induced Central Excitability	32
	1.4 Aims of the Project	33
	Chapter 2: Experimental Methods	36

2.1 Overview	36
2.2 Experimental Animals	36
2.3 Anesthesia Protocols	37
2.3.1 Induction of Anaesthesia	38
2.3.2 Reversal of Anaesthesia	40
2.4 Auditory Brainstem Response Recordings.....	41
2.4.1 Recording Set-up & Calibration	41
2.4.2 The Recording Procedure & Data Collection	41
2.4.3 Analysis of Data.....	42
2.5 Sound Exposure	44
2.5.1 Sound Exposure Protocol.....	44
2.5.2 Calibration of Equipment.....	44
2.5.3 Evans Blue for Blood-Labyrinth-Barrier Integrity	46
2.6 Tissue Dissection.....	48
2.6.1 Modioli	48
2.6.2 Cochlear Nuclei	50
2.6.3 Dorsal Root Ganglia	50
2.7 Transcriptomics.....	51
2.7.1 RNA Extraction	51
2.7.2 RNA-Seq Data Collection.....	52
2.7.3 Microarray Data Collection	52
2.7.4 Analysis of Results.....	53
2.8 Histological Methods	55
2.8.1 Solutions	55
2.8.2 General Histology.....	56
2.8.3 Immunohistochemistry.....	56

2.9 Western Blotting.....	58
2.9.1 Solutions	58
2.9.2 Protein Extraction	59
2.9.3 Running of the Gel & Transfer to Membrane.....	59
2.9.4 Antibody Staining & Imaging	60
2.9.5 Analysis	60
Chapter 3: Noise Exposure and the Characterisation of Hearing in the Mouse	62
3.1 Introduction	62
3.2 Results: ABR Measurements of the Unexposed Mouse.....	64
3.2.1 Auditory Brainstem Response in CBA/Ca Mice at 5 -7 Weeks of Age.....	64
3.2.2 Small Changes to Threshold Occur Between 5 – 13 Weeks of Age.....	68
3.3 Results: ABR Measurements of the Noise Exposed Mouse.....	70
3.3.1 ABR One Day after Noise Exposure	70
3.3.2 ABR Seven Days after Noise Exposure.....	74
3.3.3 ABR 28 Days after Noise Exposure	77
3.4 Discussion	80
3.4.1 Assessment of the CBA/Ca Auditory Brainstem Response.....	81
3.4.2 A Model of Semi-Permanent Noise Exposure	85
3.4.3 Summary	90
Chapter 4: mRNA Sequencing of the Auditory Pathway	91
4.1 Introduction	91
4.2 Comparison of RNAseq to Microarray.....	92
4.2.1 Comparison of Platforms	92
4.2.2 Defining a “Present” Gene.....	95
4.2.3 RNAseq Run Statistics	97
4.3 Ion Channel Expression in the Auditory System.....	101

4.3.1 Voltage-Gated Sodium Channels	102
4.3.2 Voltage-Gated Potassium Channels	106
4.3.3 Glutamate Receptors	111
4.4 Discussion	115
4.4.1 Gene Expression in RNASeq is Comparable to Microarray	115
4.4.2 Ion Channel Expression in the Auditory System	117
4.4.3 Ion Channel Expression Changes Occur Beyond P40	117
4.4.4 Summary	119
Chapter 5: Gene Expression Changes in the Modiolus Follow Noise Exposure	120
5.1 Introduction	120
5.2 Gene Expression Changes One Day after Noise Exposure.....	121
5.3 Gene Expression Changes Seven Days after Noise Exposure	126
5.4 Gene Expression Changes 28 Days after Noise Exposure.....	130
5.5 Neuron Specific Changes in the Modiolus	133
5.5.1 P2rx3	137
5.6 Acute Phase Proteins and the Immune Response.....	141
5.7 Programmed Cell Death.....	143
5.8 Discussion	146
5.8.1 Sustained Changes in Gene Expression	148
5.8.2 Changes to the Ribbon Synapse	155
5.8.3 Evidence of Cell Death	157
5.8.4 The Immune Response	159
5.8.5 Summary	160
Chapter 6: Gene Expression Changes in the Cochlear Nucleus Following Noise Exposure	162
6.1 Introduction	162

6.2 Gene Expression Changes on Day One	162
6.3 Gene Expression Changes on Day Seven	166
6.4 Gene Expression Changes on Day 28.....	168
6.5 Neuron Specific Changes	171
6.5.1 Aquaporin-1	174
6.6 Discussion	177
6.6.1 Sustained Changes in Gene Expression	177
6.6.2 Neuron Specific Changes	181
6.6.3 Summary	183
Chapter 7: Final Conclusions.....	184
Appendix 1 : Kv3 in the Auditory Pathway	192
A1.1 Immunolocalisation of Kv3s in the Auditory System	193
A1.2 Kv3 Expression Increases with Age	203
A1.3 Auditory Brainstem Response recordings	204
A1.4 Summary.....	210
Appendix 2 : Exemplar Scripts	211
References	214

iii. List of Tables

Table 2.1: Primary and Secondary Antibodies used for Immunohistochemistry	61
Table 2.2: Primary and Secondary Antibodies used for Western Blots	61
Table 4.1: Voltage gated sodium channels with expression in the cochlear nucleus and modiolus control samples.....	105
Table 4.2: Voltage gated potassium channels with expression in the cochlear nucleus and modiolus control samples	109
Table 4.3: Ionotropic glutamate receptors with expression in the cochlear nucleus and modiolus control samples.....	114
Table 5.1: Differentially expressed genes at day one in the modiolus	123
Table 5.2: Day one changes for which fold change cannot be calculated in the modiolus.....	124
Table 5.3: The top 10 Gene Ontology results for genes upregulated at day one in the modiolus	125
Table 5.4 The top 10 Gene Ontology results for genes downregulated at day one in the modiolus	125
Table 5.5 Differentially expressed genes at day seven in the modiolus	128
Table 5.6 Day seven changes for which fold change cannot be calculated in the modiolus.....	128
Table 5.7: The top 10 Gene Ontology results for genes upregulated at day seven in the modiolus.....	129
Table 5.8: The top 10 Gene Ontology results for genes downregulated at day seven in the modiolus....	129
Table 5.9: Differentially expressed genes at day 28 in the modiolus	131
Table 5.10 Day 28 changes for which fold change cannot be calculated in the modiolus.....	132
Table 5.11: The top 10 Gene Ontology results for genes upregulated at day 28 in the modiolus	132
Table 5.12: Neuron specific genes upregulated at each time point in the modiolus	134
Table 5.13: Neuron specific genes downregulated at each time point in the modiolus	135
Table 5.14 Summary of changes to acute phase proteins over time in the modiolus.....	142
Table 5.15: Cell death associated genes upregulated at each time point in the modiolus	144
Table 5.16: Cell death associated genes downregulated at each time point in the modiolus.....	145
Table 5.17: Genes differentially expressed at all three time points in the modiolus	152
Table 5.18: Early upregulated genes in the modiolus	153
Table 5.19: Early downregulated genes in the modiolus	153
Table 5.20: Late upregulated genes in the modiolus.....	154
Table 6.1: Differentially expressed genes at day one in the cochlear nucleus.....	164
Table 6.2: Day one changes for which fold change cannot be calculated in the cochlear nucleus	165
Table 6.3: Gene Ontology results for genes upregulated at day one in the cochlear nucleus.....	165
Table 6.4 Gene Ontology results for genes downregulated at day one in the cochlear nucleus	165
Table 6.5: Differentially expressed genes at day seven in the cochlear nucleus	167
Table 6.6: Differentially expressed genes at day 28 in the cochlear nucleus.....	169
Table 6.7 The top 10 Gene Ontology results for genes upregulated at day 28 in the cochlear nucleus...	170
Table 6.8: Neuron specific genes upregulated at each time point in the cochlear nucleus.....	172

Table 6.9 Neuron specific genes downregulated at each time point in the cochlear nucleus.....	173
Table 6.10: Genes differentially expressed at all three time points in the cochlear nucleus.....	179
Table 6.11: Early upregulated genes in the cochlear nucleus.....	180
Table 6.12: Late upregulated genes in the cochlear nucleus.....	180
Table 6.13: Late downregulated genes in the cochlear nucleus	180

iv. List of Figures

Figure 1.1: The hearing ranges of some common laboratory animals compared to human	15
Figure 1.2: Structure of the mammalian ear	16
Figure 1.3: Diagram of the mouse ascending auditory pathway	26
Figure 1.4: Diagram of the mammalian cochlea	27
Figure 1.5: Movement of the stereocilia results in an alternating current in the inner hair cell	28
Figure 1.6: The cellular effects of noise exposure in the CBA/Ca mouse	30
Figure 2.1: Flow chart of study	36
Figure 2.2: Age and weights of experimental mice used.....	37
Figure 2.3: Auditory brainstem recording equipment set up.....	43
Figure 2.4: Noise exposure equipment set up and calibration	45
Figure 2.5: Presence of Evans blue does not differ in the noise exposed mouse	47
Figure 2.6: Isolation of the Modiolus.....	49
Figure 3.1: Example auditory brainstem response (ABR) traces for each frequency tested.....	65
Figure 3.2: Amplitude and latency of waves I, III, and VI.....	67
Figure 3.3: CBA/Ca hearing between 5 – 13 weeks	69
Figure 3.4: Comparison of ABR thresholds before and after sham exposure	69
Figure 3.5: Significant shifts in ABR thresholds are seen in the auditory over exposed (AOE) mice at one day following noise exposure.....	71
Figure 3.6: Click ABR waveform properties of AOE and Sham mice at one day following exposure	73
Figure 3.7: An increase in ABR thresholds are seen in the auditory over exposed (AOE) mice at seven days following noise exposure.....	74
Figure 3.8: Click ABR waveform properties of AOE and Sham mice at seven days following exposure	76
Figure 3.9: An increase in high frequency thresholds is seen in the auditory over exposed (AOE) mice 28 days following noise exposure	77
Figure 3.10: Click ABR waveform properties of AOE and Sham mice at 28 days following exposure	79
Figure 3.11: A summary of threshold elevations of auditory overexposed (AOE) mice	80
Figure 3.12: Mouse auditory sensitivity and ABR	84
Figure 3.13: Ratio of the absolute amplitude of wave IV to wave I	89
Figure 4.1: Comparison of 8M and 15M RNAseq reads with Microarray analysis of the same samples	94
Figure 4.2: Comparison between microarray detection and FPKM for estimation of present genes	96
Figure 4.3: Examples of low-expression and high-expression in relation to protein	96
Figure 4.4: Read numbers and coverage of cochlear nucleus samples	98
Figure 4.5: Number of genes “present” in cochlear nucleus	98
Figure 4.6 Read numbers and coverage of modiolus samples.....	100
Figure 4.7: Number of genes “present” in the modiolus.	100
Figure 4.8: Voltage gated sodium channels with changed expression over time in the cochlear nucleus	105

Figure 4.9: Family specific kinetics of the potassium current.	107
Figure 4.10: Voltage gated potassium channels with changed expression over time in the cochlear nucleus	110
Figure 4.11: Voltage gated potassium channels with changed expression over time in the cochlear nucleus.	110
Figure 4.12: Ionotropic glutamate receptors with changed expression over time in the cochlear nucleus.	114
Figure 5.1 Volcano and MA plot of differentially expressed genes at day one in the modiolus.....	122
Figure 5.2: Volcano and MA plot of differentially expressed genes at day seven in the modiolus.....	127
Figure 5.3 Volcano and MA plot of differentially expressed genes at day 28 in the modiolus	131
Figure 5.4 mRNA and protein expression levels of P2X ₃ following noise exposure	139
Figure 5.5 P2X ₃ expression in the cochlea at three different developmental time points	139
Figure 5.6 P2X ₃ labelling is present in spiral ganglion cells in the adult cochlea	140
Figure 5.7 Location of Iba-1 positive cochlear macrophages seven days following noise ..	142
Figure 5.8: Summary of the number of genes differentially expressed in the modiolus	147
Figure 6.1: Volcano and MA plot of differentially expressed genes at day one in the cochlear nucleus ..	164
Figure 6.2 Volcano and MA plot of differentially expressed genes at day seven in the cochlear nucleus	167
Figure 6.3: Volcano and MA plot of differentially expressed genes at day 28 in the cochlear nucleus	169
Figure 6.4: mRNA expression of Aqp1 following noise exposure	175
Figure 6.5: Immunolocalisation of Aquaporin 1 in the cochlear nucleus	176
Figure 6.6: Summary of the number of genes differentially expressed in the cochlear nucleus.....	179
Figure A1.1: Immunolocalisation of K _v 3s in the spiral ganglion.....	195
Figure A1.2: Immunolocalisation of K _v 3s in the cochlear nucleus	196
Figure A1.3: Immunolocalisation of K _v 3s in the superior olivary complex	197
Figure A1.4: K _v 3.1 and K _v 3.3 are the predominant K _v 3s in the superior olivary complex	198
Figure A1.5: K _v 3.1 antibody validation	199
Figure A1.6: K _v 3.1 antibody validation by Western Blot	199
Figure A1.7: K _v 3.2 antibody validation	200
Figure A1.8: K _v 3.3 antibody validation	201
Figure A1.9: K _v 3.3 antibody validation by Western Blot	201
Figure A1.10: K _v 3.4 antibody validation	202
Figure A1.16: K _v 3 expression in the brainstem increases with age	203
Figure A1.11: Auditory thresholds of K _v 3.1 ^{-/-} mice	206
Figure A1.12: Auditory thresholds of K _v 3.3 ^{-/-} mice	206
Figure A1.13: The ABR waveform in 6 month old K _v 3.1 ^{-/-} mice	207
Figure A1.14: The ABR waveform in 1 month K _v 3.3 ^{-/-} mice	208
Figure A1.15: The ABR waveform in 6 month old K _v 3.3 ^{-/-} mice	209

v. List of Abbreviations

ABR	Auditory brainstem response
AOE	Acoustic overexposure
APP	Acute phase protein
AMPA	α -amino-3-hydroxy-5-methyl-4-isoxazolepropionic acid
cDNA	Complementary deoxyribonucleic acid
CN	Cochlear Nucleus
cRNA	Complementary ribonucleic acid
Δ	Fold change
Day 1	Time point: 1 day following exposure
Day 7	Time point: 7 days following exposure
Day 28	Time point: 28 days following exposure
dB SPL	Decibel, Sound Pressure Level
dB re: threshold	Decibels above threshold of an individual
FDR	False discovery rate
FPKM	Fragments per kilobase of transcript per million mapped reads
IHC	Inner hair cells
LSO	Lateral Superior Olive
μ	Mean
mRNA	Messenger RNA
Mod	Modiolus
MNTB	Medial Nucleus of the Trapezoid Body
NIHL	Noise-induced hearing loss
NMDA	<i>N</i> -Methyl- <i>D</i> -aspartic acid
OHC	Outer hair cell
P(#)	Postnatal day (#)
qPCR	Quantitative polymerase chain reaction
RNASeq	RNA-Sequencing
RNA	Ribonucleic acid
σ	Standard deviation
SEM	Standard error of the mean
SGN	Spiral ganglion neurons
SOC	Superior Olivary Complex
Suprathreshold	Decibels above threshold of an individual

Chapter 1: Introduction

As hearing loss in humans is largely self-reported, estimating the incidence in a population is problematic. A 2015 report by Action on Hearing Loss estimated that upwards of 11 million people in the UK are thought to suffer from some form of measurable hearing loss. This could result from any combination of presbycusis, exposure to loud sound, ototoxic damage, infectious disease, complications at birth, genetic predisposition, or traumatic injury. While presbycusis is currently listed as the most common cause of hearing loss, the extent of age related degeneration is primarily influenced by both a genetic predisposition to hearing loss and environmental factors, such as noise exposure, earlier in life (Kujawa and Liberman, 2006).

In the early 2000s, it was estimated that up to 1.3 million individuals were at risk of hearing impairment due to excessive noise at work (Sheild, 2006). To combat this, the European Control of Noise at Work regulations (2006) now sets an exposure limit of an unlimited duration of 80dB (A-weighted) in the workplace. However, exposure to sound in the workplace only accounts for a small fraction of NIHL. A study conducted by Dehnert et al. (2015) found that approximately 40% of adolescents are regularly exposed to hazardous levels of noise during recreational activities.

Hearing loss has a stark social and economic impact. Economically, it has been estimated that up to £13 billion is lost in the UK each year through unemployment due to hearing loss (Sheild, 2006). On an individual level, hearing loss commonly leads to withdrawal from social activities, often with an impact on the individual's relationship with their family or partner (Brooks et al., 2001). Perhaps unsurprisingly, a study into these effects on the elderly found that those with hearing loss were over twice as likely to develop depression (Saito et al., 2010) and show a higher incidence of dementia (Lin et al., 2011a, Gurgel et al., 2014). It

is therefore important that the mechanisms leading to hearing loss are understood in order to lessen the medial, social, and economic impact over time.

1.1 The Physics of Sound

1.1.1 What is Sound?

Sound is caused by the vibration of objects and is nothing more than a travelling pressure wave which displaces the molecules of the medium in which they are travelling. It was George Berkeley that said "To be is to be perceived"; all things that we believe to exist are derived from what we perceive. It is only in the complexity of the anatomy and physiology of the ear where pressure waves become something which is heard.

1.1.2 Nature of Sound Waves

Sound waves can be simplified as sinusoidal with two properties: amplitude and frequency.

The amplitude, or intensity, of the wave is a measure of the magnitude of movement in a given medium, and the power of the wave transmitted through a unit area of space. It is directly related to the loudness of a perceived sound, with higher intensity meaning louder sounds. The intensity (I) of a sound dissipates over the distance from its source. In the absence of reflection or reverberation, intensity will reduce according to the inverse square law:

$$I = \frac{P}{4\pi r^2}$$

where r is the distance from source and P is the power at origin.

The loudness of a sound is measured in decibels (dB) which is found using the ratio of the intensity of a sound (I) to a certain reference intensity (I₀) and representing this on a logarithmic scale,

$$dB = 10 \log_{10} \frac{I}{I_0} .$$

Introduction

Commonly the chosen reference is taken as the lowest sound pressure that can be detected by humans. This is determined by calculating the root mean square (RMS) pressure of the waveform and is referred to as dB SPL (sound pressure level). As the intensity of a sound varies with the square of the pressure, dB SPL is calculated as,

$$dB = 20 \log_{10} \frac{p}{p_0}$$

where p is the pressure of the wave and the reference pressure, p_0 is given as $2 \times 10^5 \text{ N/m}^2$.

The frequency of a sound wave is a measure of how many cycles of the wave pass through a given space in one second. This feature of the wave, measured in hertz (Hz) correlates to the perceived pitch of a sound, with high frequencies appearing higher in pitch. The auditory system differs subtly between species, adapted to be most sensitive at different ranges of frequencies, as shown in Figure 1.1.

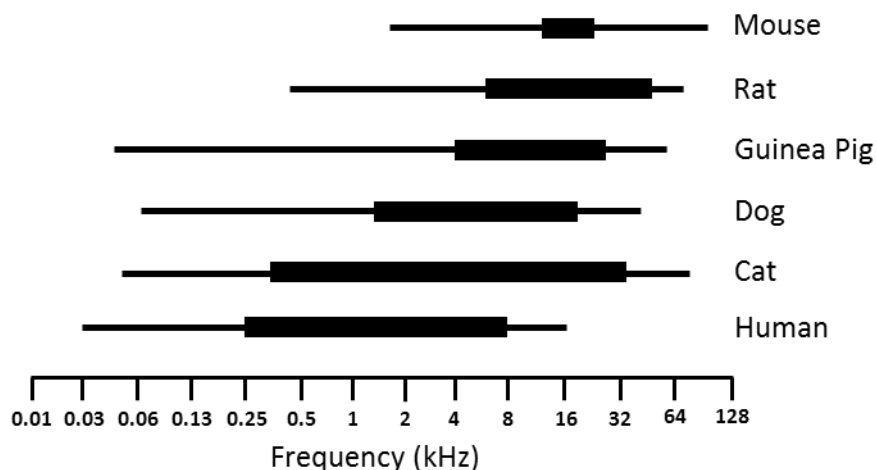


Figure 1.1: The hearing ranges of some common laboratory animals compared to human. Thin lines represent hearing range and are estimations of frequencies perceived at 60dB SPL and thick lines represent those "best frequencies", and are those perceived at 10dB SPL. Image produced from data from Heffner and Heffner (2007).

1.2 The Anatomy & Physiology of the Mammalian Ear

The auditory system as a whole can be roughly divided into two: the peripheral auditory system, which includes the ear, auditory nerve, and neurons of the spiral ganglia; and the central auditory system which includes the auditory brainstem nuclei and auditory cortex.

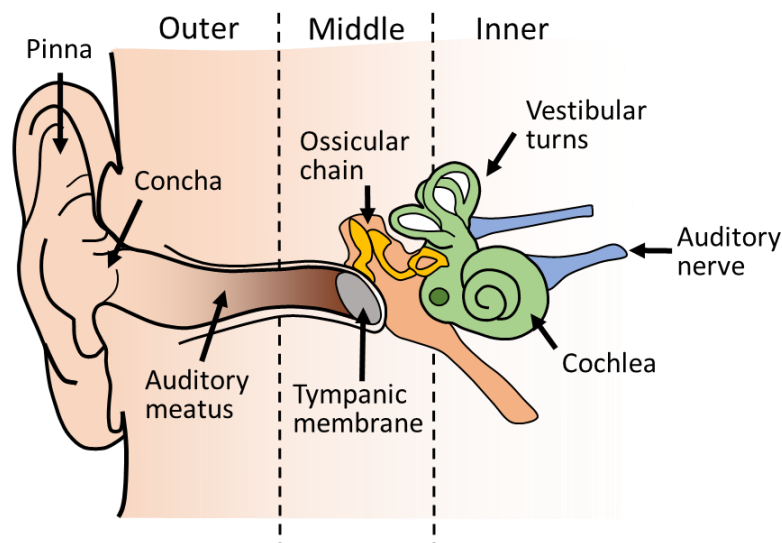


Figure 1.2: Structure of the mammalian ear. Figure shows a diagram of the human ear showing the outer, middle, and inner ear structures. This general structure is conserved across all mammals. Incoming sound is funneled into the auditory meatus, by the outer ear structures. The oscillating pressure difference causes the tympanic membrane to vibrate, and is converted into a back and forth movement at the oval window by the ossicular chain. In the fluid filled cochlea, pressure waves are converted into an electrical signal which is passed to the brainstem via the auditory nerve.

1.2.1 The Outer & Middle Ear

The ear itself can be divided into the outer ear, the middle ear, and the inner ear (Figure 1.2). The outer ear consists of the external pinna (or auricle), the auditory meatus (auditory canal).

The pinna, concha, and meatus act as an acoustic resonator, which in humans selectively increases the intensity of sound waves in the region of 2.5 kHz. As sound is channelled down the meatus, it reaches the middle ear at the tympanic membrane (ear drum) – a large, movable plate receiver for sound. The tympanic membrane is connected to a series of small bones: the malleus, incus, and stapes, collectively known as the ossicular chain. These bones act as an impedance transformer, transferring energy between the low impedance tympanic membrane to the higher impedance of the cochlear fluids of the inner ear.

The movements of the ossicular chain are under active control by two muscles; the tensor tympani, which connects the malleus, and the stapedius which connects to the stapes. These muscles reflexively contract in response to loud sound, vocalisation, and a variety of bodily movements (Carmel and Starr, 1963), protecting the ear from prolonged exposure to noise and attenuating frequency input to the cochlea.

1.2.2 The Inner Ear

The inner ear includes both the vestibular system, which is dedicated to balance, and the cochlea, which is dedicated to hearing. Here, the focus will be on the cochlea. The cochlea is hollow, conical, and spiral in shape; wrapped around a central bony structure called the modiolus. The interior of this hollow space is divided into three sub compartments – the scala vestibuli, the scala tympani, and the scala media.

Uncoiled, the cochlea can be depicted as in Figure 1.4A, with the scala vestibuli and scala tympani meeting at the helicotrema at the apex of the cochlea. Unlike the outer and middle ear, the inner ear is a fluid filled space with these outer regions filled with perilymph – an extracellular fluid rich in sodium (Na^+).

The scala media is an isolated compartment, separated from the perilymph by Reissner's membrane and the basilar membrane (Figure 1.4A-B). This compartment is filled with potassium (K^+) rich endolymph. This high concentration of K^+ in the scala media is replenished and maintained by ion channel pumps in the stria vascularis on the outer wall of the cochlea (Thalman et al., 1981). The differing concentrations of ions in each compartment is such that a large electrochemical gradient with a potential of between +80 to +100mV is maintained (Sterkers et al., 1984).

Organ of Corti

Sitting on top of the Basilar membrane, within the scala media, is the organ of Corti (Figure 1.4B-C). The organ of Corti can be thought of as the true organ of hearing. Here, specialised hair cells transform sound pressure waves into electrical signals. The hair cells are arranged on the organ of Corti as three rows of outer hair cells (OHCs) and a single row of inner hair cells (IHCs), as shown in Figure 1.4C. Tight junctions at the upper surface of the organ of Corti separate the scala tympani and scala media. These tight junctions allow the hair cell bodies to be surrounded by perilymph while their apex are bathed in endolymph.

1.2.3 Hair Cells Convert Sound into an Electrochemical Stimulus

IHCs convert the mechanical action of sound into an electrochemical signal which can be processed by the central auditory pathway, whereas the more abundant OHCs create active amplification by oscillating in length in response to transmembrane voltage changes (Brownell et al., 1985).

At the apex of each hair cell is a bundle of hair like projections called stereocilia which are lined up in several rows of increasing height. Stereocilia are connected to one another via "tip-link" proteins; a fine molecular braiding which joins non-selective mechano-electrical transduction (MET) channels on the apex of one stereocilium to the side of the longest adjacent stereocilium.

Movement by the stapes on the oval window creates 'pulses' of pressure changes in the perilymph. This causes the basilar membrane to oscillate (Figure 1.4) relative to the tectorial membrane, causing a shearing force to be exerted on the stereocilia. When the stereocilia are deflected away from the modiolus, the stereocilia move away from one another and the MET channels are opened (Figure 1.5). This allows K^+ influx into the hair cell along the large electrochemical gradient. Rapid depolarisation of the hair cell opens voltage sensitive Ca^{2+} channels and the subsequent release of neurotransmitter at the basal region of the cell. Voltage sensitive and Ca^{2+} sensitive K^+ channels allow K^+ efflux from the hair cell which is recycled back to the endolymph via the stria vascularis.

At rest approximately 10% of MET channels are open, which allows for a small amount of K^+ leak. Thus, displacement of the stereocilia towards the modiolus inhibits the influx of K^+ whilst continuing K^+ efflux, hyperpolarising the cell. The periodic excitation and inhibition caused by the sound-induced sinusoidal oscillations of the basilar membrane therefore creates a similar sinusoidal membrane potential in the hair cells (Figure 1.5).

1.2.4 Synaptic Transmission within the Cochlea

The Spiral Ganglia

Hair cells are innervated by bipolar spiral ganglion neurons (SGNs) which are located in enclosed canals within the bony modiolus (see Figure 1.4). SGNs can be divided into two broad categories: large, myelinated type I SGNs and small, unmyelinated type II.

In the adult mouse cochlea, there are approximately 800 IHCs which are each innervated by between five and 30 type I SGNs. These type I cells make up about 95% of the total SGN population (Lu et al., 2016). Type I fibres can also be subdivided further, with SGNs projecting onto the medial side of IHCs having higher thresholds and low spontaneous discharge rates compared to those projecting to the lateral side (Liberman and Oliver, 1984).

Type II SGNs make up the remaining 5% of cell bodies, which innervate OHCs. While each type I SGN makes connection with just one IHC, each type II SGN will directly connect with multiple OHCs, and each OHC will be connected to between two and five type II SGNs. The function of type II SGNs is not yet clear, however their action potential thresholds and kinetics are distinctly different from type I SGNs, suggesting a unique role (Zhang and Coate, 2016).

The majority of OHC innervation is from efferent input which originates from the contralateral Superior Olivary Complex (SOC). The principle efferent neurotransmitter is believed to be acetylcholine (ACh) which acts on $\alpha 9\alpha 10$ nicotinic receptors on the OHC, allowing the influx of Ca^{2+} and activating Ca^{2+} -sensitive K^+ channels (Wersinger and Fuchs, 2011). The OHC efferents act to modulate afferent stimulation at the IHCs by actively dampening the oscillations of the basilar membrane. As such, the protracted hyperpolarisation of OHCs reduces the sensitivity of the cochlea during noise exposure, and essentially protecting against noise-induced hearing damage.

Introduction

Sparse efferent innervation of IHCs is also found, however these form synapses with the receiving dendritic processes of type I SGNs. Efferent innervation of IHCs is distinct, formed by descending processes from the lateral SOC.

The Hair Cell Ribbon Synapse

Rapid transfer of afferent information (IHC to SGN) is facilitated by a specialised synapse, characterised by a presynaptic organelle referred to as a synaptic ribbon or dense body. The synaptic ribbon is a large, electron dense structure in the active zone of the hair cell synapse, which acts to tether synaptic vesicles and biochemically prepare them for exocytosis. For review, see Nouvian et al. (2006).

During depolarisation of the hair cell L-type voltage-gated Ca^{2+} channels open to allow influx of Ca^{2+} into the cell, triggering the release of glutamate (Nordang et al., 2000). There are two phases which occur during the elevation of intracellular Ca^{2+} . The first is an initial fast phase ($\tau = 1$ ms) in which five to eight readily-releasable vesicles, collected by the ribbon are released (Mennerick and Matthews, 1996). After this a slower, sustained phase of release ($\tau = 300$ ms) is maintained through the release of vesicles which are stored further away in the cell. This mechanism allows for synaptic transmission to be temporally precise and able to encode prolonged stimuli.

Once glutamate is released, it acts on AMPA receptors on the SGN afferents; principally GluA2, GluA3, and GluA4 (Nouvian et al., 2006, Glowatzki and Fuchs, 2002). Excess glutamate is taken up from the synapse via glutamate-aspartate transporters (GLAST or Slc1a3) and vesicular glutamate transporters (VGlut1), which are expressed on the IHCs and surrounding supporting cells (Furness and Lawton, 2003).

1.2.5 The Central Pathway

Spiral ganglion neuron axons exit the cochlea bundled as the auditory nerve (VIIIth cranial nerve), through the central column of the modiolus (Figure 1.4B), and project to the cochlear nucleus (CN) in the brainstem. At this level, the pathway

Introduction

divides into two main streams. Branches terminating in the dorsal cochlear nucleus (DCN) project directly to the contralateral nuclei of the lateral lemniscus and the inferior colliculus. This pathway conveys information about the identity of a sound, temporal variation, and frequency. The second pathway is projected into the ventral cochlear nucleus (VCN) which projects to both the contralateral and ipsilateral SOC (Figure 1.3). As each SOC receives input from both ears, sound localisation can be determined by comparing the inter-aural time and intensity differences. From here, this pathway ascends via the lateral lemniscus where it will form a synapse with either the inferior colliculus or with the medial geniculate body of the thalamus, before reaching the auditory cortex.

The Cochlear Nucleus

The cochlear nucleus (CN) is not homogeneous in structure and can be divided into three distinct subdivisions: the dorsal cochlear nucleus (DCN), and the ventral CN (VCN), which itself can be further divided into the anteroventral (AVCN) and posteroventral CN (PVCN). Several distinct cell types can also be found throughout the cochlear nucleus. These consist of spherical cells, which are located in the AVCN; multipolar cells and globular neurons which are located in both the AVCN and PVCN; octopus cells, which are located in the PCVN; giant cells, which are located in the DCN; and finally pyramidal cells which are located at the outer edge of the DCN. Granule cells can also be found at the periphery and small cells can be found throughout the CN.

In this study, the CN was taken and analysed alongside samples from the cochlea. However, as no effort was made to distinguish differing cell types in the CN, and because the CN was not the primary site of insult after noise, the characteristics of each cell type will not be discussed here. It is, nevertheless worth noting that each of the differing cell types has unique responses to input from the cochlea, including inhibitory components. Thus a diverse population of ion channels and neurotransmitter transporters can be found in the CN.

1.2.6 Tonotopy in the Auditory System

The Organ of Corti

The Basilar membrane varies in thickness and flexibility along its length, with the base being thick and stiff and the apex relatively thin and flexible. Because of this, different regions of the basilar membrane are “tuned” to different frequencies. Passive oscillation of the basilar membrane is such that peak displacement of the membrane will occur at its resonant frequency. This follows a simple harmonic motion, where frequency (f) is relative to mass of the membrane (m), and its stiffness (k),

$$f = \frac{1}{2\pi} \sqrt{\frac{k}{m}} .$$

Therefore, high frequency sounds will have the greatest response at the base of the cochlea (high stiffness) and low frequency sounds will have the greatest response at the apex (low stiffness). Displacement amplitude is also affected by the active mechanical processes produced by OHCs, which amplifies oscillations in an “active region” about the tuned area (Neely and Kim, 1986, Ashmore, 2008).

In response to a low intensity stimulus (20 – 40 dB SPL) peak vibration is sharply localised to one area, but at higher intensities (>80 dB SPL) this peak broadens (Russell and Nilsen, 1997). Past the active region of the membrane, the travelling wave amplitude quickly diminishes as the mass of the basilar membrane and cochlear fluid is large enough to limit movement. This means that damage from high intensity noise will damage regions of the cochlea up to the resonant point more than lower frequency regions beyond this.

The mapping of constituent frequencies onto different regions of the cochlea also allows for frequency specific physiological adaptations of the hair cell. Stereocilia, for example, are greatest in length at the apex in both IHCs and OHCs, and become more abundant at the base in OHCs. Graduations in their length and

Introduction

orientation to the basilar membrane also vary, adapted for the varying levels of energy at each frequency (Corwin and Warchol, 1991).

The Hair Cell Synapse and Spiral Ganglion

In addition to the mechanical adaptations, the inner ear must also adapt to the differing firing rates between the base and the apex. Thus, voltage-gated ion channel distribution and density differs along the length of the cochlea. For example, voltage-gated potassium channels, $K_v1.1$, $K_v1.2$, and $K_v3.1$, have all been shown to be enriched at the base of the cochlea, whilst $K_v4.2$ has an opposing distribution (Davis, 2003). Given the vast range of frequencies the mammalian cochlea responds to, it is likely that many proteins expressed in the hair cells and spiral ganglion possess a tonotopic gradient.

This tonotopic axis is thought to be established in part through spontaneous firing of the immature hair cells, driven through an increased response to ATP (Jovanovic et al., 2017, Sendin et al., 2014). The axis is also established and maintained by a differential distribution in neurotrophins: brain derived neurotrophic factor (BDNF) and neurotrophin-3 (NT-3) which have reciprocal expression gradients along the axis. In embryonic stages, NT-3 is enriched at the base of the cochlea, while high concentrations of BDNF can be found at the apex; however postnatally this gradient is reversed, with high NT-3 seen at the apex and high BDNF seen at the base (Davis, 2003).

The Central Auditory System

Just like the cochlea, nuclei within the central auditory pathway are thought to contain tonotopic organisation with distinct regions specialised to receive and process a "best frequency". Low frequency nerve fibres originating from the cochlear nucleus innervate the ventral portion of each CN region, while high frequencies terminate dorsally. Also like the cochlea, CN neurons must therefore be able to meet the electrophysiological and metabolic demands of a higher rate of firing.

Phase Locking at the Auditory Nerve

In the absence of stimulus, auditory nerve fibres fire spontaneously. At frequencies less than 3 kHz spike intervals will occur at integer multiples of the stimulus, i.e. firing at every 2 or more cycles. For most low frequency stimuli the frequency of the stimulus will not increase the rate of firing, but rather alter the firing pattern. This phenomenon is referred to as phase locking. With high frequency tones, the phase locking response becomes weaker and may instead spike at random intervals, so no information about frequency is encoded. This is where the tonotopic organisation of the cochlea becomes important. As the intensity of sound is encoded by the rate of firing (i.e. spikes per second), fibres at the resonant frequency will fire at a higher rate than the regions around it, so the frequency can be encoded by integrating this information.

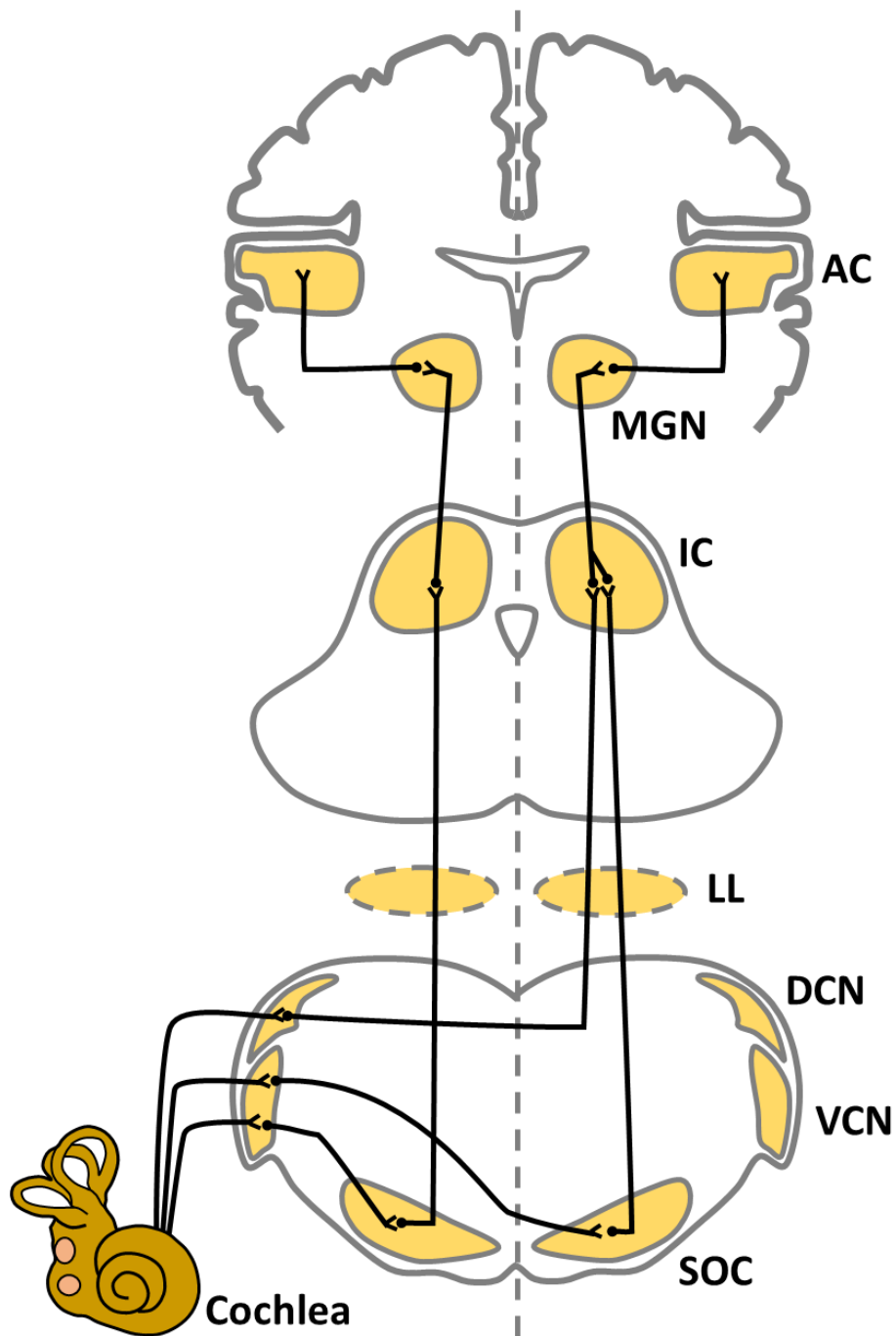


Figure 1.3: Simplified diagram of the mouse ascending auditory pathway. Signal from the cochlea passed along the VIIIth nerve, which bifurcates into both the ventral cochlear nucleus (VCN) and dorsal cochlear nucleus (DCN). The DCN then projects and synapses first through the contralateral lateral lemniscus (LL) to the inferior colliculus (IC), which then projects to the medial geniculate body (MGN) before ending at the auditory cortex. The VCN, on the other hand, first projects to the ipsilateral and contralateral superior olivary complex (SOC), before following the same ascending route. This means that each nuclei in the ascending pathway receives input from both ears.

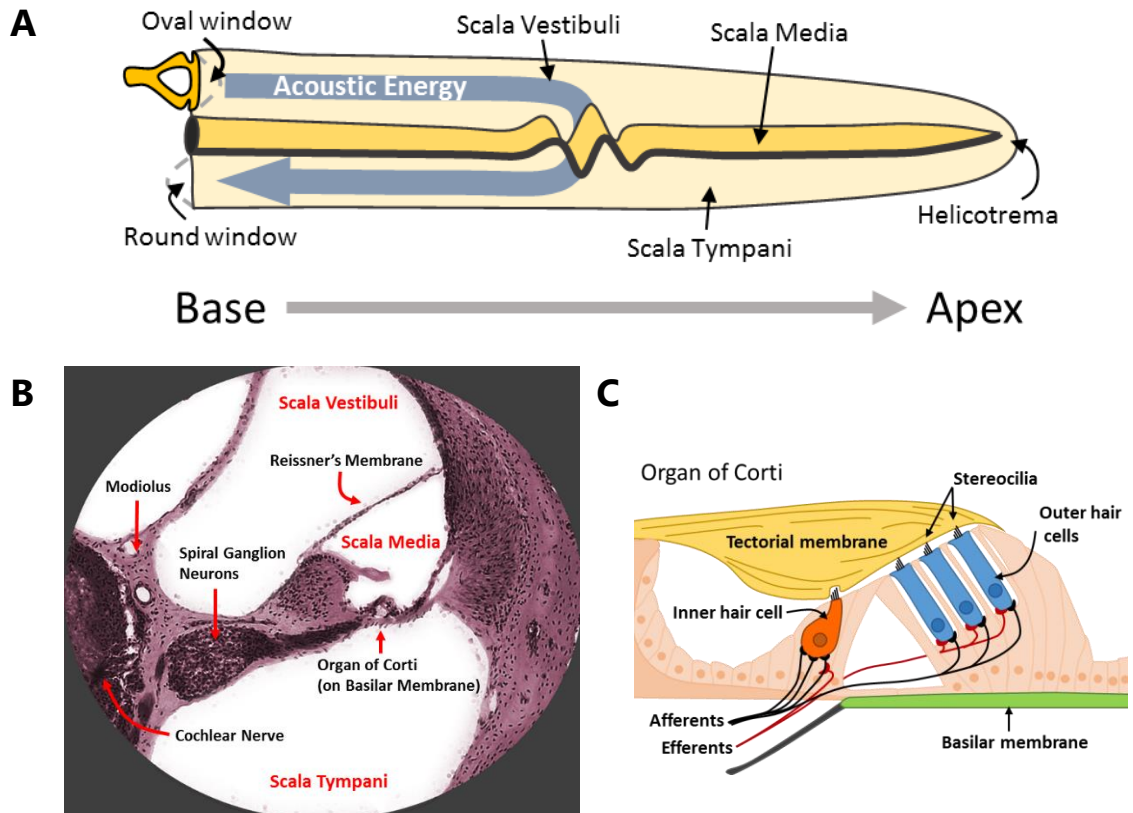


Figure 1.4: Diagram of the mammalian cochlea. (A) The cochlea is divided up into three fluid filled spaces, the Scala Vesibuli, Scala Media, and Scala Tympani. Acoustic energy is transferred into the fluid filled cochlea at the oval window where it will impart energy onto the basillar membrane. (B) Cross section of the cochlea shows the three fluid filled compartments. Between the Scala Vestibuli and Scala Tympani lies the organ of Corti (C) where the mechanical energy in the basilar membrane is converted into an electrical signal.

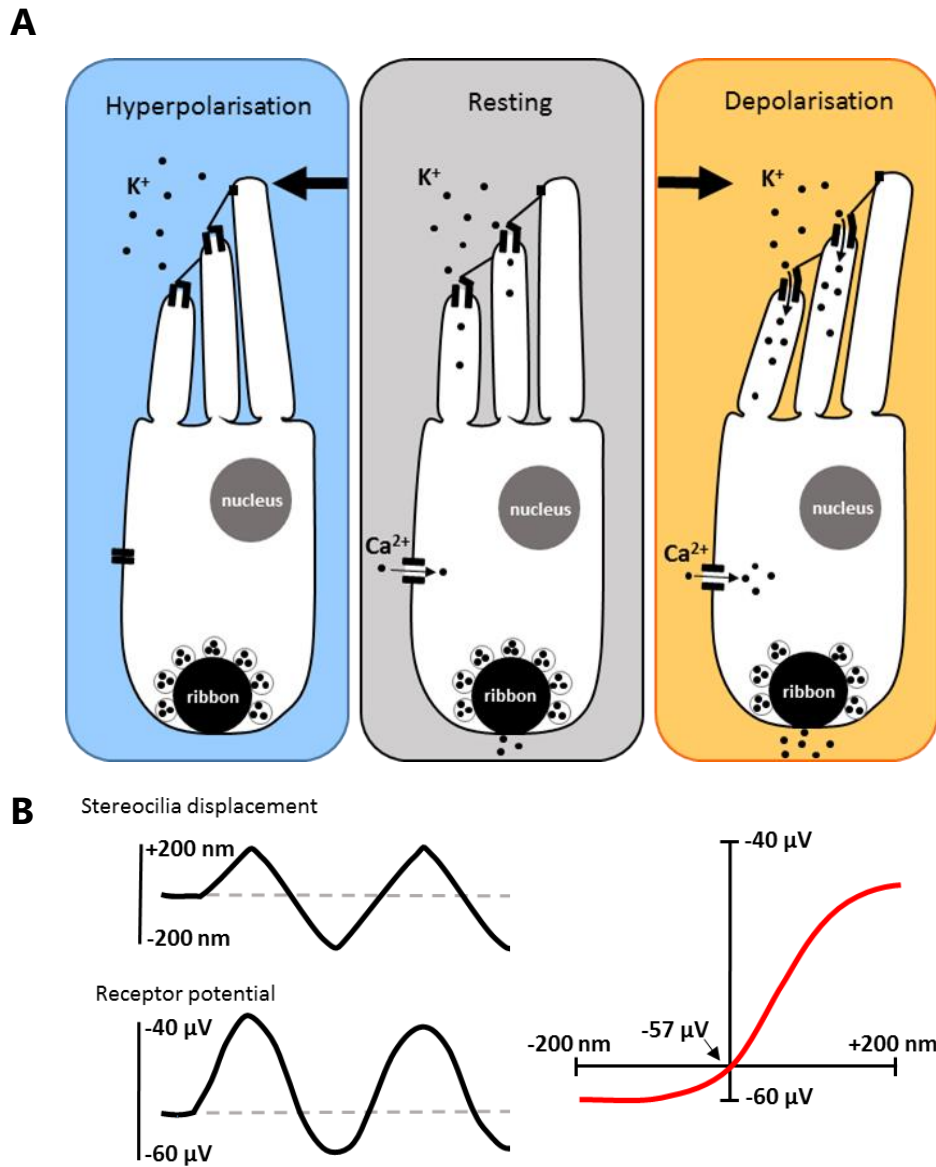


Figure 1.5: Movement of the stereocilia results in an alternating current in the inner hair cell. (A) At rest, approximately 10% of mechanotransduction channels on the inner hair cells are partially open, and can either be depolarised or hyperpolarised depending on which direction the stereocilia are moved. (B) Oscillations at the basilar membrane produce an oscillatory receptor potential in the inner hair cells. Change in receptor potential is greater in depolarisation than in hyperpolarisation.

1.3 Hearing Loss & Dysfunction

1.3.1 The Causes of Hearing Damage

Hearing loss can occur at any stage in life, with early stage hearing loss due to a genetic predisposition, ototoxic damage, physical injury, or through exposure to damagingly loud sounds. The damage incurred by exposure to sound can affect the cochlear hair cells and the auditory nerve (sensorineural damage), and can alter the propagation of energy along the basilar membrane. The extent of this damage largely depends on the intensity of noise to which the individual is exposed.

Noise induced hearing loss (NIHL) can be divided into two broad categories, characterised by the recovery of an individual's hearing thresholds after noise exposure. Permanent threshold shifts (PTS) describe an initial loss of hearing sensitivity (increase of threshold) which does not recover over time, whereas in temporary threshold shifts (TTS) the individual's hearing will return to normal over a period of several days.

1.3.2 Permanent Threshold Shifts

PTS can occur in a number of different situations. The most damaging exposures, such as high intensity blast exposures and exposure to prolonged noise in excess of 125 dB SPL can lead to catastrophic, irreversible damage to the cochlear structures, in particular at the organ of Corti (Saunders et al., 1985). However, lower intensities of noise (>106 dB SPL) can also damage and disrupt the organisation of stereocilia on both the IHCs and OHCs, while leaving surrounding structures intact.

Damage to OHCs, the tectorial membrane, and the supporting cells are thought to be the main contributing factors in PTS, as the IHCs are relatively insensitive to noise-induced cell death (Shi et al., 2016a).

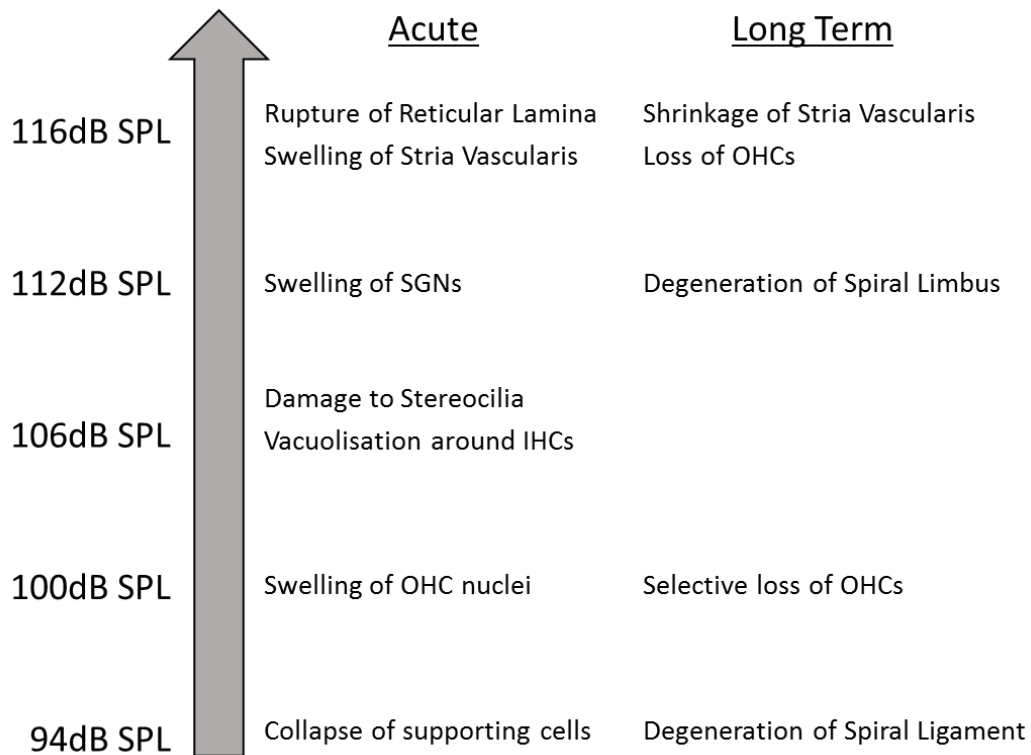


Figure 1.6: The cellular effects of noise exposure in the CBA/Ca mouse. Mice exposed to octave band noise showed varying damage to the cochlear structures dependent on intensity of noise delivered. All five intensities shown are enough to induce a permanent threshold shifts. Figure created with reference to (Wang et al., 2002).

1.3.3 Temporary Threshold Shifts

TTS occurs when the intensity of noise is not energetic enough to cause substantial physical, structural damage to the cochlea. While TTS is associated with less severe noise insults the initial loss of sensitivity is not necessarily indicative of whether the threshold shift will be permanent, as shifts of 40 dB SPL can recover to normal levels over time (Kujawa and Liberman, 2009).

Several different mechanisms are thought to contribute to TTS, which may be a combination of damage and protective adaptations. For example, a small degree of the TTS is due to the opening of non-selective cation channel P2x2, which opens in the presence of extracellular ATP (Housley et al., 2013).

One of the largest contributors to PTS is thought to be caused by glutamate excitotoxicity at the primary afferent synapses. Following noise exposure,

Introduction

excitotoxicity causes acute swelling and retraction of the SGN dendrites (Robertson, 1983, Puel et al., 1998, Kujawa and Liberman, 2009) in addition to swelling and distortions of the synaptic ribbon (Song et al., 2016).

It was previously thought that once this swelling had subsided, and threshold levels have returned to those seen pre-exposure, there was no lasting damage to the auditory pathway. However, it has recently been shown that a TTS is accompanied by a delayed and progressive loss of SGN cell bodies, which occurs even when the IHC survive undamaged (Kujawa and Liberman, 2006, Kujawa and Liberman, 2009, Lin et al., 2011b, Zilberstein et al., 2012a, Fernandez et al., 2015). There is currently no evidence to suggest that glutamate excitotoxicity has any effect on type II SGN terminals and is it the high-threshold, low spontaneous rate SGN fibres which are most sensitive to damage following acoustic overexposure (Furman et al., 2013, Liberman et al., 2015).

This type of hearing damage has been termed “hidden hearing loss” as it cannot be detected by standard threshold tests. However, the progressive loss of high-threshold SGN and afferent synapses results in deficits in temporal processing and hearing in noisy environments (Shi et al., 2016b).

1.3.4 Neuronal Death

Glutamate excitotoxicity has been implicated in a wide range of neurodegenerative disorders such as amyotrophic lateral sclerosis (King et al., 2016), Parkinson’s (Ambrosi et al., 2014), and Alzheimer’s (Zadori et al., 2014). Moreover, the excessive release of glutamate following CNS trauma can lead to the progressive degeneration which can be seen in cases like ischemic stroke (Paschen, 1996).

While SGN cell death is accompanied by the loss of connections at the hair cell synapse, this uncoupling is not likely to be the cause of degeneration as SGNs have been shown to survive after controlled ablation of IHCs (Zilberstein et al., 2012b, Kurioka et al., 2016). This suggests that SGN degeneration following TTS

Introduction

is a result of the initial noise insult, and not due to loss of function at the afferent terminal.

In the cochlea excitotoxicity first involves a large influx of water and other ions which causes the observed swelling of the terminals. This is followed by excessive influx of Ca^{2+} into the cell, mediated by prolonged depolarisation of the cell membrane (Pujol and Puel, 1999). In other areas of the nervous system, Ca^{2+} dysregulation is known to cause a number of downstream cascades which ultimately lead to death of the neuron (Szydłowska and Tymianski, 2010).

1.3.5 Noise Induced Central Excitability

Tinnitus describes the phenomenon of the perception of sound in the absence of acoustic stimulus. Approximately 10% of adults in the UK are thought to suffer some form of tinnitus (Action on Hearing Loss). Tinnitus can originate from the central auditory system or the peripheral auditory system, and can be caused by neuronal dysfunction or a physiological dysfunction, such as abnormalities in the vasculature system (Miller et al., 2016). Perhaps one of the most common causes of tinnitus is through exposure to loud noises. There is strong correlation between hearing loss and tinnitus, with the risk of tinnitus increasing with the severity of hearing loss (Chung et al., 1984). This has also been well demonstrated in a variety of animal models (Brozoski et al., 2002, Heffner and Harrington, 2002, Turner et al., 2006, Dehmel et al., 2012, Longenecker and Galazyuk, 2011).

The neurological cause of tinnitus is still relatively poorly understood, and it is likely that there are many different regions of the auditory pathway from which the phenomenon could arise. However, recent studies have shown that the generation of tinnitus via acoustic overexposure is likely to originate in the cochlear nuclei, and is accompanied with an increase in spontaneous firing and a change of firing patterns at the dorsal cochlear nucleus (Kaltenbach and Afman, 2000, Brozoski et al., 2002, Kaltenbach et al., 2004, Pilati et al., 2012b, Luo et al., 2014), which spreads to the inferior colliculus (Niu et al., 2013, Berger et al., 2014,

Ropp et al., 2014). While the most obvious cause for increased spontaneous excitability would be a decrease in inhibitory input, there is also evidence of increases in the excitatory input from the somatosensory system (Dehmel et al, 2012). This strengthening of excitatory input to the dorsal cochlear nucleus contributes to the phenomenon of tinnitus, counteracting the decrease in input originating from the peripheral auditory system.

Taking this into account, while alterations to the firing of action potentials at the cochlear nucleus are probably related to changes to ion channel composition at the cell surface; changes to gene expression in the CN following noise are likely to be associated with both excitatory and inhibitory transmission, and contribute to both increases and decreases to cellular excitability.

1.4 Aims of the Project

Gene expression analysis allows the researcher to probe changes in the synthesis of functional gene products in a region of interest. This is most commonly probed at the level of mRNA as this allows for the accurate detection of activated genes without the worry of nonspecific antibody binding.

There have been several studies to probe the differential expression of genes following noise exposure in several regions of the auditory pathway. For example, previously at the University of Leicester, it was shown that there was a change in the expression in voltage-gated sodium channels Nav1.1, 1.6, and 1.7 in spiral ganglion neurons following a noise challenge in rat (Fryatt et al., 2011).

Other studies have looked at related genes and gene pathways to investigate why certain physiological changes happen following noise. For example, in order to investigate apoptotic pathways in the hair cells and lateral wall of the cochlea following noise (Hu et al., 2009) looked at panel of apoptotic related genes following moderate noise exposure.

Since the first demonstration of the Microarray by (Schena et al., 1995), on chip hybridisation of complementary DNA has been the first choice for experiments

Introduction

which intend to probe whole genome gene expression changes. However, in recent times, the use of whole transcriptome sequencing (RNASeq) is replacing microarray in many cases as a more sensitive and reliable method for detecting gene expression changes.

There have been just a handful of previous studies which have employed these techniques on the cochlea following various models of noise exposure, such as blast exposure (Kirkegaard et al., 2006), and noise which induces severe permanent threshold shifts (Cho et al., 2004). However, none of these whole transcriptome studies have looked specifically at changes to the spiral ganglion following noise exposure.

The aim of this project is to gain insight into what happens on a molecular level following moderate noise-induced hearing loss. To achieve this, mice were exposed to noise in order to elicit a marked threshold shift, which will recover partially over time. Tissue was collected, and RNA Sequencing (RNAseq) was employed to highlight potential genes of interest. Work by Kujawa and Liberman (2009) suggests that significant changes occur to the SGNs and cochlear nerve following acoustic overexposure; which due to their size and location in the cochlea, could be overshadowed by the large inflammatory response in the whole cochlea. By micro-dissecting the modiolus, which contains the SGNs and cochlear nerve, this allows for better insight into molecular changes at the primary auditory neuron.

As cell death in the SGNs is typically observed several months following acoustic insult (Kujawa and Liberman, 2009) this project looks at three time points following exposure in order to probe both acute and long term or chronic changes in expression. The time points chosen were one day, seven days, and 28 days. This time scale allows for the identification of long-term changes, while avoiding the period (> 6 months) in which the consequences of cell death will inevitably cause additional inflammatory responses.

Introduction

Although the main focus of this study is to look at the SGNs and cochlear nerve, exposure to noise is also known to induce changes in excitability at the cochlear nucleus following noise, contributing to the phenomenon of tinnitus (Kaltenbach and Afman, 2000, Pilati et al., 2012a). For this reason, in addition to the modiolus, cochlear nucleus was also taken and analysed in parallel.

By highlighting gene expression changes in both specific genes and families of genes, the data collected here provides a foundation for the further study of mechanisms contributing to noise-induced damage and recovery; and reveals potential mechanisms for SGN cell death following noise exposure.

Chapter 2: Experimental Methods

2.1 Overview

This chapter will cover the experimental methods used throughout this study. An experimental flow chart has been provided below (Figure 2.1).

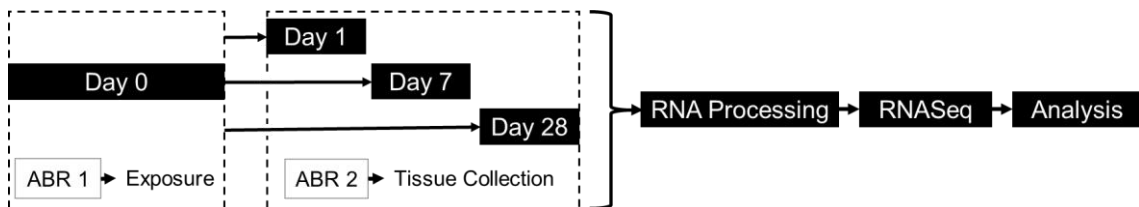


Figure 2.1: Flow chart of study. In order to gain insight into what happens on a molecular level following moderate noise-induced hearing loss, mice were exposed to noise (§2.5) and left to recover for a period of one, seven, or 28 days. In addition to noise exposed mice, matched sham exposed controls were included for each recovery group. In order to assess damage to hearing caused by the insult, mice underwent auditory brainstem response testing (ABR, §2.4) immediately before the noise exposure (ABR 1) and immediately after the recovery period (ABR 2). Following the recovery period, modiolar and cochlear nucleus tissue was collected (§2.6), and processed for whole transcriptome sequencing (RNASeq, §2.7). Differential expression analysis was performed between noise and sham exposed mice, and follow up immunohistochemistry (§2.8) and western blots (§2.9) to further support the results.

2.2 Experimental Animals

All procedures carried out were approved in local ethical reviews, overseen by a Named Veterinary Surgeon, and regulated under the Animals (Scientific Procedures) Act 1986. Described work was licensed under personal license (PIL) 70/26046 and project license (PPL) 60/4353, and carried out at a Home Office approved registered establishment (X1798C4D2).

CBA/Ca mice were bred in house at the Central Research Facility (University of Leicester). All animals were bred and kept in the same room throughout their lifetime with a 12-hour light cycle to ensure little variation between ambient noise and light levels. Food and water was provided *ad libitum*.

The animals were aged to between post-natal day 38 to 50 ($\mu = 43$, median = 43, see Figure 2.2A) before exposure (noise or sham) to ensure the inner ear could be considered mature in both its morphology and electrophysiological properties

Experimental Methods

(Lim and Anniko, 1985, Marcotti et al., 2003, Hafidi et al., 2005, Bulankina and Moser, 2012). At this age, weights were centred about a mean value of 17.4g and did not vary more than 3σ ($\sigma = 1.4\text{g}$, see Figure 2.2B). Gender was also restricted to female mice to minimise intra-animal variation.

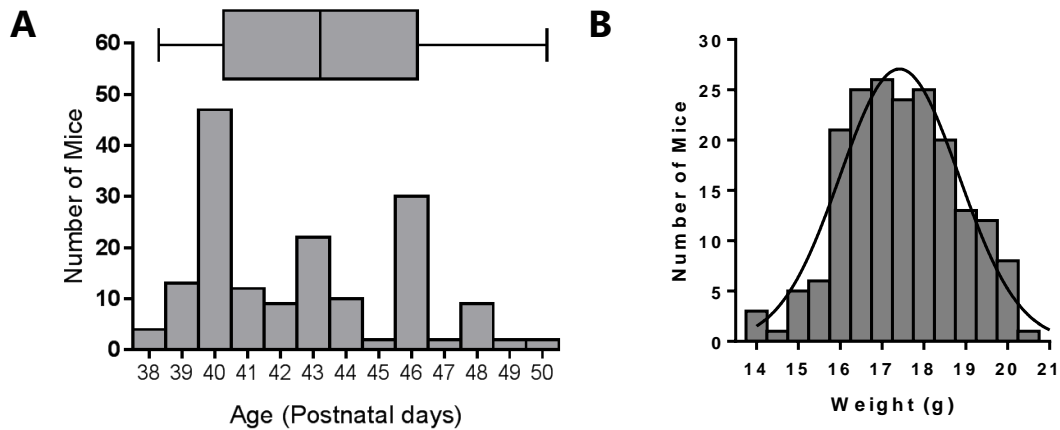


Figure 2.2: Age and weights of experimental mice used. (A) Mice were aged between P38 to P40 at the beginning of experiments with a median postnatal age of P43. **(B)** Within this age range, weights were approximately normally distributed about a central value of 17.4g ($\sigma = 1.4\text{g}$), and did not differ more than 3 standard deviations away from the mean.

2.3 Anesthesia Protocols

All experimental animals were anaesthetised to minimize trauma during noise exposure (§2.5), and to ensure that the mice remained in a consistent, prone position, free of myogenic activity during auditory brainstem response (ABR) recordings (§2.4).

Although popular practice in pre-clinical science, anaesthesia in the mouse is particularly challenging due to the animal's small size, high surface area to weight ratio, and rapid metabolism. The anaesthetic must also be carefully selected so as not to interfere with any experimental procedures.

While a combination of ketamine and xylazine does not significantly alter the auditory brainstem response (Smith and Mills, 1989), and is thus commonly used,

Experimental Methods

for this study must be avoided as NMDA agonists such as ketamine have been shown to be protective against tinnitus after noise insult and may have an effect on glutamate excitotoxicity (Guitton and Dudai, 2007). In addition other commonly used anaesthetics such as the volatile inhalation agent, isoflurane, is not suitable as prolonged exposure to the drug caused a diminishing of the ABR waveform until it was no longer recordable (Fryatt, 2010).

For this study, neuroleptanalgesia in the mice was produced with a combination of fentanyl, midazolam and medetomidine (Thal and Plesnila, 2007). Midazolam is a water-soluble benzodiazepine, and are hypnotics, muscle relaxants and minor tranquilisers. It is a short acting drug with a rapid onset and acts as a GABA_A agonist, enhancing GABA activity in the CNS. Although midazolam is effective in the induction of anaesthetic, it cannot be used alone for the maintenance of adequate anaesthesia (Reves et al., 1985).

Medetomidine is an α_2 agonist which provides sedation, hypnosis and mild analgesia. It acts by binding to α_2 -adrenergic receptors in the CNS, which inhibits the release of acetylcholine and norepinephrine. Due to the longevity of the effects of medetomidine a suitable antagonist, such as atipamezol, can be used to reverse the effects of medetomidine and speed up recovery (Cruz et al., 1998). As medetomidine only possesses mild analgesic properties, for effective anaesthesia, it is combined with the potent, synthetic opioid agonist, fentanyl.

2.3.1 Induction of Anaesthesia

Anaesthesia protocol was decided in consultation with the Division for Biomedical Services (Leicester) Named Veterinary Surgeon (NVS), and trialled with the assistance of the Senior Veterinary Services technician. Doses are based on those used in Thal and Plesnila (2007), but at a reduced (80%) rate. This dose, stated below, was found to produce a fast induction of anaesthesia (<20 mins), a long sedation period (>1 hour), and a fast recovery when reversed (<30 mins).

Experimental Methods

Mice were anaesthetised using a cocktail of fentanyl (0.04mg.kg⁻¹), midazolam¹ (4mg.kg⁻¹), and medetomidine² (0.4mg.kg⁻¹), delivered by a single intraperitoneal (IP) injection. Total volume of injection was between 78 – 114 µL, dependant on weight of animal; calculated as

$$\text{amount (mL)} = \frac{\text{dose rate (mg.kg}^{-1}) \times \text{weight of mouse (kg)}}{\text{concentration of drug (mg.mL}^{-1})},$$

with all drugs used at stock concentrations, with the exception of medetomidine which was diluted 1:10 before use.

Supplementary top-up injections (0.01mg.kg⁻¹ fentanyl, 0.1mg.kg⁻¹ midazolam) were provided up to two times if the anaesthetic became too light during procedure.

During induction of anaesthesia and during long noise exposure protocols, oxygen was delivered free field to the mouse to mitigate the decreased respiratory rate and an ocular lubricant (Lacrilube®, Allergan) was applied to the eyes to ensure they remained moist during anaesthesia. Body temperature was maintained using a homeothermic blanket set to 37°C. To prevent dehydration and to facilitate easy recovery, warmed saline solution (0.9% w/v)³ was administered subcutaneously at a rate of 100 µL per hour.

Procedures were only begun once the animal was deeply anaesthetised; this was determined by the absence of a pedal reflex on hind paw pinching. During recordings, the mouse was monitored for signs of respiratory and cardiac distress, and for signs of inadequate anaesthesia, using an oscilloscope connected to the ABR recording equipment. If the mouse showed any signs of distress, the procedure was paused until any issue was resolved.

¹ Both Fentanyl and Midazolam were obtained from National Veterinary Services Limited through the Division for Biomedical Services, Leicester.

² Medetomidine hydrochloride is sold by Dechra under the name Sedetor®.

³ Saline solution was sold by Dechra under the registered trademark Vetivex®.

Experimental Methods

On the first day of experiment, mice were kept under sedation for both ABR and following exposure. Total time under anaesthetic (before reversal) ranged between 100 – 193 minutes, with a median time of 138 minutes.

2.3.2 Reversal of Anaesthesia

The mice were recovered with a 1mg.kg^{-1} dose of atipamezol⁴ diluted to a concentration of 1:10 with sterilised water and delivered by IP injection. During recovery, mice were returned to a clean, warm cage and placed in an area free of bedding. Supplemental oxygen was provided and the mice were closely monitored until showing signs of normal behaviour, i.e. walking, cleaning, or eating when they were transferred to an individually ventilated cage rack kept at approximately 23°C, where they were left overnight. Wet food was provided on the floor of the cage to encourage the mouse to eat as soon as possible after the reversal of the anaesthesia.

⁴ Atipamezole hydrochloride is sold by Dechra under the name Atipam®

2.4 Auditory Brainstem Response Recordings

2.4.1 Recording Set-up & Calibration

Auditory brainstem response (ABR) recording equipment was sourced from Tucker-Davis Technologies (TDT) and set up according to the methods outlined in Ingham et al. (2011), see Figure 2.3. Briefly, the TDT set up was routed so that the speaker, pre-amp, and head-stage were isolated within a sound-attenuating chamber. Custom Averager software, provided by the Wellcome Trust Sanger Institute (WTSI), generates a series of tone pips or click stimuli, which is delivered to the mouse. The signal from the electrodes placed subcutaneously (see §2.4.2) is then amplified and returned back to the system for filtering and sampling.

Automatic calibration was performed by the WTSI software before the initial ABR recording each day to account for varying pressure levels and background noise. The equipment was calibrated using a PCB microphone preamplifier (model 426B03) with a 1/4" pre-polarised condenser microphone, driven through a PCB signal conditioner (model 480C02), and returned to the MA3 Stereo microphone amplifier (Figure 2.3). The microphone was placed at a height and distance away from the speaker equal to where the animal's head would lay during recordings, and automatic calibration was performed within the WTSI Averager software.

2.4.2 The Recording Procedure & Data Collection

Animals were anaesthetised as described in §2.3.1 and placed on a homeothermic blanket (Figure 2.3) in a nose-forward, prone, unrestrained position. Stainless steel, 12mm, 28 gauge needles electrodes were obtained from Chalgren Enterprises (112-812-48TP) and bent clockwise at two 90° angles (see Figure 2.3C). This modification facilitated placement of the electrodes and ensured minimum movement during recording.

The recording electrode was placed subdermally at the vertex of the head, and reference and ground needle electrodes were placed subdermally in the patch of bare skin behind the left and right ear, respectively (Figure 2.3B).

Experimental Methods

Two ABR protocols were run sequentially during each recording. The click protocol is designed to stimulate the auditory system over a broadband of frequencies and is presented as a 0.01ms square-wave, recorded between 0-100 dB SPL in rising steps and averaged 512 times per step (rate of 42.6/s). Tone pip recordings were performed for five discrete frequencies presented as a 5ms (1ms rise/fall time) tone between 0-95 dB SPL in rising steps, and averaged 258 times per step (rate of 42.6/s). For tone pip recordings frequencies were presented sequentially for each intensity level. These are summarised in Figure 2.3D. All recordings were averaged over a 20ms period with a 300-3000Hz bandwidth filter and a gain of 25000x.

2.4.3 Analysis of Data

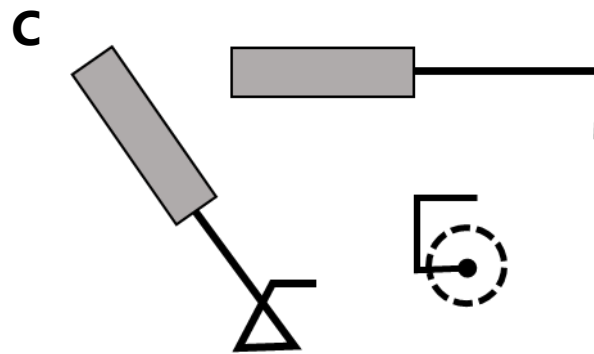
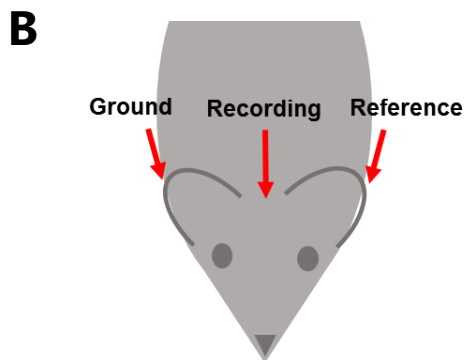
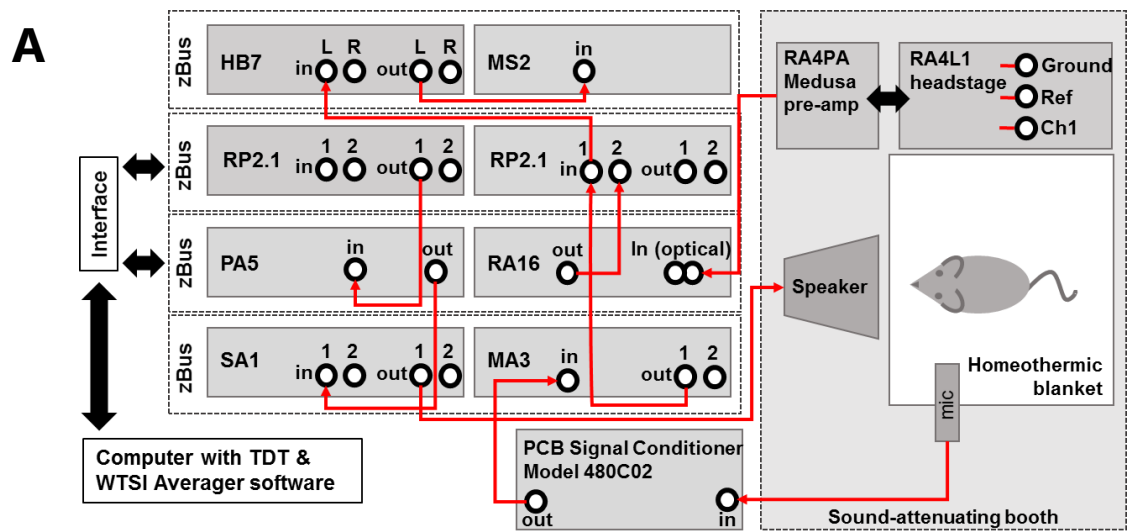
All ABR recordings were output as .csv files through the WTSI Averager and exported into individual frequency .txt files containing the measured amplitude (μV) over time (ms) at each intensity (dB SPL) using WSTI TraceView. At this stage, traces were initially checked for quality.

For threshold determination, traces were stacked in increasing intensity and threshold is estimated as the lowest stimulus intensity that any component of the waveform can be identified and reliably traced up the stimulus levels; usually this would be either wave I, II, or IV, as waves III and V were the first to diminish as intensity decreases.

ABR waveforms were also analysed to determine peak amplitude and latency using the Auditory Wave Analysis Python script developed by Bradley Buran (Eaton-Peabody Laboratory)⁵. Using the script, waveform components were manually selected and absolute amplitude and latency were output as .txt files.

Further analysis was performed using Microsoft Excel or R and plotted in GraphPad Prism.

⁵ Freely available through <https://bitbucket.org/bburan/auditory-wave-analysis>



D Summary of ABR protocols

ABR Protocol	Frequency (kHz)	Start (dB)	Final (dB)	Interval (dB)	Duration (ms)	Ramp time (ms)	N° Averaged
Click	Broadband	0	100	5	0.01	0	512
Tone Pip	6, 12, 18, 24, 30	0	95	5	5	1	256

Figure 2.3: Auditory brainstem recording equipment set up. (A) Set up of the Tucker Davis Technology (TDT) hardware as described in Ingham et al. (2011). ABR stimuli are automatically generated through the Wellcome Trust Sanger Institute (WTSI) Averager interface and presented via an open field speaker in a sound-attenuating booth. (B) Once a surgical plane of anaesthesia was reached, electrodes were placed in the patch of bare skin under each ear and at the vertex of the head. (C) In order to facilitate the placement of electrodes the tips were bent clockwise, as demonstrated above. This shape also ensured electrodes remained in place during recording. Images in A-C adapted from Ingham et al. (2011). Summary of ABR protocols shown in (D).

2.5 Sound Exposure

2.5.1 Sound Exposure Protocol

Anaesthetised mice were transferred to a sound attenuated booth and placed on a homeothermic blanket in a nose-forward, prone, unrestrained position, 15cm from the speaker (Figure 2.4A). In groups of 2 - 5, the mice were exposed 105 dB SPL generated by a custom built white noise generator and amplified by a Cambridge Audio Topaz AM1 Integrated Amplifier. The noise exposed condition will be hereafter referred to as acoustic over exposure (AOE). Sham exposed mice were anaesthetised and treated identically in preparation, however noise was not delivered.

Mice were exposed between 12:00 and 17:00; approximately the second half of daylight hours (7AM-7PM cycle). This period is during mouse inactive phase, which has been previously shown to be the period in which mice are less vulnerable to permanent thresholds shifts following AOE (Meltser et al., 2014). While all efforts were made to reduce the variability of exposure time, experiments occasionally had to be split into two sessions, resulting in a bimodal distribution (Figure 2.4D). Using the elevation of click threshold 24 hours following exposure as a metric of hearing damage, Spearman rank correlation was used to test relationships between threshold shift and hour of day ($P = 0.1638$), age of mouse ($P = 0.1019$) and position in noise exposure booth ($P = 0.8482$). There was no significant correlation with any of the three variables.

2.5.2 Calibration of Equipment

Calibration of the free field noise exposure speaker was performed using a Brüel & Kjær ½ inch free field microphone (type 4191) and pre-amplifier (type 2669-C), connected to the Agilent HP3566A Dynamic signal analyser (Figure 2.4). Equipment was tested and calibrated using a Brüel & Kjær acoustic calibrator (type 4231), before measuring speaker output at 15cm away. Recordings taken in

Experimental Methods

dBV were converted to dB SPL using recordings taken of a 1kHz reference tone of 94dB SPL, generated by a Brüel & Kjær Sound Calibrator (Type 4231).

Sound pressure level was set to a broadband noise of 105 dB SPL (total power), with peaks at ~8kHz and ~20kHz (Figure 2.4B); these measurements did not differ by more than +3dB SPL along the width of the sound attenuated chamber.

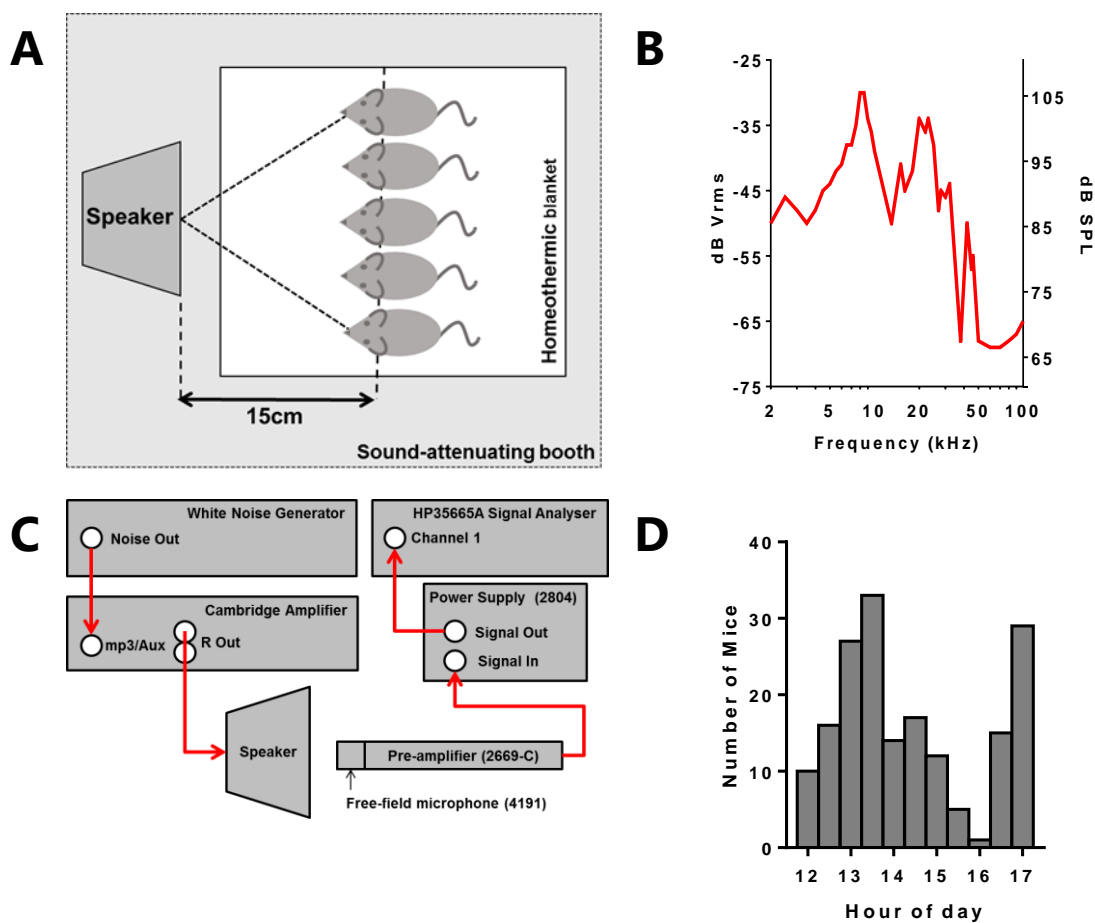


Figure 2.4: Noise exposure equipment set up and calibration. (A) Up to five mice per session were exposed to 105dB SPL for 1.5 hours. Mice were anaesthetised and placed on a homeothermic blanket within a sound-attenuating booth. **(B-C)** Noise was generated using a custom built white noise generator and amplified through a Cambridge Audio Topaz AM1 Integrated Amplifier to produce a broadband signal 105 dB peaking at ~ 8 and 20kHz. A HP35665A signal analyser and a Brüel & Kjær free field microphone was used to calibrate the equipment. **(D)** Plot showing the start time of noise exposure. Exposure was performed during the daylight cycle, between 12:00 and 17:00 which falls within the inactive phase for mice.

2.5.3 Evans Blue for Blood-Labyrinth-Barrier Integrity

Certain noise exposure protocols have previously reported blood-labyrinth-barrier (BLB) breakdown in the cochlea (Wu et al., 2014), increasing the permeability of serum proteins to the perilymph. The extravasation of serum proteins can be assessed through the intravenous injection of Evans blue, a dye which binds with high affinity to serum albumin. Thus presence of Evans blue in tissue is indicative of vascular permeability. To assess whether the noise exposure method used in this study had any effect on BLB permeability in the modiolus, the following Evans blue protocol was performed.

Evans blue (Sigma E2129, lot MKBV014V) was made up 1% w/v in sterile saline and filtered through 0.2µm cellulose acetate syringe filter. Solution was injected intravenously at a dose of 4 mL.kg⁻¹. After 10 minutes observation, mice were anaesthetised as previously described (§2.3.1) and exposed to noise or silence (§2.5.1). Immediately following exposure mice were culled by decapitation and cochlea, brain, and kidney harvested and fixed by submersion in 4% PFA at 4°C for 24hrs. Tissue was processed for sectioning using a method appropriate to tissue type.

Evans blue has a broad excitation spectra with peaks at 470nm and 540nm and an emission peak at 680nm (Hed et al., 1983), and thus will appear red under fluorescence. Exposure times were set using kidney sections as a positive control. As shown in Figure 2.5 there was no difference between the sham exposed and noise exposed cochlea, suggesting the BLB is not affected immediately following noise exposure.

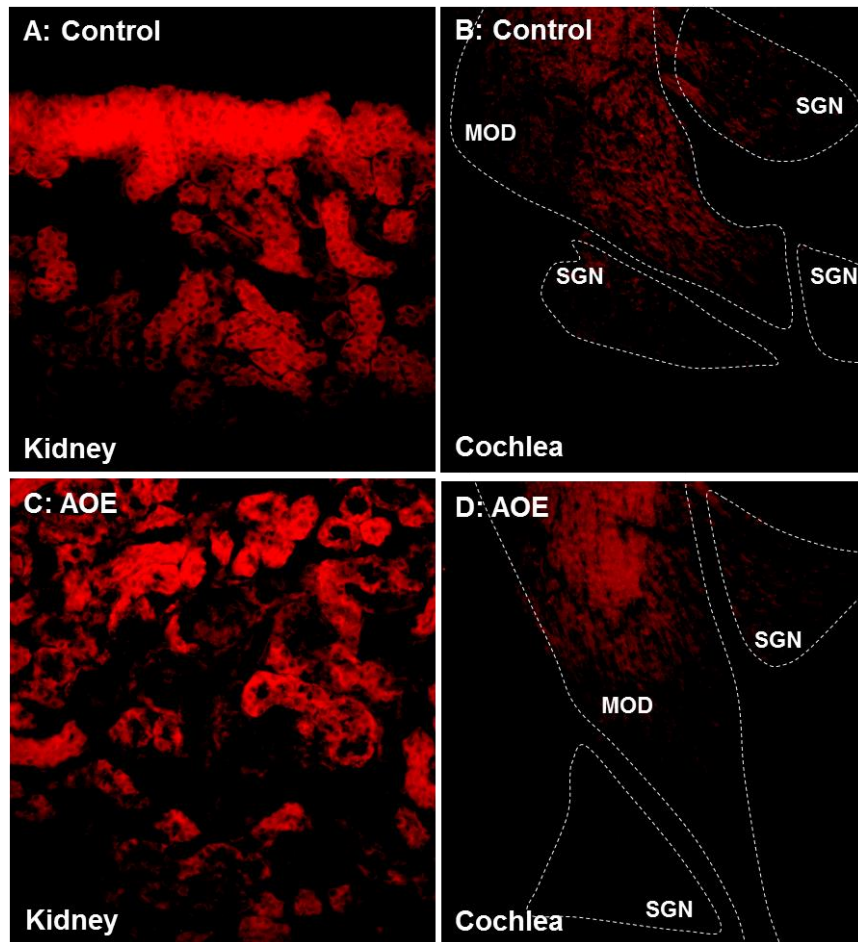


Figure 2.5: Presence of Evans blue does not differ in the noise exposed mouse. Evans blue (red) was injected intravenously prior to noise exposure. Immediately following noise exposure, mice were sacrificed and cochleae were fixed and processed for cryosections. Kidney was used for positive staining for both control (A) and noise exposed mouse (AOE) (C). There was no visible increase in fluorescent signal in the modiolus of noise exposed mouse (D) compared to control (B).

2.6 Tissue Dissection

2.6.1 *Modioli*

For RNASeq

All animals were culled by decapitation as licensed under PPL 60/4353, 19b:D1 or 19b:AR1. Immediately following decapitation, the intact brain and brainstem was rapidly removed and set aside for further dissection (see §2.6.2) and the temporal bones were extracted from the base of the skull. Work from this point was performed submerged in ice cold PBS and under stereoscopic microscope.

The tympanic bulla, identified as a semi-translucent, bony capsule (Figure 2.6B) was carefully removed to reveal the cochlea. Starting at the round or oval window, the otic capsule was carefully chipped away by applying an upwards force with a pair of closed sharp forceps. Once a sufficient portion of the otic capsule had been removed (Figure 2.6D), the spiral turns of the cochlea could be removed by pinching the spiral away from the base near the hook region. Using a pair of Dumont #5 forceps additional tissue was carefully unwound from the modiolus, leaving just the bony structure (Figure 2.6E-F).

The modiolus was then removed, transferred to 100 μ L of TRI-reagent[®] (Sigma), and snap frozen on dry ice. Samples were stored at -80°C awaiting extraction of RNA. The modioli of five mice (10 total) were pooled for each RNA extraction.

For Immunohistochemistry

Whole cochleae were extracted as previously described (§2.6.1) and processed as described in §2.8.2.

For Western Blotting

Cochleae were removed from the mouse as previously described. Immediately following removal, cochleae were placed in a round bottomed 2mL Eppendorf and frozen on dry ice. Samples were stored at -80°C until needed. Tissue was processed as described in §2.9.

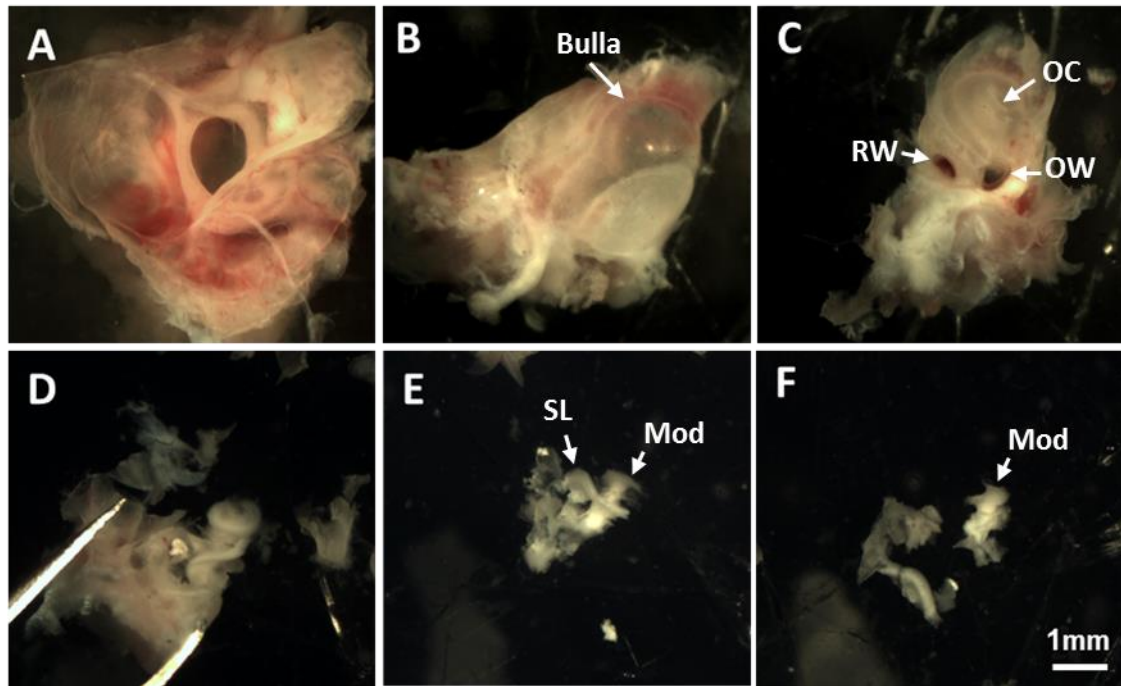


Figure 2.6: Isolation of the Modiolus. (A) Temporal bones were carefully removed from the base of the skull and transferred to ice cold PBS under stereoscopic magnification. (B) Excess tissue was trimmed to leave the semi-translucent bulla, this was carefully removed using sharp forceps. (C) Removal of the bulla reveals the cochlea. Holding the cochlea at the base, the otic capsule was chipped using sharp forceps and starting at the round (RW) or oval window (OW). (D) Once a sufficient proportion of the otic capsule (OC) was removed, the cochlear spiral was pinched off close to the hook, leaving only the modiolus (Mod) and spiral ligament (SL) (E). (F) Spiral ligament was removed leaving the bony, modiolar structure.

2.6.2 Cochlear Nuclei

For RNASeq

Brainstem was removed as previously described and immediately submerged in 500 μ L of RNAlater[®] (ThermoFisher Scientific). This was done so that both the cochlear nuclei and modiolus could be extracted from the same animal while ensuring minimal degradation of RNA. Samples were incubated in RNAlater[®] at 4°C overnight, and then stored at -80°C until further processing. Brainstem was later removed from RNAlater[®], and both cochlear nuclei were dissected under stereoscopic microscope. Cochlear nuclei were then submerged in Trizol before RNA extraction. Cochlear nuclei of three mice were pooled for each RNA extraction.

For Immunohistochemistry

Whole brain and brainstem was removed as previously described and placed into ice cold PBS. Cerebellum and brainstem were separated from cortex with a 30° incision, excess moisture was blotted away using filter paper, and the brainstem was placed into OCT embedding medium (ThermoFisher Scientific). Tissue was snap frozen on a slurry of dry ice and hexane and blocks stored at -80°C until needed.

2.6.3 Dorsal Root Ganglia

For Immunohistochemistry

Mice were culled by decapitation as previously described. The spinal column was isolated from the body by making an incision through the abdominal wall muscles and cutting the ribs parallel to the spinal column. Spine was removed from the body with a transverse cut at the level of the femurs. Vertebral bone and surrounding musculature was removed in ice cold PBS to reveal the spinal cord and dorsal root ganglia (DRG). From this point the DRG were gently teased away.

As the DRG were used only for immunohistochemistry, tissue was immediately submerged in OCT embedding medium (ThermoFisher Scientific), and snap

Experimental Methods

frozen using a slurry of dry ice and hexane. The resulting tissue blocks were kept at -80°C until required.

2.7 Transcriptomics

2.7.1 RNA Extraction

All surfaces were cleaned prior to working with 75% industrial methylated spirit and RNaseZap® (ThermoFisher Scientific) to ensure work space was clean and RNase free.

RNA extraction was achieved using a phenol extraction method, which is briefly described here. Tissue was pooled and total volume of TRI-Reagent® (Sigma) was made up to 1mL per sample. Using an IKA ULTRA-TURRAX T-8 tissue homogeniser; tissue was homogenised over ice until there were no visible pieces. At room temperature, 200µL of 1-bromo-3-chloropropane was added, shook vigorously, and left to sit for three minutes. Samples were centrifuged (12,000 RPM for 14 mins at 4°C), collecting the unwanted organic material to the bottom of the tube. The upper aqueous phase was transferred to a fresh tube and RNA was precipitated from the solution using 100% isopropanol, added at a 1:1 ratio, incubated for 10 mins at room temperature, and pelleted down by centrifugation (10,000 RPM for 15 mins at 4°C). The RNA pellet was finally washed twice with 1mL of ice cold 75% ethanol, which was discarded, and then samples were spun down and air-dried. When the pellet was dry, it was re-suspended in 20µL of nuclease-free water. Re-suspended RNA was stored at -80°C until required.

Sample purity and concentration were assessed by UV-Vis spectroscopy (Nanodrop 8000) and integrity of RNA was assessed using capillary electrophoresis (RNA Nano 6000 chip on the Agilent Bioanalyzer 2000). Only samples which had 260/280nm ratios between 1.7 - 2.0 and a RIN (RNA integrity) score >7 were selected for RNA-Seq.

2.7.2 RNA-Seq Data Collection

cDNA libraries were constructed using the NEBNext® Ultra™ Directional RNA Library Prep Kit for Illumina® sequencing and performed as per product protocol. Briefly, residual DNA was removed from the samples and mRNA was isolated from total RNA and fragmented. cDNA was then constructed using random primers and tagged with an identifying adaptor, to be used to identify samples during sequencing. Samples were then purified and then PCR enriched.

Following library construction, quality of samples was assessed using the High Sensitivity DNA chip on the Agilent Bioanalyzer 2000 to ensure samples had a narrow distribution of cDNA fragment lengths. Further purifications of samples were performed if samples had presence of a peak at 80bp (presence of primers) or 128bp (presence of adaptor-dimer). Total concentration of samples were assessed using qPCR performed by the University of Leicester Genomics service.

Samples were pooled (18 samples per run) before being sent to be sequenced at the University of Nottingham's DeepSeq facility, where sequencing was performed using Illumina's NextSeq500 High Output (v2, 150 cycles) kit and the Illumina® NextSeq500.

2.7.3 Microarray Data Collection

Three control cochlear nucleus samples were prepared for microarray for the purpose of comparison with RNA-Seq. cRNA synthesis, amplification, and hybridization to chip was performed by Dr Nicolas Sylvius of the University of Leicester Genomic Services.

Following RNA extraction (previously described, §2.7.1) cRNA was generated from total RNA using an Illumina TotalPrep RNA amplification kit (Ambion, UK). Following amplification and normalisation, samples were hybridized onto a MouseRef-8 v2.0 Expression BeadChip (Illumina) and scanned using an iScan high throughput scanner (Illumina).

2.7.4 Analysis of Results

RNA-Seq

Raw FastQ data files were generated and transferred using Illumina's cloud based service, Basespace. For each base call, a quality score (Q) is assigned, calculated as:

$$Q = -10 \log_{10} p,$$

where p is the probability of a base call error; i.e. a Q score of 30 is equivalent to a 99.9% probability of a correct base call ($p = 1 \times 10^{-3}$). Using FastQC toolkit⁶ (Babraham Bioinformatics) total reads were trimmed of low quality reads (Q<20), poly-A/T tails >10bp, and adapter sequences.

Trimmed reads were aligned to the mm10 (GRCM38⁷) mouse genome (Ensembl) and output as .BAM (binary alignment/map) files using TopHat2⁸ (Kim et al., 2013). Differential expression at each time point was calculated using Cuffdiff2 (Cufflinks⁹) (Trapnell et al., 2013) which was output as .CSV. From this a ratio (fold change) of RNA abundance (experimental/control) and a corrected significance value (FDR) was calculated for each gene. Unless otherwise stated, genes were considered to be significantly changed when FDR < 0.05 and fold change > 2 or fold change < 0.5.

Gene changes at each time point were represented using volcano plots and MA-plots. Volcano plots plot the $-\log_2(\text{FDR})$ against $\log_2(\text{fold change})$ and show the spread of changes in gene expression taking significance into account. MA-plots plot $\log_2(\text{fold change})$ against $\log_2(\text{Control FPKM})$ and show the spread of changes in the context of basal expression. Where the calculated FPKM for either control or experimental condition was 0, a value of 0 or ∞ was returned when

⁶ <http://www.bioinformatics.babraham.ac.uk/projects/fastqc/>

⁷ http://www.ensembl.org/Mus_musculus/Info/Annotation

⁸ <https://ccb.jhu.edu/software/tophat/>

⁹ <http://cole-trapnell-lab.github.io/cufflinks/>

Experimental Methods

calculating fold change; in these cases, and for the purposes of graphical representation only, $\text{Log}_2(\text{fold change})$ was set to -10 and 10 respectively. For reporting purposes “infinite” changes in gene expression were also listed separately.

Gene ontology analysis of differentially expressed genes was performed using the R package, Goseq¹⁰ (Young et al., 2010) to test for enriched pathways and terms. Goseq was chosen as the method accounts for the read bias of long transcripts. An example Goseq script has been included in Appendix 1 (Script 2.1)

Microarray

Microarray scan completed with a total background level of 115. .idat files generated by the run were loaded into Genome Studio (Illumina). Data was normalised with quantile normalisation. No background correction was applied to avoid negative values. For each sample, average signal intensity and a detection p value was exported into .txt files for further analysis. Where multiple results were generated for a single gene, these were averaged.

In Microarray data, genes are only initially identified using an Illumina Probe ID; whereas in RNA-Seq data, genes are only identified as external gene symbols which are subject to frequent change. As such, both datasets were converted to ENTREZ (NCBI)¹¹ IDs for comparison purposes. Gene lists were converted using the R library biomaRt¹² (Bioconductor), example script included in Appendix 1 (Script 2.2).

Matched data was compared using Pearson’s product-moment correlation in R, and a significance value (p) calculated. Data is considered to be correlated when $p < 0.05$.

¹⁰ <http://bioconductor.org/packages/release/bioc/html/goseq.html>

¹¹ <https://www.ncbi.nlm.nih.gov/gquery/>

¹² <https://bioconductor.org/packages/release/bioc/html/biomaRt.html>

2.8 Histological Methods

2.8.1 Solutions

All reagents were sourced from Sigma-Aldrich unless otherwise stated.

Phosphate Buffered Saline (PBS)

Stock solution of 10X concentration was made up with 1.4M NaCl, 80mM Na₂HPO₄, 15mM KH₂PO₄, 27mM KCl in distilled water. Before use, stock was diluted ten times in distilled water and pH was modified to 7.4 using 1M NaOH or 3M HCl.

Phosphate Buffered Saline–Triton (PBS-T)

For immunohistochemistry, to facilitate the permeabilization of membrane, Triton X-100 (0.1% v/v) was added to working PBS solution.

Ethylenediaminetetraacetic Acid Solution (EDTA)

EDTA solution is used for the demineralization of cochlea tissue for sectioning. 8% w/v EDTA dissolved into PBS. To facilitate this, solution was brought back to pH 7.4 using NaOH pellets. EDTA solutions were made fresh for each preparation.

4% Paraformaldehyde (PFA)

Paraformaldehyde (PFA) fixation was used to maintain morphology of tissue in immunohistochemistry protocols. To make 100mL of 4% PFA solution, 4g of PFA was added to 160mL of 0.2M Na₂HPO₄ and gently heated until dissolved. Solution was then cooled to room temperature and 40mL of 0.2M of NaH₂PO₄ and 200mL of distilled water. The PFA solution was stored at -20°C and thawed immediately before use.

30% Sucrose Solution

Sucrose solution was used to prevent ice crystal formation when freezing tissue samples. 30% w/v sucrose was added to PBS and stirred until dissolved. To prevent growth of bacteria, this solution was always made fresh immediately before use.

2.8.2 General Histology

Cochlea Processing

Cochleae were removed as described in §2.6.1 (Figure 2.6A-C). Membranes at the round and oval window were pierced using a pair of sharp forceps, and the cochlea was submerged into ice cold 4% paraformaldehyde for 30 minutes. After fixation, cochleae were briefly washed in PBS, then left to demineralise in 8% EDTA until soft (3 to 5 days at 4°C). Once soft, cochleae were briefly washed a second time in PBS and placed into a 30% sucrose solution overnight at 4°C followed by infiltration with OCT embedding medium (ThermoFisher Scientific) overnight at 4°C. Cochleae were quickly frozen in OCT on a slurry of dry ice and hexane and stored at -80°C until needed.

Sectioning

Frozen OCT embedding medium blocks containing tissue were cut to 12µm sections using a cryostat (Cryostar NX50, ThermoFisher Scientific) and melted onto Polysine™ microscope adhesion slides (ThermoFisher Scientific). Slides kept cold and stored at -20°C until required. For the cochlea, sectioning was performed at -15°C, for all other tissue types sectioning was performed at -12°C.

2.8.3 Immunohistochemistry

Indirect fluorescent immunohistochemistry allows for the cellular location and abundance of proteins to be visualized in situ. This is achieved by using a primary antibody targeted specifically against an epitope on the protein of interest. Binding of the primary antibody is then visualized through the use of a fluorescently labelled secondary antibody targeted against the host of the primary antibody.

Each primary antibody used was tested in three different fixation conditions to determine optimal protocol; these are "PFA", "PFA & Antigen retrieval", "Methanol", plus a condition where no fix is used. The preferred conditions for each antibody are outlined in Table 2.1. The full staining protocol is as follows:

Experimental Methods

(1) Slides were immediately fixed. For PFA fixation, slides were submerged in 4% PFA for 10 mins at 4°C, after which they were washed 3 x 10 mins in PBS-T. For PFA & Antigen retrieval, slides were fixed and washed as previously described, after which antigen retrieval was performed by incubating the slides in 10mM citric acid buffer (pH 6) at 80-90°C for 20 mins¹³. After cooling, slides were washed 3 x 5 mins in PBS-T. For methanol, slides were submerged into ice cold 100% methanol and incubated at -20°C for 10 minutes, after which they were washed 3 x 10 mins in PBS-T.

(2) Sections were incubated in a blocking solution of PBS-T, normal goat serum, and bovine serum albumin, in concentrations specific to each antibody (see Table 2.1), in a humidified chamber for 1 hour at room temperature.

(3) Sections were incubated in primary antibody diluted with blocking solution in a humidified chamber for 14 – 18 hours at 4°C. Dilutions for each antibody are described in Table 2.1. After incubation, slides were washed 3 x 10 mins in PBS-T.

(4) Sections were incubated in secondary antibody diluted in blocking solution (1:1000) in a humidified chamber for 2 hours at room temperature. After incubation slides were washed 3 x 20 mins in PBS-T.

(5) DAPI (ThermoFisher Scientific; D3571) was applied at 300nM and incubated at room temperature for 5 minutes. Slides were briefly washed 3 x 5 mins in PBS-T.

(6) Coverslips were mounted with Vector Hard Set Mounting Medium (Vector Laboratories, H-1400) and stored at 4°C.

Non-specific binding was identified through controls experiments where primary antibody was omitted from the incubation media. Where control peptides were

¹³ Heat mediated antigen retrieval was not used for cochlear sections, as they would frequently come away from the slide during the process. For antibodies where antigen retrieval was required, the slides were instead incubated in 1 % SDS (w/v) in PBS for 5 minutes at room temperature. This method cannot be used on brainstem sections.

Experimental Methods

available a further control condition included co-incubation of peptide with primary antibody.

Processed sections were visualized using a Leica DM 2500 microscope equipped for epifluorescence imaging and photography, with filters appropriate for Alexa Fluor 488, Alexa Fluor 546, and DAPI. Images were captured with a Retiga R6™ monochrome CCD with related QImaging software.

2.9 Western Blotting

2.9.1 Solutions

All reagents were sourced from Sigma-Aldrich unless otherwise stated.

Lysis Buffer

Lysis buffer was made up as 20mM Tris-HCL (pH 8.0), 150mM NaCl, 5mM EDTA, and 1% v/v Triton X-100 and stored at 4°C. On the day of use, the following protease inhibitors were added: 10µg/mL Leupeptin, 1µg/mL Aprotinin, 10µg/mL Antipain, and 1mM Phenylmethylsulfonyl fluoride (PMSF).

Sample Buffer

10mL of Stock concentration of 6x sample buffer was made with the following: 7mL 0.5M Tris (pH 6.8), 1g SDS, 3mL glycerol (ThermoFisher Scientific), 1.2mg bromophenol blue (Acros Organics), and 680µL β-mercaptoethanol. Solution was mixed well and stored as 0.5mL aliquots at -20°C until use.

Running Buffer

Stock 5x running buffer was made up 125mM Tris base, 1.25M glycine, and 0.005% w/v SDS, and stored at room temperature. Before use, stock was diluted 1:5.

Towbin's Buffer

Stock 10x Towbin's buffer was made as 0.25M Tris Base, and 1.92M glycine in distilled water. pH was adjusted to 8.3, and stock was stored at room temperature. For a 1L working solution, 100mL stock was added to 200mL methanol and 700mL distilled water.

Experimental Methods

Tris Buffered Saline – Tween 20 (TBS-T)

Stock 20x Tris buffered saline was made as 0.4M Tris Base and 2.7M NaCl in distilled water. pH was adjusted to 7.6, and stock was stored at room temperature. Before use, stock was diluted 1:20 in distilled water and 0.1% v/v Tween-20 (Acros Organics) was added.

Ponceau Solution

Ponceau staining solution was made as 0.5% w/v Ponceau S, and 1% v/v acetic acid in distilled water.

2.9.2 Protein Extraction

Tissue was submerged in 100 μ L 1% SDS¹⁴ (w/v in distilled water) in round bottom Eppendorfs and homogenized using an IKA ULTRA-TURRAX T-8 tissue homogenizer or by briefly sonicating. Following this, Lysis buffer was added to dilute the final concentration of SDS to 0.1%. Samples were centrifuged for 30 mins at 13,500 RPM at 4°C. After centrifugation if any remaining tissue was present at the bottom of the tube, the samples were optionally sonicated and spun a second time.

Protein concentration was determined using Bradford protein assay dye (Bio-rad, 500-0006) measured on a Jenway 7300 spectrophotometer, calibrated against increasing concentrations of bovine serum albumin. Sample protein concentration was normalised by diluting with Lysis buffer (with 0.1% SDS) and reduced using 6X sample buffer (added at a 1:5 ratio). Extracted samples were stored at -20°C until use, and were not routinely boiled before running.

2.9.3 Running of the Gel & Transfer to Membrane

SDS-Polyacrylamide gels were made, at an appropriate concentration to the molecular weight of target protein, according to protocol outlined in Sambrook (2001). Samples were loaded into the gel and ran in Running Buffer at 20mA per

¹⁴ Sodium dodecyl sulfate (SDS). For a 1mL solution of 1% SDS, 0.01g of SDS was added to 1mL of dH₂O

Experimental Methods

gel for 20 mins and 40mA per gel until the Sample Buffer had run off the end of the gel.

Proteins were transferred to nitrocellulose membranes in Towbin's buffer at 350mA for 90 mins. Protein transfer was validated by briefly staining with Ponceau solution and washed in distilled water until clear.

2.9.4 Antibody Staining & Imaging

Membranes were cut to allow simultaneous staining for protein of interest and appropriate loading control (α -actin or β -tubulin). Non-specific binding was blocked with 5% w/v Instant Dried Skimmed low fat Milk (Co-operative), diluted in TBS-T for 1 hour at room temperature. After blocking, membranes were washed 3 x 10 mins in TBS-T and primary antibody was applied at a concentration of 1:1000 in blocking solution. Membranes were incubated in primary antibody 14 – 18 hours at 4°C then washed 3 x 10 mins in TBS-T. Horseradish peroxidase (HRP) secondary antibody was applied at a concentration of 1:1000 in blocking solution, and incubated for 2 hours at room temperature. After incubation membranes were washed a further 3 x 10 mins. HRP signal was developed using BioRad clarity western electrochemiluminescence (ECL) substrate (SuperSignal™ West Pico, ThermoFisher) and photographed using a Fujifilm LAS4000 luminescence imager with associated image reader and MultiGauge software (v2.2). Antibodies used are detailed in Table 2.2.

2.9.5 Analysis

Western blot images were saved as .tiff files, and analysed using FIJI imaging software. Protein expression in each lane was normalised to the expression levels of the loading control used to give fluorescent intensity in arbitrary units (A.U.).

Experimental Methods

Table 2.1: Primary and Secondary Antibodies used for Immunohistochemistry.

Primary Antibody							
Antibody	Host	Fix	Antigen Retrieval?	Block (%v/v)	Dilution	Supplier	Product Code
IBA-1	Rabbit	PFA	Preferred	2% Goat 1% BSA	1:1000	Wako	019-19741
Fibrinogen	Rabbit	PFA	No	10% Goat 1% BSA	1:1000	Abcam	Ab34269
P2x ₃	Rabbit	PFA	No	10% Goat 1% BSA	1:1000	Antibodies Inc	61-454
Kv3.1b	Rabbit	PFA	Preferred	10% Goat 1% BSA	1:1000	Alomone	APC-014
Kv3.2	Rabbit	PFA	No	10% Goat 1% BSA	1:200	Alomone	APC-011
Kv3.3	Mouse	PFA	Required	10% Goat 1% BSA	1:3000	NeuroMab	75-354
Kv3.3	Rabbit	PFA	Required	10% Goat 1% BSA	1:1000	Alomone	APC-102
Kv3.4	Rabbit	PFA	No	10% Goat 1% BSA	1:200	Alomone	APC-019
Aquaporin1	Rabbit	PFA	Required	10% Goat 1% BSA	1:1000	Alomone	AQP-001
Secondary Antibody							
Antibody					Dilution	Product Code	
Thermo Fisher - Alexa Fluor 488 Goat Anti-Rabbit					1:1000	A-11008	
Thermo Fisher - Alexa Fluor 488 Goat Anti-Mouse					1:1000	A-11001	
Thermo Fisher - Alexa Fluor 546 Goat Anti-Rabbit					1:1000	A-11010	
Thermo Fisher - Alexa Fluor 546 Goat Anti-Mouse					1:1000	A-11003	

Table 2.2: Primary and Secondary Antibodies used for Western Blots.

Primary Antibody					
Antibody	Host	Block (%v/v)	Dilution	Supplier	Product Code
Fibrinogen	Rabbit	5% Milk	1:1000	Abcam	Ab34269
P2x ₃	Rabbit	5% Milk	1:1000	Antibodies Inc	61-454
Kv3.1b	Rabbit	5% Milk	1:1000	Alomone	APC-014
Kv3.3	Mouse	5% Milk	1:1000	NeuroMab	75-354
Secondary Antibody					
Antibody				Dilution	Product Code
GE Healthcare - ECL Anti-Rabbit IgG HRP (raised in donkey)				1:1000	NA934V
GE Healthcare - ECL Anti-Mouse IgG HRP (raised in sheep)				1:1000	NA931V

Chapter 3: Noise Exposure and the Characterisation of Hearing in the Mouse

3.1 Introduction

A large amount of variety exists in the models of noise induced hearing loss found across published literature. Differences in species, age, anaesthesia, duration, intensity, and bandwidth of noise all have the potential to alter the severity of damage caused to the auditory system. As this study was focused on the downstream effects excitotoxicity in the cochlea, it was important that the damage to hearing fell within a moderate range of damage - where a significant impact to hearing threshold could be observed, but where there is no loss of physical integrity to cochlear structures.

Broad studies into damage to the mouse (CBA/Ca) cochleae were conducted by Wang et al. (2002) and found that two hours of octave band noise between 106 – 112 dB SPL caused widespread terminal swelling, indicative of glutamate excitotoxicity (Pujol et al., 1993), whilst avoiding rupture of the reticular lamina and swelling of SGNs and stria vascularis. Unlike the study by Wang et al. (2002), the noise exposure model used here required the mice to be anaesthetised. As a variety of different anaesthetics have been shown to have protective effects in AOE (Chung et al., 2007, Norman et al., 2012, Wen et al., 2017), this makes it difficult judge an appropriate level of noise to use. It was decided that a comparable level of noise (110dB SPL) would be used. However, as we would be delivering a broadband tone, predicted to damage a greater proportion of the cochlea, this would be delivered over a shorter time period (1.5 hours).

Using ABR measurements, the first part of this chapter will describe normal hearing in the CBA/Ca mice used for these experiments using a measure of auditory threshold, and waveform amplitude and latency. Following on from this,

Noise Exposure and the Characterisation of Hearing in the Mouse

the second part of this chapter will demonstrate that the noise exposure model used here is characteristic of excitotoxicity in the cochlea.

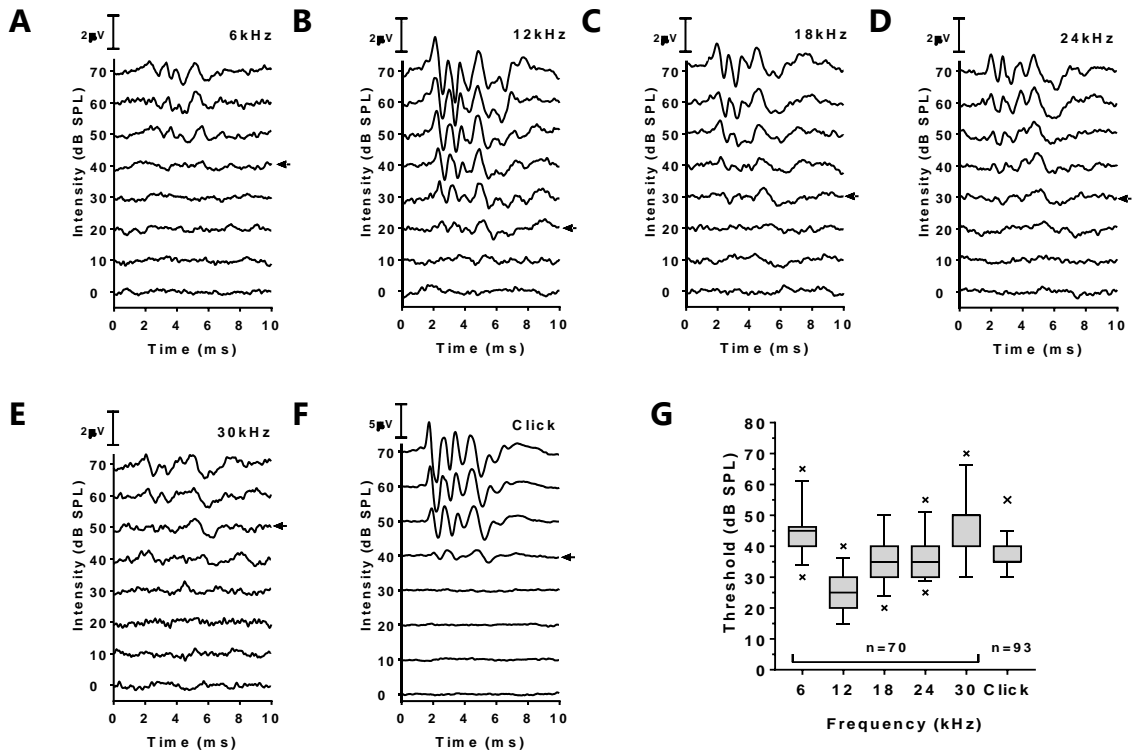
3.2 Results: ABR Measurements of the Unexposed Mouse

3.2.1 Auditory Brainstem Response in CBA/Ca Mice at 5 -7 Weeks of Age

Thresholds

Auditory brainstem response (ABR) recordings were used to determine “normal” hearing at 5 – 7 weeks of age prior to noise exposure or sham. This resulted in 93 recordings of Click ABR, of which 70 also had tone pip stimulus recordings at 6, 12, 18, 24, 30 kHz. Representative ABR traces for each frequency are shown in Figure 3.1A-F. Thresholds were defined as the lowest stimulus intensity at which any part of the ABR waveform can be distinguished above noise, which in most cases was waves I, II, or IV as waves II and V were usually the first to diminish. At this time point, thresholds ($\mu \pm SD$, rounded to the nearest integer) were determined to be 46 ± 6 dB SPL at 6 kHz, 25 ± 6 dB SPL at 12 kHz, 33 ± 6 dB SPL at 18 kHz, 37 ± 7 dB SPL at 24 kHz, 48 ± 9 dB SPL at 30 kHz, and 37 ± 4 dB SPL with Click (Figure 3.1).

Noise Exposure and the Characterisation of Hearing in the Mouse



H Threshold (dB SPL)

Frequency	Mean	S.D.	Minimum	Median	Maximum	N
6 kHz	46	6	30	45	65	70
12 kHz	25	6	15	25	40	70
18 kHz	33	6	20	35	50	70
24 kHz	38	7	25	30	55	70
30 kHz	48	9	30	50	70	70
Click	37	4	30	35	55	93

Figure 3.1: Example auditory brainstem response (ABR) traces for each frequency tested. ABRs were measured at 6 kHz (A), 12 kHz (B), 18 kHz (C), 24 kHz (D), 30 kHz (E), and Click (F) and threshold was defined as the lowest stimulus intensity at which any part of the ABR waveform can be distinguished above noise. The thresholds of mice tested at 5 – 7 weeks of age have been outlined (H) and summarised using a box and whisker plots (G) where centre indicates median value and grey box spans the interquartile range; whiskers extend from the 2.5th percentile to the 97.5th percentile (outliers are indicated as x). For the “click” ABR, n = 93, for tone pip ABRs (6, 12, 18, 24, 30 kHz) n = 70.

Waveform

In addition to thresholds, the amplitude and latency of each peak of the Click ABR was analysed using the 93 recordings at 5 - 7 weeks. From these, average and 95% confidence interval were plotted against intensity normalised to threshold (i.e. 10 dB SPL suprathreshold corresponds to 50 dB SPL where threshold is 40 dB SPL), for waves I, III, and IV (see Figure 3.2). Wave V was omitted due to its relative size, and wave II was omitted as this wave occasionally “splits” in the open-field ABR recordings, appearing as two close peaks.

Trends for amplitude and threshold appeared to follow an exponential asymptotic curve, however, within the intensities measured, a quadratic line of best fit was preferred when compared with an extra sum-of-squares F test (Figure 3.2). With the exception of Wave III amplitude, saturation of signal can be observed, on average, at approximately 40 dB SPL suprathreshold where a plateau in amplitude and latency can be observed. Equations for the line of best fit equations have been provided in Appendix 3.

Wave I has the largest increase of amplitude with relation to intensity, with values of $6.97 \pm 0.27 \mu\text{V}$ at 50 dB SPL (suprathreshold), while III and IV have values of $5.30 \pm 0.17 \mu\text{V}$ and $3.93 \pm 0.16 \mu\text{V}$ respectively. In Figure 3.2E, amplitude of wave IV appear to decrease at high intensity stimulus; however this is due to the proximity of wave V which interferes with the absolute amplitude of IV. Across, all individual waveforms measured at any intensity: wave I was present at between 1.55 – 2.37 ms after stimulus; wave III was present between 2.84 – 3.84 ms after stimulus; and wave IV was present between 3.75 – 4.94 ms after stimulus.

Noise Exposure and the Characterisation of Hearing in the Mouse

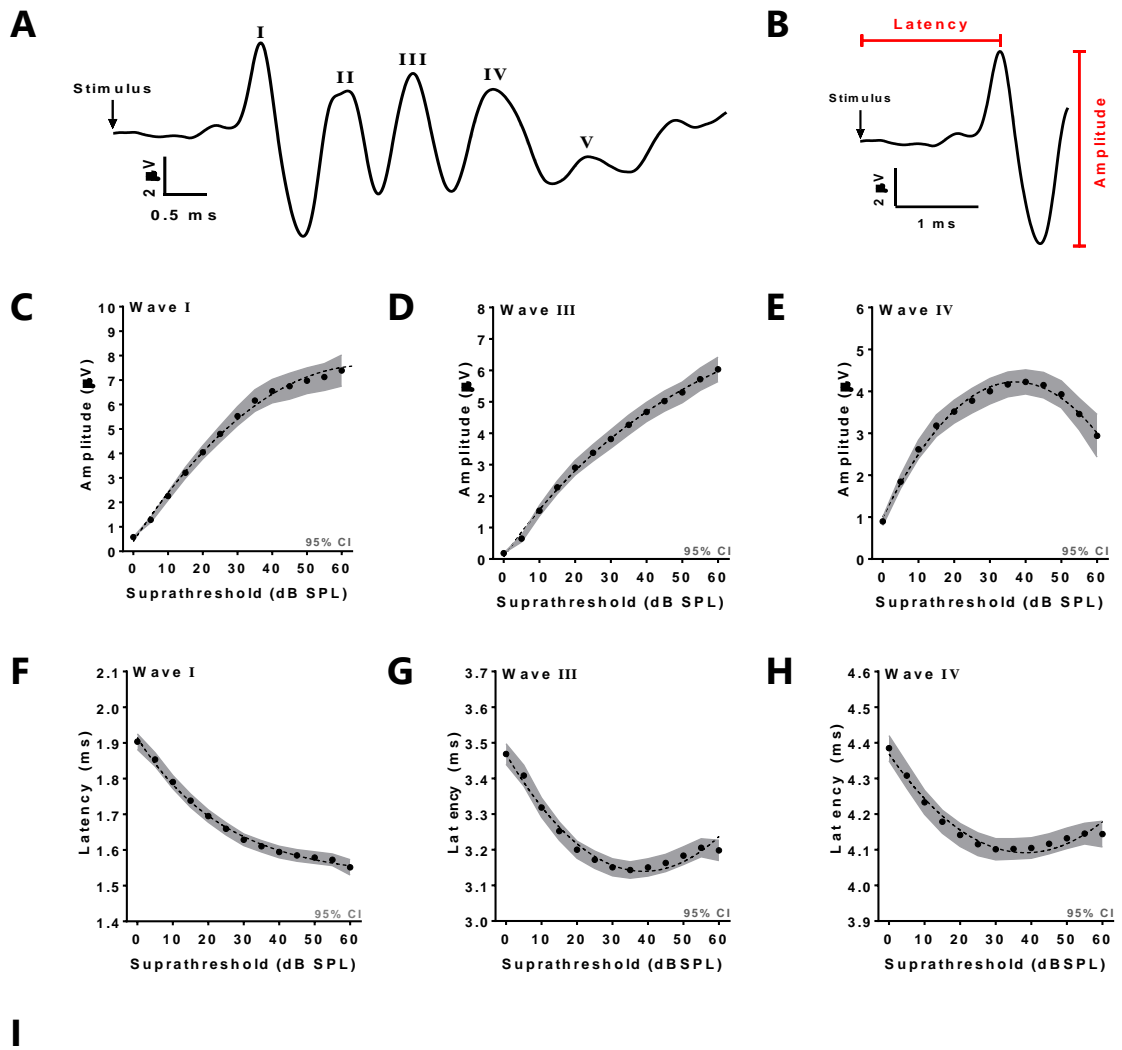


Figure 3.2: Amplitude and latency of waves I, III, and VI as a function of suprathreshold stimulus intensity. The mouse ABR waveform consists of at least five distinct peaks, denoted wave I – wave V (A). The absolute amplitude and latency (defined in B) was plotted against the intensity, normalised to threshold (suprathreshold), for waves I (C,F), III (D,G), and IV (E,H). Black points and line indicate mean values for each intensity, while grey boundaries indicate the 95% confidence interval. N = 93.

3.2.2 Small Changes to Threshold Occur Between 5 – 13 Weeks of Age

Control recordings taken at 5 - 7 weeks ($n = 70$)¹⁵, were compared with control recordings mice at 10 ($n = 5$) and 13 ($n = 10$) weeks old. Threshold for each frequency was plotted against the exact age of recording in order to assess whether any changes to normal hearing occurred over this eight-week period. Linear regression analysis was performed, and extra sum-of-squares F test was used to test if the slope of line of best fit was statistically distinguishable from zero. At 12 and 18 kHz, linear regression returned a negative non-zero gradient (m) for line of best fit ($m = -0.11 \pm 0.03$, $p = 0.005$ and $m = 0.07 \pm 0.03$, $p = 0.0128$ respectively). This corresponds to a small theoretical change of 6.3 ± 4.4 dB SPL at 12 kHz and 4.3 ± 3.5 dB SPL at 18 kHz. This change was also reflected in experiments using click stimuli (Figure 3.3).

Despite this trend, when re-testing sham exposed mice over the same time period, there is no significant difference in frequency thresholds between the first and second ABR, shown in Figure 3.4B. This could be due to the fact that the ABR recordings were made in coarse 5dB SPL increments. In the sham condition, a slight decrease, i.e. improvement, ($p = 0.0006$, after correction for multiple comparisons) in threshold at 30 kHz is seen when the ABRs are taken within a 24 - 48 hour period (Figure 3.4A) which is most likely due to desensitisation to the anaesthetic or residual effects of the reversal.

¹⁵ A proportion of the mice tested only had "click" ABRs taken. Only mice which had the full assay of "click", 6, 12, 18, 24, and 30 kHz evoked ABRs have been used for this analysis.

Noise Exposure and the Characterisation of Hearing in the Mouse

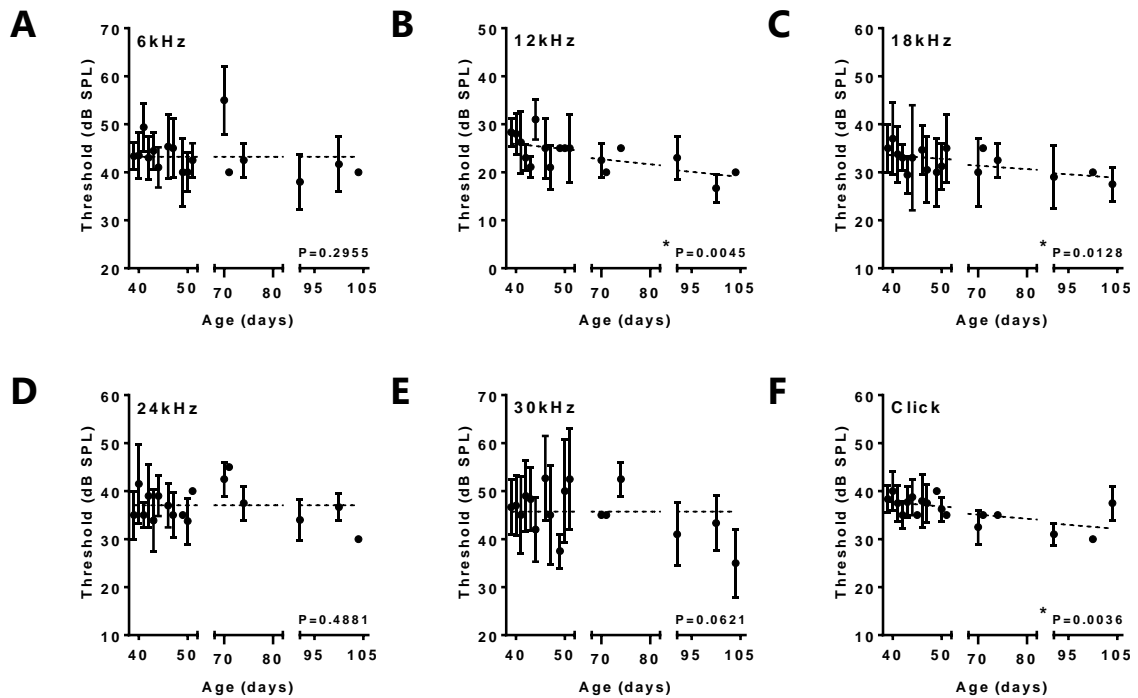


Figure 3.3: CBA/Ca hearing between 5 – 13 weeks. Hearing thresholds ($\mu \pm$ SE) recorded at 6 kHz (A), 12 kHz (B), 18 kHz (C), 24 kHz (D), 30 kHz (E), and Click (F) were plotted against time. Using a linear regression model, an extra sum-of-squares F test was used to determine if gradient of fit was significantly distinguishable from zero. At the most sensitive frequency regions (12 and 18 kHz) and with click, the gradient of the line was significantly less than zero, suggesting small improvements in threshold over this time period.

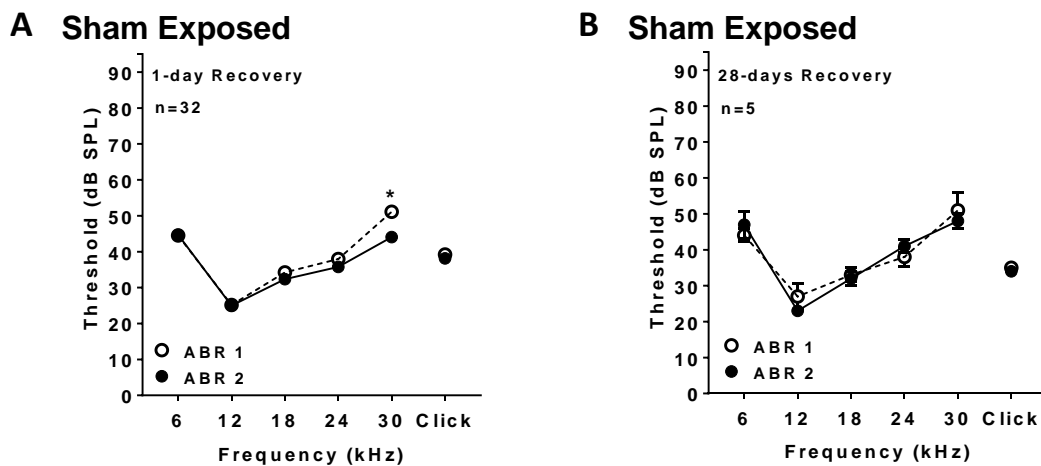


Figure 3.4: Comparison of ABR thresholds before and after sham exposure. Sham exposed mice were recovered for 1 day (A) or 28 days (B) and retested. No significant difference was found when tested with a 2-tailed paired students T-test, except at 30 kHz, on day 1 which had a small decrease of 7 ± 2 dB SPL. For 1 day recovery, $n = 32$. For 28 day recovery, $n = 5$.

3.3 Results: ABR Measurements of the Noise Exposed Mouse

CBA/Ca mice, aged 5 – 7 weeks old were anaesthetised as previously described (§2.3) and divided into two groups. One group was exposed to 110 dB SPL broadband noise for 1.5 hours (described §2.5) and will be referred to as the auditory over exposure (AOE) group. The second group was similarly exposed to silence for 1.5 hours and will be referred to as the sham group. Mice were allowed to recover for 1, 7, or 28 days following noise. ABR recordings taken immediately before exposure and after the allowed recovery period were compared to assess initial damage, and subsequent recovery of the auditory system following this noise exposure model. Here, results will be described for each recovery time individually.

3.3.1 ABR One Day after Noise Exposure

Threshold

Mice re-tested one day ($n = 25$) following auditory over exposure (AOE) showed a substantial increase in auditory threshold (compared to pre-exposure ABR). Threshold elevations were: 22 ± 3 dB SPL at 6 kHz; 31 ± 3 dB SPL at 12 kHz; 39 ± 3 dB SPL at 18 kHz; and 44 ± 3 dB SPL at both 24 and 30 kHz. Threshold in response to click was elevated 36 ± 3 dB SPL (Figure 3.5A). Comparisons between pre-exposure and post-exposure ABRs were performed using one-tailed paired T-tests, and returned values of $p \ll 0.001$ after correction for multiple comparisons.

Four of the 25 AOE mice showed no response to a 30 kHz stimulus over the tested intensities (0-95 dB SPL); in these cases, a theoretical value of 100 dB SPL was assigned. Matched sham mice ($n = 32$) showed no difference in thresholds at 1 day, with the exception of 30 kHz ($p = 0.0006$, after correction for multiple comparisons). This was previously discussed (§3.2.2).

AOE threshold elevations were compared to threshold elevations in matched sham mice using a one-tailed unpaired T-test with a Holm-Sidak¹⁶ correction for multiple comparisons. In AOE, thresholds were significantly ($p \ll 0.001$) increased (Figure 3.5B).

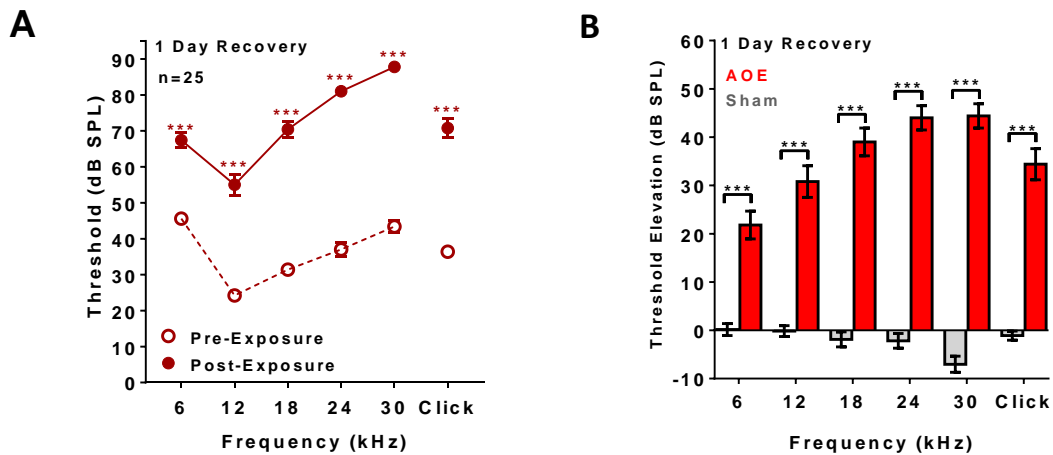


Figure 3.5: Significant shifts in ABR thresholds are seen in the auditory over exposed (AOE) mice at one day following noise exposure. (A) Thresholds measured in the AOE group (ABR 2) were compared to pre-exposure ABRs (ABR 1) using one-tailed paired T-test. At all frequencies, thresholds were significantly increased ($p < 0.001$) by up to 44 ± 3 dB SPL. **(B)** These threshold elevations were compared to differences observed in the matched sham exposed group using a one-tailed, unpaired T-test. At all frequencies these were also considered to be significant to $p < 0.001$. All T-tests were corrected using a Holm-Sidak correction for multiple comparisons. $N = 25$.

Waveform

Post-exposure ABR waveforms of the AOE mice with a suprathreshold response ($n = 21$) were compared to Click ABRs taken from sham mice at the same time-point ($n = 32$). Suprathreshold absolute amplitude and latency were calculated as previously described (§3.2.1), and are summarised in Figure 3.6. Intensities which did not have at least three repeat suprathreshold recordings were excluded. The trends for average amplitude and latency against intensity were compared with a

¹⁶ The Holm-Sidak correction was chosen throughout, unless otherwise noted, to control for multiple comparisons made between the two groups (control vs. AOE). This correction was chosen on the basis that it is more powerful than the Bonferroni or Tukey methods (Seaman et al., 1991), and therefore less likely to produce type II statistical errors (false positives).

two-way ANOVA which will be referred to as significance values for trend. Further comparisons were made for each intensity using unpaired T-tests, with a Holm-Sidak correction for multiple comparisons, which will be stated when referring to changes in amplitude or latency.

For latency, only small changes were seen to the suprathreshold trend in wave I ($p < 0.001$), and no change was observed in waves III ($p = 0.281$) or IV ($p = 0.557$), see Figure 3.6C. However, for amplitude, suprathreshold trends were significantly different across waves I, III, and IV ($p < 0.001$). In addition the trend seen in the amplitude of the AOE ABR is more linear with no evidence of “saturation” like that is seen in the sham exposed mice Figure 3.6B. This is particularly evident between 10 – 30 dB SPL suprathreshold where the largest changes are seen.

At 20 dB SPL suprathreshold (Figure 3.8A), wave I amplitude of the AOE mice decreased $3.20 \pm 0.46 \mu\text{V}$ ($p < 0.001$), a change of ~35% from sham amplitude. At the same intensity wave I latency was increased by $0.123 \pm 0.035 \text{ ms}$ ($p = 0.003$). Similarly, amplitudes of wave III and wave IV were reduced, $1.34 \pm 0.24 \mu\text{V}$ and $1.50 \pm 0.38 \mu\text{V}$ respectively ($p < 0.001$ for both), without a change in latency (see Figure 3.6).

It should be noted that the ABR amplitude of wave I in the sham exposed mice was significantly higher than when tested on day one, which fell within the 95% confidence interval shown in Figure 3.2C. This increase in amplitude is, again, likely due to desensitisation to the anaesthetic, residual effects of the reversal, or other unidentified outcomes of the long term anaesthetic regime presented the day before. This increase in amplitude is only seen in the sham mice on the first day and is not present in either wave III or wave IV.

Noise Exposure and the Characterisation of Hearing in the Mouse

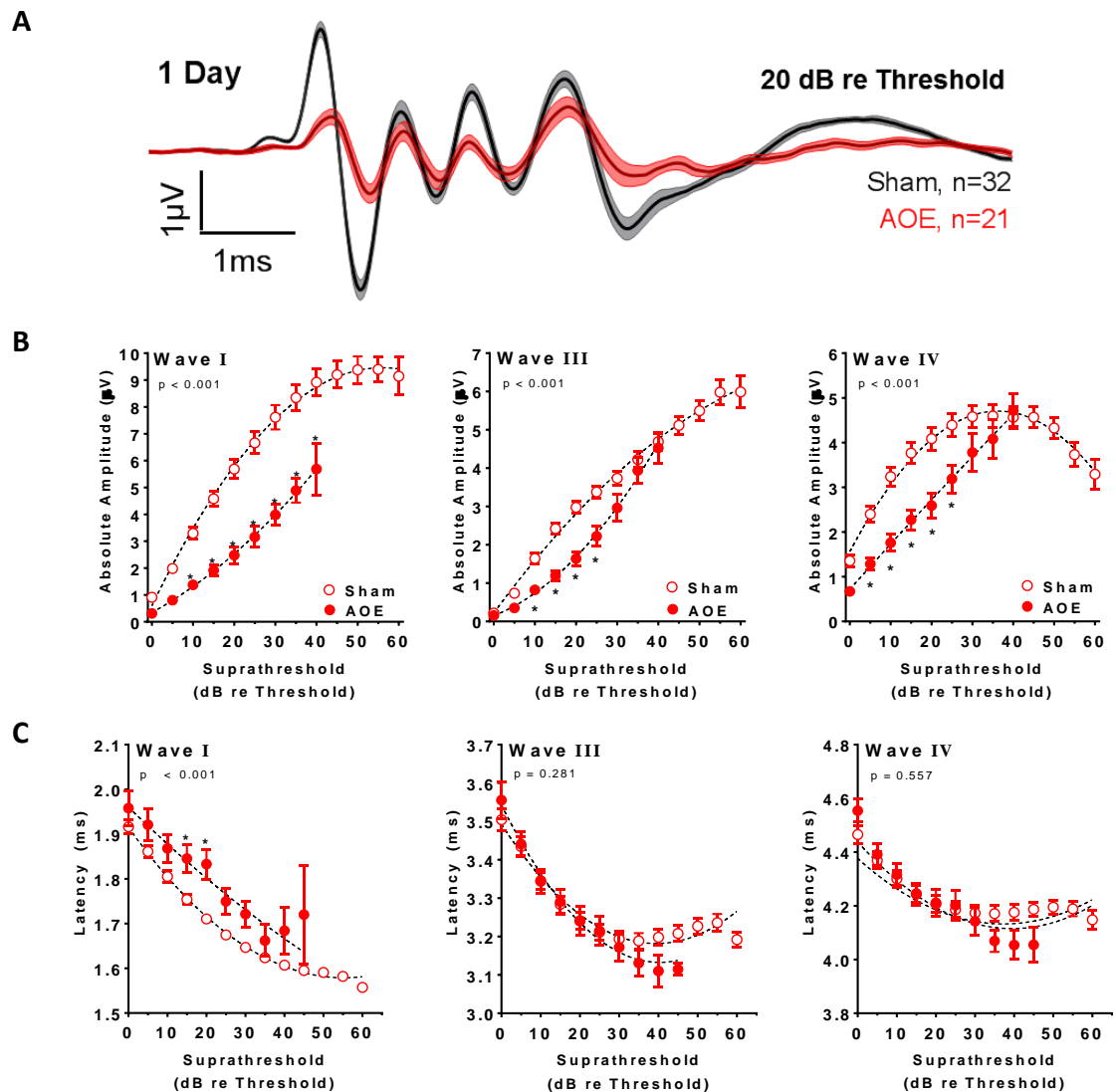


Figure 3.6: Click ABR waveform properties of AOE and Sham mice at one day following exposure. In addition to threshold, the absolute amplitude (B) and latency (C), normalised to threshold (suprathreshold), was recorded for the AOE and sham exposed mice. Amplitude was depressed across the whole waveform (A,B), and a small shift in latency could be observed at wave I only (A,C). Amplitudes and latencies were compared with a two-way ANOVA (significance displayed on plot) with multiple comparisons (Holm-Sidak correction, shown as *, where $p < 0.05$). Significant suprathreshold intensities are denoted with an asterix (*: $p < 0.05$). For sham mice, $n = 32$, for AOE mice, $n = 21$.

3.3.2 ABR Seven Days after Noise Exposure

Threshold

Mice re-tested at seven days (n = 22) following AOE had significantly ($p < 0.001$) increased threshold across all tested frequencies when compared to the pre-exposure ABR (Figure 3.7) using a one-tailed paired T-test (Holm-Sidak correction). Threshold elevations were: 8 ± 2 dB SPL at 6 kHz; 18 ± 3 dB SPL at 12 kHz; 18 ± 3 dB SPL at 18 kHz; and 28 ± 4 dB SPL at both 24 and 30 kHz. Threshold in response to click was elevated 17 ± 2 dB SPL.

Due to time constraints, individual frequency ABR recordings were not taken for the matched sham mice (n = 4). For Click, there was no change in threshold in the control condition over the seven days between testing, when using a two-tailed, paired T-test ($p = 0.235$).

At seven days following exposure, threshold elevation of AOE mice were significantly elevated in Click compared to sham exposed mice (Figure 3.7), but significantly reduced ($p < 0.01$) across all frequencies when compared to elevations seen at day one (Figure 3.11).

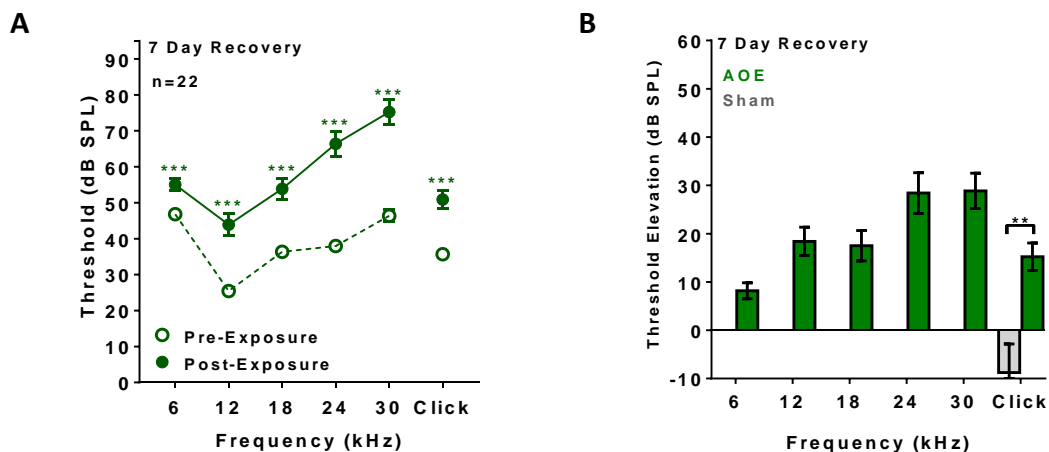


Figure 3.7: An increase in ABR thresholds are seen in the auditory over exposed (AOE) mice at seven days following noise exposure. (A) Thresholds measured in the AOE group post-noise (ABR 2) were compared to pre-exposure ABRs (ABR 1) using one-tailed paired T-tests. At all frequencies, thresholds were significantly increased ($p < 0.001$) by up to 28 ± 4 dB SPL. **(B)** Due to time constraints, matched sham mice only had Click ABR recordings taken. Threshold elevations of AOE were compared to sham using a one-tailed, unpaired T-test showed a significant difference in Click ($p = 0.03$). All T-tests were corrected using a Holm-Sidak correction for multiple comparisons. N = 22.

Waveform

Post-exposure ABR waveforms of the AOE mice (n = 22) were compared to Click ABRs taken from sham mice at the same time-point (n = 4). Suprathreshold absolute amplitude and latency were calculated as previously described (§3.2.1), and are summarised in Figure 3.8. Intensities which did not have at least three repeat suprathreshold recordings were excluded from comparison. The trends for average amplitude and latency against intensity were compared with a two-way ANOVA which will be referred to as significance values for trend. Further comparisons were made for each intensity using unpaired T-tests, with a Holm-Sidak correction for multiple comparisons, which will be stated when referring to changes in amplitude or latency.

As with day one, the trend in latency is significantly slower in wave I ($p = 0.001$); however changes to trends are also seen in wave III ($p < 0.001$) and wave IV ($p < 0.001$), although no individual intensity is significant after correction for multiple comparisons (Figure 3.8C). Similarly, trend in amplitude is significantly changed ($p < 0.001$) in the AOE group, and with the exception of wave IV, trends appear linear, as with day one, with no evidence of "saturation".

Comparison between AOE and sham at 20 dB SPL suprathreshold showed a significant decrease in absolute amplitude in waves I and III, $2.18 \pm 0.70 \mu\text{V}$ ($p = 0.001$) and $3.36 \pm 0.36 \mu\text{V}$ ($p < 0.001$) respectively (Figure 3.8A-B). Wave IV was not significantly decreased at any intensity when corrected for multiple comparisons (Figure 3.8B), although this may be due to lower number of repeats in the sham condition, as the wave appears to be depressed when compared at 20 dB SPL suprathreshold (Figure 3.8A).

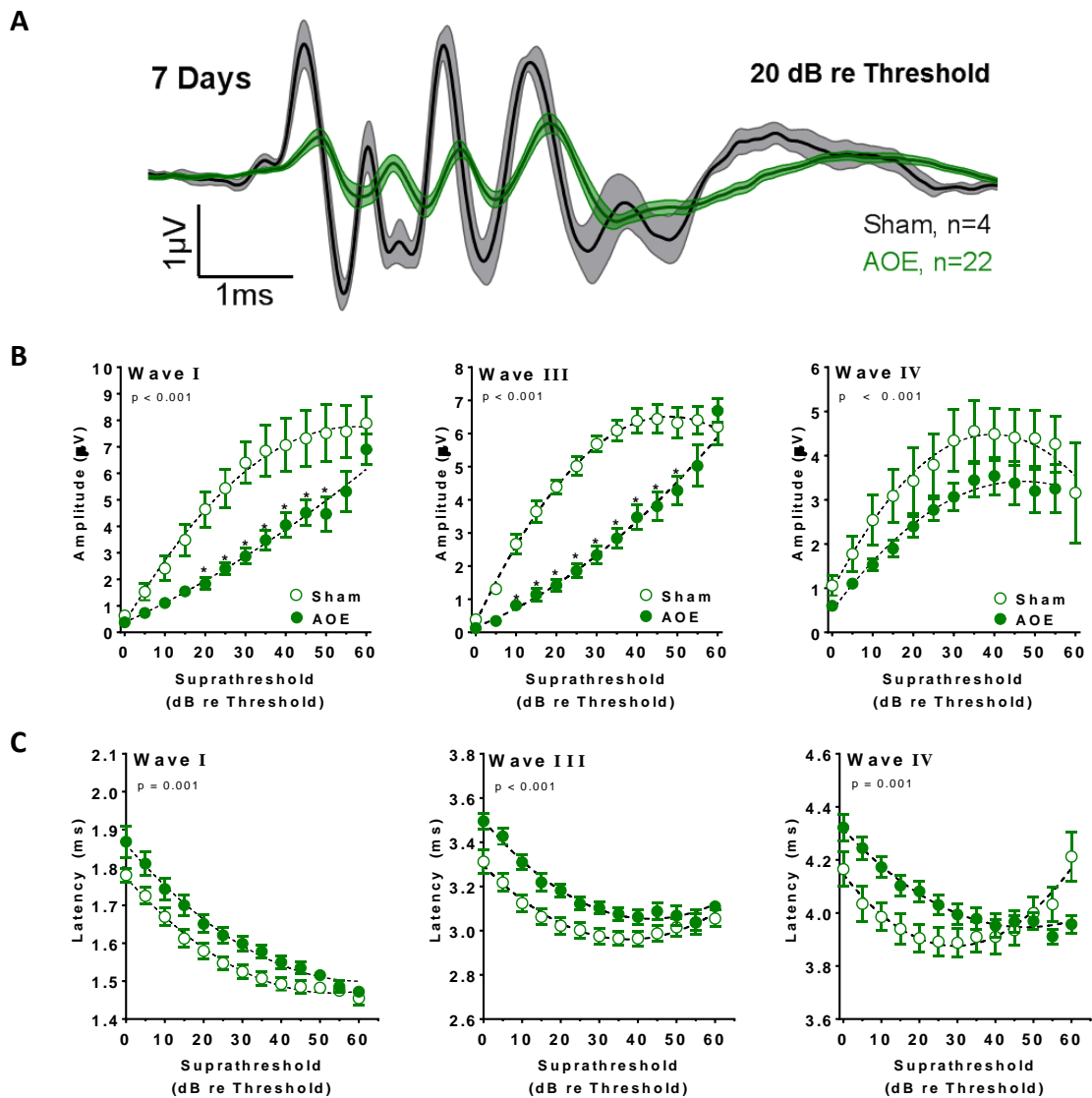


Figure 3.8: Click ABR waveform properties of AOE and Sham mice at seven days following exposure. In addition to threshold, the absolute amplitude (B) and latency (C), normalised to threshold (suprathreshold), was recorded for the AOE and sham exposed mice. Amplitudes are depressed across the ABR waveform (A,B) and follow a more linear trend although some recovery in trend can be seen in wave IV. The shift in latency in wave I is also reflected downstream, with significant changes to wave III and IV trends, although no single intensity is significant (A,C). Amplitudes and latencies were compared with a two-way ANOVA (significance displayed on plot) with multiple comparisons (Holm-Sidak correction, shown as *, where $p < 0.05$). Significant suprathreshold intensities are denoted with an asterisk (*: $p < 0.05$). For Sham mice, $n = 4$, for AOE mice $n = 22$.

3.3.3 ABR 28 Days after Noise Exposure

Threshold

Mice re-tested 28 days (n = 17) following AOE had significantly increased thresholds at 12 kHz (p = 0.015), 18 kHz (p = 0.009), 24 kHz (p < 0.001), and 30 kHz (p < 0.001), but not at 6 kHz (p = 0.460), when compared to the pre-exposure ABR (Figure 3.9A). This elevation was also reflected in the Click ABR (p = 0.011). The threshold elevations at day 28 were: 11 ± 3 dB SPL at 12 kHz; 13 ± 4 dB SPL at 18 kHz; 26 ± 4 dB SPL at 24 kHz; and 30 ± 4 dB SPL at 30 kHz. Threshold in response to click was elevated 11 ± 3 dB SPL.

When compared to age and condition matched sham mice (n = 5), the threshold elevations of AOE mice were only significant at 24 (p = 0.045) and 30 kHz (p < 0.001); however results for 12 kHz, 18 kHz, and Click would likely become significant with more sham repeats (Figure 3.9B). There was no significant change in the ABR threshold of sham mice over the 28 day period (Figure 3.4).

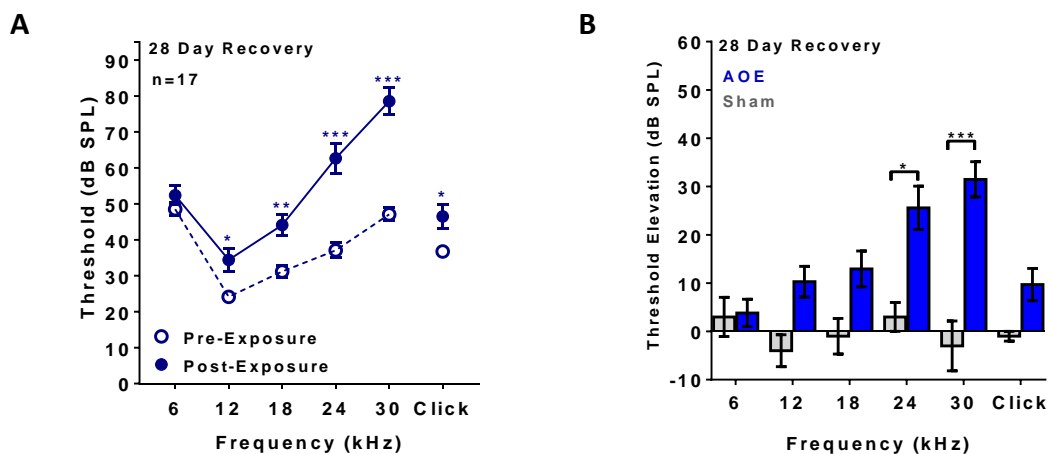


Figure 3.9: An increase in high frequency thresholds is seen in the auditory over exposed (AOE) mice 28 days following noise exposure. (A) Thresholds measured in the AOR group post-noise (ABR2) were compared to pre-exposure ABRs (ABR 1) using one-tailed paired T-tests. Thresholds were significantly increase at 12, 18, 24, 30 kHz and Click. **(B)** Threshold elevations in AOE mice were compared to sham using a one-tailed unpaired T-test, and showed significantly elevated thresholds at 24 and 30 kHz as a result of noise exposure. All T-tests were corrected using a Holm-Sidak correction for multiple comparisons. N = 17.

Threshold elevations do not significantly reduce between seven and 28 days, although downwards trends are seen in 6 kHz, 12 kHz, 18 kHz, and Click (Figure 3.11).

Waveform

Post-exposure ABR waveforms of AOE mice ($n = 17$) were compared to Click ABRs taken from sham mice at the same time-point ($n = 5$). Suprathreshold absolute amplitude and latency were calculated as previously described (§3.2.1), and are summarised in Figure 3.10. Intensities which did not have at least three repeat suprathreshold recordings were excluded from comparison. The trends for average amplitude and latency against intensity were compared with a two-way ANOVA which will be referred to as significance values for trend.

As with day seven, the suprathreshold trend in latency is significantly altered in wave I ($p < 0.001$), and wave III ($p = 0.001$), but not at wave IV ($p=0.06$). At 20 dB SPL suprathreshold, this corresponds to a latency increase of 0.123 ± 0.030 ms for wave I, and an increase of 0.071 ± 0.042 ms for wave III (Figure 3.10C).

Trends in suprathreshold amplitude are also changed for wave I ($p < 0.001$) and wave III ($p < 0.001$), but the trend is unchanged for wave VI; these changes are only significantly different beyond 20 dB SPL suprathreshold (Figure 3.10A-B). Although the trend in wave III remains linear, and despite the high intensity depression, wave I follows a similar saturating amplitude increase at suprathresholds to the sham exposed controls.

Noise Exposure and the Characterisation of Hearing in the Mouse

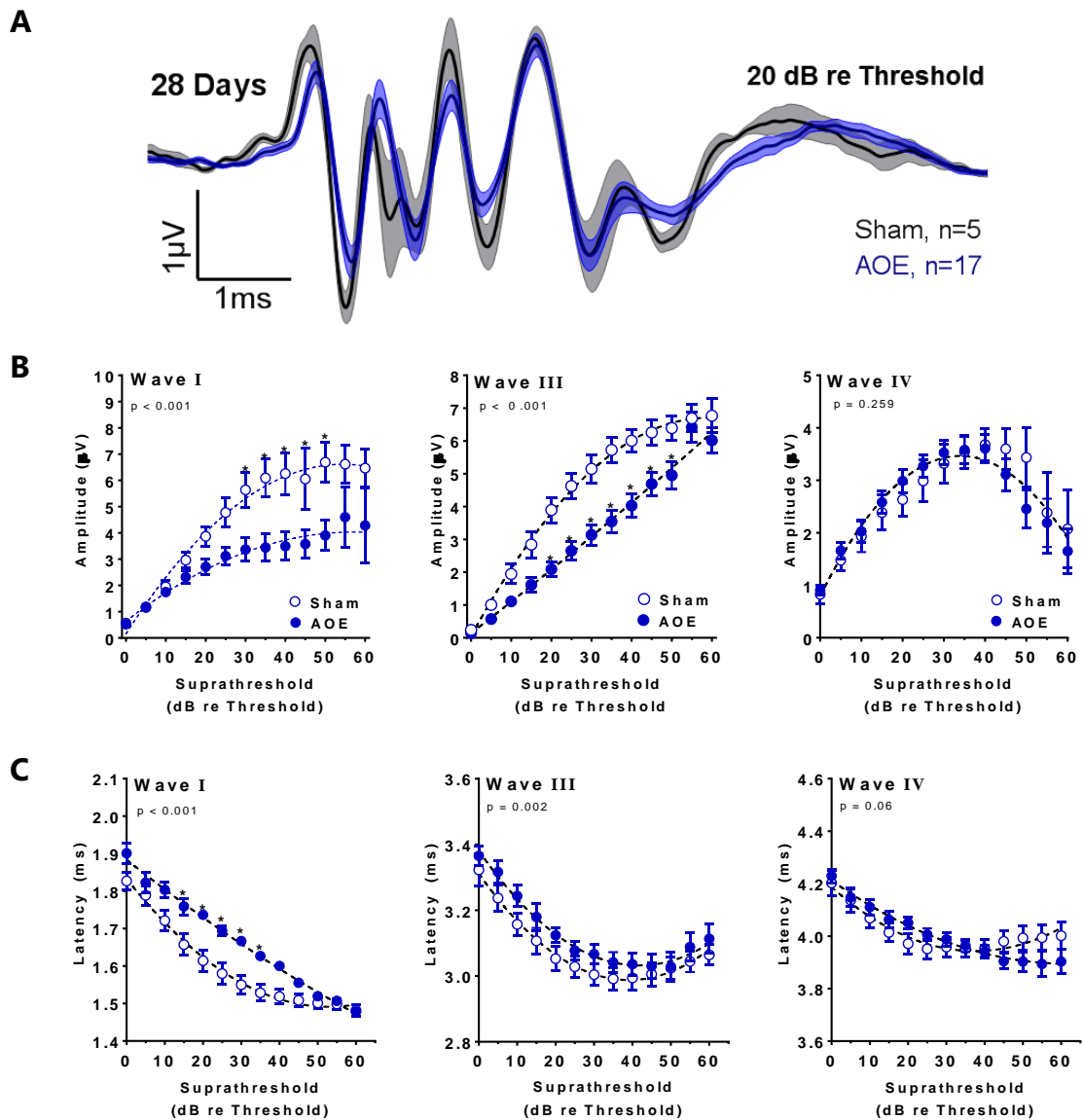


Figure 3.10: Click ABR waveform properties of AOE and Sham mice at 28 days following exposure. In addition to threshold, the absolute amplitude (**B**) and latency (**C**), normalised to threshold (suprathreshold), was recorded for the AOE and sham exposed mice. Amplitudes are depressed at high intensities for wave I and wave III, but not wave IV (**A,B**). Changes to latency can be seen in wave I and wave III, but are more pronounced for wave I (**C**). Amplitudes and latencies were compared with a two-way ANOVA (significance displayed on plot) with multiple comparisons (Holm-Sidak correction, shown as *, where $p < 0.05$). Significant suprathreshold intensities are denoted with an asterisk (*: $p < 0.05$). For Sham mice, $n = 5$. For AOE mice $n = 17$.

3.4 Discussion

The main purpose of analysis of control hearing was to assess the initial hearing capability and ABR waveform so that it can be fairly compared to control. It was also critical to assess whether “normal” hearing changes over the experimental time course. While the ABR response of the CBA/Ca was found to improve at 12 and 18 kHz between recordings at 5 and 13 weeks of age, this change was minimal, at less than one increment (5 dB SPL) of intensity.

In the noise exposed animal, hearing damage was assessed using measurements of hearing threshold and through assessment of the ABR waveform. Thresholds were acutely increased by between 22 ± 3 and $44 \pm$ dB SPL at all frequencies. Full recovery of threshold at 6 kHz stimulus was seen at 28 days following noise exposure, but only partial recovery was achieved at all other frequencies. The suprathreshold ABR waveform showed global depression of amplitude 24 hours following insult. While wave IV recovered to normal amplitudes after 28 days recovery, wave I and wave III remained depressed compared to controls throughout.

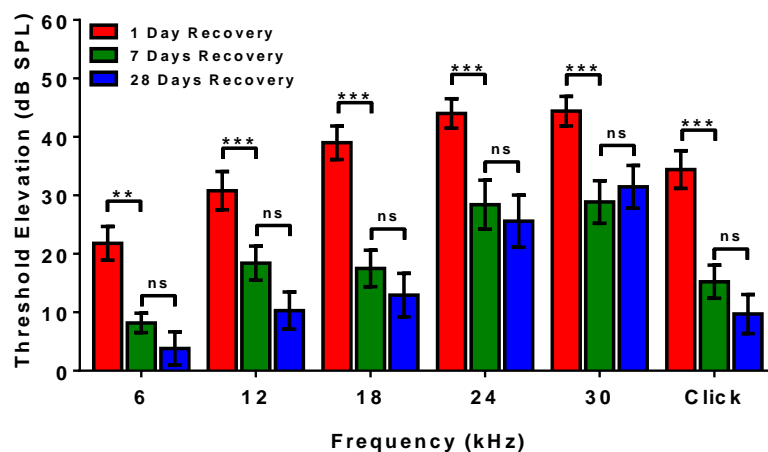


Figure 3.11: A summary of threshold elevations of auditory overexposed (AOE) mice at day one (red), day seven (green), and day 28 (blue). Substantial threshold changes are seen at every frequency at one day. Between day one and day seven, thresholds partially recover by between 18 – 77% (dependent on frequency). No further recovery of threshold is seen between days seven and 28. For 1 day n = 21, for 7 days n = 22, for 28 days n = 17. Significance is determined using a two-way ANOVA ($P < 0.001$), and corrected for multiple comparisons using a Holm-Sidak correction.

3.4.1 Assessment of the CBA/Ca Auditory Brainstem Response

Thresholds

The Auditory brainstem response (ABR) test is an electroencephalograph (EEG) recording of the neural activity of a subject when presented auditory stimuli. The ABR is used as a non-invasive method of determining auditory threshold of an individual, and more efficient than behavioural testing, as no training sessions are required. In the ABR recording, a brief acoustic stimulus is presented either as a single tone frequency (tone pip) or as a square wave, broadband stimulus (click). As the number of individual frequencies tested is time limited, tone pips are typically recorded at 6, 12, 18, 24, and 30 kHz, which represents the most sensitive frequencies in mouse.

In behavioural tests of auditory threshold, measured thresholds are typically lower than those measured with ABR; with best frequencies (12 kHz) in a CBA mouse registered at between 0-10 dB SPL (Figure 3.12A). However, in the ABR recording of mouse, thresholds can be up to 20 dB SPL higher than those measured by behaviour (Heffner and Heffner, 2003). One theory for this is that these differences are thought to arise from the relatively “impure” tones presented in ABR analyses, caused by the rapid onset and offset of the tone pips, compared to the longer (400 ms) tones presented in behavioural studies. Despite best efforts, it is also likely that the use of anaesthetics and electrical background noise also interferes with the estimation of threshold.

In this study, inbred CBA/Ca mice were found to have a “best” threshold of 25 ± 6 dB SPL at 12 kHz, which drops off to 46 ± 6 dB SPL and 48 ± 9 dB SPL at 6 and 30 kHz, respectively. Click thresholds were found to be 37 ± 4 dB SPL. These measurements are in agreement with previous recordings of the CBA/Ca mouse (Muller et al., 2005, Zhou et al., 2006, Ingham et al., 2011, Pilati et al., 2016). While most previous ABR studies have routinely used an anaesthetic mixture of ketamine and xylazine, Pilati et al (2016) and Muller et al. (2005) both used anaesthetic combinations similar to those used in this study. Agreements

between these recordings and those taken under different anaesthetic protocols suggests that there is very little difference in ABR thresholds tested under the anaesthetic used in this study and those tested using the more commonly used ketamine/xylazine mix.

ABR thresholds continue to mature up to 13 weeks of age

At 5 – 7 weeks old, mice reach sexual maturity and can be considered as young adults. As onset of hearing occurs at postnatal day 12 – 15 (Pilati et al., 2016) it was assumed that hearing thresholds would be stable by arounds post-natal day 40 where the inner ear is considered mature in both its morphology and electrophysiological properties (Lim and Anniko, 1985, Marcotti et al., 2003, Hafidi et al., 2005, Bulankina and Moser, 2012). Here, threshold data collected between 5 - 13 weeks of age suggests that the auditory system is still becoming sensitised to mid-range frequencies (12 – 18 kHz) over this time period. Although it is not clear from these recordings if thresholds become truly “stable”, the change seen here is minimal and presumably thresholds do not change considerably beyond this window and before age-related degeneration.

It should be noted that these profiles of hearing thresholds over time may be specific to the CBA/Ca mouse and unlike other commonly used inbred mouse strains such as C57BL/6 mice, which show accelerated presbycusis with hearing deficits seen as early as 6 months of age (Kane et al., 2012).

Waveform

ABRs differ between species with the number of identifiable waveforms present dependent on species. The mouse ABR consists of five waves (I-V) which are present within 8ms of the stimulus being received and are produced by distinct regions in the auditory pathway (Willott, 2006). In addition to the five waveforms, a small summing potential (SP) can also be seen, presenting as either a positive or a negative peak. Although the contribution of the regions to each waveform is still debated, the most likely origins are summarised in Figure 3.12B.

Noise Exposure and the Characterisation of Hearing in the Mouse

The Click ABR waveform was assessed using measurements of amplitude and latency of waves I, III, and IV. Wave V was omitted due to its relative size, and wave II was omitted as this wave occasionally “splits” in the open-field ABR recordings, appearing as two close peaks. For each measure, intensity was normalised to hearing threshold (suprathreshold, dB re: Threshold). In total, 90 Click recordings were collected for control animals aged between 5 and 7 weeks of age; all 90 of which were used for assessment of amplitude and latency.

On average, the first peak of the ABR waveform (wave I) occurred between 1.5 and 1.9 ms after stimulus. Wave III subsequently peaked at between 3.1 and 3.4 ms, and wave IV between 4.1 and 4.4 ms. All five waveforms were present within 6 ms after stimulus. Wave I typically had the largest peak, which on average grew to $6.974 \pm 0.266 \mu\text{V}$ at 60 dB re: Threshold; however peaks of up to 15 μV were recorded.

Click ABR waveform properties of adult mice have previously been characterised across a variety of inbred strains (Zhou et al., 2006), where in smaller groups ($n = 10$), both amplitude and latency appears to have a linear relationship with intensity of stimulus. In the data collected here, using a larger cohort ($n = 93$), on average, both amplitude and latency begin to reach a plateau at between 30 and 50 dB SPL suprathreshold.

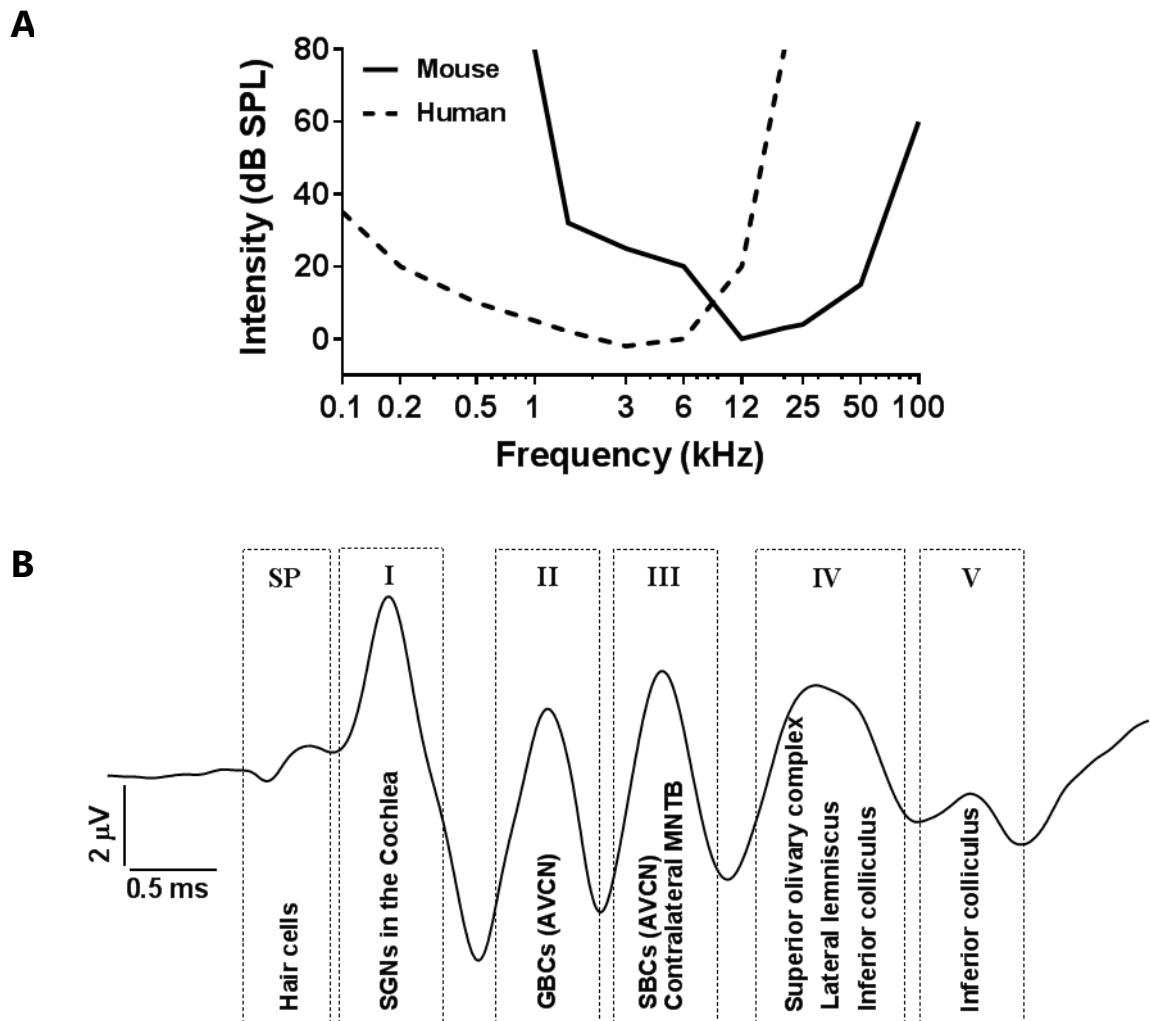


Figure 3.12: Mouse auditory sensitivity and ABR. (A) An approximation of the behavioural auditory threshold in both mouse and human shows little overlap. Although the recorded auditory threshold differs between tests, strain, and recording conditions, the most sensitive frequencies for mice are found in the region of 12-30 kHz. Figure produced with reference to (Heffner and Heffner, 2007) and Turner et al. (2005) **(B)** Wave I is generated by the cochlear spiral ganglion (SGN); Wave II by the globular bushy cells (GBCs) of the anterior ventral cochlear nucleus (AVCN); Wave III by the spherical bushy cells (SBCs) of the AVCN and the principle cells of the contralateral medial nucleus of the trapezoid body (MNTB)(Jalabi et al., 2013); Wave VI is most likely generated by the superior olivary complex, lateral lemniscus, and some contribution from the inferior colliculus; and Wave V by the inferior colliculus (Henry, 1979, Melcher and Kiang, 1996, Land et al., 2016). A proportion of recorded ABRs will also show a summing potential (SP) which is generated by the inner hair cells (Johnstone and Sellick, 1972); as the SP amplitude is approximately proportional to the RMS of the SPL of the stimulus, it is more likely to be present at higher intensities.

3.4.2 A Model of Semi-Permanent Noise Exposure

The effects of noise exposure to the ABR

The results presented in this chapter demonstrate that the sound exposure model used results in an immediate and profound elevation of ABR threshold at all frequencies tested within the first 24 hours following AOE, followed a recovery of threshold dependent on frequency over the subsequent 28 day period. Threshold elevations at each time point have been summarised in Figure 3.11, which shows that the majority of recovery occurs in the first 7 days following AOE. At 28 days, threshold elevation at 6, 12, or 18 kHz were not statistically significant from control mice after correction for multiple corrections, however more recovery was seen at 6kHz compared to 12 or 18 kHz.

In addition to threshold elevation, changes to suprathreshold ABR waveform amplitude in wave I and wave III were also observed out to 28 days. Despite no change in threshold, some recovery of wave I amplitude is observed between seven and 28 days suggesting that full recovery of ABR waveform properties may continue outside of these tested time-points.

The use of a broadband noise produced a larger increase in hearing threshold in a shorter period of time in comparison to the use of a filtered bandpass (Kujawa and Liberman, 2009, 2006) or a single tone exposure (Fryatt et al., 2011). While this model of hearing loss cannot be classed as “hidden” hearing loss, the permanent threshold shifts observed at 28 days in 24 and 30 kHz regions would be considered as a “mild loss” if the same changes were seen in the evaluation of human hearing (Niskar et al., 1998).

What the ABR tells us about damage to the peripheral auditory system

In previous models of “hidden” hearing loss, where thresholds return to baseline, this total recovery occurred within the first two weeks following AOE (Kujawa and Liberman, 2009). While it is currently unknown whether thresholds would return to control levels if left to recover beyond 28 days, given the apparent stagnation of recovery between 7 and 28 days, the significant differences seen in the high frequency regions should be considered as a permanent threshold shift (PTS). It is assumed that any mild to moderate damage seen at the IHC synapse (in the absence of any other damage) is eventually hidden from threshold tests due to a functional redundancy of hair cell afferents. With this in mind it is likely that there is some degree of irreversible physical damage that has occurred in high frequency regions of the cochlea as a result of the auditory insult. This damage is most likely to be related to disruption of stereocilia bundles, which has been observed at noise levels as low as 106 dB SPL (filtered bandpass); while more severe damage such as rupture of the reticular lamina or degeneration in the stria vascularis or spiral limbus occurs at higher intensity noise insults than those used here (Wang et al., 2002).

While the suprathreshold ABR amplitude of wave IV recovers by 28 days following exposure, there is still significant reduction in the growth of ABR wave I which corresponds to the inner ear. Recent studies have found that a reduction in amplitude of wave I is correlated with reductions in functioning afferent synapses at the inner hair cell (Jensen et al., 2015, Tong et al., 2016). Furthermore, shifts of 40 – 50 dB SPL immediately following noise exposure have been shown to be sufficient to induce glutamate excitotoxicity at the hair cell terminal and subsequent loss of synaptic connections (Robertson, 1983, Puel et al., 1998, Ruel et al., 2000). This chronic suppression of wave I suggests that it is highly likely that the noise model used here is enough to induce acute glutamate excitotoxicity at the afferent terminals which does not fully regenerate over the 28 day period.

Noise Exposure and the Characterisation of Hearing in the Mouse

Based on the data collected from control animals, wave I amplitudes begin to saturate (i.e. are non-linear) at 30 dB SPL above threshold. This trend is seen in sham exposed mice at one (Figure 3.6B) and seven days (Figure 3.8B). However, after noise exposure, the relationship between suprathreshold, and absolute amplitude is linear over the same relative intensities, rather than saturating. Thus, the saturating response is either absent, or has not been reached within the limits of the tested intensities (0-100 dB SPL). This linear growth response could suggest that some damage has occurred to the outer hair cells, as the saturating response arises from the active mechanical process in the inner ear. This linear response after acoustic trauma has been previously demonstrated in the displacement of the basilar membrane by (Johnstone et al., 1986). By 28 days following noise exposure, the saturating response of wave one returns (Figure 3.10B) suggesting that although input from the inner hair cells is permanently disrupted, outer hair cell function returns over time.

In addition to changes in amplitude, the latency of wave I appears to be permanently shifted as a result of acoustic overexposure, with significant alterations to suprathreshold latencies at one, seven, and 28 days following exposure. This delay is could reflect changes to myelin structure along the auditory nerve, like that which has been demonstrated before in rat following noise insult (Tagoe et al., 2014). Here, they found that structural alterations at the nodes of Ranvier following exposure significantly reduced nerve conduction velocity. If these changes occurred at the periphery, this would alter the observed latency of wave I.

What the ABR tells us about damage to the cochlear nucleus

While the changes to the peripheral auditory system following noise insult are well described, not as much is known about the effect of AOE on the central auditory system. Noise induced hearing loss often gives rise to central tinnitus and hyperacusis for which one proposed cause is an increase in spontaneous firing and hyperactivity in the dorsal cochlear nucleus (Kaltenbach and Afman,

2000, Pilati et al., 2012b). In these cases, while activity arising from the cochlea is decreased as a result of peripheral damage, sound evoked neural activity in higher structures such as the inferior colliculus is increased.

Thus, it is reasonable to suggest that the presence of tinnitus would alter the ratio between stimulus evoked auditory potentials arising from higher structures such as the inferior colliculus compared to cochlear input. Using the ABRs this was assessed by comparing the ratio of wave VI to wave I (Figure 3.13). This showed that in the AOE mice, wave IV amplitude is consistently larger in relation to wave I in comparison to sham exposed controls, suggesting hyperactivity in the central auditory system. In addition, tinnitus-inducing alterations to the dorsal cochlear nucleus have demonstrated in noise models which elicit similar temporary threshold shifts of 20 - 40 dB SPL (Pilati et al., 2012a).

However, ABR thresholds alone do not provide enough information to confirm the presence of tinnitus in the noise exposed animal as hearing loss and tinnitus are not always correlated (Brozoski et al., 2002). While the ratio of wave IV to wave I can sometimes be used as an approximation of central gain, this data can be easily skewed by changes to both inhibitory and excitatory networks within the auditory brainstem. Despite this, the ABR data is indicative, although not conclusive, that this noise model increases spontaneous activity in the cochlear nucleus, and is thus likely to induce tinnitus in the mouse. Going forward, a more traditional test, such as gap detection, should be used to confirm the presence of tinnitus in this model of noise exposure.

Noise Exposure and the Characterisation of Hearing in the Mouse

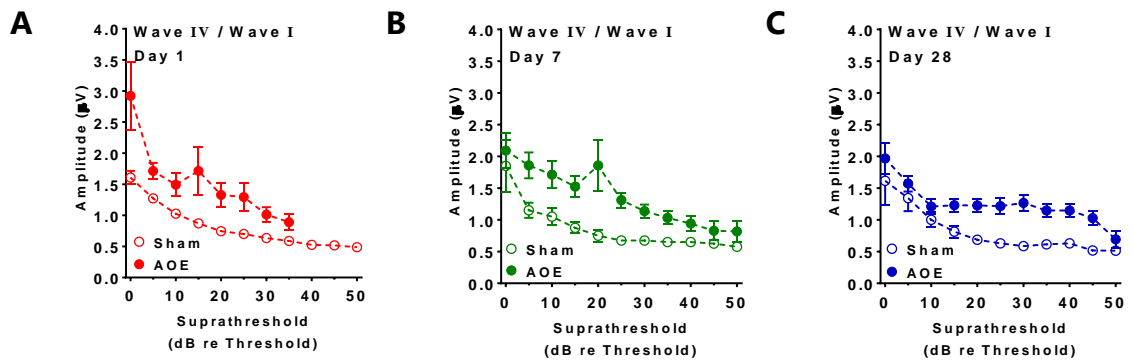


Figure 3.13: Ratio of the absolute amplitude of wave IV to wave I at day one (A), day seven (B), and day 28 (C). Wave VI / Wave I ratio are used as a measure of central gain in the auditory system, with an increase suggesting an increase of gain. Comparisons between AOE and sham mice were made with an ordinary two-way ANOVA. At all three time points, suprathreshold trend is significantly shifted upwards (significance displayed on plot).

3.4.3 Summary

Here, a noise model has been established which induces a semi-permanent threshold shift following one session of acoustic overexposure of the anaesthetised mouse. Although not conclusively confirmed, this model is highly likely to produce an excitotoxic glutamate insult at the inner hair cell synapse, resulting in a retraction of the spiral ganglion dendrite and initiating the long term degeneration of the spiral ganglion neurons like that seen by Kujawa et al. (2006, 2009). In addition to this, the ABR data presented here demonstrates an increase in central excitability following noise exposure, which is likely to originate from the cochlear nucleus or the VIIIth nerve.

In order to assess the molecular changes accompanying this damage, modiolus and cochlear nucleus will be analysed using RNA-Sequencing. As the method of RNA-Sequencing is new to this group, having recently used Microarray, the next chapter will discuss the comparability of the data collected between the two platforms and look at some of the endogenously expressed ion channels in both auditory regions.

Chapter 4: mRNA Sequencing of the Auditory Pathway

4.1 Introduction

RNASeq, or RNA sequencing, uses next generation sequencing to identify and determine the abundance of RNA sequences in biological samples. Prior to sequencing, RNAs were isolated from collected tissue samples. Once the quantity and quality of extracted RNA had been determined the RNA was then converted into a cDNA library which, after amplification, retain the relative abundance of RNA sequences present in the original sample. Tagged reads are then read on a sequencing platform strand by strand and collected data is assembled with the aid of the mouse genome.

Different RNA Sequencing technologies have been developed by several different companies; these include SOLiD sequencing (Applied Biosystems), SMRT (Pacific Biosciences), and (the now obsolete) 454 sequencing (Roche). However, it is the Illumina sequencing platform which is most frequently employed for whole transcriptome sequencing.

This chapter will discuss the use of RNASeq as a method for the discovery of differentially expressed genes as a comparison to Microarray. The basic statistics and run details have also been discussed. Following this, and owing to the large amount of data that can be collected in an RNASeq study, the control expression levels of several ion channels have been presented for both the cochlear nucleus and the modiolus samples.

4.2 Comparison of RNAseq to Microarray

Depending on the platform and choice of reagents, current Illumina technology is capable of reading up to 400 million strands of sequence in one run. This means that in a library which is assembled to have 150 nucleotides (nt) per strand, if a single sample was sequenced, a total of 150 x 800M nt would be collected for analysis. However the cost of performing a single run per sample would be prohibitively expensive for most experiments. Because of this, it has become necessary to multiplex samples; where, barcode sequences are annealed onto sample strands before amplification so that multiple samples can be run at the same time. In designing a RNASeq experiment, a compromise must therefore be made between sequencing depth (number of reads) and biological replication (number of samples). One of the biggest questions at this time is "how many reads is enough?"

To address this, a comparison was made between two RNA sequencing runs, achieving on average 8 million and 15 million reads, and the same samples which has been analysed using the Illumina MouseRef-8 v2.0 Expression BeadChip, a platform which was commonly used until its discontinuation in 2015.

4.2.1 Comparison of Platforms

Control cochlear nucleus samples (n = 3) were analysed using the recently discontinued Illumina Mouse Ref-8 Microarray. In parallel, using the same samples, RNAseq was ran twice to generate approximately 8 million reads per sample (8M) and approximately 15 million reads per sample (15M).

Microarray was independently compared with both RNAseq runs. After cross-matching Entrez IDs, 15,886 gene IDs had expression results in both Microarray and 8M read run, and 15,187 had results in both Microarray and 15M read run. Gene expression levels were reported as relative fluorescence intensity for microarray and fragments per kilobase of transcript per million mapped reads (FPKM) for RNAseq. For the microarray, a proportion of genes had expression

mRNA Sequencing of the Auditory Pathway

results over multiple probes. These were included correlation. mRNA Expression values for each gene were matched across platforms, and correlation coefficients were calculated using Spearman's correlation. In both cases, the datasets were highly correlated ($p < 0.001$), with correlation coefficients of $R = 0.7507$ and $R = 0.7452$, respectively (Figure 4.1A-B).

The correlation coefficients for 8M and 15M reads were compared using a two-tailed Fisher Z-Transformation. From this, there was no significant difference between either of the conditions ($p = 0.2714$). In addition to this, the correlation between the 8M read sample group and 15M read sample group was highly significant, with a Spearman rank correlation coefficient of $R = 0.9919$ (Figure 4.1C). However, when the relative distributions of FPKM values were compared using a Kolmogorov-Smirnov test, there was a significant difference ($p = 0.0471$) in distributions. This was most apparent in the difference number of reads of genes with mid-range expression levels (Figure 4.1D).

From the frequency distribution of both runs, the modal level of expression across all genes was approximately 11 FPKM. Although the data is not truly normally distributed due to the skew of data < 1 FPKM, 11 FPKM can be used as a benchmark for "average" expression levels. A decrease in correlation was seen at low mRNA expression levels (FPKM < 1), which is reflected not only in the comparison between the two sequencing runs (Figure 4.1C), but also in their comparison with microarray (Figure 4.1A-B).

Final control modiolus samples were also compared to Microarray data of P15 spiral ganglion cells available on the Shared Harvard Inner-Ear Laboratory Database (SHIELD) (Shen et al., 2015). The calculated Spearman's Rank correlation coefficient was $R = 0.5867$. For this R value, the probability that the datasets are not correlated is $P < 0.0001$ when tested across 16,144 matched genes; thus the datasets are considered to be significantly correlated.

mRNA Sequencing of the Auditory Pathway

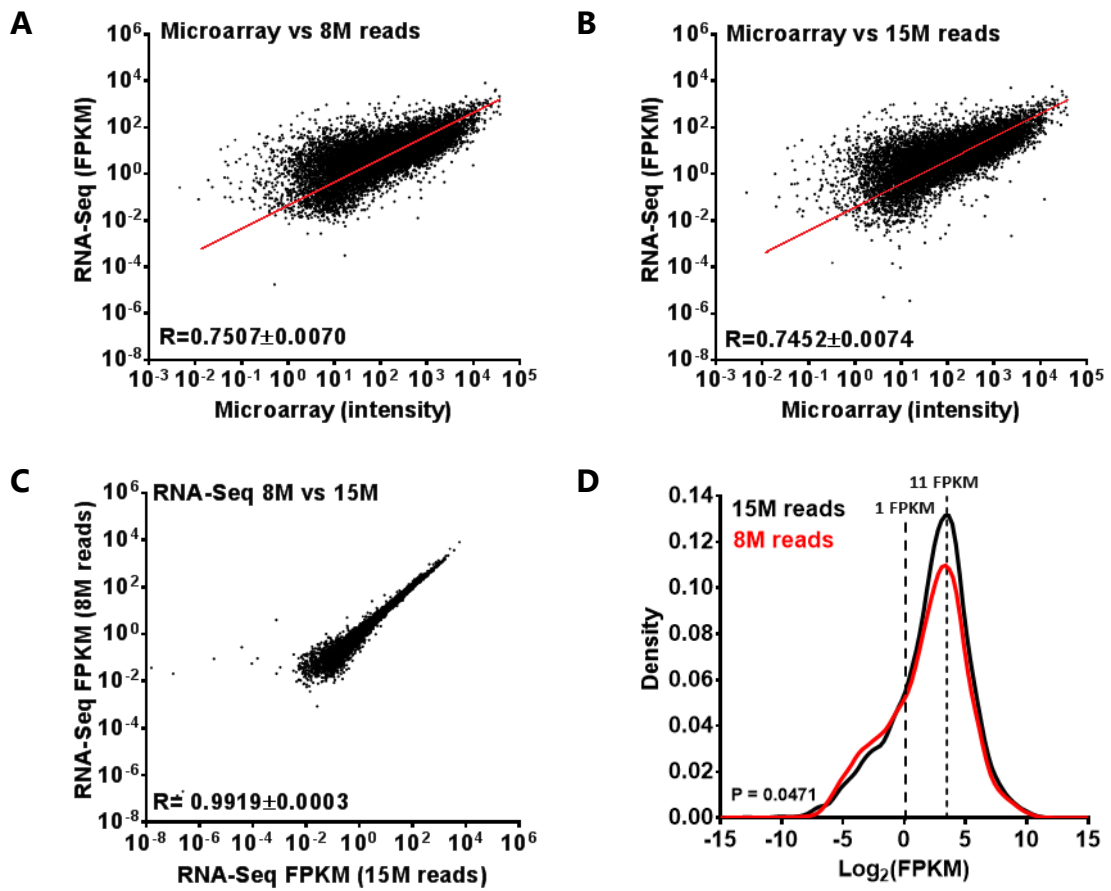


Figure 4.1: Comparison of 8M and 15M RNAseq reads with Microarray analysis of the same samples. Three control cochlear nucleus samples were run on both platforms. Average Microarray fluorescent intensity for each sample was highly correlated with FPKM values from the 8M reads (A) and the 15M reads (B). There was very little divergence in FPKM between both sequencing depths (C); however density plots showed a higher proportion of mid-range expression genes at 15M reads compared to 8M.

4.2.2 Defining a “Present” Gene

One of the fundamental questions to ask with any transcriptomic study is “when is a gene present?” in any one of the tested samples. Microarray platforms address this with a “present call”, which uses matched positive and negative probes to provide the user with a probability (p) of the gene being absent. Therefore, a (typical) value of $p < 0.05$ would indicate the gene was present in the sample. There is no such measure when using RNAseq with cut off values arbitrarily assigned as anywhere between 0.3 – 1 FPKM (Hart et al., 2013).

To address this, the number of unique transcripts, as a percentage of sampled genes, were compared between groups. At a “present call” value of $p < 0.05$, 0.55 ± 0.01 of assayed transcripts were found to be present in the microarray samples (Figure 4.2A). For the same percentage of assayed genes, this was approximately equivalent to a cut-off value of between $\text{FPKM} \geq 0.6$ and $\text{FPKM} \geq 1.0$ (Figure 4.2B).

The cut-off value of $\text{FPKM} \geq 0.6$ was further investigated using a gene at the limit of detection. Control samples of modiolus returned a value of 0.5 ± 0.1 FPKM for *Scn9a* (see Figure 4.1), which encodes voltage-gated sodium channel $\text{Nav}1.7$. Using immunohistochemistry, $\text{Nav}1.7$ was found to be expressed in select cells of the spiral ganglion (Figure 4.3A); a result which is in line with what has previously been shown in rat (Fryatt, 2010). This was also compared to the more highly expressed gene *Kcnc3* (40.9 ± 5.2 FPKM, see Table 4.2), encoding voltage-gated potassium channel $\text{Kv}3.3$, which has a more uniform and abundant expression pattern in the spiral ganglion neurons (Figure 4.3B).

This way of comparing is not without flaw. The Illumina Microarray assayed just 9,857 unique genes whereas the RNAseq results were assembled referencing 23,847 genes. Given that protein was reliably detected for genes with mRNA expression levels at this limit, a cut-off of $\text{FPKM} \geq 0.6$ represents a conservative estimate of the detectability of a gene in any given sample.

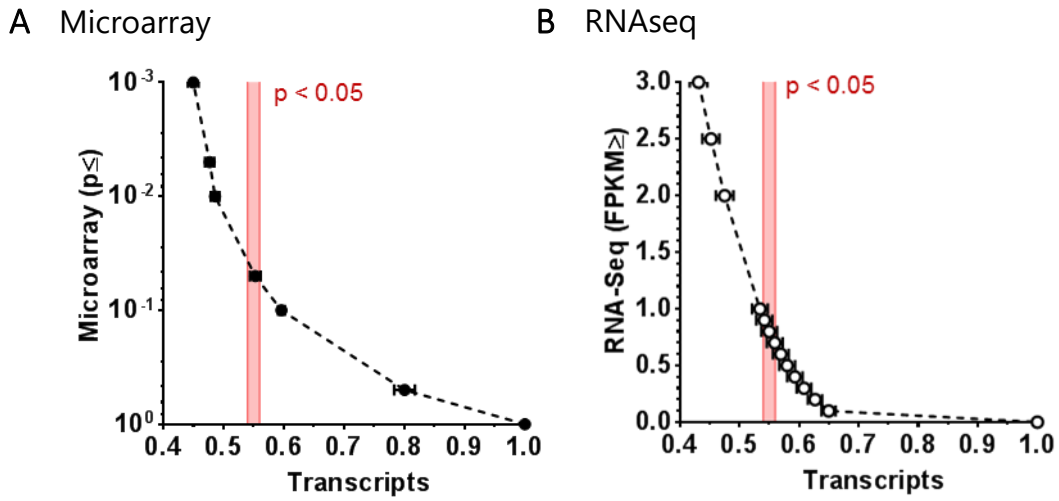


Figure 4.2: Comparison between microarray detection and FPKM for estimation of present genes. Microarray analysis conventionally uses a “present call” ($P < 0.05$) value to determine whether a gene is expressed within a sample. In the Microarray samples 0.55 ± 0.01 of the samples had a present call value of $P < 0.05$. This is equivalent to an FPKM value of between 0.6 - 1.0.

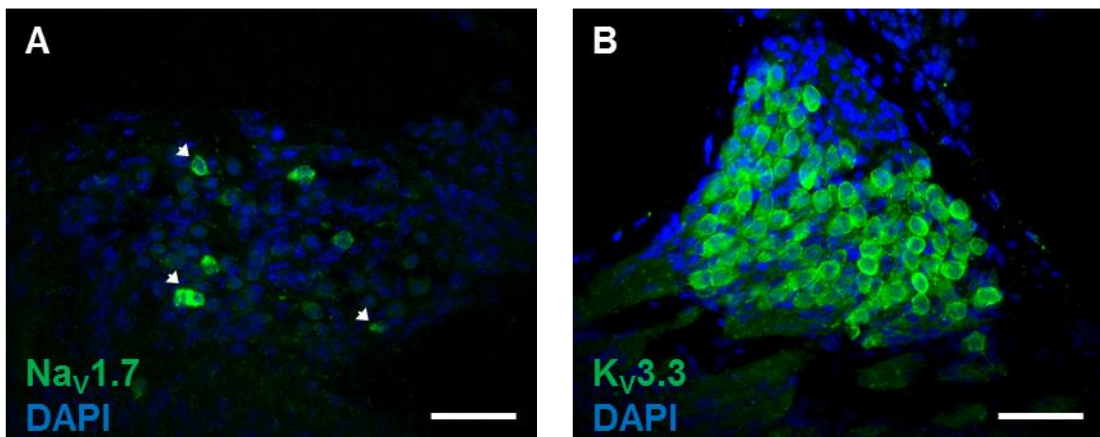


Figure 4.3: Examples of low-expression and high-expression in relation to protein. In the modiolus samples Na_v1.7, which is only expressed in a small proportion of SGN cells (A) achieved a low average value of 0.5 ± 0.1 FPKM. More widely expressed K_v3.3 (B) had a much larger average value of 40.9 ± 5.2 FPKM. Scale bar = 50 μm.

4.2.3 RNAseq Run Statistics

Cochlear Nucleus

Three cochlear nucleus samples were run per condition. Within each of these samples three mice (or six cochlear nuclei) were pooled. Therefore, each group can be thought of as $n = 3$ (samples / replicates), or $n = 9$ (mice).

Following quality control trimming, cochlear nucleus groups achieved an average of between 9.2 – 35.7 million reads. Read numbers of the experimental and control conditions were compared, and no significant difference was found at any time point (Figure 4.4A). Each group achieved a minimum of 14 times (X) coverage of coding region (calculated as total number of bases / size of category) with some groups achieving in excess of 40X coverage (Figure 4.4B); but as with read count, no significant difference was found between conditions.

Using a cut off value of $FPKM \geq 0.6$, numbers of expressed genes across each group ranged from 12,961 to 14,048 (Figure 4.5A-B), with an average of $13,655 \pm 94$ across all three control conditions. Gene ontology analysis was used to categorise genes present in control samples based on annotations for their cellular location (Figure 4.5C). From this, the top annotations returned were cell part (3078), organelle (1943), macromolecular complex (1104), membrane (1070), extracellular region (338), extracellular matrix (113), cell junction (61), and synapse (43).

mRNA Sequencing of the Auditory Pathway

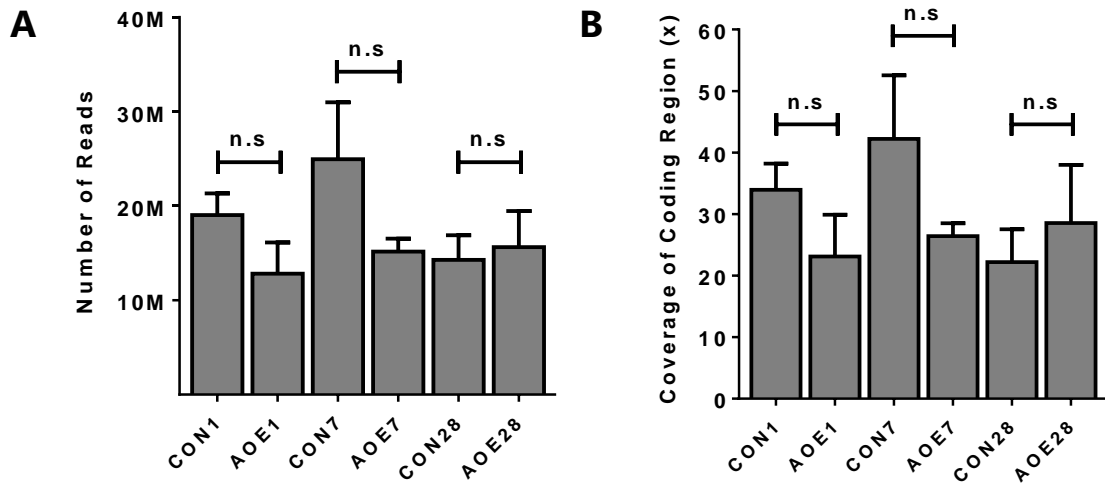


Figure 4.4: Read numbers and coverage of cochlear nucleus samples. Average number of reads per group, and thus the coding of coverage region (B) did not differ at any of the three time points. For each group $n = 3$ (replicates), or $n = 9$ (mice).

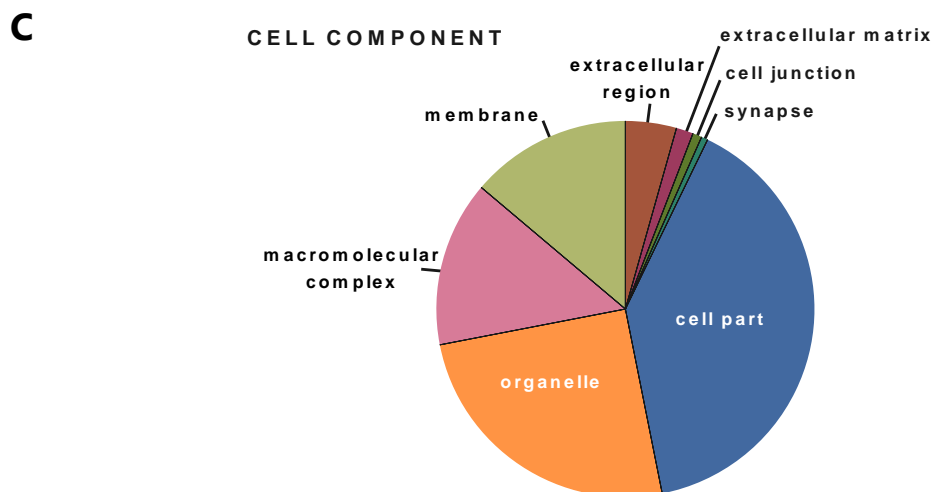
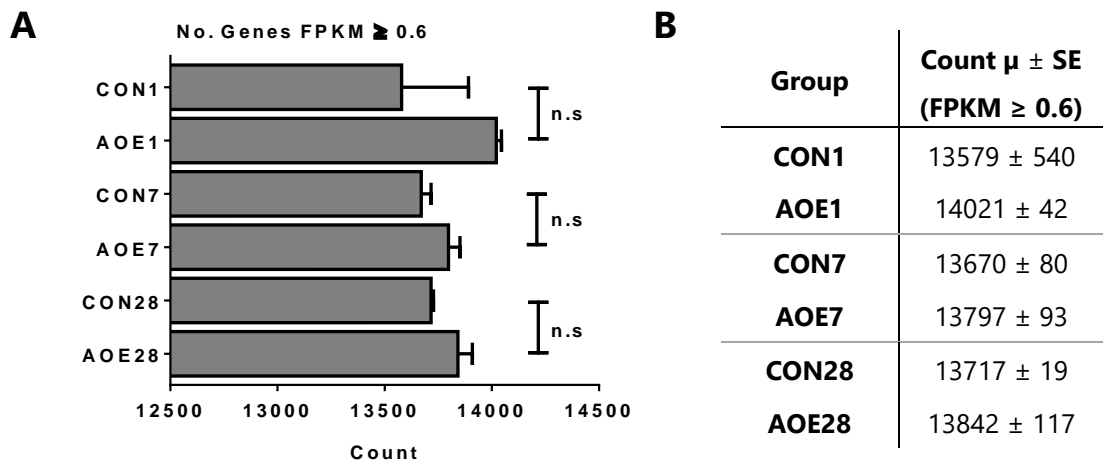


Figure 4.5: Number of transcripts "present" in cochlear nucleus. Approximately 13000 – 14000 had FPKM values ≥ 0.6 in the cochlear nucleus samples (A-B). Gene ontology analysis of present genes was performed to categorise genes based on their cellular location (C). For each group $n = 3$ (replicates), or $n = 9$ (mice).

mRNA Sequencing of the Auditory Pathway

Modiolus

Three modiolus samples were run per condition. Within each of these samples five mice (or 10 modiolus) were pooled. Therefore, each group can be thought of as $n = 3$ (samples / replicates), or $n = 15$ (mice).

Following quality control and trimming, modiolus groups achieved an average of between 15.3 – 45.7 million reads (Figure 4.6). Read numbers of the experimental and control conditions were compared, and no significant differences were found at one and 28 days. At 7 days, control samples achieved, on average, significantly more reads than the noise exposed samples (45.7 ± 1.1 million vs 20.0 ± 0.9 million, $p = 0.009$). Each group achieved a minimum of 25 times (X) coverage of coding region (calculated as total number of bases / size of category). As with read number, at seven days, the control group performed significantly better than the noise exposed group (70.0 ± 12.2 X vs 30.7 ± 9.3 X, $p = 0.032$), as shown in Figure 4.6.

Using a cut off value of FPKM ≥ 0.6 , numbers of expressed genes across each group ranged from 13,975 to 14,788 (Figure 4.7A-B), with an average of $14,381 \pm 75$ across all three control conditions. Gene ontology analysis was used to categorise genes present in the control samples based on their cellular location (Figure 4.7C). From this, the top annotations returned were cell part (3200), organelle (2030), macromolecular complex (1132), membrane (1107), extracellular region (402), extracellular matrix (133), cell junction (65), and synapse (40).

mRNA Sequencing of the Auditory Pathway

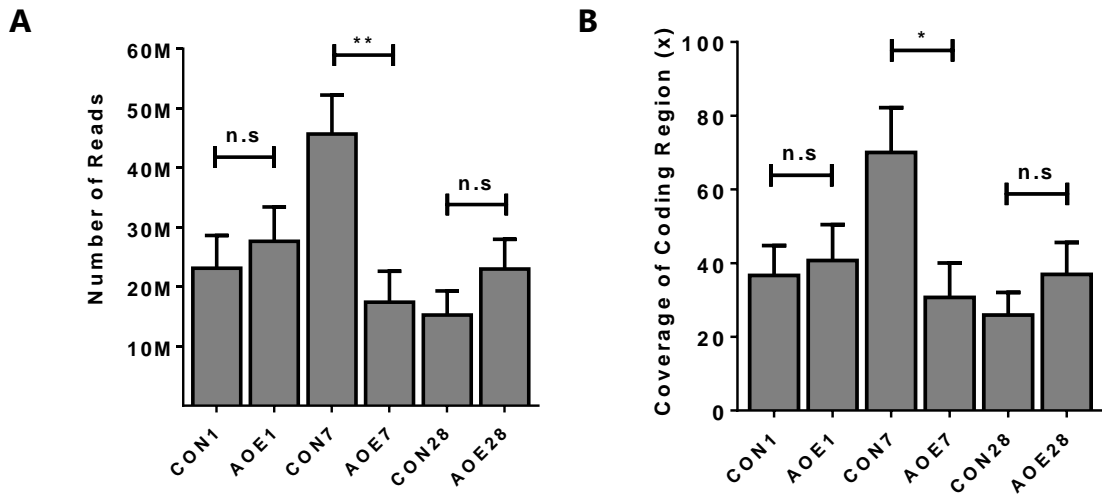


Figure 4.6 Read numbers and coverage of modiolus samples. Average number of reads and coverage of coding region did not differ between groups at one and 28 days. At seven days, the control modiolus samples achieved more reads than the AOE samples. For each group $n = 3$ (replicates), or $n = 15$ (mice).

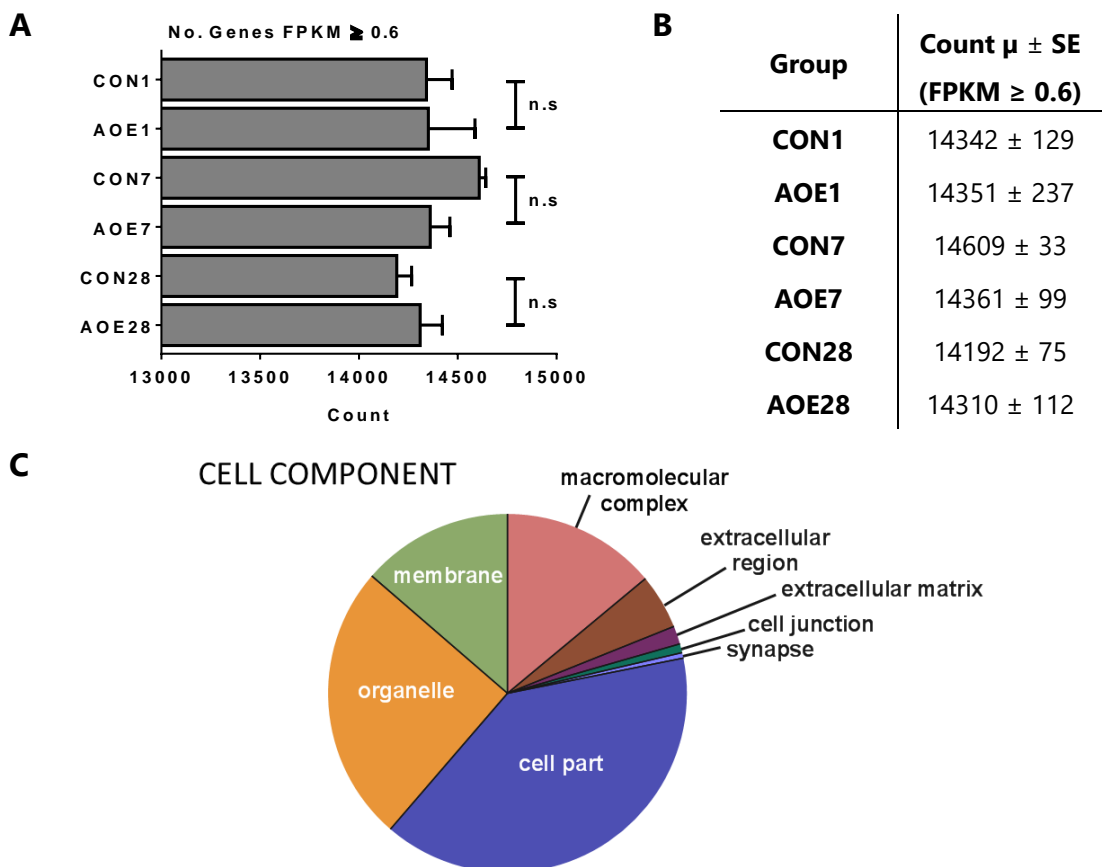


Figure 4.7: Number of transcripts "present" in the modiolus. Approximately 14000 – 15000 had FPKM values ≥ 0.6 in the modiolus samples (A-B). Gene ontology analysis of present genes was performed to categorise genes based on their cellular location (C). For each group $n = 3$ (replicates), or $n = 15$ (mice).

4.3 Ion Channel Expression in the Auditory System

Although the description of ion channel expression was not an initial aim of the project, the collected control samples presented an opportunity to look at relative RNA expression of several key voltage-gated ion channels in the cochlear nucleus and modiolar samples.

List of expression levels for each control replicate at the three time points were compiled and averaged. From this, the list was filtered to include all known voltage gated Na⁺ α subunits, voltage gated K⁺ α subunits, and ionotropic glutamate subunits. Auxiliary subunits have been omitted from this study. Any gene which had an average (\pm SE) FPKM levels was considered "present" within the sample and listed in the following sections.

To address the fact that expression of these genes could change over time, average expression of each gene was compared between each time point using a Two-way ANOVA with multiple comparisons and corrected with a Benjamini Hochberg False Discovery Rate (FDR)¹⁷. Genes which differ between time points will be highlighted in each section.

¹⁷ This method of multiple corrections was chosen to be consistent with later tests for differential expression between control and AOE.

4.3.1 Voltage-Gated Sodium Channels

Transmembrane voltage-gated sodium channels (Na_v) allow the influx of sodium into a neuron, causing the depolarisation of the neuronal membrane and the subsequent rising phase of an action potential. Na_v s consist of a single 260kDa pore forming α subunit, which although sufficient for functional expression, can be associated with one more of four auxiliary β subunits, which modify channel kinetics and facilitate trafficking to the cell membrane (Namadurai et al., 2015). Each α subunit consists of four repeats of six transmembrane domains which contains a voltage sensing region (S4), pore (S5-6), and an inactivating intracellular loop.

There are ten known genes which encode Na_v channels, classified as the tetrodotoxin-sensitive $\text{Na}_v1.1$ - $\text{Na}_v1.9$, and the structurally related tetrodotoxin-resistant Na_x . Unlike the Na_v1 s, Na_x is not voltage sensitive, and is found in ependymal and glial cells where they respond to rising concentrations of extracellular sodium (Hiyama et al., 2002). The voltage sensitive Na_v1 isoforms differ in their electrophysiological properties and distribution of expression. In the central nervous system, neurons predominantly express $\text{Na}_v1.1$, 1.2, 1.6, and 1.3 (Whitaker et al., 2001), whereas expression of $\text{Na}_v1.7$, 1.8 and 1.9 is typically restricted to the peripheral nervous system (Toledo-Aral et al., 1997, Dib-Hajj et al., 1998a, 1998b).

Voltage Gated Sodium Channels in the Cochlear Nucleus

Of the nine described Nav channels, five had expression levels of FPKM ≥ 0.6 in the cochlear nucleus after RNASeq analysis (Table 4.1). Those with the highest levels were *Scn1a* (Nav1.1; 42.2 ± 3.6 FPKM) and *Scn8a* (Nav1.6; 22.6 ± 3.5 FPKM). In addition to this, *Scn2a1* (Nav1.2), *Scn3a* (Nav1.3), and *Scn9a* (Nav1.7) were also expressed.

Of the five detected genes, two had age-related increases in control expression. Both *Scn1a* (Nav1.1), and *Scn8a* (Nav1.6) showed increased levels of expression over time, increasing by 22.2 ± 4.1 FPKM (70.3 ± 13.0 %) and 21.9 ± 4.5 FPKM (197.2 ± 40.5 %), respectively (Figure 4.8).

Both Nav1.1 and Nav1.6 are abundantly expressed in the CNS, and are critical components of the axon initial segment and nodes of Ranvier. In addition, Nav1.6 is expressed in several different cell types in the mammalian cochlear nucleus (Manis et al., 2003, Bal et al., 2009, Bal and Baydas, 2009), and has been shown to be critical for spontaneous activity in cartwheel neurons (Chen et al., 1999).

Nav1.9 expression has also previously been demonstrated in cartwheel cells of the dorsal cochlear nucleus (Yan et al., 2015), however in this study mRNA levels of the encoding gene (*Scn11a*) was too low to be considered present (0.03 ± 0.03 FPKM).

Voltage Gated Sodium Channels in the Modiolus

Of the nine described Nav channels, four had expression levels of FPKM ≥ 0.6 in the modiolus after RNASeq analysis (Table 4.1). Those with the highest levels of expression were *Scn1a* (Nav1.1; 7.1 ± 1.1 FPKM) and *Scn8a* (Nav1.6; 9.4 ± 1.5 FPKM). In addition to this, *Scn2a1* (Nav1.2), *Scn9a* (Nav1.7), and the related sodium subunit *Scn7a* (Nax) was also found to be expressed.

None of the detected genes had differing levels of expression with age.

Sodium channel expression in the rat spiral ganglion has previously been characterised by Fryatt et al. (2009), and largely agrees with the mRNA data presented here for mouse. Fryatt et al. (2009) also found that Nav1.6 and Nav1.7 is expressed in the SGN cell bodies and Nav1.1 is localised to axonal processes. Although there is no evidence of Nav1.2 expression in the SGNs, it is found in the efferent processes innervating IHCs and OHCs (Hossain et al., 2005), which could explain the presence of *Scn2a1* mRNA in these results.

The presence of Nax has not previously been investigated in the cochlea and is typically associated with circumventricular regions in the CNS, acting as a sodium level sensor of body fluid. However, there is strong evidence to suggest functional expression of the protein in the dorsal root ganglion neurons and non-myelinating Schwann cells (Hiyama et al., 2002, Watanabe et al., 2002) suggesting a peripheral role for Nax.

Table 4.1: Voltage gated sodium channels with expression in the cochlear nucleus and modiolus control samples. List of genes with average control levels of > 0.6 FPKM in the cochlear nucleus and modiolus samples. Values averaged over all nine control samples and mean (μ) and standard error (SE) has been given. Genes which had significantly different levels of expression between time points have been highlighted with an asterix (*).

Cochlear Nucleus				Modiolus			
Symbol	Protein	μ	SE	Symbol	Protein	μ	SE
<i>Scn1a</i> *	Nav1.1	42.2	3.6	<i>Scn1a</i>	Nav1.1	7.1	1.1
<i>Scn2a1</i>	Nav1.2	7.5	0.6	<i>Scn2a1</i>	Nav1.2	1.0	0.2
<i>Scn3a</i>	Nav1.3	2.1	0.2	<i>Scn8a</i>	Nav1.6	9.4	1.5
<i>Scn8a</i> *	Nav1.6	22.6	3.5	<i>Scn9a</i>	Nav1.7	0.5	0.1
<i>Scn9a</i>	Nav1.7	0.8	0.1	<i>Scn7a</i>	Nav _x	2.5	0.7

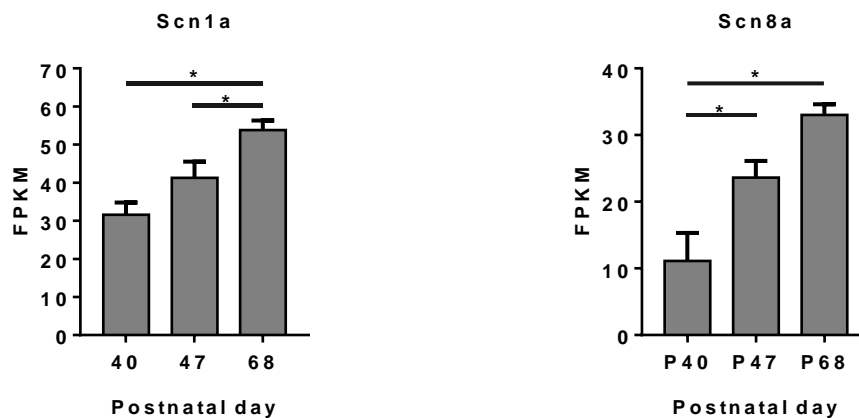


Figure 4.8: Voltage gated sodium channels with changed expression over time in the control cochlear nucleus. Two genes (*Scn1a* and *Scn8a*) were found to have significantly different levels of expression between one or more of the groups: control 1 (~P40), control 7 (~P47) and control 28 (~P68). For each group n = 3 (replicates), or n = 9 (mice).

4.3.2 Voltage-Gated Potassium Channels

The potassium channel family is the largest ion channel family with over 70 identified subunits. Of the extensive population of genes encoding K⁺ channel subunits. Here, the focus will be on voltage-gated K⁺ channels (K_V) which by itself consists of 40 α subunits divided into 12 families (K_V1 – K_V12).

K_V channels are homomeric or heteromeric structures consisting of four α subunits. These associated subunits are typically from within the same family, however “modifying” subunits from the K_V5, K_V6, K_V8, and K_V9 families are only able to form functional channels when combined with other K_Vα subunits. Each α subunit consists of six transmembrane domains and includes a voltage sensor region (S4), a pore forming P loop between S5 and S6 and an inactivating intracellular loop at the N-terminus. Like with Na_V channels, several auxiliary β subunits can associate with functional K_V channels to modify the activity of the channel.

The different families of α subunits have an array of biophysical properties. A simplified summary of these properties is shown in Figure 4.9. This diversification allows a membrane to express a combination of channel types so that the cell can perform a more specific physiological function.

In addition to the data collected from RNAseq, additional information about the role of K_V3s in the auditory pathway has been collected and included in Appendix 1.

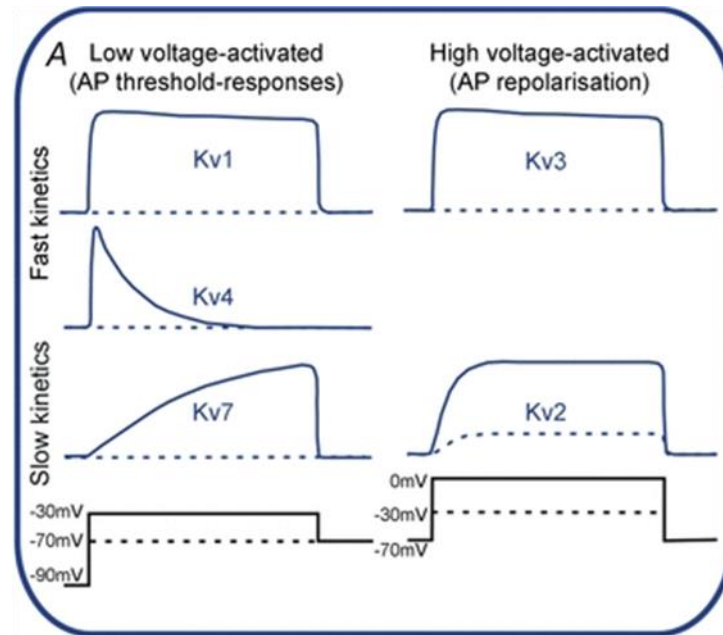


Figure 4.9: Family specific kinetics of the potassium current. Kv1, Kv4, and Kv7 channels are low-voltage activated channels whereas Kv2 and Kv3 are high-voltage activated. The channels can be characterised by their rapid activation (Kv1, Kv4, Kv3) or slow activation (Kv2, Kv7), or by their inactivation kinetics (i.e. Kv1 vs. Kv7). Reproduced from Johnston et al. (2010) with permission.

Voltage Gated Potassium Channels in the Cochlear Nucleus

Using a cut off value of FPKM ≥ 0.6 , 29 Kv α subunits were present in the control cochlear nucleus (Table 4.2). Of these, five most abundant consisted of the high-voltage activated *Kcnc1* (Kv3.1; 89.5 ± 7.3 FPKM) and *Kcnc3* (Kv3.3; 54.7 ± 6.9 FPKM), the low voltage activated *Kcna1* (Kv1.1; 56.4 ± 4.6 FPKM) and *Kcna2* (Kv1.2; 38.1 ± 3.4 FPKM), and *Kcnh2* which encodes Ether-à-go-go- related gene (ERG, Kv11.1; 30.0 ± 1.5 FPKM).

Of those detected, five of the genes showed age-related increases in control expression between the first time point (\sim P40) and the last time point (\sim P68), as shown in (Figure 4.10). These were: *Kcna1* (Kv1.1), which increased by 28.1 ± 4.5 FPKM (69.6 ± 11.1 %); *Kcna2* (Kv1.2), which increased by 19.0 ± 2.6 FPKM (66.0 ± 9.0 %); *Kcnc1* (Kv3.1), which increased by 36.2 ± 15.4 FPKM (104.6 ± 44.5 %); *Kcnc3* (Kv3.3), which increased by 47.5 ± 6.3 FPKM (164.9 ± 9.3 %); and *Kcnq2* (Kv7.2), which increased by 2.6 ± 0.8 FPKM (66.7 ± 20.5 %).

mRNA Sequencing of the Auditory Pathway

K_v3s were further investigated using immunohistochemistry (Figure A1.2) which confirmed K_v3.1 and K_v3.3 as the predominant K_v3 channels in the cochlear nucleus. Only a small amount of K_v3.2 was present, and while K_v3.4 was present, it did not appear to be expressed in the cell membrane of principle cells, but instead appears to be localised to an internal cell structure or in surrounding glia.

The presence of K_v1.1, 1.2, 1.4, 1.6, 3.1, 3.4, 4.2, 4.3, 7.2, 7.3, and 7.5 has previously been reported in the cochlear nucleus (Jung et al., 2005, Pal et al., 2005, Caminos et al., 2007, Friedland et al., 2007, Rusznak et al., 2008, Li et al., 2015). Here, the data collected shows that mRNA is present for an additional 15 K_v subunits, shown in Table 4.2.

Voltage Gated Potassium Channels in the Modiolus

Using a cut-off value of FPKM ≥ 0.6 , 22 K⁺ channel subunits were found to be expressed in the control modiolus (Table 4.2). Like in the cochlear nucleus, four of the top five were the high-voltage activated *Kcnc1* (K_v3.1; 35.6 ± 4.5 FPKM) and *Kcnc3* (K_v3.3; 40.9 ± 5.2 FPKM), the low-voltage activated *Kcna1* (K_v1.1; 46.4 ± 15.1 FPKM), and *Kcnh2* which encodes Ether-à-go-go- related gene (ERG, K_v11.1; 22.4 ± 2.4 FPKM). In addition to these, *Kcns1* which encodes the K_v2 modulating α subunit K_v9.1 is also highly expressed (23.7 ± 1.8 FPKM).

Both of the highly expressed K_v3 subunits, *Kcnc1* and *Kcnc3*, showed age-related increases in control expression between the first time point (~P40) and the last time point (~P68), as shown in Figure 4.11. *Kcnc1* (K_v3.1) increased by 12.3 ± 9.7 FPKM (37.5 ± 29.6 %) and *Kcnc3* also increased by 15.9 ± 10.2 FPKM (44.3 ± 28.4 %).

K_v3 channel expression in the spiral ganglion were further investigated using immunohistochemistry (Figure A1.1). K_v3.1 and K_v3.1 were both found to be expressed in the spiral ganglia cell bodies as well as axonal processes, with clustering at what appears to be the nodes of Ranvier. K_v3.2 protein was completely absent from the spiral ganglion, and no other staining was noted in

mRNA Sequencing of the Auditory Pathway

the cochlea. Surprisingly, Kv3.4 protein was found in the SGN membrane, despite the low levels of mRNA present in the RNASeq results.

In the mammalian spiral ganglia, the presence Kv1.1, 1.2, 1.4, 1.6, 3.1, 3.4, 4.2, 4.3, 7.2, and 7.3 have previously been demonstrated (Chen and Davis, 2006, Rusznak et al., 2008, Jin et al., 2009).

Table 4.2: Voltage gated potassium channels with expression in the cochlear nucleus and modiolus control samples. List of genes with average control levels of > 0.6 FPKM in the cochlear nucleus and modiolus samples. Values averaged over all nine control samples and mean (μ) and standard error (SE) has been given. Genes which had significantly different levels of expression between time points have been highlighted with an asterix (*).

Cochlear Nucleus				Modiolus			
Gene	Protein	μ	SE	Gene	Protein	μ	SE
<i>Kcna1*</i>	Kv1.1	56.4	4.6	<i>Kcna1</i>	Kv1.1	46.4	15.1
<i>Kcna2*</i>	Kv1.2	38.1	3.4	<i>Kcna2</i>	Kv1.2	22.1	7.0
<i>Kcna3</i>	Kv1.3	0.9	0.2	<i>Kcna5</i>	Kv1.5	0.4	0.3
<i>Kcna4</i>	Kv1.4	1.1	0.2	<i>Kcna6</i>	Kv1.6	2.7	0.5
<i>Kcna5</i>	Kv1.5	0.9	0.1	<i>Kcna10</i>	Kv1.8	10.5	3.9
<i>Kcna6</i>	Kv1.6	18.3	1.2	<i>Kcnb1</i>	Kv2.1	1.0	0.1
<i>Kcnb1</i>	Kv2.1	2.6	0.3	<i>Kcnc1*</i>	Kv3.1	35.6	4.5
<i>Kcnc1*</i>	Kv3.1	54.7	6.9	<i>Kcnc2</i>	Kv3.2	2.2	0.3
<i>Kcnc2</i>	Kv3.2	12.5	0.7	<i>Kcnc3*</i>	Kv3.3	40.9	5.2
<i>Kcnc3*</i>	Kv3.3	89.5	7.3	<i>Kcnc4</i>	Kv3.4	1.5	0.1
<i>Kcnc4</i>	Kv3.4	17.0	1.3	<i>Kcnd1</i>	Kv4.1	1.6	0.3
<i>Kcnd1</i>	Kv4.1	3.1	0.3	<i>Kcnd2</i>	Kv4.2	0.9	0.1
<i>Kcnd2</i>	Kv4.2	20.7	0.5	<i>Kcnd3</i>	Kv4.3	0.7	0.1
<i>Kcnd3</i>	Kv4.3	6.4	0.4	<i>Kcnq1</i>	Kv7.1	2.9	0.5
<i>Kcnq2*</i>	Kv7.2	21.4	3.1	<i>Kcnq2</i>	Kv7.2	9.1	1.0
<i>Kcnq3</i>	Kv7.3	5.3	0.6	<i>Kcnq3</i>	Kv7.3	0.6	0.2
<i>Kcnq4</i>	Kv7.4	12.0	0.4	<i>Kcnq4</i>	Kv7.4	3.1	1.1
<i>Kcnq5</i>	Kv7.5	1.8	0.2	<i>Kcns1</i>	Kv9.1	23.7	1.8
<i>Kcns1</i>	Kv9.1	1.5	0.1	<i>Kcns3</i>	Kv9.3	9.5	0.6
<i>Kcns2</i>	Kv9.2	1.3	0.1	<i>Kcnh5</i>	Kv10.2	0.8	0.2
<i>Kcns3</i>	Kv9.3	4.0	0.6	<i>Kcnh2</i>	Kv11.1	22.4	2.5
<i>Kcnh1</i>	Kv10.1	2.6	0.3				
<i>Kcnh5</i>	Kv10.2	2.6	0.3				
<i>Kcnh2</i>	Kv11.1	30.0	1.5				
<i>Kcnh7</i>	Kv11.2	1.6	0.3				
<i>Kcnh8</i>	Kv12.1	1.6	0.3				

Cochlear Nucleus

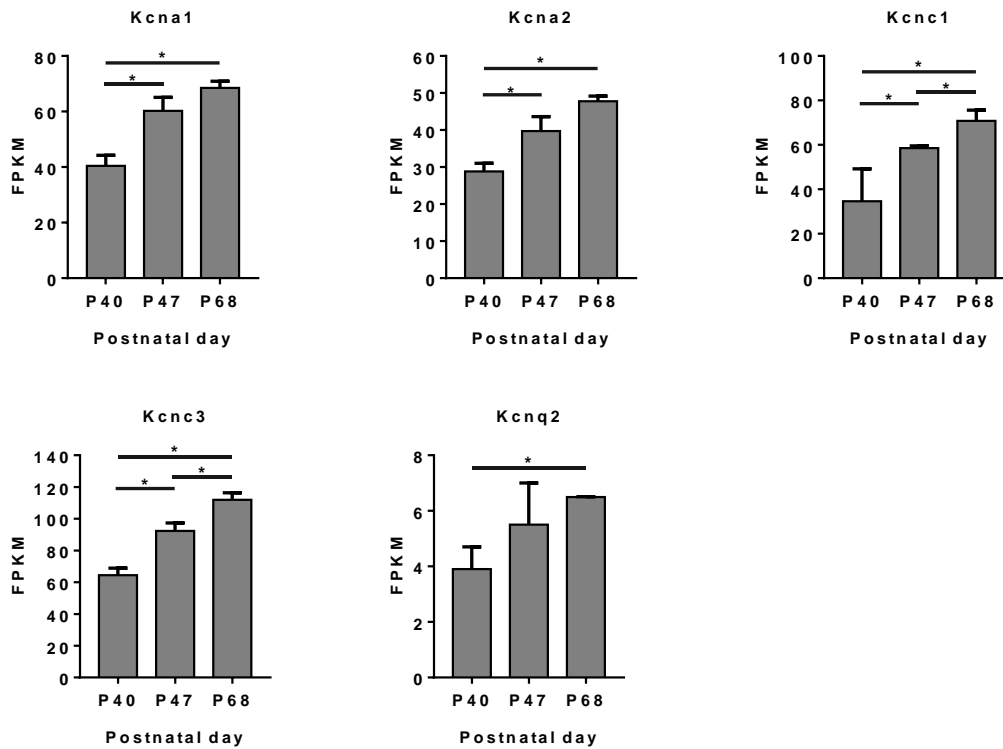


Figure 4.10: Voltage gated potassium channels with changed expression over time in the control cochlear nucleus. Five genes (*Kcna1*, *Kcna2*, *Kcnc1*, *Kcnc3*, and *Kcnq2*) were found to have significantly different levels of expression between one or more of the groups: control 1 (~P40), control 7 (~P47) and control 28 (~P68). For each group n = 3 (replicates), or n = 9 (mice).

Modiolus

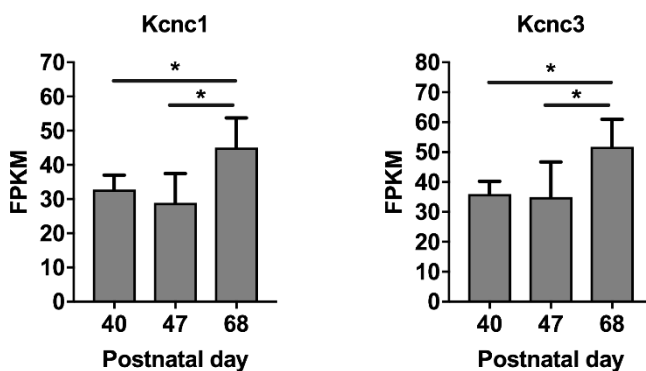


Figure 4.11: Voltage gated potassium channels with changed expression over time in the control modiolus. Two genes (*Kcnc1* and *Kcnc3*) were found to have significantly different levels of expression between one or more of the groups: control 1 (~P40), control 7 (~P47) and control 28 (~P68). For each group n = 3 (replicates), or n = 15 (mice).

4.3.3 Glutamate Receptors

Glutamate is the major excitatory neurotransmitter in the mammalian nervous system, and the principle neurotransmitter in the peripheral auditory system. Glutamate receptors can be divided in the G-protein coupled metabotropic receptors (mGluRs), and the ligand-gated ionotropic glutamate receptors; which in turn can be further divided into AMPA (GluAs), Kainate (GluKs), and NMDA receptors (GluNs). While metabotropic receptors associate with G-proteins to form functional channels, ionotropic channels are formed of clusters of subunits, which form around a central channel. As metabotropic receptors can produce either excitation or inhibition, this section has focused on ionotropic glutamate receptors.

Ionotropic glutamate receptors can be divided into two main categories, N-methyl-D-aspartate (NMDA) receptors, and non-NMDA receptors; which includes α -amino-3-hydroxy-5-methylisoxazol-4-propionic acid (AMPA) and kainate receptors. Each of the receptors are named for the synthetic glutamate analogue which activates them.

Non-NMDA receptor-channels (AMPA and kainate) are homomeric or heteromeric channels formed of four subunits. These channels, when formed, are permeable to Na^+ and K^+ when bound by their agonist. NMDA receptor-channels, on the other hand, are tetramers formed of GluN1 and two of the four GluN2 subunits. Although there is only one gene which encodes GluN1 (*Grin1*), eight variants of this channel are created through alternative splicing. More recently, the presence of two additional GluN3 subunits have been discovered in the CNS (GluN3a and GluN3b) although it is not clear what role they play when substituted into NMDA receptors (Perez-Otano et al., 2016).

NMDA receptors have a larger conductance than non-NMDA channels, and in addition to Na^+ and K^+ are permeable to Ca^{2+} when open. However, the opening of the channel is dependent on the presence of not only NMDA, but glycine and

mRNA Sequencing of the Auditory Pathway

a depolarisation of the cell membrane before maximal conductance can be reached.

Glutamate Receptors in the Cochlear Nucleus

In the cochlear nucleus all four AMPA (GluA1-4), all five kainate (GluK1-5), and all seven known NMDA (*Grin1*, *2a-d*, *3a-b*) subunits were considered present (Table 4.3), with the highest levels of expression seen in *Grin1* (GluN1, 61.7 ± 5.6 FPKM), and *Gria4* (GluA4, 42.9 ± 4.0 FPKM).

Age-related increases in control expression was seen in the AMPA subunit *Gria4* (GluA4), and the NMDA subunit *Grin1* (GluN1) between the first time point (~P40) and the last time point (~P68); see Figure 4.12. Over the 28 day period, mRNA for *Gria4* increased by 18.7 ± 9.6 FPKM (58.3 ± 29.9 %) and *Grin1* had a smaller increase of 18.7 ± 16.8 FPKM (35.1 ± 31.5 %).

The distribution of AMPA and NMDA glutamate receptors have been well documented in the cochlear nucleus, whereas less is known about kainate receptors (Petralia et al., 2000). Expression of both GluA2 and GluA4 has been demonstrated in all of the major neuron types across the cochlear nucleus. On the other hand, GluA1 expression is more restricted, limited to cartwheel and small stellate cells of the dorsal cochlear nucleus. GluA3 is also only found as protein on small subpopulations of cells, despite being ubiquitously expressed as mRNA (Petralia et al., 1997, Wang et al., 1998, Petralia et al., 1996).

As an integral component of NMDA receptor channels, GluN1 has also been shown to be expressed in all major neuronal types in the brainstem (Watanabe et al., 1994). The presence of all four N2 subunits and the two N3 subunits suggests the potential for a diversity of NMDA receptor-channels in the cochlear nucleus.

Glutamate Receptors in the Modiolus

In the modiolus mRNA was detected for all four AMPA subunits (GluA1-4), all five kainate (GluK1-5), NMDA subunit GluN1, and two of the N2 subunits (GluN2c and GluN2d), as shown in Table 4.3. Those with the highest levels of expression were *Grin1* (GluN1; 26.1 ± 3.0 FPKM), *Gria3* (GluA3; 13.3 ± 1.5 FPKM), and *Gria4* (GluA4 11.9 ± 1.3 FPKM).

None of the detected genes had differing levels of expression with age.

In situ hybridisation and immunohistochemical analysis in previous studies have shown the presence of GluN1, GluN2A-D, GluA2-4, and GluK1-5 in the spiral ganglion (Niedzielski and Wenthold, 1995, Ruel et al., 2007). It is thought that afferent transmission at the ribbon synapse is dominated by AMPA receptors, with GluA2/3 heteromers and GluA4 being expressed abundantly on the terminals (Matsubara et al., 1999). However more recently it has been shown that kainate receptors are also present in at the ribbon synapse (Peppi et al., 2012). Previous literature on the expression of GluA1 mRNA in the mammalian spiral ganglion is mixed, with some studies reporting it absent (Safieddine and Eybalin, 1992), while some report labelling (Luo et al., 1995). Here, the data would suggest that GluA1 is present in the modiolar samples, but at lower levels than the other AMPA receptor subunits.

Table 4.3: Ionotropic glutamate receptors with expression in the cochlear nucleus and modiolus control samples. List of genes with average control levels of > 0.6 FPKM in the cochlear nucleus and modiolus samples. Values averaged over all nine control samples and mean (μ) and standard error (SE) has been given. Genes which had significantly different levels of expression between time points have been highlighted with an asterix (*).

Cochlear Nucleus				Modiolus			
AMPA				AMPA			
Gene	Protein	μ	SE	Gene	Protein	μ	SE
<i>Gria1</i>	GluA1	17.8	1.5	<i>Gria1</i>	GluA1	2.2	0.2
<i>Gria2</i>	GluA2	24.3	3.2	<i>Gria2</i>	GluA2	3.6	0.6
<i>Gria3</i>	GluA3	21.6	1.2	<i>Gria3</i>	GluA3	13.3	1.5
<i>Gria4*</i>	GluA4	42.9	4.0	<i>Gria4</i>	GluA4	11.9	1.3
Kainate				Kainate			
Gene	Protein	μ	SE	Gene	Protein	μ	SE
<i>Grik1</i>	GluK1	5.8	0.4	<i>Grik1</i>	GluK1	0.7	0.1
<i>Grik2</i>	GluK2	4.3	0.2	<i>Grik2</i>	GluK2	0.7	0.1
<i>Grik3</i>	GluK3	5.1	0.3	<i>Grik3</i>	GluK3	0.5	0.1
<i>Grik4</i>	GluK4	5.8	0.2	<i>Grik4</i>	GluK4	2.9	0.4
<i>Grik5</i>	GluK5	15.2	0.3	<i>Grik5</i>	GluK5	10.5	0.5
NMDA				NMDA			
Gene	Protein	μ	SE	Gene	Protein	μ	SE
<i>Grin1*</i>	GluN1	61.7	5.6	<i>Grin1</i>	GluN1	26.1	3.0
<i>Grin2a</i>	GluN2A	1.9	0.2	<i>Grin2c</i>	GluN2c	0.6	0.2
<i>Grin2b</i>	GluN2B	0.8	0.1	<i>Grin2d</i>	GluN2d	0.9	0.2
<i>Grin2c</i>	GluN2c	10.8	0.8				
<i>Grin2d</i>	GluN2d	3.1	0.4				
<i>Grin3a</i>	GluN3A	6.6	0.6				
<i>Grin3b</i>	GluN3B	1.0	0.1				

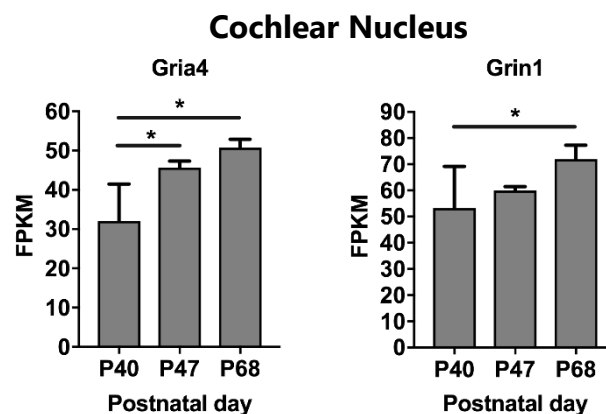


Figure 4.12: Ionotropic glutamate receptors with changed expression over time in the control cochlear nucleus. Two genes (*Gria4* and *Grin1*), which encode GluA4 and GluN1, were found to have significantly different levels of expression between one or more of the groups: control 1 (~P40), control 7 (~P47) and control 28 (~P68). For each group n = 3 (replicates), or n = 9 (mice).

4.4 Discussion

The main purpose of this chapter was to assess the comparability of RNA-Sequencing used here, to the previously used Illumina Microarray and to outline some of the basic statistics of the RNA-Sequencing run. The data collected here demonstrates that the RNA-Sequencing parameters used here is comparable to data which may be collected from the Microarray.

In order to exploit the vast amount of data that is obtained from RNA-Sequencing, this chapter also looked at the endogenous expression of a number of key voltage-gated and glutamate receptor ion channels in the modiolus and cochlear nucleus. The data collected here from control samples allows us to gain insight into the relative expression levels of these ion channels in the auditory system.

4.4.1 Gene Expression in RNASeq is Comparable to Microarray

The National Centre for Biotechnology Information (NCBI) currently has the mouse genome at approximately 2.7×10^9 base pairs long. If it is assumed that only around 3% of the genome encodes exons (Sakharkar et al., 2005), this would leave 81 million base pairs of coding region. As it was only mRNA which was isolated for sequencing and each read was 150 base pairs (150bp) in length, this means that approximately every 0.5 million reads would theoretically cover the assayed genome once.

There is currently no clear consensus on how many reads is required for a whole transcriptome RNASeq experiment. For experiments where low-abundance gene discovery is vital, or experiments looking at alternative splicing it is typically recommended that 50-100 million reads is achieved for each sample; whereas experiments relying on *de novo* builds benefit from 100-150 million reads (Liu et al., 2013b). However, for differential expression studies 10 – 25 million reads may be sufficient (Liu et al., 2014).

mRNA Sequencing of the Auditory Pathway

In this study, cochlear nucleus samples achieved between 9.2 – 35.7 million reads, while the modiolus samples did better than this at between 15.3 – 45.7 million reads. This meant a coverage depth of approximately 14 – 70 times the assayed genome. The large variance between the sample read depths is particularly apparent in the modiolus samples where control samples at day seven achieved significantly more reads than noise exposed samples at the same time point (Figure 4.6). As FPKM values are normalised to the number of reads in a run, the fact that the number of present genes was not significantly different between these two groups suggests that this discrepancy did not affect downstream analysis (Figure 4.7).

Here, the comparison between Microarray and RNASeq shows high correlation between the two platforms (Figure 4.1). While the two different RNASeq read depths (8M and 15M) were highly correlated, density plots of the two were significantly different (Figure 4.1), with the 15M read run having less genes at $FPKM < 1$. This suggests that 15M read run was marginally better for the detection of lowly expressed genes.

A direct comparison was not made in this study between Microarray and RNA sequencing of the modiolus samples. To help mitigate this, control modiolus samples were compared with SGN Microarray results collected as part of the Shared Harvard Inner-Ear Laboratory Database (SHIELD) (Shen et al., 2015). Despite the fact the SHEILD samples included only SGNs at an age point (P15) distinctly different from that used here, both datasets were significantly correlated.

While there is no disadvantage to increasing read depth in an RNASeq study (besides financially), this data would suggest that ~15 million reads is at least as good as Microarray in the quantitative analysis of mRNA counts.

4.4.2 Ion Channel Expression in the Auditory System

Using the proportion of expressed genes as measure, an FPKM ≥ 0.6 was equivalent to the classically used "present call" detection method on Illumina Microarray. Using this as a cut off, an average of $13,655 \pm 93$ genes were expressed in the cochlear nucleus, and $14,381 \pm 75$ genes were expressed in the modiolus. While the cochlear nucleus has a more diverse population of neuronal cells types, the differences in number of expressed genes is likely to be due to the inclusion of bone in the modiolus samples.

The cochlear nucleus samples collected contained both anterior and dorsal portions of the cochlear nucleus. This means that the samples would include the five types of principle cell plus surrounding glia; and due to how the samples were collected ependyma would also be included. While the data collected here has identified mRNA for five Na_v , 26 K_v , and 16 glutamate receptor channel subunits to be present in the cochlear nucleus, it would be impossible to determine the significance of their presence without knowing which cell types they are expressed in.

Similarly, modiolus samples not only contained SGNs, but also bone and glia. In addition to this, this mRNA of four Na_v , 21 K_v , 12 glutamate receptor, and the sodium sensing Na_x channels in the modiolus. Further RNA *in-situ* hybridisation studies would be required to determine the localisation of the mRNA while western blotting and immunohistochemical experiments would also determine the presence and location of any translated protein.

4.4.3 Ion Channel Expression Changes Occur Beyond P40

Auditory brainstem response recordings from control animals, collected in Chapter 3, suggested that auditory threshold continues to mature beyond P40. Here, over 28 days following P40, there is evidence of the upregulation of several of Na_v , K_v and glutamate receptor channel subunits in the auditory pathway.

mRNA Sequencing of the Auditory Pathway

With the exception of Kv3.1 and Kv3.3 (discussed in Appendix 1), changes to translated protein were not investigated. In addition to this, as the first collected time point (P40) was just 24 hours following the sham exposure, any changes could be an effect of stresses caused by long duration anaesthetic and recovery rather than developmental changes. Because of this, all changes would need to be investigated further before any strong conclusions could be made.

Nav Subunits

Of the Nav subunits, there were no changes in expression over time in the modiolus samples. However, two Nav subunits, *Scn1a* (Nav1.1) and *Scn8a* (Nav1.6) were significantly upregulated in the cochlear nucleus. These two channels are highly expressed across the CNS and are found in axon initial segments and the nodes of Ranvier. Upregulation of these channels could, potentially, increase the rate of spontaneous activity in the cochlear nucleus as both are thought to be involved in the generation of a resurgent sodium current when expressed (Lewis and Raman, 2014).

Kv Subunits

The cochlear nucleus saw upregulation of two Kv1 subunits, *Kcna1* (Kv1.1), *Kcna2* (Kv1.2). This contrasts with previously published data on the development of these channels in the rat cochlear nucleus by Caminos et al. (2005), who found that Nav1.1 and 1.2 progressively decreased after 21 days of age. In addition to this, *Kcnc1* (Kv3.1) and *Kcnc3* (Kv3.3) were significantly upregulated over time in both the cochlear nucleus (Figure 4.10) and modiolus (Figure 4.11). These changes are discussed in Appendix 1.

Glutamate Receptor Subunits

In the cochlear nucleus, mRNA for genes encoding the AMPA subunit GluA4 (*Gria4*) and the NMDA subunit GluN1 (*Grin1*) were significantly upregulated between P40 and P68.

Increases of GluA4 after hearing onset has previously been demonstrated across the superior olivary complex (Pilati et al., 2016); this change was observed

mRNA Sequencing of the Auditory Pathway

between P12-15 and measured out to P29-36. The data collected here suggests an upregulation of GluA4 in the CN beyond this time point which would lead an acceleration in the rate of evoked excitatory postsynaptic potentials. Unpublished data from the same study also looked at two of the alternative splice variants of *Grin1* (GluN1), NR1a and NR1b, and found that expression of the subunit decreased in the SOC following hearing onset. Data collected here for the cochlear nucleus suggests not only that there is still a substantial amount of mRNA present at P40 but that this mRNA increase after this time point.

4.4.4 Summary

Here, RNA-Sequencing has been compared against the Illumina Microarray and the two platforms have been found to be comparable in the distribution of data collected, and with high correlation between relative abundance of genes in each sample. This chapter has also confirmed the presence of five Nav α subunits in the modiolus and cochlear nucleus, 21 and 26 Kv α subunits in the modiolus and cochlear nucleus respectively, and 12 and 16 Glutamate receptor α subunits in the modiolus and cochlear nucleus respectively.

The next chapter, chapter five, will discuss changes in the modiolus in a model of noise induced hearing loss by comparing AOE samples to control samples at one, seven, and 28 days following exposure. Following this, chapter six will discuss the changes to the cochlear nucleus following noise exposure across the same time points.

Chapter 5: Gene Expression Changes in the Modiolus Follow Noise Exposure

5.1 Introduction

Modiolus RNASeq results at each experimental time-point were compared with condition matched sham controls. In this chapter these comparisons will be described at each time point. Following this, a more integrative approach will be taken to address the following questions: what is the immune response to noise in the modiolus?; what neuron specific changes can be seen?; and is there any evidence of the involvement of cell death pathways following noise exposure?

While the aim of this chapter is to represent as much data as possible from the RNASeq dataset, not every significantly changed gene can be discussed. As such, gene ontology analysis has been used to consolidate the data into groups and pathways. Just one protein of interest, P2x₃ was chosen for further discussion and was selected based on its association with neuron specific annotations.

5.2 Gene Expression Changes One Day after Noise Exposure

After one day recovery noise exposed modiolus had 166 differentially expressed genes compared to sham exposed control. Of these, 110 were upregulated ($\Delta > 2.0$, FDR < 0.05) and 56 were downregulated ($\Delta < 0.5$, FDR < 0.05). The top 20 upregulated and downregulated genes are shown in Table 5.1.

Plots of the distribution of fold changes show a greater spread of upregulated genes, an even distribution about zero of non-significant changes, and an even spread of differentially expressed genes based on their control levels (Figure 5.1). Predictably, fewer downregulated changes were seen in genes lowly expressed in control conditions as there is generally lower resolution for the detection of these genes.

Of the 110 upregulated genes, 29 genes had a control FPKM of zero; and of the 56 downregulated genes 13 were reduced to zero in the AOE (see Table 5.2). The largest of these changes was Serum Amyloid P (*Apcs*) which increased to 20.20 FPKM in experimental conditions. This change, is one of nine acute phase proteins (*Apcs*, *Crp*, *Fgb*, *Hp*, *Orm1*, *Orm2*, *Saa1*, *Saa2*, and *Saa4*) upregulated at day 1; this is further discussed in §5.6.

The largest measurable fold change was serum Albumin (*Alb*) with which had experimental expression 150x higher than control; this was the largest change seen over all three time points. Related serum protein Transthyretin (*Ttr*) was also highly upregulated at this time point with an experimental expression 35x control expression.

Gene ontology analysis of genes upregulated at day one returned 31 "over-represented" terms ($P < 0.05$). 23 of the 31 terms were related to either immune systems process or stress response to stimulus, including nine of the top 10 terms (see Table 5.3). The complement cascade was one of the most enriched pathways with members of the C1-complex (*C1qa*, *C1qb*, *C1qc*), *C3*, *C4b*, *C8a*, complement

Gene Expression Changes in the Modiolus Follow Noise Exposure

factor B (*Cfb*), C-reactive protein (*Crp*), and Mannan-binding lectin (*Mbl1*) all significantly upregulated. Although neither pathway is fully represented, upregulation of these complement proteins suggest activation of the alternative or lectin pathway within the first 24 hours of recovery.

Gene ontology of downregulated genes returned 93 significant ($P < 0.05$) terms, with the top 10 terms relating to extracellular matrix organisation and the development of bone and cartilage (Table 5.4). This is primarily due to the downregulation of 6 fibrillar collagen genes (*Col1a1*, *Col2a1*, *Col5a1*, *Col11a1*, *Col11a2*, and *Col22a1*).

Following from short term changes at day one, the next section will discuss changes which occur after seven days recovery.

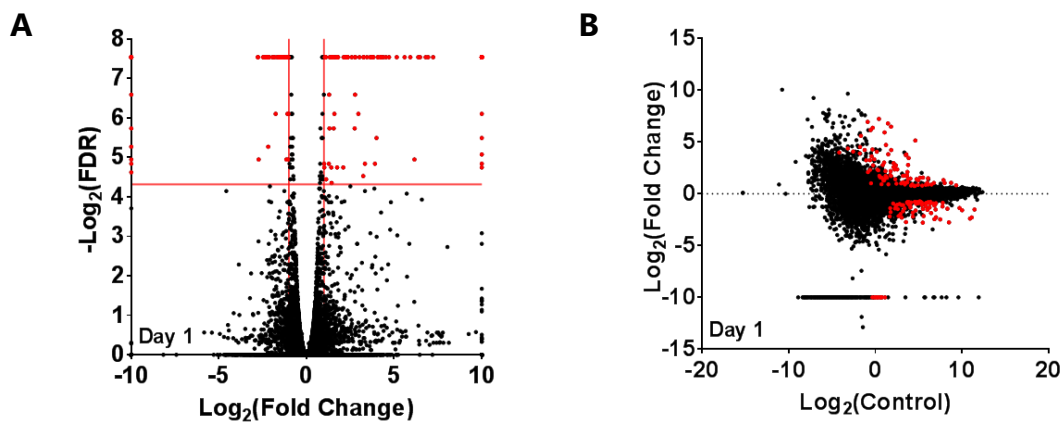


Figure 5.1 Volcano (A) and MA plot (B) of differentially expressed genes at day one in the modiolus. Plots were constructed using a Log_2 transforms of fold change (Δ), false discovery rate (FDR) and mean control FPKM. Red lines represent cut off values of $\text{FDR} < 0.05$ and $\Delta > 2$ or $\Delta < -2$. Genes which satisfy these conditions have been coloured red.

Gene Expression Changes in the Modiolus Follow Noise Exposure

Table 5.1: Differentially expressed genes at day one in the modiolus. The top 20 changed genes at day one listed in order of biggest change. For each gene, the average control and experimental (AOE) FPKM values are listed along with a Log₂ transform of fold change (Δ) and the significance value (FDR). For changes where either control or AOE FPKM equal zero, a true ratio of change cannot be determined; these changes are shown in Table 5.2.

Top 20 Upregulated					Top 20 Downregulated				
Gene	Control	AOE	Log ₂ Δ	FDR	Gene	Control	AOE	Log ₂ Δ	FDR
<i>Alb</i>	1.33	199.73	7.23	0.005	<i>Prg2</i>	44.21	6.44	-2.78	0.005
<i>Fgb</i>	0.54	66.22	6.94	0.005	<i>Camp</i>	361.01	53.41	-2.76	0.005
<i>Saa2</i>	2.72	303.63	6.80	0.005	<i>Adipoq</i>	11.53	1.74	-2.73	0.032
<i>Saa1</i>	3.48	311.70	6.48	0.005	<i>Ngp</i>	178.78	32.24	-2.47	0.005
<i>Serpina3k</i>	0.81	67.51	6.39	0.005	<i>Fabp4</i>	113.09	20.89	-2.44	0.005
<i>Apoa1</i>	0.68	49.06	6.16	0.032	<i>S100a9</i>	1934.17	371.73	-2.38	0.005
<i>Hpx</i>	2.08	126.82	5.93	0.005	<i>Slc4a1</i>	8.28	1.69	-2.29	0.005
<i>Myh4</i>	0.31	15.28	5.60	0.005	<i>S100a8</i>	2223.62	457.05	-2.28	0.005
<i>Ttr</i>	24.51	871.45	5.15	0.005	<i>Retnlg</i>	127.81	26.60	-2.26	0.005
<i>Ckm</i>	2.33	61.12	4.72	0.005	<i>Chi3l3</i>	20.22	4.43	-2.19	0.005
<i>Myh1</i>	0.29	6.77	4.53	0.005	<i>Dkk2</i>	3.16	0.70	-2.18	0.026
<i>Apob</i>	0.11	2.29	4.39	0.005	<i>Cd177</i>	6.37	1.44	-2.14	0.005
<i>Serpina3n</i>	0.79	15.40	4.28	0.005	<i>Ltf</i>	47.44	10.81	-2.13	0.005
<i>Orm1</i>	3.52	66.26	4.23	0.005	<i>Mmp9</i>	7.45	1.92	-1.95	0.005
<i>Plg</i>	0.42	7.92	4.23	0.005	<i>Bglap2</i>	85.81	23.69	-1.86	0.005
<i>Myh2</i>	0.17	2.85	4.08	0.005	<i>Alas2</i>	19.98	5.69	-1.81	0.005
<i>Apoh</i>	1.12	18.77	4.07	0.005	<i>Col22a1</i>	3.39	1.00	-1.76	0.015
<i>Prlr</i>	0.06	0.88	4.00	0.022	<i>Fbxo40</i>	9.17	2.86	-1.68	0.005
<i>Hspb7</i>	0.28	4.28	3.91	0.035	<i>Mpo</i>	24.83	8.13	-1.61	0.005
<i>Calca</i>	2.78	39.44	3.83	0.005	<i>Bpifa1</i>	1033.94	346.36	-1.58	0.005

Gene Expression Changes in the Modiolus Follow Noise Exposure

Table 5.2: Day one changes for which fold change cannot be calculated in the modiolus. Differentially expressed genes which have a control or experimental value of zero have been excluded from the top 20 changed genes as fold change cannot be determined. For each gene, the average control and experimental (AOE) FPKM values are listed along the significance value (FDR).

Upregulated				Downregulated			
Gene	Control	AOE	FDR	Gene	Control	AOE	FDR
<i>Apcs</i>	0	20.20	0.005	<i>Gm14743</i>	2.15	0	0.005
<i>Orm2</i>	0	6.95	0.005	<i>Calm4</i>	1.68	0	0.005
<i>Sult2a1</i>	0	5.87	0.005	<i>Scgb2b24</i>	1.63	0	0.040
<i>Ankrd1</i>	0	5.82	0.005	<i>Defb42</i>	1.44	0	0.005
<i>Leap2</i>	0	5.37	0.005	<i>Defb1</i>	1.23	0	0.005
<i>Hpd</i>	0	4.76	0.005	<i>Krtap7-1</i>	1.18	0	0.035
<i>Calcb</i>	0	3.01	0.005	<i>Gm94</i>	1.16	0	0.019
<i>Mbl1</i>	0	3.01	0.005	<i>Crct1</i>	1.00	0	0.010
<i>Crp</i>	0	2.97	0.005	<i>Cnfn</i>	0.99	0	0.026
<i>Lect2</i>	0	2.72	0.005	<i>Wfdc12</i>	0.98	0	0.032
<i>Akr1c6</i>	0	2.35	0.005	<i>Rnf151</i>	0.96	0	0.005
<i>Apon</i>	0	2.24	0.005	<i>Gm13710</i>	0.93	0	0.005
<i>Agxt</i>	0	1.88	0.005	<i>Krt77</i>	0.78	0	0.005
<i>Cyp2d10</i>	0	1.62	0.005				
<i>Afm</i>	0	1.43	0.005				
<i>Aadac</i>	0	1.43	0.005				
<i>Prodh2</i>	0	1.41	0.005				
<i>Saa4</i>	0	1.37	0.005				
<i>Proc</i>	0	1.37	0.005				
<i>Ces1c</i>	0	1.30	0.005				
<i>Cyp2c37</i>	0	1.18	0.005				
<i>Dusp13</i>	0	1.03	0.005				
<i>1110059M19Rik</i>	0	0.98	0.005				
<i>C8a</i>	0	0.95	0.005				
<i>Ugt2b36</i>	0	0.94	0.005				
<i>Sult2a6</i>	0	0.90	0.005				
<i>Cyp4a32</i>	0	0.75	0.005				
<i>Ugt2b5</i>	0	0.72	0.005				
<i>Otc</i>	0	0.72	0.005				

Gene Expression Changes in the Modiolus Follow Noise Exposure

Table 5.3: The top 10 Gene Ontology results for genes upregulated at day one in the modiolus. Genes upregulated at day one were analysed for enriched biological function terms using the gene ontology package GOSep. 31 significant terms ($P < 0.05$) were returned and ordered by significance.

	GO ID	Term	P
1	GO:0072376	Protein activation cascade	9.98×10^{-8}
2	GO:0006952	Defense response	1.19×10^{-7}
3	GO:0006956	Complement activation	3.83×10^{-7}
4	GO:0002455	Humoral immune response mediated by circulating immunoglobulin	4.11×10^{-6}
5	GO:0006958	Complement activation, classical pathway	5.13×10^{-6}
6	GO:0006953	Acute-phase response	5.13×10^{-6}
7	GO:0006936	Muscle contraction	1.54×10^{-5}
8	GO:0002526	Acute inflammatory response	1.54×10^{-5}
9	GO:0016064	Immunoglobulin mediated immune response	7.56×10^{-5}
10	GO:0019724	B cell mediated immunity	8.61×10^{-5}

Table 5.4 The top 10 Gene Ontology results for genes downregulated at day one in the modiolus. Genes upregulated at day one were analysed for enriched biological function terms using the gene ontology package GOSep. 93 significant terms ($P < 0.05$) were returned and ordered by significance.

	GO ID	Term	P
1	GO:0061448	Connective tissue development	8.20×10^{-5}
2	GO:0030199	Collagen fibril organization	1.25×10^{-4}
3	GO:0001501	Skeletal system development	1.87×10^{-4}
4	GO:0032501	Multicellular organismal process	1.96×10^{-4}
5	GO:0048705	Skeletal system morphogenesis	1.96×10^{-4}
6	GO:0030198	Extracellular matrix organization	1.96×10^{-4}
7	GO:0043062	Extracellular structure organization	1.96×10^{-4}
8	GO:0044707	Single-multicellular organism process	2.14×10^{-4}
9	GO:0006952	Defense response	2.36×10^{-4}
10	GO:0051216	Cartilage development	2.38×10^{-4}

5.3 Gene Expression Changes Seven Days after Noise Exposure

After 7 days recovery, noise exposed modiolus had 188 genes differentially expressed compared to sham exposed controls. Of these, 57 genes were significantly upregulated ($\Delta > 2.0$, FDR < 0.05) and 131 genes were significantly downregulated ($\Delta < 0.5$, FDR < 0.05). The top 20 upregulated and downregulated genes are shown in Table 5.5. Plots of the data show a skew to overall fold changes which were more concentrated at $\Delta < 1.0$ (Figure 5.2A). This could suggest that the higher proportion of downregulated genes is due to a change in the distribution of control data; although this is not reflected in Figure 5.2B.

Shown in Table 5.6, 16 genes were upregulated from zero FPKM in control and 6 genes were downregulated to zero FPKM after AOE. Of these, the largest change seen is fatty acid binding protein 1 (*Fabp1*) which was increased to 25.38 FPKM after noise. Like with the day 1 group, serum Albumin (*Alb*) remains highly upregulated at 72x control. The largest upwards changes seen at day seven include all three fibrinogen subunits (*Fga*, *Fgb*, and *Fgg*), three Serum Amyloid A subunits (*Saa1*, *Saa2*, *Saa3*), and five apolipoproteins (*Apoa1*, *Apob*, *Apoc1*, *Apoc3*, and *ApoH*).

Nine of the top 20 upregulated genes had been previously changed at day one. Of the top 20 downregulated, just one had previously been downregulated at day one; however these two time points shared many other downregulated genes such as integrins $\beta 3$ (*Itgb3*) and $\alpha 2b$ (*Itga2b*), calprotectin genes calgranulin A (*S100a8*) and calgranulin B (*S100a9*), and fibrillar collagens 11 $\alpha 1$ (*Col11a1*), 22 $\alpha 1$ (*Col22a1*), 5 $\alpha 1$ (*Col5a1*).

Downregulated changes to the modiolus include platelet associated proteins, Pro-platelet basic protein (*Ppbp*) and Tubulin $\beta 1$ (*Tubb1*), and several muscle associated proteins such as members of the Myosin superfamily: *Myh2*, *Myh4*, *Mylpf*, and *Myoz1*.

Gene Expression Changes in the Modiolus Follow Noise Exposure

The upregulated Ribonuclease P RNA-like 2 (*Rprl2*) has reads of 10.66 FPKM after AOE (Table 5.6); however this gene transcribes non-coding RNA and has unknown function, so few conclusions could be drawn about its effects here. Ankyrin repeat domain 1 (*Ankrd1*) is downregulated in Table 5.6; however as the controls for day one and day 28 have zero reads for Ankrd1 this may be a false reading.

Gene ontology of upregulated genes returned 54 significant terms ($P < 0.05$). The top 20 of these are shown in (Table 5.8).

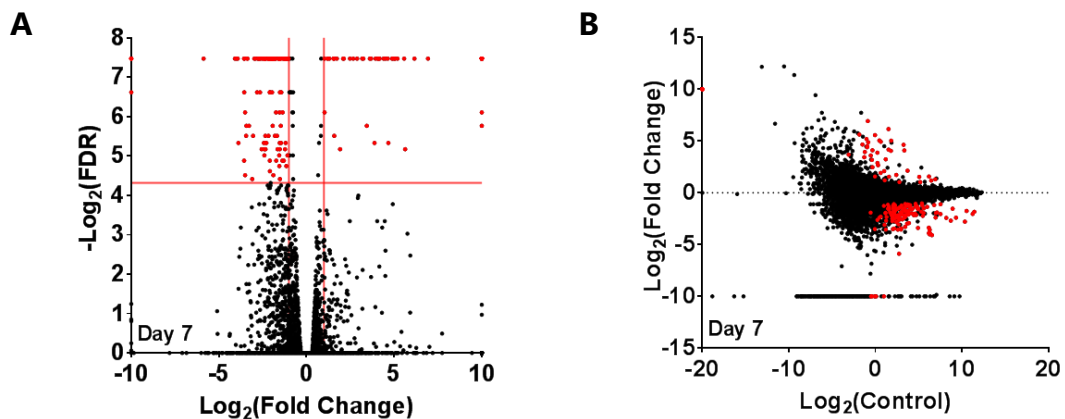


Figure 5.2: Volcano (A) and MA plot (B) of differentially expressed genes at day seven in the modiolus. Plots were constructed using a Log_2 transforms of fold change (Δ), false discovery rate (FDR) and mean control FPKM. Red lines represent cut off values of $\text{FDR} < 0.05$ and $\Delta > 2$ or $\Delta < 0.5$. Genes which satisfy these conditions have been coloured red.

Gene Expression Changes in the Modiolus Follow Noise Exposure

Table 5.5 Differentially expressed genes at day seven in the modiolus. The top 20 changed genes at day seven listed in order of biggest change. For each gene, the average control and experimental (AOE) FPKM values are listed along with a Log₂ transform of fold change (Δ) and the significance value (FDR). Genes which also had differential expression at day one are highlighted by asterisk (*). For changes where either control or AOE FPKM equal zero, a true ratio of change cannot be determined; these changes are shown in Table 5.6.

Top 20 Upregulated					Top 20 Downregulated				
Gene	Control	AOE	Log ₂ Δ	FDR	Gene	Control	AOE	Log ₂ Δ	FDR
<i>Fgb*</i>	0.54	66.14	6.93	0.006	<i>Myh4</i>	6.63	0.11	-5.87	0.006
<i>Alb*</i>	2.86	205.00	6.16	0.006	<i>Ppbbp*</i>	92.77	5.48	-4.08	0.006
<i>Serpina1b</i>	0.28	13.69	5.63	0.028	<i>Tnnc2</i>	77.27	4.83	-4.00	0.006
<i>Apoa1*</i>	0.96	45.97	5.57	0.006	<i>Mylpf</i>	80.63	5.32	-3.92	0.006
<i>Fga</i>	0.49	17.96	5.19	0.006	<i>Tnnt3</i>	71.83	4.86	-3.89	0.025
<i>Serpina3k*</i>	1.37	45.69	5.06	0.006	<i>Acta1</i>	76.67	6.50	-3.56	0.006
<i>Hpx*</i>	3.54	115.77	5.03	0.006	<i>Klhl41</i>	2.28	0.19	-3.56	0.034
<i>Fgg</i>	1.53	46.94	4.94	0.006	<i>Rgs18</i>	5.99	0.51	-3.55	0.010
<i>Itih4</i>	0.57	16.72	4.89	0.006	<i>Clec1b</i>	7.73	0.67	-3.54	0.006
<i>Serpina1d</i>	0.35	9.02	4.67	0.025	<i>Myh2</i>	0.95	0.08	-3.50	0.044
<i>Saa2*</i>	9.55	237.81	4.64	0.006	<i>Gp5</i>	4.03	0.36	-3.50	0.014
<i>Ambp</i>	0.52	11.82	4.51	0.006	<i>Tubb1</i>	4.55	0.42	-3.45	0.022
<i>Gc</i>	0.51	10.85	4.41	0.006	<i>Myoz1</i>	7.85	0.73	-3.43	0.018
<i>Ahsg</i>	2.87	51.79	4.17	0.006	<i>Ckm</i>	30.25	2.88	-3.39	0.006
<i>Apoh*</i>	0.79	13.63	4.11	0.006	<i>Tnni2</i>	71.87	7.01	-3.36	0.006
<i>Saa1*</i>	10.12	173.81	4.10	0.006	<i>Atp2a1</i>	10.76	1.11	-3.28	0.018
<i>Orm1*</i>	3.47	57.84	4.06	0.006	<i>Spib</i>	2.08	0.24	-3.10	0.047
<i>Aldob</i>	0.43	6.56	3.94	0.006	<i>Nrgn</i>	6.37	0.77	-3.05	0.022
<i>Apoc3</i>	1.17	17.31	3.88	0.025	<i>Slc4a1</i>	12.64	1.62	-2.97	0.006
<i>Apob*</i>	0.12	1.50	3.68	0.006	<i>Car1</i>	14.59	1.93	-2.92	0.006

Table 5.6 Day seven changes for which fold change cannot be calculated in the modiolus. Differentially expressed genes which have a control or experimental value of zero have been excluded from the top 20 changed genes as fold change cannot be determined. For each gene, the average control and experimental (AOE) FPKM values are listed along the significance value (FDR). Genes which also had differential expression at day one are highlighted by asterisk (*).

Upregulated				Downregulated			
Gene	Control	AOE	FDR	Gene	Control	AOE	FDR
<i>Fabp1</i>	0	25.38	0.006	<i>Ankrd1</i>	1.99	0	0.006
<i>Rprl2</i>	0	10.66	0.006	<i>4930444P10Rik</i>	1.06	0	0.006
<i>Igfbp1</i>	0	3.11	0.006	<i>Gm12839</i>	0.94	0	0.010
<i>Afm*</i>	0	1.84	0.006	<i>Dsccl</i>	0.76	0	0.006
<i>Itih1</i>	0	1.71	0.006	<i>Tceal7</i>	0.74	0	0.006
<i>Leap2</i>	0	1.51	0.014	<i>4833423E24Rik</i>	0.71	0	0.006
<i>Cyp2c70</i>	0	1.24	0.006				
<i>C4bp</i>	0	1.23	0.006				
<i>Lect2*</i>	0	1.15	0.006				
<i>Sult2a2</i>	0	1.08	0.006				
<i>Sult2a5</i>	0	1.02	0.006				
<i>Mup3</i>	0	0.98	0.006				
<i>Sult2a6</i>	0	0.83	0.006				
<i>Agxt</i>	0	0.82	0.006				
<i>Prodh2</i>	0	0.81	0.006				
<i>Ugt2b36</i>	0	0.67	0.006				

Gene Expression Changes in the Modiolus Follow Noise Exposure

Table 5.7: The top 10 Gene Ontology results for genes upregulated at day seven in the modiolus. Genes

upregulated at day one were analysed for enriched biological function terms using the gene ontology package GOSep. 54 significant terms ($P < 0.05$) were returned and ordered by significance.

	GO ID	Term	P
1	GO:0002526	Acute inflammatory response	$< 1.00 \times 10^{-12}$
2	GO:0006953	Acute-phase response	$< 1.00 \times 10^{-12}$
3	GO:0010466	Negative regulation of peptidase activity	1.68×10^{-6}
4	GO:0051346	Negative regulation of hydrolase activity	6.80×10^{-6}
5	GO:0043086	Negative regulation of catalytic activity	5.15×10^{-5}
6	GO:0052547	Regulation of peptidase activity	1.32×10^{-4}
7	GO:0006954	Inflammatory response	1.32×10^{-4}
8	GO:0008202	Steroid metabolic process	2.56×10^{-4}
9	GO:0010951	Negative regulation of endopeptidase activity	4.41×10^{-4}
10	GO:0006641	Triglyceride metabolic process	4.41×10^{-4}

Table 5.8: The top 10 Gene Ontology results for genes downregulated at day seven in the modiolus. Genes upregulated at day one were analysed for enriched biological function terms using the gene ontology package GOSep. 118 significant terms ($P < 0.05$) were returned and ordered by significance.

	GO ID	Term	P
1	GO:0044707	Single-multicellular organism process	5.68×10^{-12}
2	GO:0032501	Multicellular organismal process	1.09×10^{-11}
3	GO:0002376	Immune system process	1.37×10^{-9}
4	GO:0044699	Single-organism process	2.66×10^{-5}
5	GO:0009605	Response to external stimulus	5.49×10^{-5}
6	GO:0034109	Homotypic cell-cell adhesion	6.37×10^{-5}
7	GO:0006936	Muscle contraction	7.43×10^{-5}
8	GO:0048513	Organ development	2.97×10^{-4}
9	GO:0050900	Leukocyte migration	2.97×10^{-4}
10	GO:0042742	Defense response to bacterium	3.00×10^{-4}

5.4 Gene Expression Changes 28 Days after Noise Exposure

After 28 days recovery, noise exposed modiolus had 113 differentially expressed genes compared to sham exposed controls. Of these, 60 genes were significantly upregulated ($\Delta > 2.0$, FDR < 0.05), and 53 significantly downregulated ($\Delta < 0.5$, FDR < 0.05). The top 20 upregulated and downregulated genes are summarised in Table 5.9. Plots of the data shows that significant changes were clustered around genes which were expressed at low to mid-levels in control (Figure 5.3B), and more variation in the magnitude of significantly upregulated genes (Figure 5.3A).

Shown in Table 5.10, eight genes were upregulated from zero FPKM in control and just one gene was downregulated to zero FPKM after AOE. Like with day seven, the largest of these changes was seen in *Fabp1*, which is upregulated to 6.8 FPKM after AOE. In addition to this, the related fatty acid binding protein (*Fabp4*) is also upregulated at 28 days (20x control). The largest downregulated change at day 28 is seen with Gamma-aminobutyric acid (GABA) receptor B2 (*Gabbr2*), which is expressed at 0.26x control levels following noise.

A high proportion of the highest upregulated changes are chronically expressed, with 17 of the 20 also upregulated at day seven, of which 8 have been upregulated since day one. None of the downregulated genes at day 28 had previously been changed at either of the prior time points.

Gene ontology analysis of significantly upregulated genes returned 206 significant terms ($P < 0.05$), the top 10 of these are shown in Table 5.11. As with the first two time points, the top 2 terms are related to the acute phase and inflammatory response. However, at this time point many of the top terms were associated with lipid localisation, metabolism, and storage.

Gene ontology of downregulated genes returned no significantly over represented terms.

Gene Expression Changes in the Modiolus Follow Noise Exposure

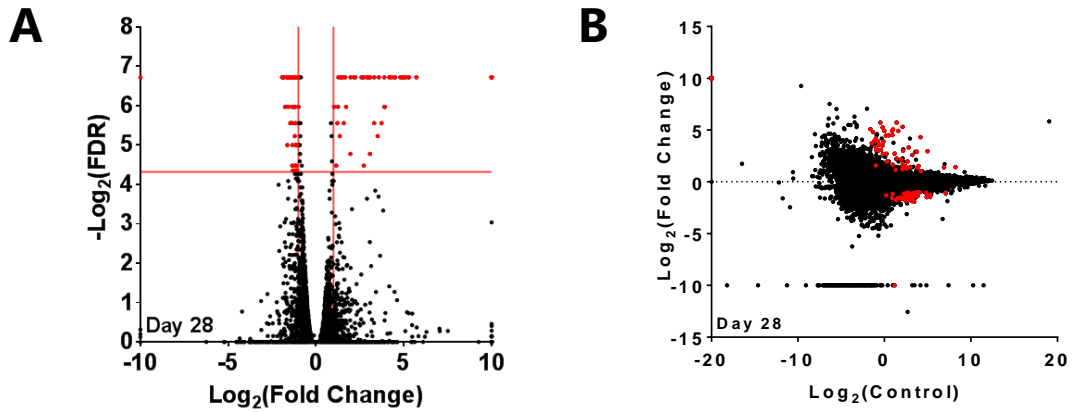


Figure 5.3 Volcano (A) and MA plot (B) of differentially expressed genes at day 28 in the modiolus. Plots were constructed using a Log_2 transforms of fold change (Δ), false discovery rate (FDR) and mean control FPKM. Red lines represent cut off values of $\text{FDR} < 0.05$ and $\Delta > 2$ or $\Delta < 0.5$. Genes which satisfy these conditions have been coloured red.

Table 5.9: Differentially expressed genes at day 28 in the modiolus. The top 20 changed genes at day seven listed in order of biggest change. For each gene, the average control and experimental (AOE) FPKM values are listed along with a Log_2 transform of fold change (Δ) and the significance value (FDR). Genes which also had differential expression at day seven are highlighted by asterix (*), and genes which were changed at day seven and day one are denoted by a double asterix (**). For changes where either control or AOE FPKM equal zero, a true ratio of change cannot be determined; these changes are shown in Table 5.10.

Top 20 Upregulated					Top 20 Downregulated				
Gene	Control	AOE	$\text{Log}_2\Delta$	FDR	Gene	Control	AOE	$\text{Log}_2\Delta$	FDR
<i>Saa1</i> **	2.63	139.02	5.72	0.009	<i>Gabbr2</i>	10.82	2.84	-1.93	0.009
<i>Fgb</i> **	0.72	37.92	5.72	0.009	<i>Uhmk1</i>	8.95	2.47	-1.86	0.009
<i>Saa2</i> **	4.28	169.54	5.31	0.009	<i>Bmpr2</i>	5.43	1.54	-1.82	0.009
<i>Fgg</i> *	0.86	32.91	5.26	0.009	<i>Npas2</i>	2.56	0.75	-1.76	0.016
<i>Itih4</i> *	0.32	11.05	5.09	0.009	<i>Crhr1</i>	6.97	2.20	-1.66	0.009
<i>Hpx</i> **	2.00	66.60	5.06	0.009	<i>Sv2c</i>	6.25	1.98	-1.66	0.009
<i>Serpina3k</i> **	0.99	30.20	4.93	0.009	<i>Nos1</i>	6.84	2.19	-1.64	0.009
<i>Alb</i> **	3.03	91.55	4.92	0.009	<i>Cacng2</i>	3.87	1.26	-1.62	0.031
<i>Ucp1</i>	1.84	55.58	4.91	0.009	<i>Dvl3</i>	9.61	3.17	-1.60	0.009
<i>Fga</i> *	0.40	11.15	4.80	0.009	<i>Lnpep</i>	2.84	0.95	-1.58	0.009
<i>Orm1</i> **	1.89	43.30	4.51	0.009	<i>Spred2</i>	4.63	1.55	-1.58	0.016
<i>Ahsg</i> *	1.41	31.91	4.50	0.009	<i>Eif2c2</i>	1.86	0.63	-1.57	0.009
<i>Apoa1</i> **	1.12	24.76	4.47	0.009	<i>Sned1</i>	7.41	2.54	-1.54	0.009
<i>Fabp4</i>	17.96	356.96	4.31	0.009	<i>Trip11</i>	3.64	1.30	-1.48	0.009
<i>Cidec</i>	0.50	9.08	4.18	0.009	<i>Syt2</i>	29.53	10.62	-1.48	0.009
<i>Gc</i> *	0.44	6.79	3.93	0.016	<i>Stx1b</i>	38.69	13.99	-1.47	0.009
<i>Adipoq</i>	0.92	13.67	3.89	0.009	<i>Lancl3</i>	5.25	1.91	-1.46	0.021
<i>H2-Q10</i>	0.59	8.79	3.89	0.016	<i>Ptch1</i>	5.54	2.04	-1.44	0.009
<i>Mat1a</i> *	0.36	4.82	3.73	0.021	<i>Kcnq4</i>	6.18	2.29	-1.43	0.021
<i>Pck1</i>	0.66	7.91	3.59	0.009	<i>Peg3</i>	9.58	3.60	-1.41	0.009

Gene Expression Changes in the Modiolus Follow Noise Exposure

Table 5.10 Day 28 changes for which fold change cannot be calculated in the modiolus.

Differentially expressed genes which have a control or experimental value of zero have been excluded from the top 20 changed genes as fold change cannot be determined. For each gene, the average control and experimental (AOE) FPKM values are listed along the significance value (FDR).

Upregulated				Downregulated			
Gene	Control	AOE	FDR	Gene	Control	AOE	FDR
<i>Fabp1</i>	0	6.81	0.009	<i>Lgals7</i>	2.26	0	0.009
<i>Apoc4</i>	0	4.08	0.009				
<i>Orm2</i>	0	3.80	0.009				
<i>Ttc36</i>	0	3.02	0.009				
<i>Serpina3m</i>	0	2.54	0.009				
<i>Azgp1</i>	0	2.28	0.009				
<i>Apom</i>	0	1.30	0.009				
<i>Saa4</i>	0	1.02	0.009				

Table 5.11: The top 10 Gene Ontology results for genes upregulated at day 28 in the modiolus. Genes upregulated at day one were analysed for enriched biological function terms using the gene ontology package GOSeq. 206 significant terms ($P < 0.05$) were returned and ordered by significance.

	GO ID	Term	P
1	GO:0002526	Acute inflammatory response	$< 1.00 \times 10^{-12}$
2	GO:0006953	Acute-phase response	$< 1.00 \times 10^{-12}$
3	GO:0010876	Lipid localization	$< 1.00 \times 10^{-12}$
4	GO:0006954	Inflammatory response	9.84×10^{-8}
5	GO:0006641	Triglyceride metabolic process	6.67×10^{-7}
6	GO:0006629	Lipid metabolic process	1.57×10^{-6}
7	GO:0006639	Acylglycerol metabolic process	2.09×10^{-6}
8	GO:0019915	Lipid storage	2.09×10^{-6}
9	GO:0046486	Glycerolipid metabolic process	2.09×10^{-6}
10	GO:0006638	Neutral lipid metabolic process	2.09×10^{-6}

5.5 Neuron Specific Changes in the Modiolus

From each modiolus, a variety of tissue types will be present in the tissue taken. In addition to the SGNs samples will contain bone, connective tissue, and glia. To assess any neuron specific changes, gene lists were filtered base on published gene ontology data.

Differentially expressed genes at each time point were cross matched against a list of 1529 genes with the annotation "neuronal part" (GO:0097458), which was downloaded from the AmiGO gene ontology online resource. From the total list of differentially expressed genes, 57 had the annotation neuronal part. Of these, 17 were upregulated at one or more time point (see Table 5.12), and 40 downregulated at one or more time point (see Table 5.13).

The majority of genes identified as neuron specific appear in just one time point, with the exception of: Apolipoprotein B (*Apob*) and P2X purinoceptor 3 (*P2xr3*) which were upregulated at day one and seven; Group specific component (*Gc*) which was upregulated at day seven and 28; and Bone γ -carboxyglutamate protein 1 and 2 (*Bglap*, *Bglap2*) and cytochrome b-245 β (*Cybb*) which were downregulated at day one and seven.

Early upregulated gene *P2rx3* is discussed in §5.5.1.

Gene Expression Changes in the Modiolus Follow Noise Exposure

Table 5.12: Neuron specific genes upregulated at each time point in the modiolus. Genes highlighted at significantly upregulated (FDR < 0.05) were filtered based on annotations for the gene ontology term "neuron part" (GO: 0097458). For each gene, the average control and experimental (AOE) FPKM values are listed along with a Log₂ transform of fold change (Δ) and the significance value (FDR).

Day 1: Upregulated					
Gene	Protein	Control	AOE	Log ₂ Δ	FDR
<i>Crp</i>	C-reactive protein	0.0	3.0	∞	5.4×10^{-3}
<i>Apob</i>	Apolipoprotein B	0.1	2.3	4.4	5.4×10^{-3}
<i>Calca</i>	Calcitonin α	2.8	39.4	3.8	5.4×10^{-3}
<i>Synpr</i>	Synaptoporin	0.6	6.2	3.3	5.4×10^{-3}
<i>Htr3a</i>	5-hydroxytryptamine receptor 3A	0.5	4.5	3.2	4.3×10^{-2}
<i>Prph</i>	Peripherin	4.2	25.3	2.6	5.4×10^{-3}
<i>Tac1</i>	Tachykinin 1	5.7	29.2	2.4	5.4×10^{-3}
<i>P2rx3</i>	P2X, ligand-gated ion channel, 3	0.5	2.4	2.1	3.7×10^{-2}
<i>Gad1</i>	Glutamate Decarboxylase 1	2.1	5.6	1.4	4.9×10^{-2}
<i>Pcp4</i>	Purkinje cell protein 4	233.7	586.9	1.3	5.4×10^{-3}
<i>Syt1</i>	Synaptotagmin I	1.9	4.6	1.3	3.5×10^{-2}
<i>C4b</i>	Complement component 4B	5.4	10.7	1.0	1.0×10^{-2}
<i>Gria2</i>	Glutamate receptor, ionotropic, AMPA2 (α 2)	2.8	5.3	0.9	4.6×10^{-2}
<i>Stmn4</i>	Stathmin-like 4	88.8	165.2	0.9	5.8×10^{-3}
<i>Sncg</i>	Synuclein, γ	640.5	1137.1	0.8	4.1×10^{-2}
<i>Calb1</i>	Calbindin 1	17.3	30.1	0.8	1.9×10^{-2}

Day 7: Upregulated					
Gene	Protein	Control	AOE	Log ₂ Δ	FDR
<i>Gc</i>	Group specific component	0.5	10.8	4.4	5.6×10^{-3}
<i>Apob</i>	Apolipoprotein B	0.1	1.5	3.7	5.6×10^{-3}
<i>P2rx3</i>	P2X, ligand-gated ion channel, 3	1.0	2.9	1.6	2.2×10^{-2}

Day 28: Upregulated					
Gene	Protein	Control	AOE	Log ₂ Δ	FDR
<i>Gc</i>	Group specific component	0.4	6.8	3.9	1.6×10^{-2}
<i>Prph</i>	Peripherin	5.3	15.4	1.5	9.5×10^{-3}
<i>Stmn4</i>	Stathmin-like 4	57.8	104.7	0.9	2.1×10^{-2}

Gene Expression Changes in the Modiolus Follow Noise Exposure

Table 5.13: Neuron specific genes downregulated at each time point in the modiolus. Genes highlighted at significantly downregulated (FDR < 0.05) were filtered based on annotations for the gene ontology term "neuron part" (GO: 0097458). For each gene, the average control and experimental (AOE) FPKM values are listed along with a Log₂ transform of fold change (Δ) and the significance value (FDR).

Day 1: Downregulated					
Gene	Protein	Control	AOE	Log ₂ Δ	FDR
<i>Bglap2</i>	Bone γ-carboxyglutamate protein 2	85.8	23.7	-1.9	5.4x10 ⁻³
<i>Crhbp</i>	Corticotropin releasing hormone binding	124.2	43.3	-1.5	5.4x10 ⁻³
<i>Bglap</i>	Bone γ-carboxyglutamate protein	320.1	118.3	-1.4	5.4x10 ⁻³
<i>Syt2</i>	Synaptotagmin II	16.5	6.6	-1.3	5.4x10 ⁻³
<i>Cybb</i>	Cytochrome b-245, β polypeptide	5.1	2.3	-1.1	3.2x10 ⁻²
<i>Clstn1</i>	Calsyntenin 1	126.8	68.1	-0.9	2.2x10 ⁻²
<i>Brsk1</i>	BR serine/threonine kinase 1	33.9	18.8	-0.8	3.7x10 ⁻²
<i>Kcnc3</i>	Potassium voltage gated channel Kv3.3	40.5	22.8	-0.8	1.5x10 ⁻²
<i>Pacsin1</i>	Protein kinase C substrate in neurons 1	31.9	18.3	-0.8	2.2x10 ⁻²
<i>Rgma</i>	Repulsive guidance molecule member A	23.2	13.6	-0.8	2.2x10 ⁻²
<i>Slc6a17</i>	Solute carrier family 6, member 17	34.1	20.5	-0.7	4.6x10 ⁻²

Day 7: Downregulated					
Gene	Protein	Control	AOE	Log ₂ Δ	FDR
<i>Nrgn</i>	Neurogranin	6.4	0.8	-3.0	2.2x10 ⁻²
<i>Spta1</i>	Spectrin α, erythrocytic 1	1.2	0.2	-2.6	5.6x10 ⁻³
<i>Bglap</i>	Bone γ-carboxyglutamate protein	637.7	120.5	-2.4	5.6x10 ⁻³
<i>Calca</i>	Calcitonin	14.8	3.8	-2.0	1.0x10 ⁻²
<i>Bglap2</i>	Bone γ-carboxyglutamate protein 2	126.4	32.8	-1.9	5.6x10 ⁻³
<i>Slc40a1</i>	Solute carrier family 40), member 1	5.0	1.8	-1.5	1.0x10 ⁻²
<i>Coro1a</i>	Coronin, actin binding protein 1A	41.5	20.6	-1.0	5.6x10 ⁻³
<i>Cybb</i>	Cytochrome b-245, beta polypeptide	5.3	2.7	-1.0	3.1x10 ⁻²
<i>Ncf1</i>	Neutrophil cytosolic factor 1	12.4	6.5	-0.9	1.0x10 ⁻²
<i>Hmbs</i>	Hydroxymethylbilane synthase	32.4	19.1	-0.8	1.4x10 ⁻²
<i>Otof</i>	Otofelin	11.1	6.6	-0.8	1.0x10 ⁻²

Day 28: Downregulated					
Gene	Protein	Control	AOE	Log ₂ Δ	FDR
<i>Gabbr2</i>	Gamma-aminobutyric acid (GABA) B2	10.8	2.8	-1.9	9.5x10 ⁻³
<i>Uhmk1</i>	U2AF homology motif (UHM) kinase 1	8.9	2.5	-1.9	9.5x10 ⁻³
<i>Bmpr2</i>	Bone morphogenetic protein receptor (II)	5.4	1.5	-1.8	9.5x10 ⁻³
<i>Crhr1</i>	Corticotropin releasing hormone receptor 1	7.0	2.2	-1.7	9.5x10 ⁻³
<i>Sv2c</i>	Synaptic vesicle glycoprotein 2c	6.2	2.0	-1.7	9.5x10 ⁻³
<i>Nos1</i>	Nitric oxide synthase 1, neuronal	6.8	2.2	-1.6	9.5x10 ⁻³
<i>Syt2</i>	Synaptotagmin II	29.5	10.6	-1.5	9.5x10 ⁻³
<i>Stx1b</i>	Syntaxin 1B	38.7	14.0	-1.5	9.5x10 ⁻³
<i>Ptch1</i>	Patched 1	5.5	2.0	-1.4	9.5x10 ⁻³
<i>Kcnq4</i>	Potassium voltage-gated channel, Kv7.4	6.2	2.3	-1.4	2.1x10 ⁻²
<i>Dpysl3</i>	Dihydropyrimidinase-like 3	11.3	4.9	-1.2	2.7x10 ⁻²
<i>Crtac1</i>	Cartilage acidic protein 1	11.6	5.1	-1.2	1.6x10 ⁻²
<i>Adcy9</i>	Adenylate cyclase 9	4.8	2.1	-1.2	4.5x10 ⁻²
<i>Fos</i>	FBJ osteosarcoma oncogene	9.0	4.0	-1.2	4.9x10 ⁻²
<i>Mib1</i>	Mindbomb E3 ubiquitin protein ligase 1	5.8	2.6	-1.2	3.1x10 ⁻²
<i>Crhbp</i>	Corticotropin releasing hormone binding	135.7	62.1	-1.1	9.5x10 ⁻³

Gene Expression Changes in the Modiolus Follow Noise Exposure

Table 5.13 continued: Neuron specific genes downregulated at each time point in the modiolus. Genes highlighted at significantly downregulated (FDR < 0.05) were filtered based on annotations for the gene ontology term “neuron part” (GO: 0097458). For each gene, the average control and experimental (AOE) FPKM values are listed along with a Log₂ transform of fold change (Δ) and the significance value (FDR).

Day 28: Downregulated					
Gene	Protein	Control	AOE	Log ₂ Δ	FDR
<i>Ptpn5</i>	Protein tyrosine phosphatase non-receptor 5	10.7	5.0	-1.1	3.1x10 ⁻²
<i>Rph3a</i>	Rabphilin 3A	28.7	14.0	-1.0	9.5x10 ⁻³
<i>Plcb4</i>	Phospholipase C, beta 4	13.8	6.9	-1.0	1.6x10 ⁻²
<i>Shank1</i>	SH3/ankyrin domain gene 1	5.1	2.6	-1.0	1.6x10 ⁻²
<i>Dst</i>	Dystonin	36.6	18.8	-1.0	3.1x10 ⁻²
<i>Rap1gap2</i>	RAP1 GTPase activating protein 2	8.4	4.5	-0.9	3.1x10 ⁻²
<i>Pacsin1</i>	Protein kinase C substrate in neurons 1	47.7	26.4	-0.9	9.5x10 ⁻³
<i>Cntnap1</i>	Contactin associated protein-like 1	21.4	12.2	-0.8	4.5x10 ⁻²

5.5.1 *P2rx3*

P2X purinoceptor 3 (*P2rx3*) encodes the P2X₃ receptor protein to form a non-selective, ATP-gated, ion channel expressed in sensory ganglia (Collo et al., 1996). In the mouse cochleae, P2X₃ is shown to be transiently expressed in the hair cells and SGN soma but only in the embryo and first 10 days postnatally, before onset of hearing (Huang et al., 2006).

Here, in the modiolus samples, the P2X₃ transcript has average control expression of 0.54 ± 0.17 FPKM placing it just at the limits of being detectable (0.6 - 1.0 FPKM, see §4.2.2 for a discussion of this cut off value). After noise, *P2rx3* was significantly upregulated, more than 2-fold, at one and seven days (see Table 5.12). This upregulation was consistent across all 12 coding exons (Figure 5.4A).

To investigate whether this change in transcript translates to a change of protein cochleae western blots were performed on control and AOE whole cochleae samples at one day recovery (Figure 5.4). Western blotting results from the noise exposed cochlea were inconclusive, showing a large range of intra-animal variability in levels of expression; however P2X₃ was detected consistently in all 4 control (adult) samples (Figure 5.4C), which does not support data shown by Huang et al. (2006).

Validation of the P2X₃ antibody was performed on whole brain lysate and in adult dorsal root ganglion (DRG) sections where it was shown to have consistent patterns of expression to that which has been previously published (Bradbury et al., 1998, Vulchanova et al., 1998, Petruska et al., 2000). Furthermore, staining was blocked when incubated with equal concentrations of peptide. Sections of P4 and P11 cochleae were taken to be compared against the P40 cochlea. Immunolabelling at P4 was consistent with results reported by (Huang et al., 2006), and was reduced by P11 (Figure 5.5A-B).

In the P40 cochlea signal was still apparent, but concentrated to a single area of punctate staining in each SGN cell body (Figure 5.5C). From these experiments,

Gene Expression Changes in the Modiolus Follow Noise Exposure

the location of P2X₃ in the adult could not be determined, but could be associated with the axon initial segment, or internalised in the endoplasmic reticulum. To test specificity of the antibody, sections co-incubated with blocking peptide (Figure 5.6); punctate staining of SGNs was absent in both the secondary antibody control and in the peptide block absorption controls. Sections from noise exposed cochleae showed a staining pattern identical to that seen in the control P40 animal.

Based on RNASeq results at one and seven days mRNA expression of P2X₃ appears to be increased in the spiral ganglion following noise exposure. This would be a significant result as P2X_{2/3} heteromultimeric channels have been suggested to be responsible for an increase in ATP induced inward currents in neonate rat SGN (Salih et al., 2002), increasing excitability. Based on the western blotting and immunohistochemistry, it is not clear whether this change is translated to protein consistently across the noise exposed modiolus, or whether P2X₃ is able to form functional channels in the adult SGN. Given that the amount of protein extracted from the modioli of a single cochlea is small, it is likely that the amount of P2X₃ present in the lysate is small, and close to detection limits. By increasing the protein concentration and relative P2X₃ concentration a clearer result may be obtained. This could be achieved either through the pooling of both cochleae or by collecting and pooling several isolated modioli in each group.

Gene Expression Changes in the Modiolus Follow Noise Exposure

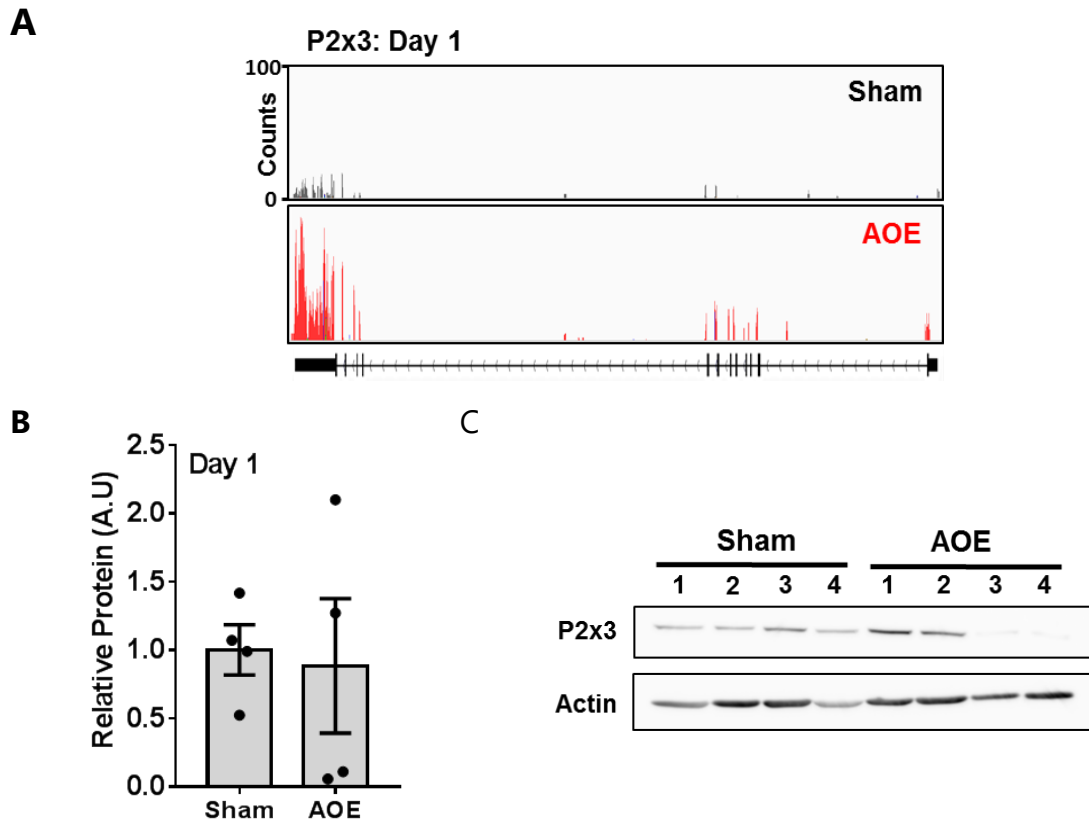


Figure 5.4 mRNA and protein expression levels of P2X₃ following noise exposure. (A) At day one, RNASeq results show a 4.28 fold increase of *P2rx3* mRNA in the noise exposed animals. (B-C) immunoblots of whole cochlea showed variable changes in protein levels P2X₃, with just one sample being significantly higher than control ($P = 0.009$), and two samples being significantly lower ($P = 0.016$ and $P = 0.014$) than control when measured with one-sample Student's T test (corrected for multiple comparisons). Sham exposed animals had consistent expression of P2X₃ protein.

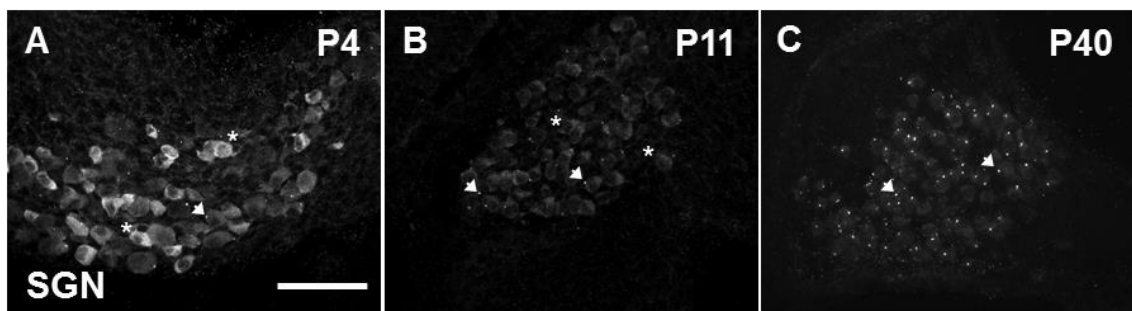


Figure 5.5 P2X₃ expression in the cochlea at three different developmental time points. (A) As previously reported by Huang et al. (2006), P2X₃ staining is apparent in SGN cell bodies pre-hearing (P4). (B) Around hearing onset (P11) staining is reduced, with a mixture of cell body staining (*) and punctate staining (arrow). (C) By P40, signal is concentrated to a single area of punctate labelling per SGN. Scale bar = 50 μ m.

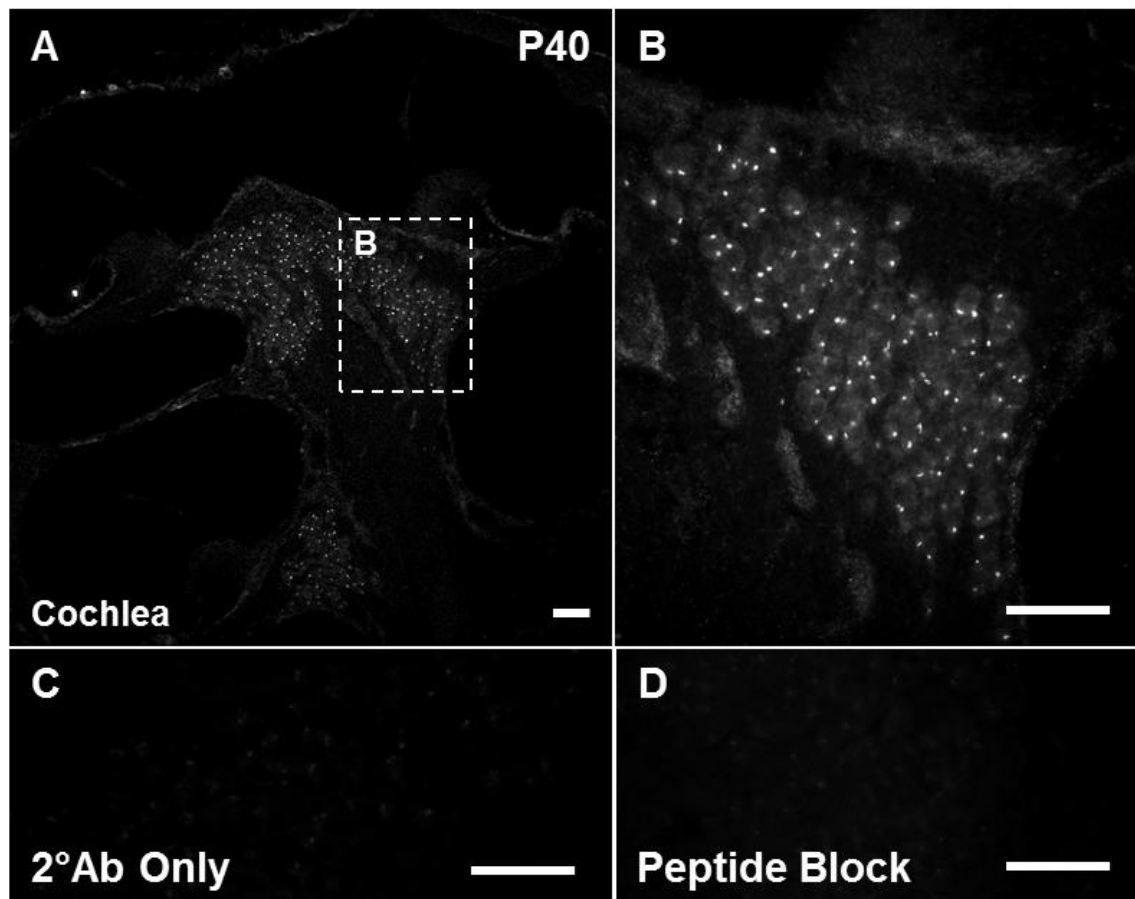


Figure 5.6 P2X₃ labelling is present in spiral ganglion cells in the adult cochlea. (A) Mid-modiolar sections of P40 cochlea show P2X₃ staining in SGNs at apical and basal regions. **(B)** Signal was observed at a 1:1 ratio with cell body, and appeared to be present in all SGNs imaged. **(C-D)** Staining was validated using secondary antibody controls and a peptide block. Scale bar = 50 μ m.

5.6 Acute Phase Proteins and the Immune Response

Gene ontology analysis at each individual time point showed upregulation of acute phase proteins (APPs) which persists to 28 days following auditory overexposure. APPs are proteins have differential concentrations (positive or negative) in response to infection, inflammation, or stress. Typically peaking within 24 - 48 hours following the triggering event, the acute phase response has a wide range of biological effects such as complement activation, leukocyte recruitment, and opsonisation (Suffredini et al., 1999).

In a review of APPs, (Cray et al., 2009) categorised APPs as either having a major positive response (>10x change), a moderate positive response (2 - 10x change), or minor positive response (minimal change). In mouse, haptoglobin (*Hp*), serum amyloid A (*Saa1-4*), and serum amyloid P (*Apcs*) are considered major APPs, whereas C-reactive protein (*Crp*), fibrinogen (*Fga*, *Fgb*, *Fgg*), and orosomucoid (*Orm1-2*) are considered moderate APPs.

Each of the identified major and moderate APPs are found to be upregulated at one or more time point in the modiolus samples following noise exposure (summarised in Table 5.14). Across species, the serum albumin is involved in the major negative response APP, however in the noise exposed modiolus *Alb* is the highest upregulated gene to be changed at all three time points (see Table 5.1, Table 5.5, and Table 5.9).

To assess the immune response at the spiral ganglion as a result of this acute phase response, the Iba-1 positive cochlear macrophages were compared between AOE and sham mice at day seven (Figure 5.7). Although there was not a marked increase in Iba-1 positive cells in the cochlea following AOE, more staining was observed around SGN dendrites in the osseous lamina following noise.

Gene Expression Changes in the Modiolus Follow Noise Exposure

Table 5.14 Summary of changes to acute phase proteins over time in the modiolus. 12 major and moderate acute phase proteins were identified as being differentially regulated at one or more time point over the 28 day period following noise. For each gene a Log₂ fold change (Δ) and significance value (FDR) is listed for each time point. Bold values signify significantly upregulated values (FDR < 0.05).

Acute Phase Proteins		Day 1		Day 7		Day 28	
Gene	Protein	Log ₂ Δ	FDR	Log ₂ Δ	FDR	Log ₂ Δ	FDR
<i>Hp</i>	Haptoglobin	1.6	5.4x10⁻³	1.5	5.6x10⁻³	3.3	9.5x10⁻³
<i>Saa1</i>	Serum amyloid A1	6.5	5.4x10⁻³	4.1	5.6x10⁻³	5.7	9.5x10⁻³
<i>Saa2</i>	Serum amyloid A2	6.8	5.4x10⁻³	4.6	5.6x10⁻³	5.3	9.5x10⁻³
<i>Saa3</i>	Serum amyloid A3	6.2	3.9x10 ⁻¹	3.2	5.6x10⁻³	4.6	4.8x10 ⁻¹
<i>Saa4</i>	Serum amyloid A4	∞	5.4x10⁻³	4.6	8.8x10 ⁻¹	∞	9.5x10⁻³
<i>Apcs</i>	Serum amyloid P	∞	5.4x10⁻³	4.5	9.8x10 ⁻²	6.3	8.4x10 ⁻¹
<i>Crp</i>	C-reactive protein	∞	5.4x10⁻³	NOTEST	1	NOTEST	1
<i>Fga</i>	Fibrinogen α	7.2	7.1x10 ⁻¹	5.2	5.6x10⁻³	4.8	9.5x10⁻³
<i>Fgb</i>	Fibrinogen β	6.9	5.4x10⁻³	6.9	5.6x10⁻³	5.7	9.5x10⁻³
<i>Fgg</i>	Fibrinogen γ	8.0	1.5x10 ⁻¹	4.9	5.6x10⁻³	5.3	9.5x10⁻³
<i>Orm1</i>	Orosomuroid 1	4.2	5.0x10⁻⁵	4.1	5.6x10⁻³	4.5	9.5x10⁻³
<i>Orm2</i>	Orosomuroid 2	∞	5.0x10⁻⁵	6.2	1	∞	9.5x10⁻³

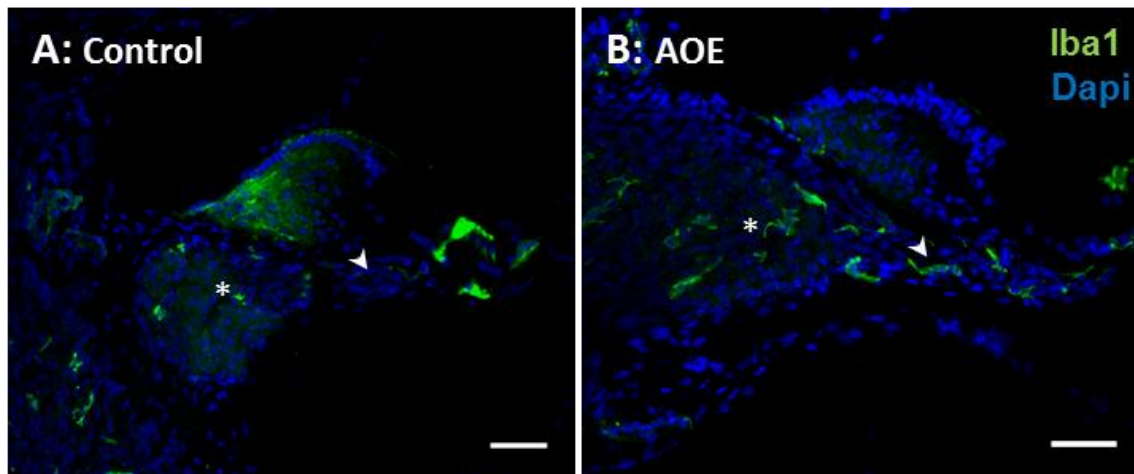


Figure 5.7 Location of Iba-1 positive cochlear macrophages seven days following noise. Although there was no marked increase in Iba-1 positive cells in the noise exposed cochlea (B) compared to sham exposed control (A), more staining was observed around the spiral ganglion dendrites (arrow) and cell bodies (*). Only one cochlea was taken for each condition. Scale bar = 50 μ m.

5.7 Programmed Cell Death

Based on previous work by Kujawa and Liberman (2006), one of the questions that we aimed to address was the cause of spiral ganglion cell loss following noise exposure. For this, gene lists were filtered by association to cell death pathways.

Differentially expressed genes at each time point were cross matched against a list of 1767 genes with the annotation "programmed cell death" (GO:0016244), which was downloaded from the AmiGO gene ontology online resource. From the total list of differentially expressed genes, 51 had the annotation neuronal part. Of these, 18 were upregulated at one or more time point (see Table 5.15), and 33 downregulated at one or more time point (see Table 5.16).

A persistent upregulation of fibrinogen β -chain (*Fgb*), serum albumin (*Alb*), and apolipoprotein H (*ApoH*) was seen at all three time points, while fibrinogen α -chain (*Fga*), fibrinogen γ -chain (*Fgg*), and fatty acid binding protein 1 (*Fabp1*) were upregulated at both seven days and 28 days post-AOE. Of the downregulated proteins, there were no genes changed over all three time points, but calcium binding proteins A8 (*S100a8*) and A9 (*S100a9*), matrix metalloproteinase 9 (*Mmp9*), and thrombospondin 1 (*Thbs1*) were downregulated at both one and seven days post-AOE.

Gene Expression Changes in the Modiolus Follow Noise Exposure

Table 5.15: Cell death associated genes upregulated at each time point in the modiolus.

Genes highlighted at significantly upregulated (FDR < 0.05) were filtered based on annotations for the gene ontology term “programmed cell death” (GO: 0016244). For each gene, the average control and experimental (AOE) FPKM values are listed along with a Log₂ transform of fold change (Δ) and the significance value (FDR).

Day 1: Upregulated					
Gene	Protein	Control	AOE	Log ₂ Δ	FDR
<i>Ankrd1</i>	Ankyrin repeat domain 1	0.0	5.8	∞	5.4x10 ⁻³
<i>Proc</i>	Protein C	0.0	1.4	∞	5.4x10 ⁻³
<i>Alb</i>	Albumin	1.3	199.7	7.2	5.4x10 ⁻³
<i>Fgb</i>	Fibrinogen β chain	0.5	66.2	6.9	5.4x10 ⁻³
<i>ApoH</i>	Apolipoprotein H	1.1	18.8	4.1	5.4x10 ⁻³
<i>Ccl12</i>	Chemokine (C-C motif) ligand 12	4.3	33.6	3.0	1.5x10 ⁻²
<i>Scg2</i>	Secretogranin II	2.5	7.4	1.6	5.4x10 ⁻³
<i>Atf3</i>	Activating transcription factor 3	4.9	13.0	1.4	5.4x10 ⁻³
<i>Pcp4</i>	Purkinje cell protein 4	233.7	586.9	1.3	5.4x10 ⁻³
<i>Wdr92</i>	WD repeat domain 92	30.4	55.4	0.9	2.2x10 ⁻²

Day 7: Upregulated					
Gene	Protein	Control	AOE	Log ₂ Δ	FDR
<i>Fabp1</i>	Fatty acid binding protein 1, liver	0.0	25.4	∞	5.6x10 ⁻³
<i>Fgb</i>	Fibrinogen β chain	0.5	66.1	6.9	5.6x10 ⁻³
<i>Alb</i>	Albumin	2.9	205.0	6.2	5.6x10 ⁻³
<i>Fga</i>	Fibrinogen α chain	0.5	18.0	5.2	5.6x10 ⁻³
<i>Fgg</i>	Fibrinogen γ chain	1.5	46.9	4.9	5.6x10 ⁻³
<i>ApoH</i>	Apolipoprotein H	0.8	13.6	4.1	5.6x10 ⁻³

Day 28: Upregulated					
Gene	Protein	Control	AOE	Log ₂ Δ	FDR
<i>Fabp1</i>	Fatty acid binding protein 1, liver	0.0	6.8	∞	9.5x10 ⁻³
<i>Fgb</i>	Fibrinogen β chain	0.7	37.9	5.7	9.5x10 ⁻³
<i>Fgg</i>	Fibrinogen γ chain	0.9	32.9	5.3	9.5x10 ⁻³
<i>Alb</i>	Albumin	3.0	91.6	4.9	9.5x10 ⁻³
<i>Fga</i>	Fibrinogen α chain	0.4	11.2	4.8	9.5x10 ⁻³
<i>Cidec</i>	Cell death-inducing DFFA-like effector C	0.5	9.1	4.2	9.5x10 ⁻³
<i>Adipoq</i>	Adiponectin, C1Q and collagen domain containing	0.9	13.7	3.9	9.5x10 ⁻³
<i>ApoH</i>	Apolipoprotein H	0.8	9.7	3.5	2.7x10 ⁻²
<i>Cidea</i>	Cell death-inducing DNA fragmentation factor, α subunit-like effector A	4.4	35.3	3.0	9.5x10 ⁻³
<i>Hspa1b</i>	Heat shock protein 1B	3.7	16.7	2.2	9.5x10 ⁻³
<i>Pdk4</i>	Pyruvate dehydrogenase kinase, isoenzyme 4	7.0	13.2	0.9	4.2x10 ⁻²

Gene Expression Changes in the Modiolus Follow Noise Exposure

Table 5.16: Cell death associated genes downregulated at each time point in the modiolus.

Genes highlighted at significantly downregulated (FDR < 0.05) were filtered based on annotations for the gene ontology term “programmed cell death” (GO: 0016244). For each gene, the average control and experimental (AOE) FPKM values are listed along with a Log₂ transform of fold change (Δ) and the significance value (FDR).

Day 1: Downregulated					
Gene	Protein	Control	AOE	Log ₂ Δ	FDR
<i>Adipoq</i>	Adiponectin	11.5	1.7	-2.7	3.2x10 ⁻²
<i>S100a9</i>	S100 calcium binding protein A9	1934.2	371.7	-2.4	5.4x10 ⁻³
<i>S100a8</i>	S100 calcium binding protein A8	2223.6	457.0	-2.3	5.4x10 ⁻³
<i>Mmp9</i>	Matrix metalloproteinase 9	7.4	1.9	-2.0	5.4x10 ⁻³
<i>Pglyrp1</i>	Peptidoglycan recognition protein 1	44.8	16.2	-1.5	5.4x10 ⁻³
<i>Thbs1</i>	Thrombospondin 1	10.4	3.9	-1.4	5.4x10 ⁻³
<i>Lrp5</i>	Low density lipoprotein receptor-related 5	6.9	3.5	-1.0	3.5x10 ⁻²
<i>Col2a1</i>	Collagen, type II, α 1	41.4	21.2	-1.0	5.4x10 ⁻³
<i>Pf4</i>	Platelet factor 4	103.7	54.8	-0.9	4.6x10 ⁻²
<i>Ddit4</i>	DNA-damage-inducible transcript 4	82.2	48.2	-0.8	2.2x10 ⁻²

Day 7: Downregulated					
Gene	Protein	Control	AOE	Log ₂ Δ	FDR
<i>Ankrd1</i>	Ankyrin repeat domain 1	2.0	0.0	-∞	5.6x10 ⁻³
<i>Atp2a1</i>	ATPase, Ca ²⁺ transporting, fast twitch 1	10.8	1.1	-3.3	1.8x10 ⁻²
<i>Top2a</i>	Topoisomerase (DNA) II α	3.8	0.7	-2.5	5.6x10 ⁻³
<i>Birc5</i>	Baculoviral IAP repeat-containing 5	10.1	1.9	-2.4	5.6x10 ⁻³
<i>Pf4</i>	Platelet factor 4	124.2	23.9	-2.4	5.6x10 ⁻³
<i>S100a9</i>	S100 calcium binding protein A9	2397.6	584.3	-2.0	5.6x10 ⁻³
<i>E2f2</i>	E2F transcription factor 2	2.2	0.6	-2.0	5.6x10 ⁻³
<i>S100a8</i>	S100 calcium binding protein A8	2757.2	776.5	-1.8	5.6x10 ⁻³
<i>Pglyrp1</i>	Peptidoglycan recognition protein 1	39.1	11.1	-1.8	5.6x10 ⁻³
<i>Mmp9</i>	Matrix metalloproteinase 9	10.8	3.1	-1.8	5.6x10 ⁻³
<i>Cdk1</i>	Cyclin-dependent kinase 1	3.0	1.0	-1.6	2.8x10 ⁻²
<i>Thbs1</i>	Thrombospondin 1	17.7	5.8	-1.6	5.6x10 ⁻³
<i>Alox12</i>	Arachidonate 12-lipoxygenase	5.4	1.8	-1.6	5.6x10 ⁻³
<i>Slc40a1</i>	Solute carrier family 40 member 1	5.0	1.8	-1.5	1.0x10 ⁻²
<i>Vdr</i>	Vitamin D receptor	6.6	2.4	-1.5	5.6x10 ⁻³
<i>Hmgb2</i>	High mobility group box 2	30.5	11.0	-1.5	5.6x10 ⁻³
<i>Plac8</i>	Placenta-specific 8	27.7	11.3	-1.3	3.4x10 ⁻²
<i>Lcn2</i>	Lipocalin 2	111.1	49.0	-1.2	5.6x10 ⁻³
<i>Fap</i>	Fibroblast activation protein	24.9	12.1	-1.0	5.6x10 ⁻³
<i>Coro1a</i>	Coronin, actin binding protein 1A	41.5	20.6	-1.0	5.6x10 ⁻³
<i>Ncf1</i>	Neutrophil cytosolic factor 1	12.4	6.5	-0.9	1.0x10 ⁻²
<i>Cd44</i>	CD44 antigen	9.3	5.5	-0.8	4.7x10 ⁻²

Day 28: Downregulated					
Gene	Protein	Control	AOE	Log ₂ Δ	FDR
<i>Lgals7</i>	Lectin, galactose binding, soluble 7	2.3	0.0	-∞	9.5x10 ⁻³
<i>Bmpr2</i>	Bone morphogenetic protein receptor, type II	5.4	1.5	-1.8	9.5x10 ⁻³
<i>Nos1</i>	Nitric oxide synthase 1, neuronal	6.8	2.2	-1.6	9.5x10 ⁻³
<i>Peg3</i>	Paternally expressed 3	9.6	3.6	-1.4	9.5x10 ⁻³
<i>Peli3</i>	Pellino 3	7.3	2.9	-1.4	4.5x10 ⁻²
<i>Mef2a</i>	Myocyte enhancer factor 2A	12.5	4.9	-1.3	9.5x10 ⁻³
<i>Rps6ka3</i>	Ribosomal protein S6 kinase polypeptide 3	10.4	4.3	-1.3	1.6x10 ⁻²

5.8 Discussion

Compared to whole cochlear transcriptomics, the micro-dissection of the modiolus allowed for better insight into molecular changes at the primary auditory neuron. However, although care was taken to remove the additional cochlear structures, it is likely that the basal aspect of the inner hair cell is retained. This assumption would explain the presence of genes typically associated with the hair cell, such as otoferlin. With this in mind, the results have been interpreted with the assumption that the ribbon and synapse are present in the sample and contributing to the gene expression changes seen. While not the primary target of the study, changes to the synapse (and its connection to the ribbon) likely contributes to the long term changes to the spiral ganglion neurons and thus affects their survival.

The total number of unique genes changed at one or more time point was 421. The number of genes upregulated and downregulated at each time point has been summarised in Figure 5.8. While each gene could be playing an integral role in the damage or recovery of the spiral ganglion following noise exposure, it would not be possible to discuss each and every gene change. Instead an integrative approach to analysis has been taken. First, sustained changes and patterns of changes will be discussed. Following this, the immune response, neuron specific, and cell death associated genes will be discussed within the context of known changes to the spiral ganglion demonstrated in previous literature.

Gene Expression Changes in the Modiolus Follow Noise Exposure

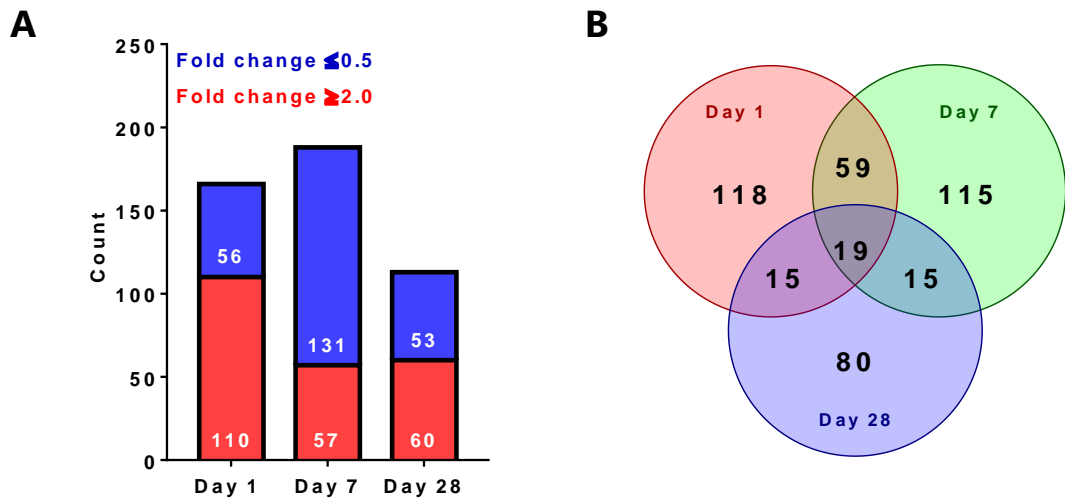


Figure 5.8: Summary of the number of genes differentially expressed in the modiolus. (A) Upregulated (fold change ≥ 2.0) and downregulated (fold change ≤ 0.5) at each time point. (B) Over the three time points, 19 genes had changes in expression across all three time points. 59 genes had altered expression levels early (day 1 and day 7) and 15 genes had altered expression levels late (day 7 and day 28).

5.8.1 Sustained Changes in Gene Expression

Of the 421 changed genes, 108 were found to be changed as a result of noise exposure at more than one time point. These genes can be divided into four categories: 1) genes which are differentially expressed chronically (at all 3 time points), as shown in Table 5.17; 2) genes which show early (i.e. at one and seven days, but not 28) changes to expression, as shown in Table 5.18 and Table 5.19; 3) genes which show late (i.e. at seven and 28 days, but not one) changes to expression, as shown in Table 5.20; and finally, 4) changes with no obvious pattern, i.e. where changes are seen at day one and 28 but not at seven or changes which occur in opposing directions. This last category (4), although potentially interesting on its own, has been omitted from this discussion.

In total, 19 genes were found to be upregulated at all three time points (Table 5.17). None of the downregulated gene changes were shared over the three time points. Many of these upregulated changes were associated with immune system processes and the acute phase response. Serum albumin (*Alb*), hemopexin (*Hpx*), high-molecular weight kininogen (*Kng1*), orosomucoid 1 (*Orm1*), plasminogen (*Plg*), serum amyloid a1 and a2 (*Saa1*, *Saa2*), and the β chain of fibrinogen (*Fgb*) are all typically known as liver expressed and free circulating proteins. However, given the large changes in mRNA expression between the sham and noise exposed groups expression of these genes is more likely to be originating from within the modiolus rather than from any plasma present in the small vascular structures. Further studies using RNA *in situ* hybridisation would be needed to identify which of the cochlear structures are transcribing these genes following noise exposure.

In addition to immune system processes, *Fgb*, *Plg*, and *Kgn1* are also associated with the coagulation of blood following injury (Lin et al., 2017). Although this may be a secondary effect of the inflammatory process, the initiation of a coagulation cascade within the cochlea could contribute to noise-induced cochlea ischemia

Gene Expression Changes in the Modiolus Follow Noise Exposure

and changes to blood flow seen following acoustic overexposure (Reif et al., 2013).

Another notable group of chronically upregulated genes are the apolipoproteins: A1 (*Apoa1*), C1 (*Apoc1*), and H (*ApoH*). In addition to these, apolipoprotein B (*ApoB*) is also upregulated across day one and day seven (see Table 5.18). Apolipoproteins are a family of proteins which bind lipids. Apolipoprotein B (*ApoB*) forms a low-density lipoprotein which is associated with an increased risk of vascular and cardiac diseases (Benn, 2009), whereas apolipoproteins A, C, and H form high-density lipoproteins which are instead thought to protect against atherosclerotic processes, acting as an anti-inflammatory (Hu et al., 2016). Compared to apolipoprotein E, which has an established role in Alzheimer's disease (for a review see Liu et al, 2013a), little is known about the presence of the other apolipoproteins in the nervous system. There is, however, evidence to suggest that apolipoproteins - in particular *Apoa1* - is protective against neuroinflammation (Paula-Lima et al., 2009) and plays a role in re-myelination of peripheral nerves following damage (Boyles et al., 1989). The increased presence of apolipoprotein mRNA, and subsequently protein, could be a repair response to the demyelination of the auditory nerve following insult, or could be a response to an increase in free lipids caused by myelin breakdown.

At one and seven days following AOE there were just nine shared upregulated genes (Table 5.18), and 26 shared downregulated genes (Table 5.19). An additional 24 genes were significantly different in both groups, but changed in opposing directions. The sudden increase in downregulated genes at day seven (see Figure 5.8), and the increase in the number of genes changing in opposing directions, may be an artefact of the increased number of reads gained for the control samples at day seven (discussed in §4.2.3) and may therefore be affecting interpretation of results at this time point.

Gene Expression Changes in the Modiolus Follow Noise Exposure

Of the genes which showed early changes in expression, several were associated with defense response or response to stimulus. These included the cathelin-related antimicrobial peptide (*Camp*), pro-platelet basic protein chemokine C-X-C motif 7 (*Ppbp*), peptidoglycan recognition protein 1 (*Pglyrp1*), and the two genes that collectively make up the calcium binding protein calprotectin (*S100a8* and *S100a9*). Proteins such as these would typically be secreted during an inflammatory response so the downregulation of these genes was unexpected given the acute phase and inflammatory response seen in other gene changes. This could suggest that these gene changes contribute to another mechanism following noise exposure such as the initiation of apoptosis; to which the downregulation of *S100a8* has been previously linked (Yaundong et al., 2014).

At day one and day seven, collagen genes: type V α 1 (*Col5a1*), type XX α 1 (*Col11a1*), and type XXII α 1, are all downregulated. In addition to this, type I α 1 (*Col1a1*), type II α 1 (*Col2a1*), and type XI α 2 (*Col11a2*) were downregulated at day one only. Several different fibrillar collagen proteins have been shown to be expressed in the osseous spiral lamina and around the VIIIth nerve in the mammalian cochlea (Slepecky et al., 1992), and the deletion of a number of collagen genes has been implicated in diseases with an auditory phenotype, such as Stickler syndrome (Robin et al., 1993) or Alport Syndrome (Alves and de, 2005). Reduction in the expression of these collagen genes could affect the structural maintenance of any number of cell types present in the modiolar samples, or conversely may be due to a loss of cells in the noise exposed animals.

Finally, 11 genes had shared upregulation at the later (seven and 28 days) time points. Like with the chronically upregulated genes, several of these were associated with immune system processes and the coagulation cascade (Table 5.20). The late upregulation of fibrinogen α chain (*Fga*) and γ chain (*Fgg*) means that all three fibrinogen subunits are upregulated at seven and 28 days following

Gene Expression Changes in the Modiolus Follow Noise Exposure

noise exposure. Increases in fibrinogen expression has previously been shown to restrict cochlear blood flow and effect hearing thresholds (Ihler et al., 2012).

Although the mechanism for an increase in fibrinogen transcription following noise is not clear, increases in the expression of fibrinogen in the modiolus could be impairing recovery from exposure or contributing to the long term cell death of the spiral ganglia through the disruption of blood flow. One quick way to test this would be to administer a defibrinogenation agent such as Ancrod, which was shown to mitigate against systemic hyperfibrinogenemia by Weiss et al. (2017), to test whether this improved recovery of thresholds following acoustic over exposure. However, this alone would not be sufficient to determine the role of modiolar fibrinogen after noise, as this experiment would not differentiate between the effects of increased blood flow to the modiolus and increased blood flow in the rest of the cochlea.

By looking at patterns of expression between time points, it is clear that apolipoproteins, collagens, and fibrinogen play some role following noise exposure. What is not clear at this stage is whether these changes are contributing to the damage or recovery of thresholds over the 28-day period. Immunohistochemistry and/or RNA *in-situ* hybridisation would first be needed to discover the source of expression and where proteins are localised following expression; while drug-induced inhibition of fibrinogenesis following noise exposure, and the use apolipoprotein deficient mouse models could elucidate whether the changes exacerbate or protect against further hearing damage following noise.

Gene Expression Changes in the Modiolus Follow Noise Exposure

Table 5.17: Genes differentially expressed at all three time points in the modiolus. All 19 genes are upregulated at all time points. Out of the 19 genes, 12 are associated with response to stress (GO:0006950). Fold change (Δ) has been \log_2 transformed.

Gene	Protein	Day 1 Log₂ Δ	Day 7 Log₂ Δ	Day 28 Log₂ Δ
<i>Alb</i>	Albumin	7.23	6.16	4.92
<i>Apoa1</i>	Apolipoprotein A1	6.16	5.58	4.47
<i>Apoc1</i>	Apolipoprotein C1	2.79	2.14	2.58
<i>ApoH</i>	Apolipoprotein H	4.07	4.11	3.51
<i>C3</i>	Complement component 3	2.41	1.72	2.23
<i>Fgb</i>	Fibrinogen beta chain	2.79	6.93	5.72
<i>Hpx</i>	Hemopexin	5.93	5.03	5.06
<i>Itih3</i>	Inter-alpha trypsin inhibitor, heavy chain 3	3.63	2.68	2.70
<i>Kng1</i>	Kininogen 1	3.28	2.89	3.31
<i>Orm1</i>	Orosomucoid 1	4.23	4.06	4.51
<i>Plg</i>	Plasminogen	4.23	3.19	3.04
<i>Saa1</i>	Serum amyloid a1	6.48	4.10	5.72
<i>Saa2</i>	Serum amyloid a2	6.80	4.64	5.31
<i>Serpina3k</i>	Serine or cysteine peptidase inhibitor, clade A, 3K	6.39	5.06	4.93
<i>Serpina3n</i>	Serine or cysteine peptidase inhibitor, clade A, 3N	4.29	2.10	3.07
<i>Slc4a1</i>	Solute carrier family 4 anion exchanger, 1	2.29	2.96	0.93

Gene Expression Changes in the Modiolus Follow Noise Exposure

Table 5.18: Early upregulated genes in the modiolus. Nine genes are upregulated at both 1 day and 7 days after AOE, but not at day 28. Fold change (Δ) has been Log_2 transformed.

Gene	Long name	Day 1 $\text{Log}_2 \Delta$	Day 7 $\text{Log}_2 \Delta$
<i>Afm</i>	Afamin	∞	∞
<i>Agxt</i>	Alanine-glyoxylate aminotransferase	∞	∞
<i>Apob</i>	Apolipoprotein b	4.39	3.69
<i>Bhmt</i>	Betaine homocystine methyltransferase	3.02	1.54
<i>Leap</i>	Liver expressed antimicrobial peptide	∞	∞
<i>Lect2</i>	Leukocyte cell-derived chemotaxin 2	∞	∞
<i>Miat</i>	Myocardial infarction associated transcript	0.93	0.85
<i>P2rx3</i>	Purigenic receptor p2x ligand gated ion channel ATP	2.10	1.58
<i>Prodh</i>	Proline dehydrogenase	∞	∞

Table 5.19: Early downregulated genes in the modiolus. 26 genes are downregulated at both 1 day and 7 days after AOE, but not at day 28. Fold change (Δ) has been Log_2 transformed.

Gene	Long name	Day 1 $\text{Log}_2 \Delta$	Day 7 $\text{Log}_2 \Delta$
<i>Beta-s</i>	Hbb-bs haemoglobin beta adult s-chain	-1.40	-2.74
<i>Bglap</i>	Bone gamma-carboxyglutamate protein	-1.43	-2.40
<i>Bglap2</i>	Bone gamma-carboxyglutamate protein 2	-1.84	-1.94
<i>Bpifa1</i>	Bpi fold containing family a member 1	-1.60	-1.79
<i>Camp</i>	Cathelicidin antimicrobial peptide	-1.60	-1.79
<i>Cd177</i>	Cd177 antigen	-2.12	-1.51
<i>Chi3l3</i>	Chtinase-like -3	-2.18	-2.06
<i>Col11a1</i>	Collagen type 11 alpha 1	-0.79	-0.92
<i>Col22a1</i>	Collagen type 22 alpha 1	-1.79	-1.51
<i>Col5a1</i>	Collagen type 5 alpha 2	-0.79	-0.81
<i>Cybb</i>	Cytochrome b -245 beta polypeptide	-1.15	-0.94
<i>Ibsp</i>	Integrin binding sialoprotein	-1.15	-1.09
<i>Itga2b</i>	Integrin subunit alpha 2b cd41	-1.03	-1.12
<i>Itgb3</i>	Integrin subunit beta 3 cd61	-1.47	-2.12
<i>Ltf</i>	Lactotransferrin	-2.12	-1.94
<i>Lyz2</i>	Lysozyme	-0.84	-0.79
<i>Mmp9</i>	Matrix metalloproteinase 9	-1.94	-1.79
<i>Mpo</i>	Myeloperoxidase	-1.60	-2.12
<i>Ngp</i>	Neutrophilic granule protein	-2.47	-2.06
<i>Pf4</i>	Platelet factor 4	-0.92	-2.40
<i>Pglyrp1</i>	Peptidoglycan recognition protein 1	-1.47	-1.84
<i>Ppbb</i>	Pro-platelet basic protein cxcl7	-2.74	-2.18
<i>Retnlg</i>	Resistin like gamma	-2.25	-1.89
<i>S100a8</i>	S100 calcium binding protein a8	-2.25	-1.84
<i>S100a9</i>	S100 calcium binding protein a9	-2.40	-2.06
<i>Thbs1</i>	Thrombospondin 1	-1.40	-1.60

Gene Expression Changes in the Modiolus Follow Noise Exposure

Table 5.20: Late upregulated genes in the modiolus. 11 genes are upregulated at both 7 day and 28 days after AOE, but not at day 1. Fold change (Δ) has been Log_2 transformed.

Gene	Long name	Day 7 $\text{Log}_2\Delta$	Day 28 $\text{Log}_2 \Delta$
<i>Ahsg</i>	Apha-2-HS-glycoprotein	4.2	4.5
<i>Fabp1</i>	Fatty acid binding protein	∞	∞
<i>Fga</i>	Fibrinogen alpha chain	5.2	4.8
<i>Fgg</i>	Fibrinogen gamma chain	4.9	5.3
<i>GC</i>	Group specific component	4.4	3.9
<i>Gh</i>	Growth hormone	1.6	1.4
<i>Itih4</i>	Inter-alpha trypsin inhibitor heavy chain	4.9	5.1
<i>King2</i>	Kininogen 2	1.9	3.1
<i>Lrrc17</i>	Leucine rich repeat containing 17	1.0	1.7
<i>Mat1a</i>	Methionine adenosyltransferase 1 alpha	3.6	3.7
<i>Tmem38b</i>	Transmembrane protein 38b	0.8	1.4

5.8.2 Changes to the Ribbon Synapse

“Cochlear synaptopathy”, which describes the loss of afferent synapses at the hair cell in the absence of hair cell loss, has been shown to occur after NIHL; even when the insult is mild. In cases of temporary threshold shifts this noise induced synaptopathy causes irreversible disruption to synaptic communication and leads to perceptual difficulties such as a reduced discrimination of speech in noisy environments.

Although the microdissection of modiolar tissue used here contains a number of different cell types, in filtering the differentially expressed genes by those associated with the neuron this study was able to highlight genes which are likely to be associated with the spiral ganglion neuron and any remaining components of the inner hair cell (see §5.5). This revealed 57 differentially expressed neuronal genes, in which 36 were changed more than two-fold control levels.

Within this group, three pre-synaptic Ca^{2+} calcium sensors were of particular interest due to their role in Ca^{2+} -mediated exocytosis. These were: synaptotagmin I, upregulated at day one; synaptotagmin II, downregulated at day one and 28; and otoferlin, downregulated at day seven. While synaptotagmin I and II are typically the most commonly found Ca^{2+} sensors, neither are expressed on the presynaptic inner hair cell in the mature mouse. Instead IHC exocytosis appears to switch to otoferlin-dependant mechanisms during IHC maturation (Beurg et al., 2010, Reisinger et al., 2011). The changes seen to synaptotagmin I and otoferlin after noise could be a consequence of synaptic loss, reverting the IHC back to an “immature” state; however, this is confounded by the fact that expression of synaptotagmin II mRNA reduces in parallel with I.

Although synaptotagmins are classically associated with the presynaptic membrane they can also be expressed post-synaptically. Thus, changes in gene expression of any of these transcripts could be representing changes to the postsynaptic membrane rather than the IHC. It is not currently clear what role

Gene Expression Changes in the Modiolus Follow Noise Exposure

synaptotagmins play on the post-synapse, however more recently they have been implicated in the recruitment of AMPA receptors to the postsynaptic membrane (Wu et al., 2017). If an upregulation of synaptotagmin I did lead to an increase of membrane-associated AMPA receptors this would potentiate any remaining synaptic connections between the IHC and SGNs. There was a transient upregulation of *Gria2* which encodes GluA2, a subunit component of the AMPA receptors classically associated with the afferent terminal, but this change was relatively small (1.74 fold) and ultimately may not translate to an increase in GluA2.

While synaptotagmins are not expressed at the mature IHC presynapse, they are expressed in the efferent fibres (Beurg et al., 2010, Reisinger et al., 2011). Therefore, it may be more sensible to suggest that changes to synaptotagmin expression occurs at efferent terminals after noise. Although synaptotagmin I and II are thought to play similar roles, they are generally found to be expressed in different populations of neurons (Fox and Sanes, 2007), which suggests differential function. Hence, the opposing changes in synaptotagmin I and II seen at day one could contribute to the alteration of efferent feedback.

There was no evidence of change to any structural proteins associated with the presynaptic ribbon such as bassoon, RIBEYE (*Ctbp2*) or Piccolo. Downregulation of the SNARE protein Syntaxin 1B was seen at 28 days following noise exposure. However, like with the synaptotagmins there is some debate as to whether the protein is functional at the hair cell ribbon synapse (Nouvian et al., 2011).

5.8.3 Evidence of Cell Death

Noise exposure and the subsequent excitotoxic insult at the SGN afferent terminals results in a significant reduction in SGN cell bodies which is delayed several months following the insult (Kujawa and Liberman, 2006). It has been hypothesised that this neural degeneration is a form of accelerated presbycusis, possibly induced by glutamate induced uncoupling of the ribbon synapses which does not fully recover over time (Kujawa and Liberman, 2015, Song et al., 2016).

It is not yet clear what the mechanism is for the SGN cell death seen after acoustic overexposure. Some recent studies have attempted to address this through *in vitro* models of excitotoxicity, which have suggested that apoptosis is the primary cause of SGN loss induced through reactive oxygen species (ROS) induced endoplasmic reticulum stress pathways (Ding et al., 2015, Bai et al., 2016), presumably triggered by excessive uptake of Ca²⁺ by the mitochondria. Both of these *in vitro* models, however, have failed to account for why cell death in the *in vivo* model of excitotoxicity is delayed by several months.

To probe for any evidence of programmed cell death in the modiolus samples following noise exposure, the list of differentially expressed genes was filtered by genes with the gene ontology annotation "programmed cell death". From this, 18 upregulated genes (Table 5.15) and 33 downregulated genes (Table 5.16) were highlighted. From these lists, no single apoptotic pathway could be identified, and many of the genes highlighted had overlaps with immune system processes. However, a number of the genes could give some insight into how a late induced cell death processes may be initiated in the spiral ganglion following noise.

At day 28 cell death-inducing DNA fragmentation factor α (*Cidea*) and related Cidea-like C (*Cidec*) are upregulated 8.0x and 18.4x (respectively) compared to control levels. Expression of *Cidea* and *Cidec* is typically associated with brown and white adipose where expression is induced in high-sucrose and high-fat diet

Gene Expression Changes in the Modiolus Follow Noise Exposure

(Jinno et al., 2010); but, mRNA expression has also been demonstrated in the mammalian brain (Li et al., 2009).

Both *Cidea* and *Cidec* are pro-apoptotic proteins, and have been shown to induce apoptosis in adipocytes, CHO, and HeLa cell lines (Valouskova et al., 2008, Ito et al., 2010) and is associated with β -cell apoptosis in models of free-fatty acid exposure (Jinno et al., 2010). Potentially acting oppositely to *Cidea* and *Cidec* is adiponectin (*Adipoq*); initially downregulated at day one (0.16x control FPKM), and upregulated at day 28 (14.9x control FPKM). Adiponectin is classically known as an adipose secreted hormone involved in the metabolism of glucose and fatty acids; however both mRNA and protein can be found expressed in a variety of different tissue types (Thundyil et al., 2012). Crucially, adiponectin has been shown to have neuroprotective properties in a manner dependant on AMPK activation which is mediated through adiponectin receptors AdipoR1 and AdipoR2 (Qiu et al., 2011, Naseer et al., 2014); both of which are expressed in the modiolus samples.

The upregulation of these genes, along with several lipid binding apolipoproteins (*Apoa1*, *Apob*, *Apoc3*, *ApoH*) and fatty acid binding proteins (*Fabp1*, *Fabp4*), over the 28 day period is suggestive of dysregulation in the production of lipids, their metabolism, or storage (see related gene ontology terms in Table 5.11). Previous evidence of increased lipid synthesis or uptake into the spiral ganglia following noise exposure has been observed by Gannouni et al. (2015); who found aggregates of lipid droplets in the endoplasmic reticulum and cytoplasm when rats were exposed to moderate levels of noise over long time periods. Hyperlipidemia is a well-established risk factor in a number of neurodegenerative diseases and lipid accumulation can result in increased expression of pro-apoptotic proteins Bcl-2, Bcl-2 associated protein X (Bax), and caspase 3 (Zhao et al., 2017). Although these genes are not seen to be upregulated in the samples collected here, cell death in the spiral ganglion is not seen until several months

following insult, meaning that the 28-day time point collected here is still in the early stages and the cell death process may not yet be triggered.

5.8.4 The Immune Response

It has been extensively demonstrated that following noise exposure, pro-inflammatory cytokines such as tumour necrosis factor α (TNF- α) and interleukin-1 β (IL-1 β), and intercellular adhesion molecule-1 (ICAM-1) are upregulated in the cochlea over the two weeks following insult (Tornabene et al., 2006, Tan et al., 2016, Yang et al., 2016). However, previous transcriptomic analysis of gene expression changes to cochlear tissue following traumatic noise exposure have used whole cochleae preparations which do not differentiate between the different cochlear structures. Furthermore, immunohistochemical analysis from these same studies show that the majority of the inflammatory response is localised to the spiral ligament where mechanical stress will be greatest. It was therefore hypothesised that by isolating the modiolus, most of this inflammatory response would be excluded from the analysis, and greater insights into spiral ganglion specific changes would be gained.

However, while this study did not show changes in any pro-inflammatory cytokines it is clear from the analysis at one, seven, and 28 days that an immune response is elicited in the modiolar samples following noise exposure. This is most evident with members of the C1-complex (*C1qa*, *C1qb*, *C1qc*), *C3*, *C4b*, *C8a*, complement factor B (*Cfb*), C-reactive protein (*Crp*), and Mannan-binding lectin (*Mbl1*) all significantly upregulated at day one, suggesting activation of one or more pathways of the complement cascade. In addition to this, while immunohistochemical analysis of Iba-1 positive cells did not indicate an increase in the number of macrophages at the spiral ganglion, there was some evidence of migration of the cells to SGN dendrites in the osseous spiral lamina, although more repeats would be needed to confirm this.

Gene Expression Changes in the Modiolus Follow Noise Exposure

Over the 28 day period gene ontology terms “acute phase response” and “acute inflammatory response”, both terms describing a group of genes (see §5.6) which are rapidly and transiently expressed following acute injury. More importantly, this response is usually resolved within hours following insult (Suffredini et al., 1999). Here, upregulation of these acute phase response genes persists out to 28 days following noise exposure, with no additional trauma in this recovery period. The only reported case of chronic inflammation involving the spiral ganglion is a study by Menardo et al. (2012), who found that in mice lacking the gene senescence-accelerated mouse prone 8 (*Samp8*) altered levels of antioxidant led to chronic inflammation characterised by a rise in pro-inflammatory cytokines. Interestingly, this chronic inflammation was also accompanied by the induction of apoptosis in the spiral ganglia, like what we expect to occur following noise; and an increase in lipid droplets aggregates like those seen by Gannouni et al. (2015) following noise.

5.8.5 Summary

This study did not find any changes to voltage-gated sodium channels following noise exposure like those reported by Fryatt et al. (2011). In fact, the only ion channel changes seen during the recorded 28 day period was an upregulation of P2X₃ at days one and seven, and a small upregulation of the AMPA receptor α 2 subunit at day one. It is not clear at this stage whether the lack of changed ion channels is to the species used (mouse), noise model, or whether changes occur but are not detected using the RNA Sequencing parameters used here.

From the results collected from the modiolus following noise exposure, there was no one group of up- or down- regulated genes which would indicate a known pathway for induced cell death in the spiral ganglion. Despite this, the study has revealed several classes of proteins which may be playing key roles in either damage or recovery processes following acoustic overexposure.

Gene Expression Changes in the Modiolus Follow Noise Exposure

The first of these is fibrinogen or its products; all three fibrinogen subunits are significantly upregulated at one or more time points over the 28-day recovery period. Increased free circulating fibrinogen has been previously linked to sudden sensorineural hearing loss and increases in the expression of fibrinogen in the modiolus could be impairing recovery from exposure or contributing to the long term cell death of the spiral ganglia through the disruption of blood flow.

Secondly, several fibrillar collagen genes were downregulated in the modiolus following noise. Without immunohistochemical localisation of these proteins, it would be difficult to comment on what role these collagens play following noise exposure, as it is not known which cell types are expressing these proteins within the modiolus.

Finally, gene ontology analysis revealed several annotations related to lipid binding, production, metabolism, or storage. The upregulation of several lipid binding apolipoproteins and fatty acid binding proteins is strongly indicative of lipid dysregulation following noise exposure. Increases in free lipids in the mouse cochlea following noise could originate from myelin break down or the death of other cell types around the spiral ganglia, or could be increased systemically. This increase in free lipids would result in lipofuscin cell inclusions, like those seen by Gannouni et al. (2015). In addition to this, it is likely that an increase in free lipid results in the upregulation of pro-apoptotic genes *Cidea* and *Cidec* which are elevated 28 days following exposure, and may ultimately result in spiral ganglion cell death.

Chapter 6: Gene Expression Changes in the Cochlear Nucleus Following Noise Exposure

6.1 Introduction

Cochlear nucleus RNASeq results at each experimental time-point were compared with condition matched sham controls. In this chapter these comparisons will be described at each time point. Following this, neuron specific genes have been highlighted.

While the aim of this chapter is to represent as much data as possible from the RNASeq dataset, not every significantly changed gene can be discussed. As such, genes which are significantly changed over one, or more time points have been preferentially discussed. Compared to the modiolus, relatively few gene expression changes were observed in the cochlear nucleus.

Just one protein of interest, Aquaporin-1 was chosen for further discussion. This immunohistochemistry data was collected under my supervision by Kishen Chahwala.

6.2 Gene Expression Changes on Day One

After one day recovery, noise exposed cochlear nuclei had 28 significantly upregulated ($\Delta \geq 2$, $FDR \leq 0.05$) and 6 significantly downregulated ($\Delta \leq 0.5$, $FDR \leq 0.05$) genes compared to sham exposed controls. An additional 38 genes had a $FDR \leq 0.05$, but were within two times control levels. The top 20 upregulated, and total downregulated genes are shown in Table 6.1. Of the 28 upregulated genes, 2 had a control FPKM of zero (see Table 6.2); these were Lutenising hormone β polypeptide (*Lhb*) and the non-coding vault RNA component 5 (*Vaultrc5*).

Gene Expression Changes in the Cochlear Nucleus Following Noise Exposure

All of the differentially expressed genes had low to moderate magnitudes of change following AOE (<10x), and had moderate levels of expression in control conditions (

Figure 6.1). The largest change seen in WD repeat domain 86 (*Wdr86*) which was expressed at 6x ($\text{Log}_2\Delta = 2.59$) control expression after noise exposure. Other upregulated genes included tight junction protein Claudin-2 (*Cldn2*, $\text{Log}_2\Delta = 1.88$) and the K⁺ channel β -subunit MinK-related peptide 1 (*Kcne2* $\text{Log}_2\Delta = 1.8$).

The top downregulated genes at this time-point included Dopamine β -hydroxylase (*Dbh*, $\text{Log}_2\Delta = -2.11$), which catalyzes the conversion of dopamine to noradrenalin, and members of the FOS gene family c-fos (*Fos*, $\text{Log}_2\Delta = -1.48$) and FosB (*Fosb*, $\text{Log}_2\Delta = -1.90$).

Gene ontology analysis of upregulated genes returned five “over-represented” biological process terms (Table 6.3). Of these, two were related to ion transportation and two were related to hormone regulation and transport.

There were six “over-represented” terms associated with downregulated genes (Table 6.4). Of the 12 downregulated genes, just five genes were associated with the significant gene ontology terms listed in Table 6.4: Inhibin β B (*Inhbb*), VGF nerve growth factor inducible (*Vgf*), Serine peptidase inhibitor A 3N (*Serpina3n*), Pituitary adenylate cyclase-activating peptide (*Adcyap1*) and Vesicular monoamine transporter 2 (*Slc18a2*).

Gene Expression Changes in the Cochlear Nucleus Following Noise Exposure

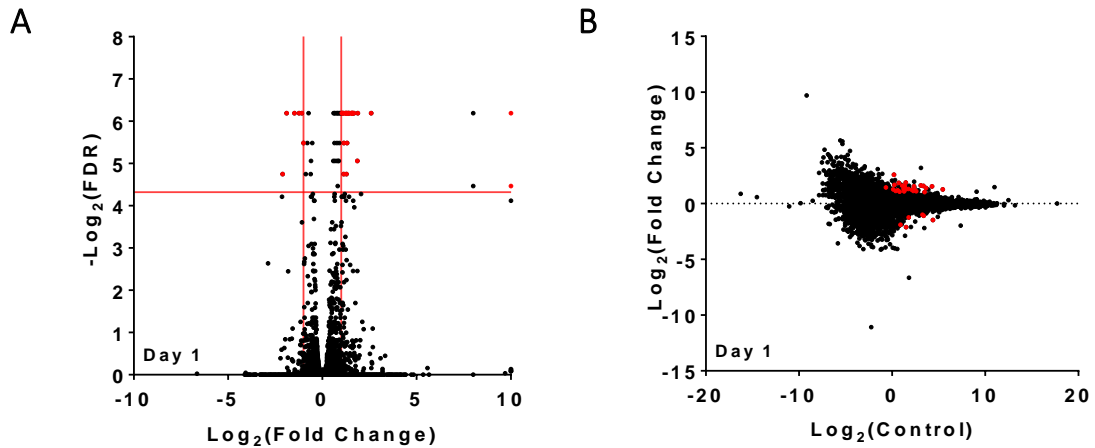


Figure 6.1: Volcano (A) and MA plot (B) of differentially expressed genes at day one in the cochlear nucleus. Plots were constructed using a Log_2 transforms of fold change (Δ), false discovery rate (FDR) and mean control FPKM. Red lines represent cut off values of $\text{FDR} < 0.05$ and $\Delta > 2$ or $\Delta < 0.5$. Genes which satisfy these conditions have been coloured red.

Table 6.1: Differentially expressed genes at day one in the cochlear nucleus. The top 20 upregulated genes at day one listed in order of biggest change. Only 12 genes were downregulated at this time point. For each gene, the average control and experimental (AOE) FPKM values are listed along with a Log_2 transform of fold change (Δ) and the significance value (FDR). For changes where either control or AOE FPKM equal zero, a true ratio of change cannot be determined; these changes are shown in Table 6.2.

Top 20 Upregulated					Downregulated				
Symbol	Control	AOE	$\text{Log}_2\Delta$	FDR	Symbol	Control	AOE	$\text{Log}_2\Delta$	FDR
<i>Wdr86</i>	1.1	6.9	2.59	0.014	<i>Dbh</i>	2.8	0.7	-2.11	0.037
<i>Cldn2</i>	2.8	10.1	1.88	0.014	<i>Fosb</i>	1.9	0.5	-1.90	0.014
<i>Kcne2</i>	1.7	6.0	1.85	0.030	<i>Fos</i>	20.7	7.4	-1.48	0.014
<i>Postn</i>	1.2	3.8	1.67	0.014	<i>Slc18a2</i>	3.4	1.4	-1.24	0.014
<i>Kl</i>	8.5	26.0	1.62	0.014	<i>Rem2</i>	10.5	4.9	-1.09	0.014
<i>Trpv4</i>	2.1	6.4	1.61	0.014	<i>Adcyap1</i>	9.5	4.7	-1.00	0.022
<i>Clic6</i>	10.2	30.5	1.58	0.014	<i>Deaf1</i>	12.6	6.9	-0.88	0.037
<i>F5</i>	2.5	7.4	1.57	0.014	<i>Serpina3n</i>	11.3	6.5	-0.80	0.022
<i>Aqp1</i>	5.1	14.9	1.56	0.014	<i>Vgf</i>	20.9	12.6	-0.74	0.014
<i>Cldn1</i>	2.6	7.5	1.54	0.014	<i>Cdkn1a</i>	24.9	16.2	-0.62	0.037
<i>Sostdc1</i>	19.4	56.4	1.54	0.014	<i>Inhbb</i>	10.0	6.6	-0.60	0.030
<i>Rbm47</i>	0.6	1.7	1.44	0.014	<i>Mfsd2a</i>	42.1	29.0	-0.53	0.022
<i>Folr1</i>	12.5	32.8	1.39	0.014					
<i>Abca4</i>	2.7	7.0	1.37	0.014					
<i>Car12</i>	5.2	13.1	1.34	0.014					
<i>Pqlc3</i>	3.4	8.3	1.31	0.022					
<i>Krt8</i>	2.3	5.7	1.28	0.037					
<i>Tmem72</i>	2.8	6.7	1.28	0.014					
<i>Atp10d</i>	1.1	2.6	1.27	0.014					
<i>Slc4a5</i>	4.3	10.1	1.23	0.014					

Gene Expression Changes in the Cochlear Nucleus Following Noise Exposure

Table 6.2: Day one changes for which fold change cannot be calculated in the cochlear nucleus. Differentially expressed genes which have a control or experimental value of zero have been excluded from the top 20 changed genes as fold change cannot be determined. There were no downregulated genes for this criteria. For each gene, the average control and experimental (AOE) FPKM values are listed along the significance value (FDR).

Upregulated				Downregulated
Symbol	Control	AOE	FDR	n/a
<i>Lhb</i>	0.0	2.3	0.014	
<i>Vaultrc5</i>	0.0	2.7	0.045	

Table 6.3: Gene Ontology results for genes upregulated at day one in the cochlear nucleus. Genes upregulated at day one were analysed for enriched biological function terms using the gene ontology package GOSep. Five significant terms ($P < 0.05$) were returned and ordered by significance.

	GO ID	Term	P
1	GO:0010817	Regulation of hormone levels	2.26×10^{-3}
2	GO:0006820	Anion transport	5.54×10^{-3}
3	GO:0006811	Ion transport	7.71×10^{-3}
4	GO:0009914	Hormone transport	4.01×10^{-2}
5	GO:0044765	Single-organism transport	4.84×10^{-2}

Table 6.4 Gene Ontology results for genes downregulated at day one in the cochlear nucleus. Genes upregulated at day one were analysed for enriched biological function terms using the gene ontology package GOSep. Six significant terms ($P < 0.05$) were returned and ordered by significance.

	GO ID	Term	P
1	GO:0030072	Peptide hormone secretion	1.96×10^{-2}
2	GO:0002790	Peptide secretion	1.96×10^{-2}
3	GO:0015833	Peptide transport	1.96×10^{-2}
4	GO:0042886	Amide transport	1.96×10^{-2}
5	GO:0046879	Hormone secretion	1.96×10^{-2}
6	GO:0009914	Hormone transport	1.96×10^{-2}

6.3 Gene Expression Changes on Day Seven

After 7 days recovery, noise exposed cochlear nucleus had 40 significantly upregulated ($\Delta > 2.0$, FDR < 0.05) and three significantly downregulated ($\Delta < 0.5$, FDR < 0.05) genes compared to sham exposed controls. An additional 27 genes had a FDR ≤ 0.05 , but were within two times control levels. The top 20 upregulated and the three downregulated genes are shown in Table 6.1.

The most highly upregulated gene at day seven was Aquaporin 1 (*Aqp1*) which was increased by 12x control levels ($\text{Log}_2\Delta = 3.64$). Other upregulated genes included Folate receptor α (*Folr1*, $\text{Log}_2\Delta = 3.12$), Claudin-2 (*Cldn2*, $\text{Log}_2\Delta = 2.69$), and Carbonic anhydrase 12 (*Car12*, $\text{Log}_2\Delta = 2.64$). Of the top 20 upregulated genes, 13 were previously upregulated at day one.

Downregulated genes were Hemoglobin β S chain (*Hbb-bs*, $\text{Log}_2\Delta = -1.44$), src homology 2 domain-containing transforming protein E (*She*, $\text{Log}_2\Delta = -1.41$), and Claudin 5 (*Cldn5*, $\text{Log}_2\Delta = -1.09$).

There were no significant gene ontology terms for either the upregulated or downregulated genes at this time-point.

Gene Expression Changes in the Cochlear Nucleus Following Noise Exposure

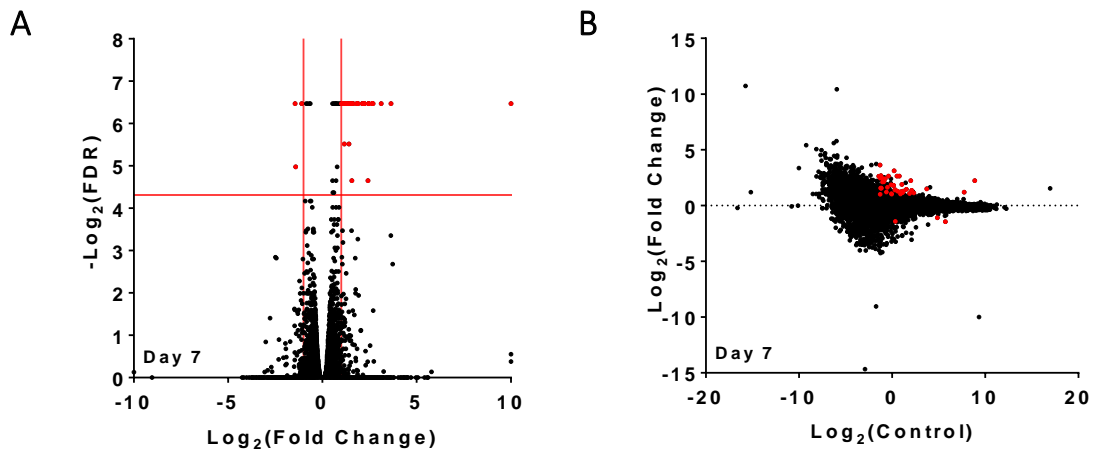


Figure 6.2 Volcano (A) and MA plot (B) of differentially expressed genes at day seven in the cochlear nucleus. Plots were constructed using a Log_2 transforms of fold change (Δ), false discovery rate (FDR) and mean control FPKM. Red lines represent cut off values of $\text{FDR} < 0.05$ and $\Delta > 2$ or $\Delta < 0.5$. Genes which satisfy these conditions have been coloured red.

Table 6.5: Differentially expressed genes at day seven in the cochlear nucleus. The top 20 upregulated genes are listed by magnitude of change. Only seven genes were downregulated at this time point. For each gene, the average control and experimental (AOE) FPKM values are listed along with a Log_2 transform of fold change (Δ) and the significance value (FDR). Genes which also had differential expression at day seven are highlighted by asterisk (*).

Top 20 Upregulated					Downregulated				
Symbol	Control	AOE	$\text{Log}_2\Delta$	FDR	Symbol	Control	AOE	$\text{Log}_2\Delta$	FDR
<i>Aqp1</i> *	0.41	5.07	3.64	0.011	<i>Hbb-bs</i>	52.63	19.29	-1.45	0.011
<i>Folr1</i> *	1.16	10.12	3.12	0.011	<i>She</i>	1.27	0.47	-1.41	0.032
<i>Cldn2</i> *	0.44	2.81	2.69	0.011	<i>Cldn5</i>	29.03	13.58	-1.10	0.011
<i>Car12</i> *	0.76	4.76	2.64	0.011	<i>Ly6c1</i>	55.31	30.62	-0.85	0.011
<i>Kl</i> *	1.44	8.97	2.64	0.011	<i>Rgs5</i>	30.80	17.85	-0.79	0.011
<i>Clic6</i> *	1.71	10.63	2.64	0.011	<i>Gpr116</i>	4.75	2.96	-0.69	0.011
<i>F5</i> *	0.37	2.29	2.63	0.011	<i>Itm2a</i>	55.92	35.83	-0.64	0.011
<i>Mpzl2</i>	0.41	2.26	2.47	0.011					
<i>Trpv4</i> *	0.49	2.63	2.44	0.011					
<i>Krt18</i>	0.60	3.19	2.41	0.040					
<i>Sostdc1</i> *	4.01	18.88	2.23	0.011					
<i>Ttr</i>	468.7	2203.4	2.23	0.011					
<i>Abca4</i> *	0.54	2.39	2.14	0.011					
<i>Tmem72</i> *	0.49	2.11	2.11	0.011					
<i>Lbp</i> *	2.05	7.65	1.90	0.011					
<i>Ccdc135</i> *	0.92	3.38	1.87	0.011					
<i>Prlr</i>	1.05	3.74	1.83	0.011					
<i>Slc4a5</i> *	1.11	3.93	1.82	0.011					
<i>Col8a1</i> *	0.71	2.20	1.64	0.011					
<i>Ccdc108</i>	0.44	1.31	1.57	0.011					

6.4 Gene Expression Changes on Day 28

After 28 days recovery, noise exposed cochlear nuclei had 46 significantly upregulated ($\Delta > 2.0$, FDR < 0.05) and four significantly downregulated ($\Delta < 0.5$, FDR < 0.05) genes compared to sham exposed controls. An additional 49 genes had a FDR ≤ 0.05 , but were within two times control levels. The top 20 upregulated and the four downregulated genes are shown in Table 6.6.

As with day seven, the largest change was seen in Aquaporin 1 (*Aqp1*, $\text{Log}_2\Delta = 4.17$). 13 of the top 20 upregulated genes were also upregulated at day seven; of these 11 were chronically upregulated since day one. None of the downregulated genes were shared with other time points, with the exception of Dopamine β -hydroxylase (*Dbh*, $\text{Log}_2\Delta = -1.19$) which was downregulated at day one ($\text{Log}_2\Delta = -2.11$, FDR = 0.037), but not at day seven ($\text{Log}_2\Delta = -0.70$, FDR = 0.378).

Gene ontology of the significantly upregulated genes returned 15 significant terms ($P < 0.05$), the top 10 of these are shown in Table 6.7. There were no significant terms returned for downregulated genes at this time-point.

Gene Expression Changes in the Cochlear Nucleus Following Noise Exposure

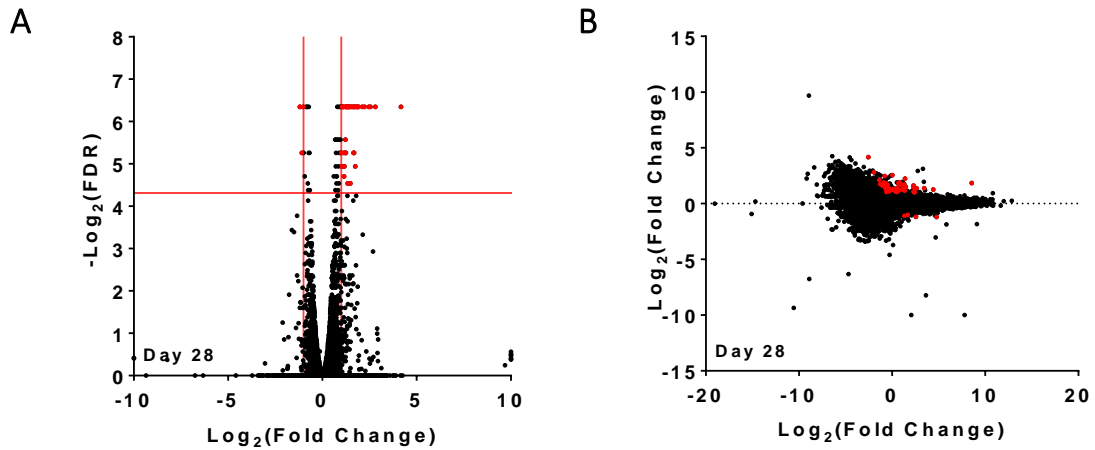


Figure 6.3: Volcano (A) and MA plot (B) of differentially expressed genes at day 28 in the cochlear nucleus. Plots were constructed using a Log_2 transforms of fold change (Δ), false discovery rate (FDR) and mean control FPKM. Red lines represent cut off values of $\text{FDR} < 0.05$ and $\Delta > 2$ or $\Delta < 0.5$. Genes which satisfy these conditions have been coloured red.

Table 6.6: Differentially expressed genes at day 28 in the cochlear nucleus. The top 20 upregulated genes are listed by magnitude of change. Only 17 genes were downregulated at this time point. For each gene, the average control and experimental (AOE) FPKM values are listed along with a Log_2 transform of fold change (Δ) and the significance value (FDR). Genes which also had differential expression at day seven are highlighted by asterix (*), and genes which were changed at day seven and day one are denoted by a double asterix (**).

Upregulated					Downregulated				
Symbol	Control	AOE	$\text{Log}_2\Delta$	FDR	Symbol	Control	AOE	$\text{Log}_2\Delta$	FDR
<i>Aqp1</i> **	0.17	3.05	4.17	0.012	<i>Rgs5</i>	27.14	11.83	-1.20	0.012
<i>F5</i> **	0.26	1.81	2.81	0.012	<i>Dbh</i>	5.87	2.57	-1.19	0.012
<i>Folr1</i> **	1.01	5.91	2.55	0.012	<i>Doc2b</i>	2.48	1.16	-1.09	0.026
<i>Car12</i> **	0.57	3.17	2.47	0.012	<i>Ets1</i>	3.19	1.58	-1.01	0.012
<i>Sostdc1</i> **	2.61	12.28	2.23	0.012	<i>Kdr</i>	2.47	1.24	-0.99	0.026
<i>Anpep</i>	0.39	1.67	2.11	0.012	<i>Slc6a2</i>	2.02	1.05	-0.94	0.038
<i>Clic6</i> **	1.78	6.70	1.92	0.012	<i>Lnpep</i>	12.37	6.68	-0.89	0.012
<i>Cldn2</i> **	0.54	2.03	1.90	0.012	<i>Bmpr2</i>	18.37	10.06	-0.87	0.012
<i>Kl</i> **	1.61	5.91	1.87	0.012	<i>Cldn5</i> *	29.49	16.34	-0.85	0.012
<i>Ttr</i> *	376.0	1342.4	1.84	0.012	<i>Flt1</i>	8.97	5.06	-0.83	0.012
<i>Mpzl2</i> *	0.61	2.16	1.83	0.012	<i>Pde10a</i>	6.55	3.83	-0.78	0.043
<i>Ttc21a</i>	0.41	1.38	1.74	0.012	<i>ErbB4</i>	5.33	3.12	-0.77	0.012
<i>Lbp</i> **	1.66	5.53	1.73	0.012	<i>Sema3c</i>	5.98	3.53	-0.76	0.043
<i>Slc6a20a</i>	2.45	8.08	1.72	0.012	<i>Slc5a7</i>	11.91	7.19	-0.73	0.048
<i>Slc22a6</i>	0.71	2.28	1.68	0.012	<i>Gucy1a2</i>	9.60	5.80	-0.73	0.026
<i>Gstm2</i>	1.97	6.28	1.67	0.012	<i>Rgs8</i>	16.89	10.54	-0.68	0.012
<i>Ccdc135</i> **	0.70	2.20	1.65	0.012	<i>Calb1</i>	26.43	16.66	-0.67	0.026
<i>Aldh1a2</i>	4.93	15.06	1.61	0.012					
<i>Abca4</i> **	0.49	1.47	1.60	0.012					
<i>Aebp1</i>	4.91	14.01	1.51	0.012					

Gene Expression Changes in the Cochlear Nucleus Following Noise Exposure

Table 6.7 The top 10 Gene Ontology results for genes upregulated at day 28 in the cochlear nucleus. Genes upregulated at day one were analysed for enriched biological function terms using the gene ontology package GOSep. 15 significant terms ($P < 0.05$) were returned and ordered by significance.

	GO ID	Term	P
1	GO:0070208	Protein heterotrimerization	9.43×10^{-4}
2	GO:0071229	Cellular response to acid chemical	3.56×10^{-3}
3	GO:0030198	Extracellular matrix organization	6.65×10^{-3}
4	GO:0043062	Extracellular structure organization	6.65×10^{-3}
5	GO:0060324	Face development	6.81×10^{-3}
6	GO:0071230	Cellular response to amino acid stimulus	9.88×10^{-3}
7	GO:0009887	Organ morphogenesis	1.39×10^{-2}
8	GO:0006820	Anion transport	1.39×10^{-2}
9	GO:0060322	Head development	1.39×10^{-2}
10	GO:0070206	Protein trimerization	1.39×10^{-2}

6.5 Neuron Specific Changes

Differentially expressed genes at each time point were cross matched against a list of 1529 genes with the annotation "neuronal part" (GO:0097458), which was downloaded from the AmiGO gene ontology online resource. From the total list of differentially expressed genes, 35 belonged to this group. Of these 20 were upregulated at one or more time point (Table 6.8), and 15 were downregulated at one or more time point (Table 6.9).

The majority (16) of upregulated genes were unique to a single time point. The exceptions to this were Transient receptor potential cation channel V4 (*Trpv4*) and bicarbonate transporter Solute carrier 4,10 (*Slc4a10*) which were upregulated at days one and seven; and Aquaporin 1 (*Aqp1*) and ATP-binding cassette A4 (*Abca4*) which were upregulated at all three time points.

Of the downregulated genes all but two were unique to a single time point. These were Dopamine β -hydroxylase (*Dbh*) which was downregulated at days 1 and 28, but not at day 7; and Claudin 5 (*Cldn5*) which was downregulated at day 7 and day 28.

The changes to *Aqp1* are further discussed in §6.5.1.

Gene Expression Changes in the Cochlear Nucleus Following Noise Exposure

Table 6.8: Neuron specific genes upregulated at each time point in the cochlear nucleus.

Genes highlighted at significantly upregulated (FDR < 0.05) were filtered based on annotations for the gene ontology term "neuron part" (GO: 0097458). For each gene, the average control and experimental (AOE) FPKM values are listed along with a Log₂ transform of fold change (Δ) and the significance value (FDR).

Day 1: Upregulated					
Gene	Protein	Control	AOE	Log ₂ Δ	FDR
<i>Trpv4</i>	Transient receptor potential cation channel, V4	2.1	6.4	1.61	0.014
<i>Aqp1</i>	Aquaporin 1	5.1	14.9	1.56	0.014
<i>Abca4</i>	ATP-binding cassette, sub-family A (ABC1), 4	2.7	7.0	1.37	0.014
<i>Htr2c</i>	5-hydroxytryptamine (serotonin) receptor 2C	6.0	12.9	1.11	0.014
<i>Slc31a1</i>	Solute carrier 31,1	12.3	19.2	0.64	0.022
<i>Slc4a10</i>	Solute carrier 4,10 (NaHCO ₃ co-transporter -like)	27.8	40.8	0.56	0.014
Day 7: Upregulated					
Gene	Protein	Control	AOE	Log ₂ Δ	FDR
<i>Aqp1</i>	Aquaporin 1	0.41	5.07	3.64	0.011
<i>Trpv4</i>	Transient receptor potential cation channel, V4	0.49	2.63	2.44	0.011
<i>Abca4</i>	ATP-binding cassette, sub-family A (ABC1), 4	0.54	2.39	2.14	0.011
<i>Otx2</i>	Orthodenticle homeobox 2	2.30	5.66	1.30	0.011
<i>Ntrk1</i>	Neurotrophic tyrosine kinase, receptor, type 1	3.68	7.81	1.09	0.011
<i>Prkcg</i>	Protein kinase C, gamma	9.68	19.19	0.99	0.011
<i>Itpr1</i>	Inositol 1,4,5-trisphosphate receptor 1	15.70	27.96	0.83	0.011
<i>Grid2</i>	Glutamate receptor, ionotropic, delta 2	8.98	15.07	0.75	0.011
<i>C4b</i>	Complement component 4B (Chido blood group)	4.04	6.71	0.73	0.011
<i>Slc4a10</i>	Solute carrier 4,10 (NaHCO ₃ co-transporter-like)	14.70	24.28	0.72	0.011
<i>Grm1</i>	Glutamate receptor, metabotropic 1	10.29	16.63	0.69	0.011
<i>Reln</i>	Reelin	4.63	7.45	0.68	0.011
<i>Cbln3</i>	Cerebellin 3 precursor protein	17.34	27.43	0.66	0.011
<i>Sgk1</i>	Serum/glucocorticoid regulated kinase 1	60.45	87.62	0.54	0.011
Day 28: Upregulated					
Gene	Protein	Control	AOE	Log ₂ Δ	FDR
<i>Aqp1</i>	Aquaporin 1	0.17	3.05	4.17	0.012
<i>Abca4</i>	ATP-binding cassette, sub-family A (ABC1), 4	0.49	1.47	1.60	0.012
<i>Cdh1</i>	Cadherin 1	0.78	2.06	1.39	0.012
<i>Slc6a12</i>	Solute carrier 6,12 (betaine/GABA transporter)	1.45	3.81	1.39	0.012
<i>Slc6a13</i>	Solute carrier 6,13 (GABA transporter)	5.01	10.39	1.05	0.012
<i>Rara</i>	Retinoic acid receptor α	3.83	6.92	0.85	0.033

Gene Expression Changes in the Cochlear Nucleus Following Noise Exposure

Table 6.9 Neuron specific genes downregulated at each time point in the cochlear nucleus. Genes highlighted at significantly downregulated (FDR < 0.05) were filtered based on annotations for the gene ontology term “neuron part” (GO: 0097458). For each gene, the average control and experimental (AOE) FPKM values are listed along with a Log₂ transform of fold change (Δ) and the significance value (FDR).

Day 1: Downregulated					
Gene	Protein	Control	AOE	Log ₂ Δ	FDR
<i>Dbh</i>	Dopamine beta hydroxylase	2.8	0.7	-2.11	0.037
<i>Fos</i>	FBJ osteosarcoma oncogene	20.7	7.4	-1.48	0.014
<i>Slc18a2</i>	Solute carrier 18,2 (vesicular monoamine)	3.4	1.4	-1.24	0.014
<i>Adcyap1</i>	Adenylate cyclase activating polypeptide 1	9.5	4.7	-1.00	0.022
<i>Vgf</i>	VGF nerve growth factor inducible	20.9	12.6	-0.74	0.014
Day 7: Downregulated					
Gene	Protein	Control	AOE	Log ₂ Δ	FDR
<i>Cldn5</i>	Claudin 5	29.03	13.58	-1.10	0.011
Day 28: Downregulated					
Gene	Protein	Control	AOE	Log ₂ Δ	FDR
<i>Dbh</i>	Dopamine beta hydroxylase	5.87	2.57	-1.19	0.012
<i>Doc2b</i>	Double C2 β	2.48	1.16	-1.09	0.026
<i>Kdr</i>	Kinase insert domain protein receptor	2.47	1.24	-0.99	0.026
<i>Slc6a2</i>	Solute carrier family 6,2 (adrenalin transporter)	2.02	1.05	-0.94	0.038
<i>Bmpr2</i>	Bone morphogenetic protein receptor II	18.37	10.06	-0.87	0.012
<i>Cldn5</i>	Claudin 5	29.49	16.34	-0.85	0.012
<i>Pde10a</i>	Phosphodiesterase 10A	6.55	3.83	-0.78	0.012
<i>ErbB4</i>	Erb-b2 receptor tyrosine kinase 4	5.33	3.12	-0.77	0.043
<i>Slc5a7</i>	Solute carrier family 5,7 (choline transporter)	11.91	7.19	-0.73	0.026
<i>Rgs8</i>	Regulator of G-protein signaling 8	16.89	10.54	-0.68	0.026
<i>Calb1</i>	Calbindin 1	26.43	16.66	-0.67	0.048

6.5.1 Aquaporin-1

Aqp1 encodes the aquaporin-1 water channel; a widely expressed water transport channel belonging to the major intrinsic protein (MIP) or aquaporin family. Consisting of homotetrameric structures, with six transmembrane regions, the protein forms a non-selective ion channel allowing the rapid movement of H₂O, NH₃, NO, CO₂, O₂, K⁺, Na⁺ and Cs⁺ across the cell membrane (Boassa et al., 2006, Endeward et al., 2006, Benga, 2012). In the brain, aquaporin-1 is most strongly expressed in the choroid plexus (Boassa et al., 2006), however expression has been demonstrated in the trigeminal tracts and is found in human astrocytes (Gao et al., 2012). While there is no evidence basal aquaporin-1 expression in rodent astrocytes, expression can be induced following injury or stress (McCoy and Sontheimer, 2010, Hoshi et al., 2016).

In the cochlear nucleus, *Aqp1* mRNA expression was found to be upregulated following acoustic overexposure, and remained elevated compared to control over the subsequent 28-day period (Figure 6.4). As *Aqp1* has been shown to be upregulated in astrocytes following injury, immunohistochemistry was performed to determine the location of Aquaporin-1 in the noise-exposed cochlear nucleus. In control cochlear nucleus, expression was seen in the choroid plexus and trigeminal system as previously reported. Additional expression could also be seen in the cochlear nucleus (Figure 6.5A-B). When counterstained with eNOS (data not shown), this fluorescence was determined to be associated with red-blood cells (Figure 6.5E). After noise exposure, there were no additional regions of expression in the cochlear nucleus (Figure 6.5C-D) suggesting that these levels of noise-trauma do not induce astrocytic expression of aquaporin-1.

Given the pattern of staining seen in the noise exposed cochlear nucleus, the origin of the additional mRNA in the noise-exposed animals is not clear. As red blood cells are anucleate, they themselves do not produce mRNA, although some mRNA may be retained within the cell. If increase in mRNA is associated with the red blood cells, it must be also elevated in their progenitor cells, which would

Gene Expression Changes in the Cochlear Nucleus Following Noise Exposure

suggest a systemic response to noise exposure. Another possible source of *Aqp1* mRNA could be from contamination of choroid plexus or trigeminal cells. However, as *Aqp1* expression is consistently seen to be upregulated in the noise exposed samples at each time point, contamination is unlikely to be the source of the difference. Of course, mRNA could be produced without being translated to protein, which would mean that any number of CN cell types could be upregulating expression of *Aqp1*, with no increase in protein expression.

Increases in upregulation of aquaporin-1 has previously been seen in the first 24-hour period following spinal injury in the dorsal root ganglion (Kaya et al., 2014) where it is thought to be involved in DRG regeneration (Zhang and Verkman, 2015). An upregulation of aquaporin-1 following noise would presumably provide a protective effect in the cochlear nucleus, either by assisting in the clearance of increased levels of nitric oxide seen after noise exposure (Coomber et al., 2014); or perhaps even associated with the increased metabolic demand of increased neuronal excitability. Without further investigation, it is not known whether this effect is local or systemic. Further study with RNA *in-situ* hybridisation would determine the location of mRNA expression in the cochlear nucleus, while the sampling of blood following noise exposure would test for systemic increases following noise.

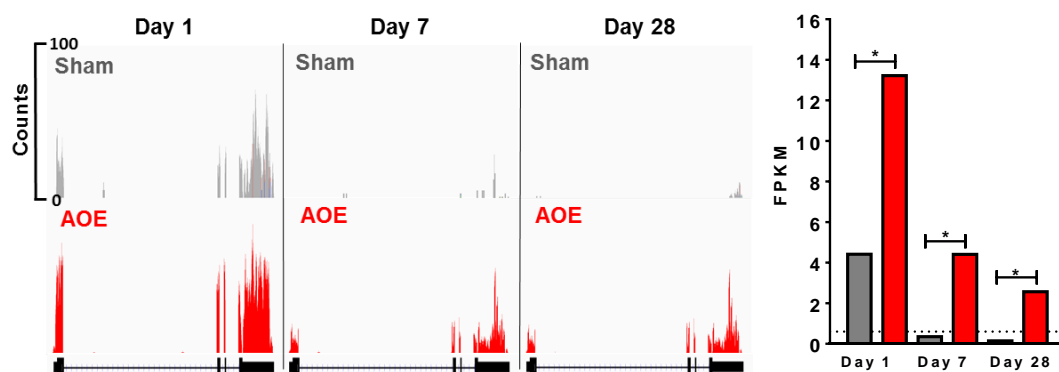


Figure 6.4: mRNA expression of *Aqp1* following noise exposure. At day one, RNASeq results showed a 2.95 fold increase in mRNA in the cochlear nucleus of noise exposed animals. This increased to a 12.47 and 18.00 fold change at seven and 28 days respectively.

Gene Expression Changes in the Cochlear Nucleus Following Noise Exposure

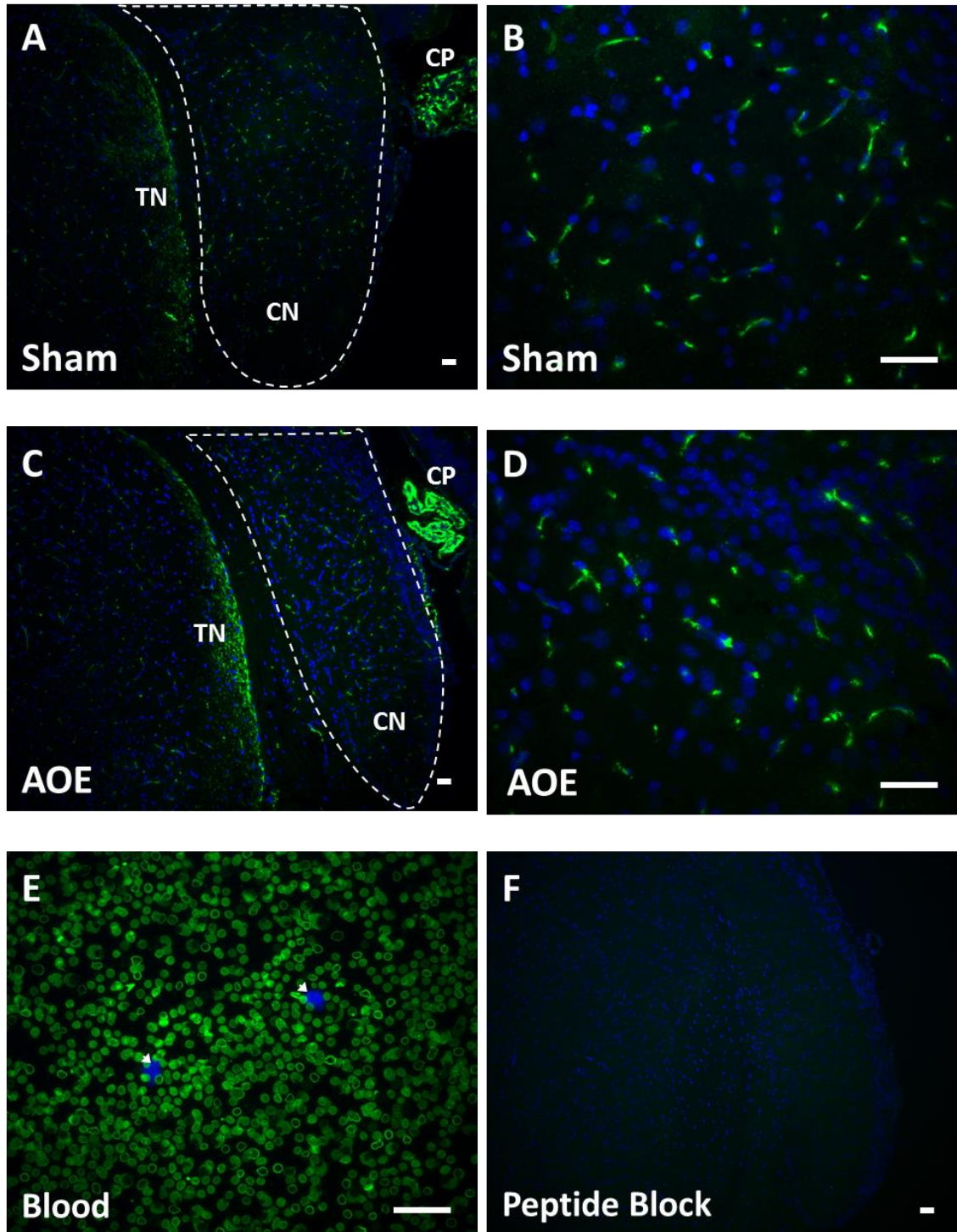


Figure 6.5: Immunolocalisation of Aquaporin 1 (green) in the cochlear nucleus. Sections were counterstained with DAPI (blue). In both the sham exposed (A-B) and acoustic overexposed (AOE; C-D) cochlear nucleus Aquaporin 1 expression was restricted to within blood vessels; this was confirmed by co-staining with eNOS (data not shown). (E) Aquaporin 1 was found to be expressed on erythrocytes, but not leukocytes (shown by arrows). There was no significant difference in immunofluorescence between the sham and AOE samples. Slides were prepared and imaged by Kishen Chahwala. Scale bar = 50 μ m.

6.6 Discussion

There were 184 unique genes found to be differentially expressed over the three time points investigated. Approximately 85% of the total gene expression changes over this period were upregulated compared to control. The number of genes upregulated and downregulated at each time point has been summarised in Figure 6.6. There were comparatively fewer changes in the cochlear nucleus than the modiolus following noise exposure, which was anticipated as damage to the cochlea is expected to be greater. Despite this, as with the modiolar samples it would be impractical to discuss every gene change seen. This section will first discuss sustained gene changes, i.e. changes seen over more than one time point. Following on from this, neuron specific changes which may affect cell excitability - and therefore potentially contribute to the phenomenon of tinnitus - will be discussed.

6.6.1 Sustained Changes in Gene Expression

Of the 184 changed genes, just 37 were found to be changed as a result of noise exposure at more than one time point. These genes can be divided into three categories: 1) genes which are differentially expressed chronically (at all three time points), as shown in Table 6.10; 2) genes which shown early changes (i.e. at one and seven days, but not 28) to expression, as shown in Table 6.11; and finally, 3) genes which shown late changes (i.e at seven and 28 days, but not one) to expression, as shown in Table 6.12 and Table 6.13.

In total, 18 genes were found to be upregulated at all three time points. The largest of these changes was to the gene encoding aquaporin-1 (*Aqp1*) which was discussed in §6.5.1. Alongside *Aqp1*, five additional genes were associated with the transport of ions either intracellularly, or across cell membranes. These were the Na⁺ / sulfate co-transporter *Slc13a4*, the NaHCO₃ co-transporter *Slc4a5*, the intracellular Cl⁻ channel *Clc6*, and *Folr1* which is capable of acting as folate co-transporter. Although it is unclear why an increase in ion transporters is seen in

Gene Expression Changes in the Cochlear Nucleus Following Noise Exposure

the 28-day period following noise exposure, one possible hypothesis of this increase is in order to handle an increase in intracellular Cl^- and bicarbonate. Such increases are proposed to happen in the inhibitory DCN cartwheel neurons following periods of activity, which leads to a decrease in intracellular pH (Kim and Trussell, 2009).

Another gene which is highly upregulated across all three time points is the *Kl*, which encodes the membrane bound protein klotho. Previous studies have found an increase in klotho to be neuroprotective through the modulation of oxidative stress and insulin-like growth factor (Igf-1) expression (Kuang et al., 2014). Increases of expression of klotho, which peaks at seven days, may be indicative of the previously described oxidative stress in the cochlear nucleus (Coomber et al., 2014).

There were just seven early upregulated genes in the cochlear nucleus (Table 6.11). Of these, the two with the largest changes were the anti-apoptotic keratin 18 gene *Krt18* (Caulin et al., 2000), and *Trpv4* which encodes the Transient receptor potential cation channel V4. *Trpv4* is discussed in §6.6.2.

Of the late gene expression changes, six were upregulated (Table 6.12) and just two were downregulated (Table 6.13). The largest of these changes were seen in tetratricopeptide repeat domain 21A (*Ttc21a*) and myelin protein zero-like 2 (*Mpzl2*) which, unlike myelin protein zero, is expressed in oligodendrocytes (Letzen et al., 2010).

Gene Expression Changes in the Cochlear Nucleus Following Noise Exposure

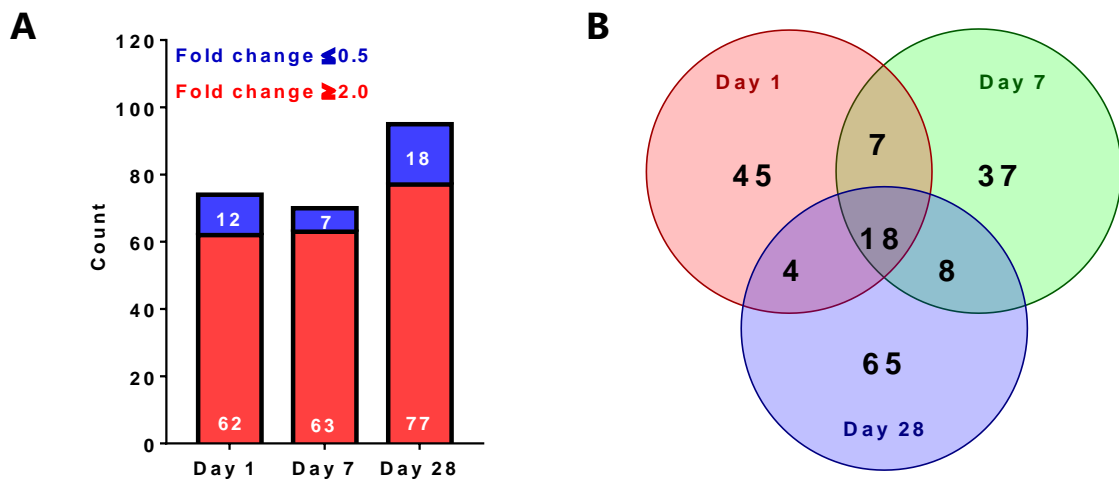


Figure 6.6: Summary of the number of genes differentially expressed in the cochlear nucleus. (A) Upregulated (fold change ≥ 2.0) and downregulated (fold change ≤ 0.5) at each time point. (B) Over the three time points, 18 genes were shared across all three time points. 7 genes can be considered to be changed early (day 1 and day 7) and 8 genes are changed late (day 7 and day 28).

Table 6.10: Genes differentially expressed at all three time points in the cochlear nucleus. All 18 genes are upregulated at all time points. Fold change (Δ) has been \log_2 transformed.

Gene	Protein	Day 1 $\log_2 \Delta$	Day 7 $\log_2 \Delta$	Day 28 $\log_2 \Delta$
<i>1500015O10Rik</i>	RIKEN cDNA 1500015O10 gene	1.3	1.5	1.4
<i>Abca4</i>	ATP-binding cassette, sub-family A	1.4	2.1	1.6
<i>Ace</i>	Angiotensin I converting enzyme 1	1.0	1.1	0.8
<i>Aqp1</i>	Aquaporin 1	1.6	3.6	4.2
<i>Car12</i>	Carbonic anhydrase 12	1.3	2.6	2.5
<i>Ccdc135</i>	Dynein regulatory complex subunit 7	0.9	1.9	1.7
<i>Cldn2</i>	Claudin 2	1.9	2.7	1.9
<i>Clic6</i>	Chloride intracellular channel 6	1.6	2.6	1.9
<i>Col8a2</i>	Collagen, type VIII, alpha 2	0.9	1.4	1.2
<i>F5</i>	Coagulation factor V	1.6	2.6	2.8
<i>Folr1</i>	Folate receptor 1 (adult)	1.4	3.1	2.5
<i>Igf2</i>	Insulin-like growth factor 2	0.6	0.6	1.3
<i>Kl</i>	Klotho	1.6	2.6	1.8
<i>Lbp</i>	Lipopolysaccharide binding protein	0.9	1.9	1.7
<i>Slc13a4</i>	Solute carrier family 13, 4	0.6	1.5	1.5
<i>Slc4a5</i>	Solute carrier family 4, 5	1.2	1.8	1.1
<i>Sostdc1</i>	Sclerostin domain containing 1	1.5	2.2	2.2
<i>Tmem72</i>	Transmembrane protein 72	1.3	2.1	1.5

Gene Expression Changes in the Cochlear Nucleus Following Noise Exposure

Table 6.11: Early upregulated genes in the cochlear nucleus. Seven genes are upregulated at both 1 day and 7 days after AOE, but not at day 28. Fold change (Δ) has been Log_2 transformed.

Gene	Long name	Day 1 $\text{Log}_2\Delta$	Day 7 $\text{Log}_2 \Delta$
<i>A2m</i>	Alpha-2-macroglobulin	0.8	0.8
<i>Col8a1</i>	Collagen, type VIII, alpha 1	0.8	1.6
<i>Col9a3</i>	Collagen, type IX, alpha 3	0.6	0.6
<i>Krt18</i>	Keratin 18	1.1	2.4
<i>Slc4a10</i>	Solute carrier family 4, 10	0.6	0.7
<i>Trpm3</i>	Transient receptor potential cation channel, M, 3	0.9	0.7
<i>Trpv4</i>	Transient receptor potential cation channel, V, 4	1.6	2.4

Table 6.12: Late upregulated genes in the cochlear nucleus. Six genes are upregulated at both 7 day and 28 days after AOE, but not at day 1. Fold change (Δ) has been Log_2 transformed.

Gene	Long name	Day 7 $\text{Log}_2\Delta$	Day 28 $\text{Log}_2 \Delta$
<i>Mpzl2</i>	myelin protein zero-like 2	2.5	1.8
<i>Pcolce</i>	procollagen C-endopeptidase enhancer protein	0.9	1.0
<i>Prlr</i>	prolactin receptor	1.8	0.9
<i>Ryr1</i>	ryanodine receptor 1, skeletal muscle	1.0	1.1
<i>Ttc21a</i>	tetratricopeptide repeat domain 21A	2.2	1.8
<i>Ttr</i>	transthyretin	1.6	1.7

Table 6.13: Late downregulated genes in the cochlear nucleus. Two genes are upregulated at both 7 day and 28 days after AOE, but not at day 1. Fold change (Δ) has been Log_2 transformed.

Gene	Long name	Day 7 $\text{Log}_2\Delta$	Day 28 $\text{Log}_2 \Delta$
<i>Cldn5</i>	Claudin 5	-1.0	-1.0
<i>Rgs5</i>	Regulator of G-protein signalling 5	-0.7	-1.3

6.6.2 Neuron Specific Changes

Noise induced hearing loss is strongly correlated with the incidence of tinnitus. As shown in Chapter 3, mice exposed to the noise model used here had ABR recordings indicative of an increase in central excitability following exposure. Furthermore, work by (Pilati et al., 2012b) showed that similar levels of noise exposure increased neuronal excitability in the murine dorsal cochlear nucleus. Increases in central excitability following noise are most likely caused by changes to ion channel composition at the cell surface.

In order to assess this, gene expression changes were filtered by those associated with neuronal parts. Of the 184 differentially expressed genes, just 35 were ontologically associated with a neuronal part. Out of the 35, 16 of the genes were changed at a single time point; and approximately 51% of all neuronal changes were changed less than 2 times control values. Besides the previously discussed *Aqp1*, the largest changes over the 28-day period were seen in transient receptor potential cation channel V4 (*Trpv4*), ATP-binding cassette A4 (*Abca4*), and dopamine β hydroxylase (*Dbh*).

Trpv4, which was upregulated both one and seven days following exposure, is a Ca^+ permeable, non-selective cation channel belonging to the transient receptor potential (TRP) family. Although widely expressed, the channel is commonly associated with primary sensory neurons, as it is opened primarily in response to heat, mechanical stimulus, hypo-osmolality, but can also be opened in response to some intracellular signalling cascades (Darby et al., 2016). In the brain, *Trpv4* is found in astrocytes, where it is expressed at their end feet (Filosa et al., 2013). Because of the channel's permeability to Ca^+ it has been shown that an increase in astrocytic *Trpv4* expression is associated with increased levels of pro-inflammatory cytokines IL-1 β and TNF- α , and increased NF- κ B activation induced by calmodulin and protein kinase C (PKC) signalling pathways (Shi et al., 2013). Here, increases in *Trpv4* do coincide with statistically significant increases in PKC γ

Gene Expression Changes in the Cochlear Nucleus Following Noise Exposure

(*Prkcg*; $\text{Log}_2\Delta = 1.00$) and PKC δ (*Prkcd*; $\text{Log}_2\Delta = 0.68$) at day seven. However, there were no observed changes to either IL-1 β or TNF- α over the 28-day time period.

In addition to its role in inflammatory processes, neuronal expression of *Trpv4* could play a key role in altering excitability following noise exposure. In the hippocampus, it has been shown that *Trpv4* protein is expressed neuronally and active at physiological temperatures. Furthermore, activation of neuronal *Trpv4* significantly increases the resting membrane potential (Shibasaki et al., 2015), thus increases in the membrane expression of *Trpv4* would conceivably increase spontaneous firing rates in the cochlear nucleus by lowering the amount of current required to trigger an action potential. Related TRP channel *Trpm3*, which is also upregulated at one and seven days following noise exposure, has also been shown to potentiate glutamatergic transmission (Zamudio-Bulcock et al., 2011); although study of *Trpm3* expression in the central nervous system is still sparse.

Just a handful of previous studies have looked at gene expression changes in the cochlear nucleus (Dong et al., 2010, Qu et al., 2015, Manohar et al., 2016). Focusing on panels of genes associated with neurotransmission, published changes include changes to GABA receptors (*Gabra1*, *Gabrag3*, *Gabbr1*, *Gabbr2*), glycine receptors (*Glr1*), glutamate receptors (*Gria2*, *Grin*) and potassium channels (*Kcnq3*, *Kcnk15*) over a 4-week period following noise exposure. Across all three studies, just one gene change was in agreement with the changes found here; this was the upregulation of *Ntrk1* ($\text{Log}_2\Delta = 1.09$), which was also seen by Manohar et al. (2016). *Ntrk1*, also known as TrkA (tryptomyosin receptor kinase A), is implicated in the generation of neuropathic pain and hyperalgesia in the dorsal root ganglion. This is initiated by the binding of nerve growth factor to TrkA which promotes upregulation of mechanoreceptors (such as TRP channels) through PKC-dependent pathways (Julius and Basbaum, 2001).

6.6.3 Summary

Fewer changes were observed in the cochlear nucleus compared to the modiolus in the 28-day period following noise. This was unsurprising, as the primary neuronal insult with noise exposure is within the cochleae. In addition to this, the changes which were seen were of smaller magnitudes compared to the modiolus, with the largest gene expression change being $\text{Log}_2\Delta = 4.2$ (compared with changes of up to $\text{Log}_2\Delta = 7.23$ in the modiolus). The subtlety of the changes seen and the absence of some of the previously reported changes is likely due to the fact that only a modest noise exposure model was used in this study.

Despite this, increases in the expression *Trpv4* and *Trpm3* could be linked to an increased rate of excitatory transmission and firing in the cochlear nucleus following noise exposure. The upregulation of these channels is potentially mediated through an increase in *Ntrk1* (TrkA) which, when bound with nerve growth factor, increases gene expression through a PKC-dependent pathway, involving PKC γ and PKC δ , at around seven days following noise exposure.

Further immunohistochemical analysis and western blots would be required to confirm increases in protein expression and location of such increases.

Chapter 7: Final Conclusions

This thesis outlines noise-induced genes expression changes in the modiolus and cochlear nucleus discovered using whole transcriptome sequencing on micro-dissected tissues. This project was distinct from previous studies in two ways. First, by micro-dissecting the modiolus instead of using whole cochleae, changes seen were specific to the spiral ganglion neurons and their immediate environment. Secondly, the noise model used here produced only mild lasting damage to auditory thresholds more analogous to leisure associated noise-induced hearing loss seen in humans. In order to collect as much information as possible from the animals used for these experiments, in addition to the modiolus, cochlear nucleus samples were also collected to look at gene expression changes in this first region of the auditory brainstem.

Noise Model

The aim of this project was to gain insight into what happens on a molecular level following moderate noise-induced hearing loss. More specifically the project was intended to investigate the phenomenon of “hidden hearing loss”, where excitotoxic synaptic degeneration leads to delayed spiral ganglion cell death in the absence of a permanent threshold shift.

ABRs were primarily obtained to ensure that the noise model used was sufficient to produce an elevation of threshold and to properly characterise this model. This amassed a considerable amount of data, both from the control (sham exposed) and the noise exposed mice. In Chapter 3, the ABR waveform of the control CBA/Ca adult mouse was described and compared against the ABR waveform for acoustic overexposed mice at three different recovery time points (1, 7, and 28 days).

The noise exposure model used here consisted of a single 1.5-hour exposure to 105 dB SPL broadband noise under anaesthesia. This resulted in immediate threshold shifts of between 22 ± 3 and 44 ± 3 dB SPL, depending on frequency

Final Conclusions

tested. Over the subsequent 28-day recovery period, threshold elevations compared to initial recording were increased between 11 ± 3 and 30 ± 4 dB SPL, suggesting partial recovery. Thresholds tested at 6, 12, and 18 kHz were statistically insignificant compared with sham exposed mice tested over the same period.

As there was not complete recovery of threshold over the 28-day period, perhaps this noise exposure model was too harsh to be considered analogous to "hidden hearing loss"; and it is possible that some of the molecular changes seen may be as a result of damage to the sensory epithelia which does not occur when full recovery is achieved. Despite this, it is reasonable to assume that the noise model used here causes a type of glutamate induced synaptopathy at the inner hair cell ribbon. There are two reasons for this; firstly, the threshold shifts seen at day one have been previously demonstrated to be sufficient to coincide with synaptic disruption (Robertson, 1983, Puel et al., 1998, Ruel et al., 2000); and secondly, the chronic suppression of wave I despite partial recovery of thresholds has been shown to be a key indicator of hidden hearing loss (Lobarinas et al, 2017). However, in addition to this, the waveform also suggested some disruption to efferent feedback, which recovered over the 28-day period, and a persistent increase in central excitability, which would suggest the presence of tinnitus.

As only a single exposure was required to elicit the required effects to hearing, this meant that the mice had minimal disturbance between the start and experimental end points. In fact, the only handling during the recovery period was to facilitate cage changes and welfare checks. Furthermore, despite the long periods of anaesthesia, the combination of drugs used here allowed for quick recovery of the mice following exposure. This ensured the good welfare of mice used for this study.

Changes to the Spiral Ganglion following Noise Exposure

Chapter 5 outlines mRNA changes to modiolar tissue collected at three recovery time points following noise exposure. By limiting the analysis of tissue to just the modiolus, it was expected that there would be fewer inflammatory genes detected within the samples following noise. Instead, what was found was an intense acute phase response which persisted over the tested period. Large increases in mRNA of serum amyloids, fibrinogens, and orosomucoids were seen out to 28 days following noise exposure suggesting the presence of chronic inflammation in the modiolar samples. What is particularly interesting is that the permanent threshold shifts observed at 28 days would be considered as just a mild loss of hearing if the same changes were seen in the evaluation of human hearing. This suggests that auditory brainstem response by itself is a poor indicator of long-term inflammatory damage to the spiral ganglion.

Previous transcriptomic analysis of noise-induced hearing loss in the cochlea have implicated the differential expression of voltage-gated sodium channels (Fryatt et al., 2011); immediate early genes such as Fos, Jun, Erg1, and Atf3 (Cho et al., 2004; Kirkegaard et al., 2006); and genes related to an oxidative stress response, such as Dusp1 and Dusp5 (Kirkegaard et al., 2006). However, Kirkegaard et al. (2006) also shows that, at least in a blast exposure model, immediate early genes are returned to control levels by 24 hours (the first time point here), which would explain their absence from this dataset. Although there is little overlap, these previous studies share a handful of similar genes changed following noise. Kininogen 1 (*Kng1*), upregulated here at all three time points, and calcitonin-related polypeptide (*Calcb*) upregulated here at day one, have both also been shown to be significantly upregulated 24 hours following blast exposure (Kirkegaard et al., 2006).

Although there was no increase here in genes classically associated with the initiation of cell death, such as Bcl-2 or any of the caspases; from the data presented here, there is a strong suggestion of disruptions to lipid binding,

Final Conclusions

production, metabolism, or storage around the spiral ganglion neurons following acoustic overexposure. Lipofuscin inclusions in the spiral ganglion have been noted before in models of chronic noise exposure, but there has been no further investigation into the role of lipids in the inner ear. Increases in free lipids in the mouse cochlea following noise could originate from myelin break down or the death of other cell types around the spiral ganglia.

In addition to the role that they play in energy storage and the maintenance of cellular structure, many lipids are also potent signalling molecules capable of mediating cell growth, death, and inflammation. It has been shown that free fatty acid levels rise following inflammatory cell activation, and their metabolites can play a multitude of both pro-inflammatory and anti-inflammatory roles (Zarate et al, 2017). While it is not clear whether the increased presence of lipid-associated molecules here would play a protective or offensive role, dyslipidaemia could ultimately be what triggers a delayed SGN cell death through the upregulation of pro-apoptotic genes *Cidea* and *Cidec* which are elevated 28 days following exposure.

Changes to the Cochlear Nucleus following Noise Exposure

Chapter 6 outlines mRNA changes to cochlear nucleus tissue collected at three recovery time points following noise exposure. There were considerably fewer, and smaller, changes in the cochlear nucleus following acoustic overexposure.

Previous gene expression studies of changes to the cochlear nucleus following hearing loss have used severe hearing loss models, and only focused on panels of genes associated with neurotransmission or pain. Published changes include changes to GABA receptors (*Gabra1*, *Gabra3*, *Gabbr1*, *Gabbr2*), glycine receptors (*Glr1*), glutamate receptors (*Gria2*, *Grin*) and potassium channels (*Kcnq3*, *Kcnk15*) over a 4-week period following noise exposure. Across all three studies, just one gene change was in agreement with the changes found here; this was

Final Conclusions

the upregulation of *Ntrk1* which was also seen by Manohar et al. (2016) following severe noise damage.

This lack of agreement in itself is not surprising as the noise insult delivered was relatively mild. While it is likely that the noise exposure delivered was tinnitus-causing, this was untested during this study. Given the mild levels of hearing elevation seen, it could be that this particular noise model was too mild to elicit and substantial changes to the cochlear nucleus.

Some observed changes, such as upregulation of *Trpv4*, *Trpm3*, and *Ntrk1* (TrkA) could potentially contribute to increases of cell excitability following noise exposure, however further study would be required to investigate this. This in itself is not surprising as the noise insult delivered was relatively mild, and the cochlear nucleus was not the primary target. While it is likely that the noise exposure delivered was tinnitus-causing, this was untested during this study. Given the mild levels of hearing elevation seen, it could be that this particular noise model was too mild to elicit and substantial changes to the cochlear nucleus.

Remaining Questions & Suggested Future Experiments

The most confounding element of the research of noise-induced hearing loss at this time is the lack of comparability between noise exposure models used between groups. Differences between species used, strain, age, and most importantly the intensity, length, and frequencies of noise delivered hampers the critical assessment of finding between experiments. In addition to this, unlike pharmacological studies, little effort has been made to create a "dose response" of noise exposure on different animal models. This creates a tendency to want to use harsher noise models, which are guaranteed to produce a threshold effect, but are likely create large inflammatory responses which mask cell specific changes.

Final Conclusions

In naivety at the beginning of this project, this work contributes yet another model of noise-exposure; thus making it difficult to make direct comparisons with other studies. To assess these subtler changes, the noise model could be refined to find the minimum exposure required to elicit the desired cellular effect. For future experiments it is suggested that the exposure should be refined to find a noise model where there was a complete recovery of threshold over the 28-day period following exposure. This would ensure that gene changes seen were due to changes to the spiral ganglion, rather than a result of cellular damage to the sensory epithelia. Such models of temporary threshold shifts are already employed (Kujawa and Liberman, 2009), but on awake mice.

Another area where this study could have been refined is in the RNA Sequencing. As a relatively new technique there is still little consensus on the limits of what is acceptable in terms of sequencing read depth. The data collected here suggests that there is good agreement between what is considered a low number of reads (15M) and the previously used Microarray. Indeed, recent studies have suggested that biological repeats are more important than read depth (Liu et al., 2014). Here, there was only enough resource for three biological repeats for each group; however, by increasing this number to at least five this would substantially increase the quality of the data collected by decreasing variability within groups, and allowing for the detection of subtler changes to gene expression.

In addition to this, the findings may also have been affected by the use of females rather than males, and by the use of a relatively wide range of ages at the time of exposure, and subsequently tissue collection. By further restricting this and the time of the day the exposure and tissue collection was carried out, this would reduce the number of non-relevant gene expression fluctuations that occur because of hormonal changes and circadian rhythm.

P2rx3 and *Aqp1* were chosen as they were chosen for further investigation as they are both ion-channels, and both had large (>2-fold) changes in gene expression

Final Conclusions

over more than one time point in the modiolus and cochlear nucleus, respectively. Despite this, no clear conclusion was reached for either gene. With the exception of *Aqp1* and *P2rx3*, none of the detected changes in gene expression were validated using a second method. Typically for whole transcriptome arrays, real time quantitative polymerase chain reaction would be employed to confirm the changed observed. There is some on-going debate as to whether this process is necessary for the validation of RNA Sequencing results, as the methods used for both are very similar. Nevertheless, any of the gene expression changes seen here should be experimentally validated before investing any time into further investigation.

For both the modiolus and cochlear nucleus samples, the first question which should be asked is where the gene is being expressed – is it neuronal, or is it expressed in the surrounding tissue? This could be achieved through immunohistochemistry, or where good antibodies are not available by RNA *in-situ* hybridization. After this, the next important question to ask would whether the increase of RNA results in an increase in protein. This could be achieved through western blotting, although this may be more difficult in the modiolar samples where protein yield is low.

Ultimately, it is the functional significance of any gene changes which is of most interest. For genes that may affect excitability in the cochlear nucleus, such as *Trpv4* and *Trpm3*, electrophysiological experiments could be conducted following noise exposure. However, this again would be challenging in the modiolus as the spiral ganglion neurons are encased in bone. For other gene changes, such as those related to fibrinogenesis and hyperlipidemia, depending on the location of the increase, it may be of interest to conduct pharmacological studies combined with noise exposure, such as the administration of a defibrinogenation agent such as Ancrod; or therapies which antagonise the production of lipofuscins, such as calorie restriction.

Final Conclusions

Finally, an estimated 50% of identified human hearing loss cases are thought to have an inheritable component. Of these, 50%, approximately 70% are non-syndromic, i.e. not associated with any other symptoms (Schrijver, 2004). Large scale genetic screening, such as the International Phenotyping Consortium (IMPC), are aiming to identify genes associated with the mammalian auditory system through the generation of null mouse mutants for every known mouse gene. To date, the approximately 2% of all mutant lines screened have been identified as having a significant hearing deficit compared to littermate controls (Bowl et al., 2017). Clearly, then genetics must play a key role in an individual's susceptibility to hearing loss.

While it is tempting to see hereditary hearing loss and NIHL as two separate conditions, proteins which have protective effects following auditory insult may be necessary to preserve auditory thresholds throughout an individual's lifetime. Thus, the use of information from this dataset should not be restricted to the study of NIHL, but be used within the wider context of hearing-loss related disorders.

Appendix 1 : Kv3 in the Auditory Pathway

The voltage gated potassium family Kv3s are a subfamily of high voltage activated K⁺ channel subunits consisting of 4 subunits (Kv3.1-3.4). The rapid kinetics associated with these channels allows for a fast repolarization of action potential, and thus a faster rate of firing (Rudy and McBain, 2001). As the auditory system relies on the ability to follow high frequency stimulus, the location and function of the Kv3s in the auditory system are a good candidate for study.

This section includes data collected for additional work unrelated to the original project presented in this thesis. This side project came about after the discovery of an age-related increase the mRNA of Kv3.1 and Kv3.3 in the auditory pathway as shown in Chapter 4. As part of another project within the group, Kv3.1^{-/-} and Kv3.3^{-/-} mice were already bred at the University of Leicester, however screening of the mutants had revealed no obvious auditory phenotype when tested shortly after hearing onset. This presented the question: if Kv3 expression increases over time in control animals, could a phenotype be observed at a later, adult, time point?

This chapter includes data collected about the presence, location, and physiological function of Kv3.1-3.4 in the mouse auditory system. As the function of Kv3s was not related to the primary aim of this thesis, this chapter is meant as a record of these recordings only, and will not include an in depth introduction or discussion of results.

The data collected here will assist other projects currently investigated within the Forsythe group, and contributes to two questions:

- 1) Which of the Kv3 subunits are expressed in the auditory system?
- 2) How does the absence of Kv3 alter hearing, as measured by the auditory brainstem response?

A1.1 Immunolocalisation of Kv3s in the Auditory System

Using immunohistochemistry, Kv3.1 – Kv3.4 were probed in three distinct areas of the auditory system: the spiral ganglion neurons, the cochlear nucleus, and the superior olivary complex. Results are outlined below.

The antibodies for Kv3.1 and Kv3.3 have been previously well validated by pre-absorption of peptides and knock out tissues in immunohistochemistry (data not shown) and immunoblots (see Figure A1.6 and Figure A1.9). Secondary antibody controls were also included in the analysis as some auto-fluorescence was detected when staining for Kv3.1 within the cochlea (see Figure A1.5). Antibodies for Kv3.2 and Kv3.4 were validated using secondary antibody and peptide pre-absorption controls, and found no non-specific staining (see Figure A1.7 and Figure A1.10).

It is worth noting that the Kv3.3 antibody used here gives poor results without an antigen retrieval method applied beforehand. For brainstem sections this was performed using a heat mediated antigen retrieval in citrate buffer. However, when the same method was applied to cochlea sections, poor adhesion of the section to the slide meant that tissue was often damaged or lost during this process. For cochlea sections, a number of room temperature antigen retrieval methods were trialed, including enzymatic antigen retrieval; however the method which produced the best results was a short incubation (5 mins) in 1% SDS. This produced the clearest staining and did not visibly alter the structure of the fixed cochlear tissues.

Spiral Ganglion Neurons

Immunohistochemistry of each of the subunits revealed the expression of Kv3.1, Kv3.3, and Kv3.4 in the spiral ganglion cell bodies (Figure A1.1). In addition to this Kv3.1 staining was apparent at nodes of Ranvier and within the SGN dendrite near the inner hair cell synapse. This pattern of Kv3.1 expression has been previously demonstrated (Kim and Rutherford, 2016). While mRNA expression of Kv3.3 has

: Kv3 in the Auditory Pathway

been shown previously in the mouse cochlea (Chen and Davis, 2006), the presence of protein has not been previously published. This data is also the first time that Kv3.4 has been shown to be present in spiral ganglion neurons.

Cochlear Nucleus

Immunohistochemistry of each of the Kv3 subunits showed clear staining of Kv3.1 and Kv3.3 in the cochlear nucleus (see Figure A1.2). For some cell types, this staining appeared to be membrane bound, although staining of the processes could be observed. Not every cell (associated with DAPI staining) showed this pattern of membrane associated staining, suggesting that only a subset of cell types express the protein. Only small amounts of Kv3.2 staining was observed in the cochlear nucleus, and Kv3.4 staining was localised to small regions around the nucleus, or perhaps just in subset of small cells or glia.

Superior Olivary Complex

Immunohistochemistry of each of the Kv3 subunits yielded similar staining patterns to those which were seen in the cochlear nucleus. Kv3.1 and Kv3.3 showed staining in each region of the SOC and in many cases appeared to be membrane bound. In the MNTB membrane associated staining of both Kv3.1 and Kv3.3 could be seen in the principle neurons (see Figure A1.4). However, in the LSO only Kv3.3 was membrane associated with the principle neurons, while Kv3.1 was restricted to surrounding processes (see Figure A1.4). There was no evidence of Kv3.2 across the SOC, and Kv3.4 was restricted to small regions around the nucleus, or within other non-principle neurons such as glia.

Given the pattern of staining, it is likely that Kv3.1 and Kv3.3 are the only subunits contributing to a Kv3 current in the superior olivary complex.

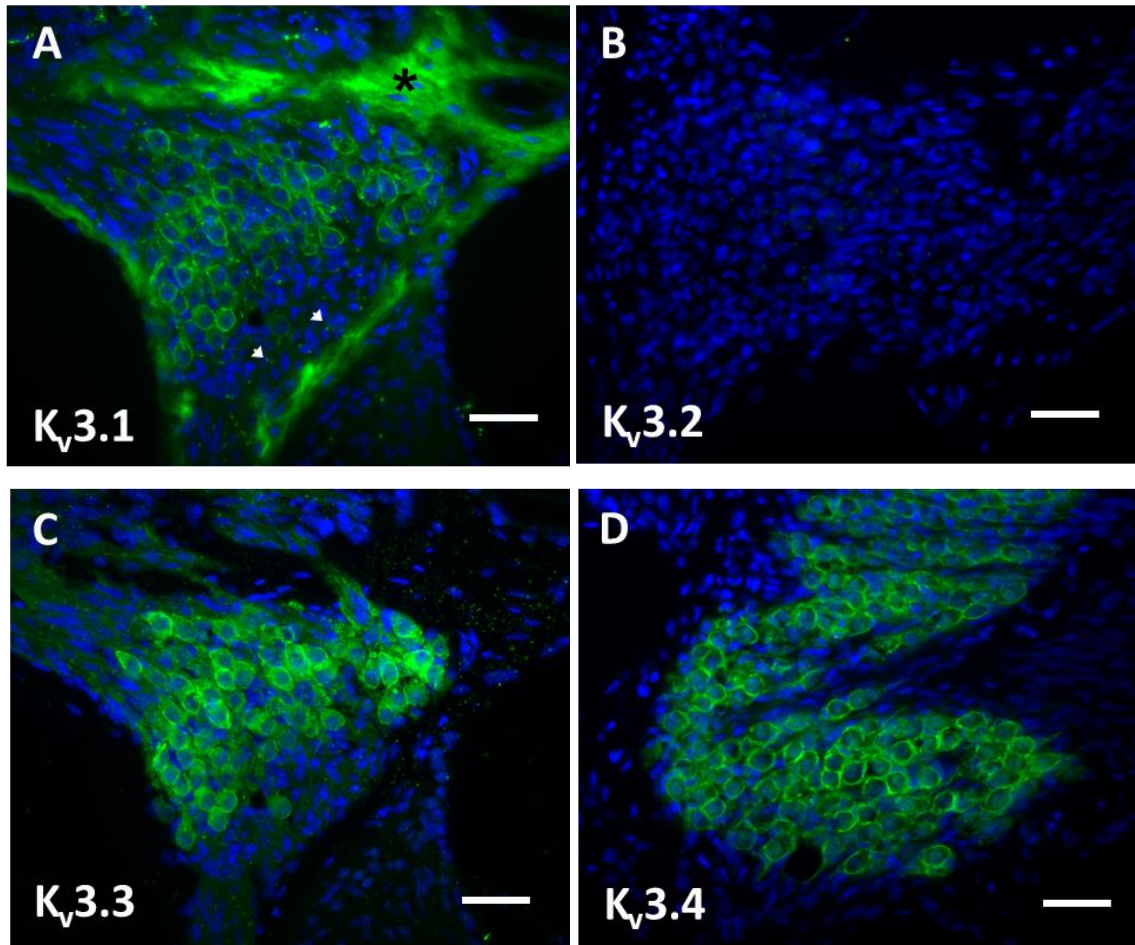


Figure A1.1: Immunolocalisation of Kv3s in the spiral ganglion. Of the Kv3 family, 3.1 (A), 3.3 (C), and 3.4 (D) were present in the spiral ganglion cell bodies when investigated using immunohistochemistry. Kv3.2 (B) was not present in the cochlea. In addition to the cell bodies, Kv3.1 was also present at nodes of Ranvier (A, arrows); the non-specific staining on bony segments of the cochlea (*) was also present when the primary antibody was omitted. Kv3.3 (C) showed faint staining in the axons and dendrites, but strongly stained the cell bodies, and Kv3.4 (D) was restricted to the cell bodies and axon initial segment. Scale bar = 50 μ m, DAPI shown in blue.

: KV3 in the Auditory Pathway

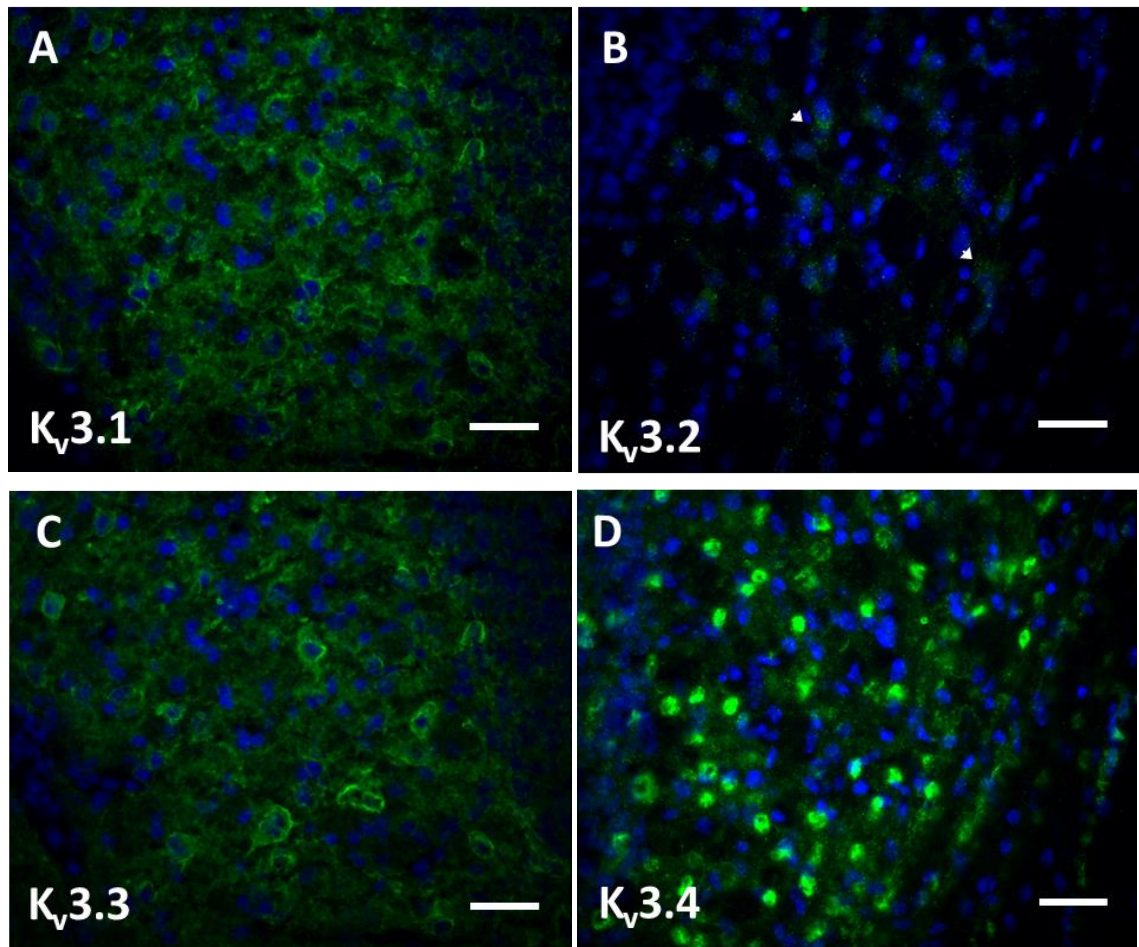


Figure A1.2: Immunolocalisation of Kv3s in the cochlear nucleus. Kv3.1 (A) and Kv3.3 (B) were found in the membrane of principle cells of the cochlear nucleus. Kv3.2 (B) showed faint staining across the cochlear nucleus, and Kv3.4 (D) was present, but did not appear to be in the membrane. Scale bar = 50 μ m, DAPI shown in blue.

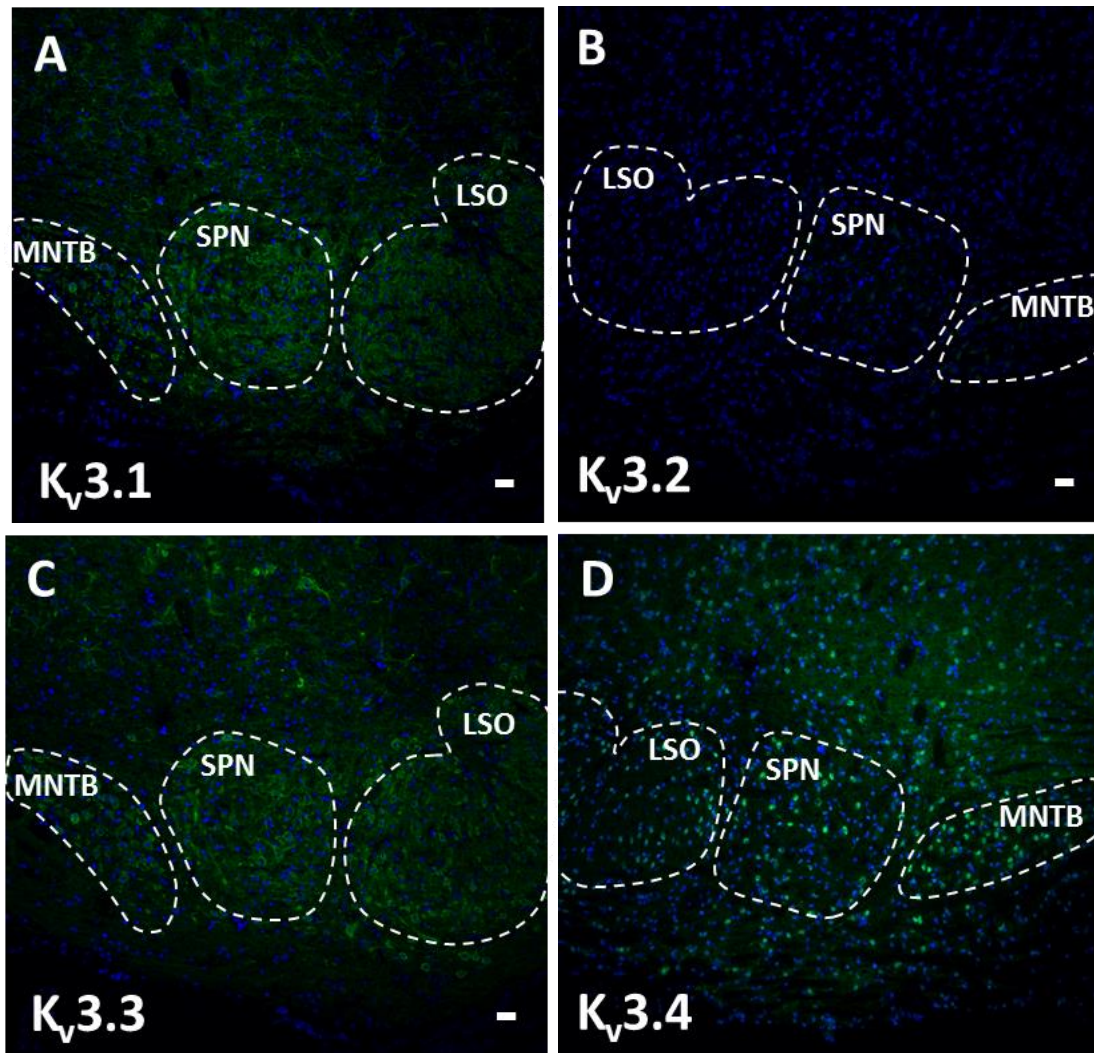


Figure A1.3: Immunolocalisation of Kv3s in the superior olivary complex. Similar patterns of staining to the cochlear nucleus were found across the medial nucleus of the trapezoid body (MNTB), superior periolivary nucleus (SPN) and lateral superior olive (LSO). Kv3.1 (A) and Kv3.3 (C) were found in the membrane of principle cell. Kv3.2 (B) was not present in any of the nuclei, and Kv3.4 (D) was present, but did not appear to be in the membrane. Scale bar = 50 μm, DAPI shown in blue.

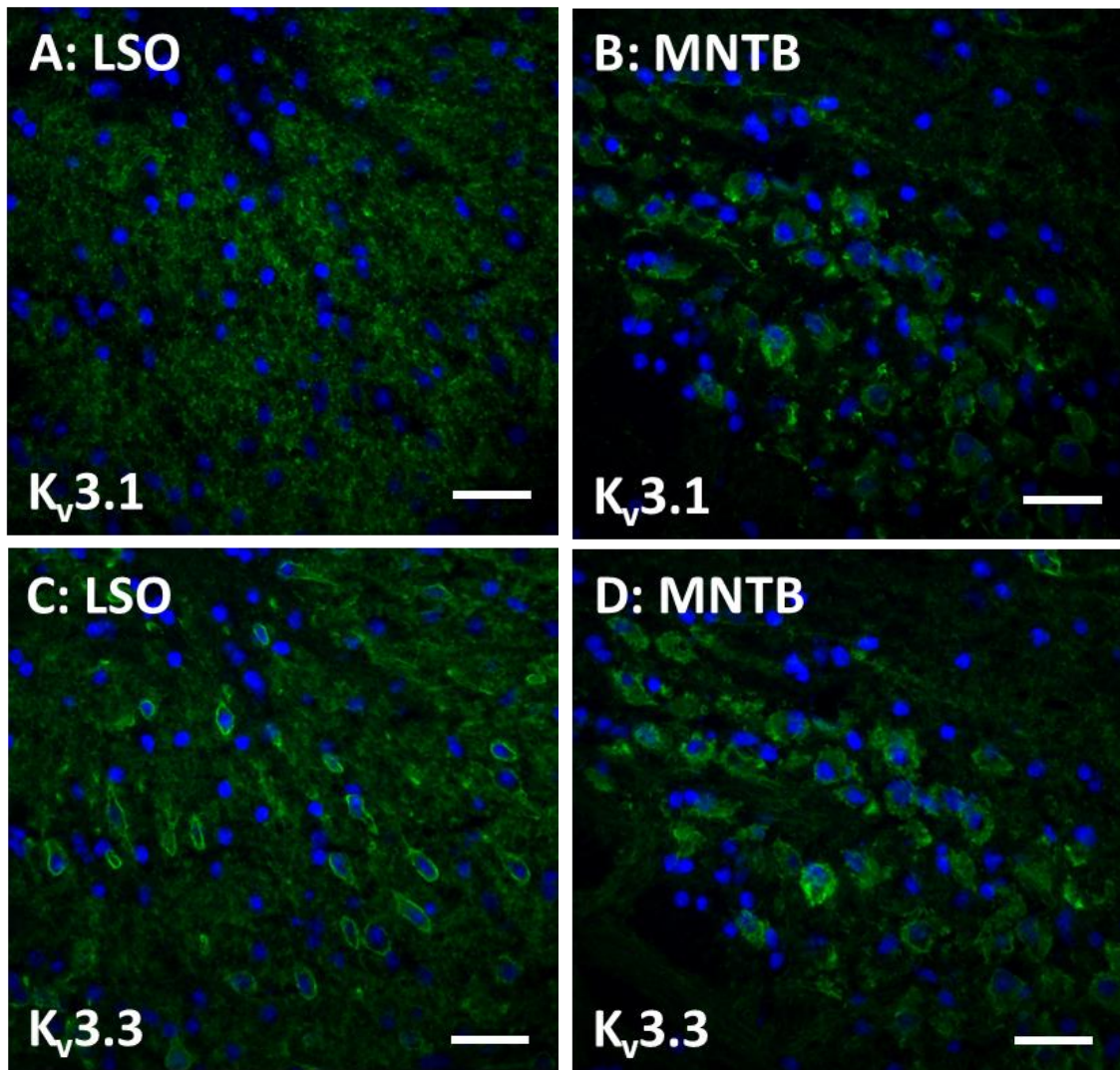


Figure A1.4: K_v3.1 and K_v3.3 are the predominant K_v3s in the superior olivary complex. In the MNTB, both K_v3.1 (B) and K_v3.3 (D) were present in the principal cells. In the LSO, K_v3.3 (C) was present in the principle cell membrane, but K_v3.1 (A) was restricted to the neuropil. Scale bar = 50 μm, DAPI shown in blue.

: Kv3 in the Auditory Pathway

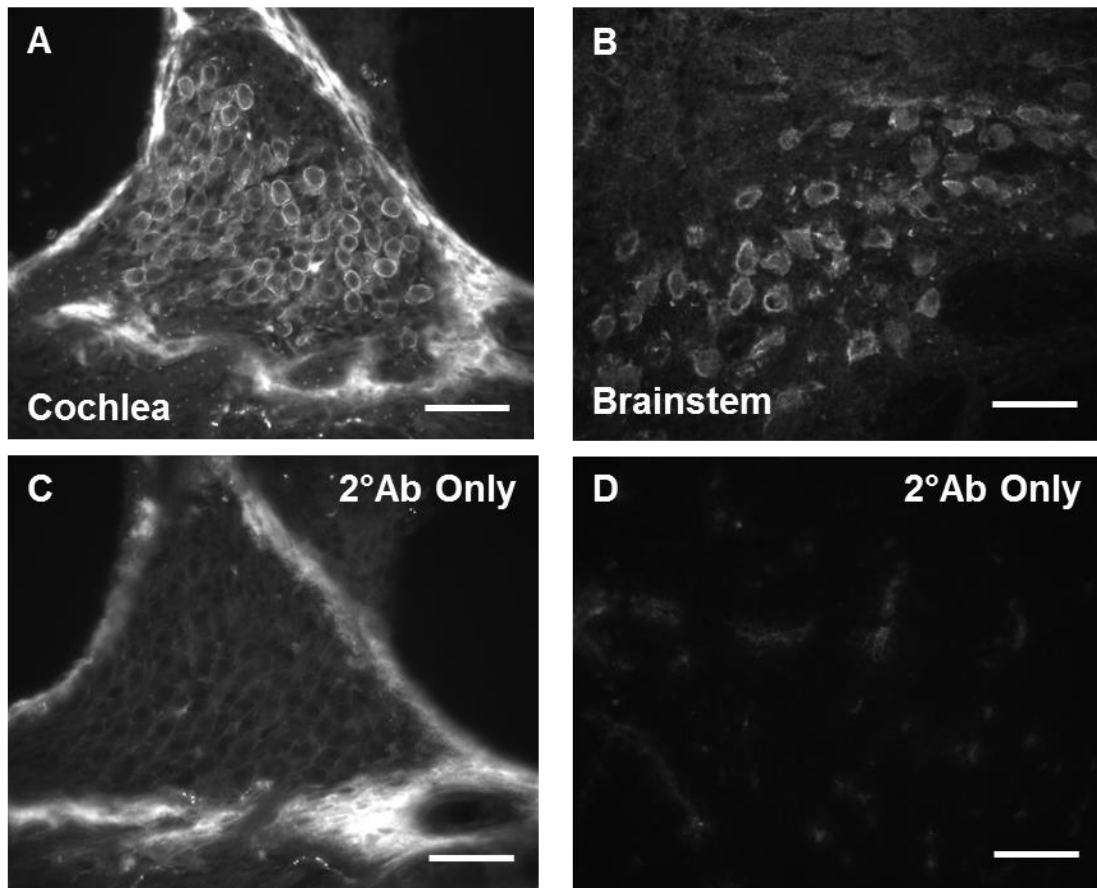


Figure A1.5: Kv3.1 antibody validation. Comparison of Kv3.1 and secondary antibody controls in the cochlea (A,C) and brainstem (MNTB) (B,D). Scale bar = 50 μ m.

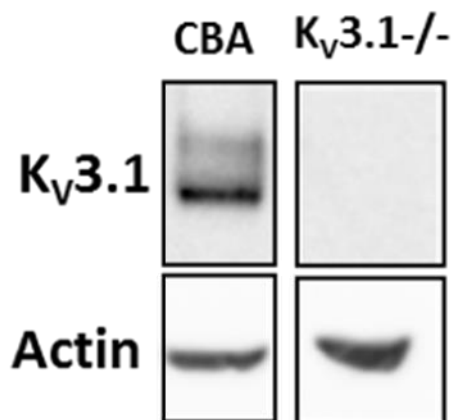


Figure A1.6: Kv3.1 antibody validation by Western Blot. The absence of non-specific binding of Kv3.1 antibody was confirmed using Kv3.1 null brain lysates. Antibody was also tested using immunohistochemistry on knock-out tissue and produced no staining (data not shown).

: KV3 in the Auditory Pathway

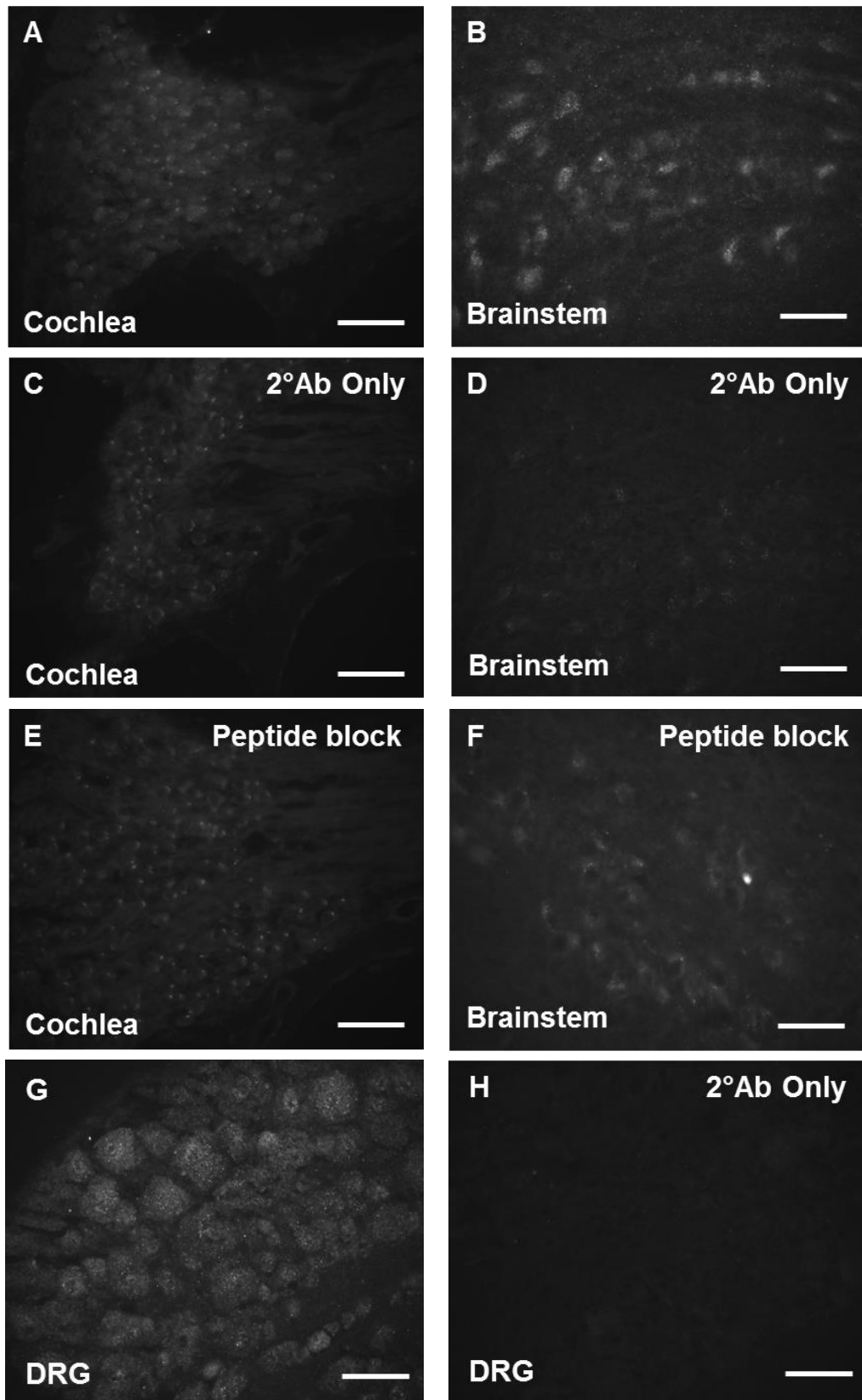


Figure A1.7: Kv3.2 antibody validation. Comparison of Kv3.2, secondary antibody controls, and peptide block absorption controls in the cochlea (A,C,E) and brainstem (MNTB) (B,D,F). There was no visible expression of Kv3.2 above the levels seen in the negative controls. Dorsal root ganglion (DRG) sections were also included as a positive control (G,H). Scale bar = 50 μ m.

: KV3 in the Auditory Pathway

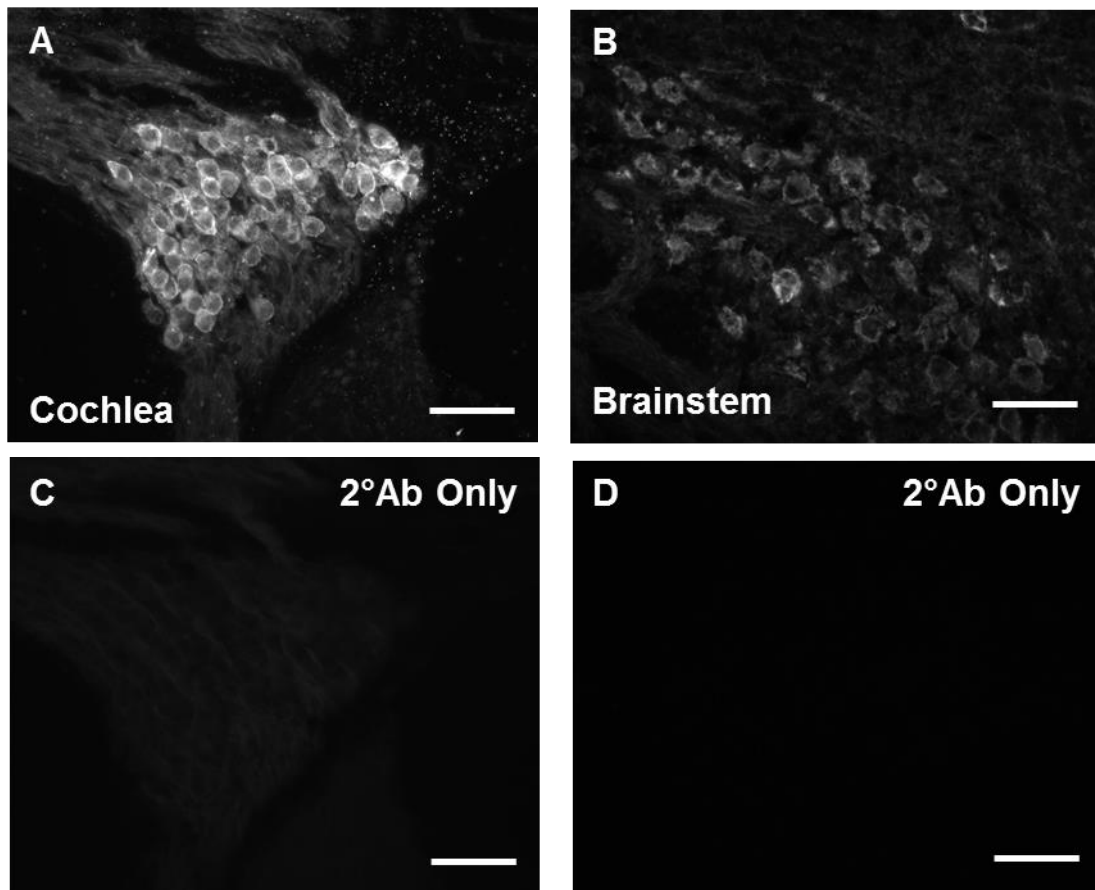


Figure A1.8: Kv3.3 antibody validation. Comparison of Kv3.3 and secondary antibody controls in the cochlea (A,C) and brainstem (MNTB) (B,D). Scale bar = 50 μ m.

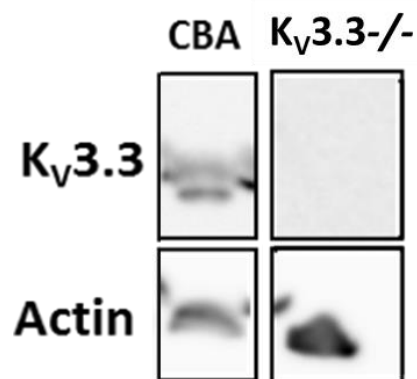


Figure A1.9: Kv3.3 antibody validation by Western Blot. The absence of non-specific binding of Kv3.3 antibody was confirmed using Kv3.3 null brain lysates. Antibody was also tested using immunohistochemistry on knock-out tissue and produced no staining (data not shown).

: Kv3 in the Auditory Pathway

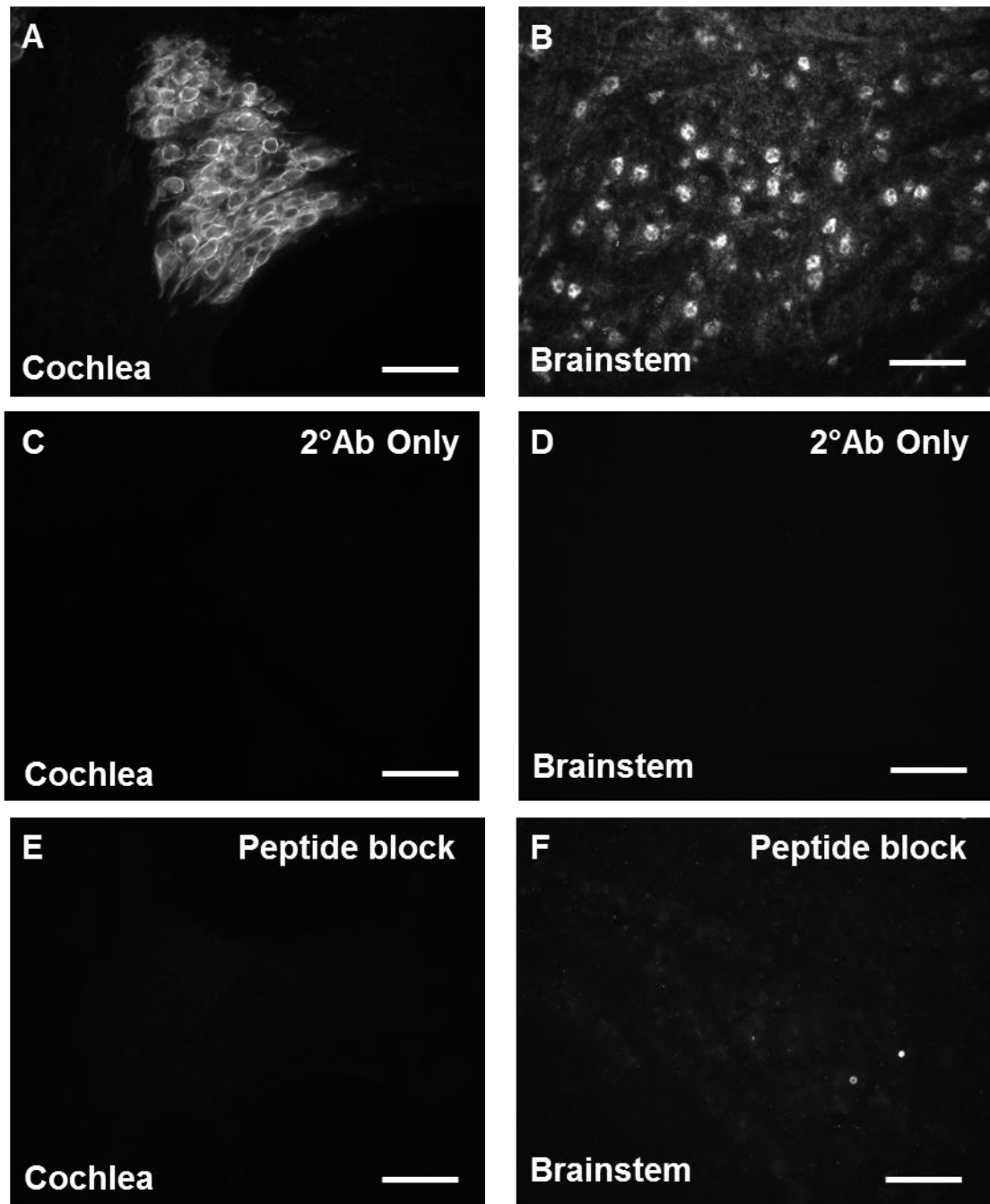


Figure A1.10: Kv3.4 antibody validation. Comparison of Kv_v3.4, secondary antibody controls, and peptide block absorption controls in the cochlea (A,C,E) and brainstem (MNTB) (B,D,F). Scale bar = 50 μ m.

A1.2 Kv3 Expression Increases with Age

Following on from the RNA Sequencing results in §4.3, which showed increasing levels of mRNA for Kv3.1 and Kv3.3 with age, brainstem (cerebellum removed) was taken from CBA/Ca mice aged 1 month old (1Mo), and mice aged to 6 months (6Mo). Western blots showed a large and significant increase in both subunits over this time period (Figure A1.11). A similar increase in Kv3.1 expression was seen even in the absence of Kv3.3.

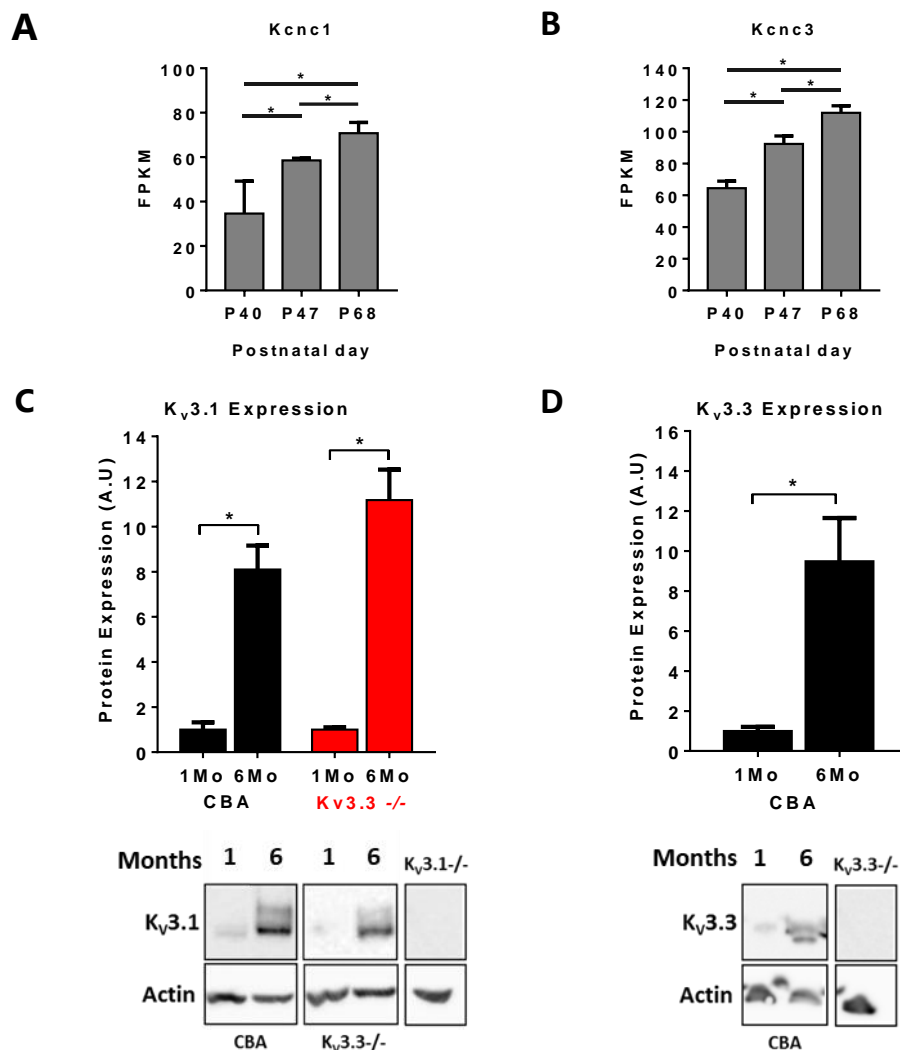


Figure A1.11: Kv3 expression in the brainstem increases with age. mRNA data from the cochlear nucleus showed increases in expression (FPKM, Fragments per kilobase of transcript per million mapped reads) of (A) *Kcnc1* (Kv3.1) and (B) *Kcnc3* (Kv3.3,) between P40 and P68 (data taken from RNASeq results). To see whether this translated to an increase of protein, whole brainstem sections were taken at 1 month of age (~P30) and 6 months of age (~P180) and western blots performed. Both Kv3.1 (C) and Kv3.3 (D) were significantly increased in the 6 month old CBA mouse. In addition to this, similar increases in Kv3.1 expression in the absence of Kv3.3 (C).

: KV3 in the Auditory Pathway

A1.3 Auditory Brainstem Response recordings

Following on from the confirmation of presence and location of Kv3.1 and Kv3.3 in the auditory brainstem, hearing in Kv3.1^{-/-} and Kv3.3^{-/-} was assessed using the ABR response. In human cases of Kv3 dysfunction, such as spinocerebellar ataxia type 13, deficits in hearing and sound localization is observed, but this is often late to manifest (Middlebrooks et al., 2013). Because of this, and because initial screening of adolescent mice showed no apparent phenotype, mice were aged to approximately 6 months prior to testing. For Kv3.3 additional recordings at approximately 1 month of age have also been taken and recorded. This section will outline the findings from analysis of the ABR.

The Kv3.3 mice were bred as homozygous mutants, so littermate controls could not be used. In each case the mice homozygous for the knock out allele are on a background of CBA/Ca mice, and have therefore been compared to inbred CBA/Ca colony bred at the University of Leicester.

Auditory Brainstem Response in the Kv3.1^{-/-} mouse

At 6 months of age, Kv3.1^{-/-} mice showed slightly elevated thresholds, in particular at high frequency; however these were not statistically significant when compared to control (Figure A1.12). Visual inspection of the ABR waveforms suggested that the ^{-/-} mice had a depressed waveform with globally depressed amplitudes. Amplitude of wave I and wave IV was measured for ABRs recorded using 12kHz and 24kHz stimuli; which for the purpose of discussion will be considered low frequency and high frequency, respectively. At low frequency (12kHz) wave I was marginally depressed while wave IV was indistinguishable from control (Figure A1.12A-C). However, at high frequencies (24kHz) both wave I ($P = 0.0005$) and wave IV ($P = 0.0415$) were significantly decreased in the ^{-/-} mouse (Figure A1.12D-F), when compared using a two-way ANOVA.

Compared to wild-type, variability was increased in the ^{-/-} mouse, as can be seen in the ABR traces in Figure A1.12.

: KV3 in the Auditory Pathway

Auditory Brainstem Response in the Kv3.3^{-/-} mouse

At 1 month of age, ABR thresholds of Kv3.3^{-/-} were decreased compared to control (Figure A1.13A-B). This was accompanied by an abnormally large amplitude for wave I at low frequency (12kHz), which was significantly elevated compared to control (Figure A1.15A-C, $P = 0.0236$). At high frequency (24kHz), while wave I was indistinguishable from control, wave IV was significantly depressed ($P = 0.0215$); in fact wave IV was only just distinguishable from wave III when the data was averaged (Figure A1.15D-F). The apparent shift in latency at 30dB re: threshold (Figure A1.15a) was not significant following statistical tests.

At 6 months of age while auditory thresholds are indistinguishable from controls (Figure A1.13C-D), there is a significant decrease in wave I at both low (12kHz, $P = 0.0193$) and high (24kHz, $P = 0.0011$) frequencies. In addition to this, at high frequency wave IV is almost absent from the ABR waveform (Figure A1.16D-F, $P = 0.0002$), suggesting severe deficits in the regions associated with this area (see Figure 3.12B).

Interestingly, the CBA thresholds are significantly decreased between 1 month and 6 months, but Kv3.3^{-/-} are unchanged. This means that the lack of difference seen at 6 month it is not due Kv3.3^{-/-} thresholds increasing, but rather CBA thresholds improving; this could indicate either accelerated maturation of the primary auditory neurons or an initial hyperacusis.

: KV3 in the Auditory Pathway

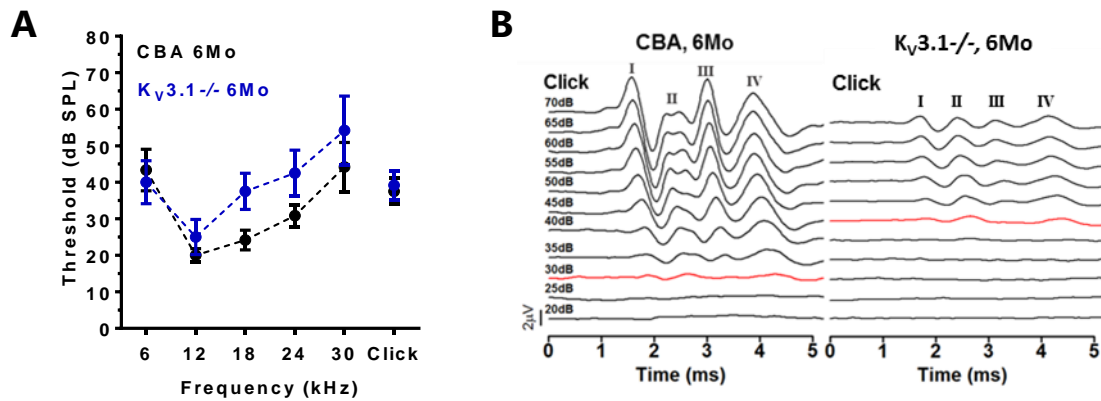


Figure A1.12: Auditory thresholds of $Kv3.1^{-/-}$ mice. ABR thresholds (A) were not significantly different to age matched controls. However, slight elevations could be seen at higher frequencies. Visual inspection of the ABR waveform for Click stimulus suggested deficits in waveform amplitude (B). $Kv3.1^{-/-}$ n = 5, CBA n = 10.

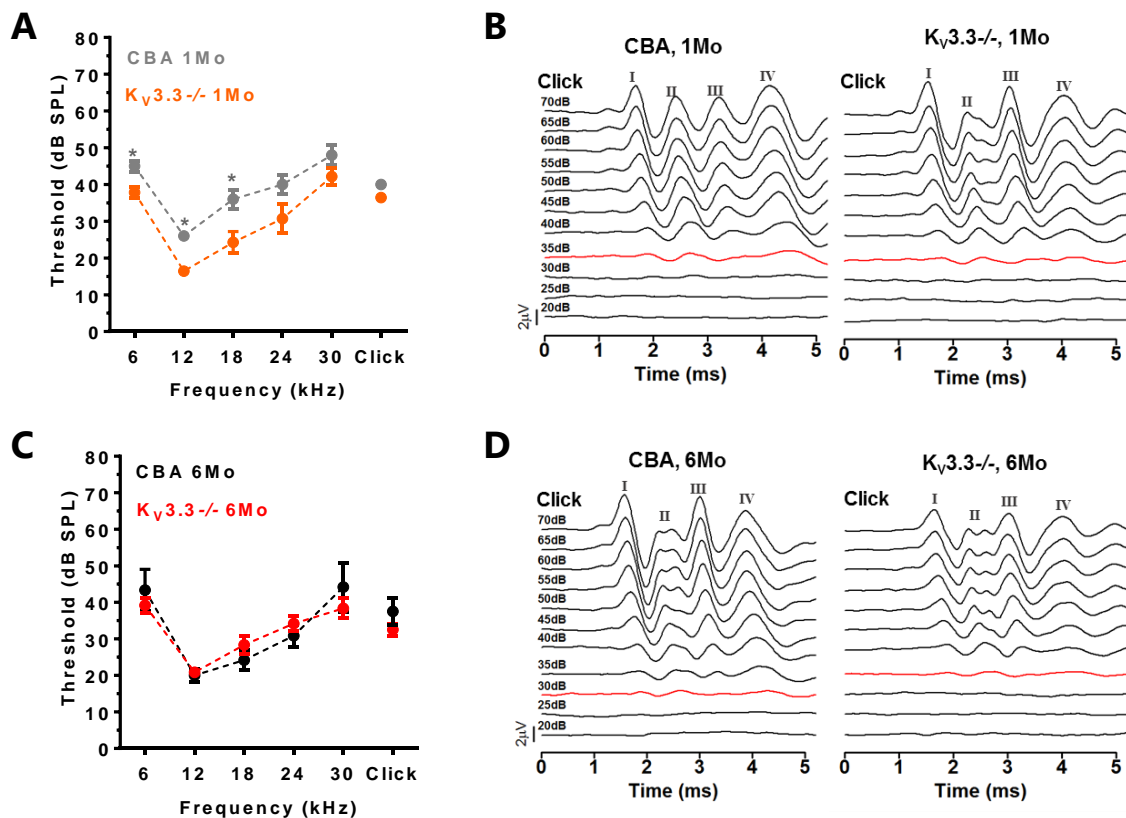


Figure A1.13: Auditory thresholds of $Kv3.3^{-/-}$ mice. At 1 month of age (A-B) $Kv3.3^{-/-}$ mice had slightly better thresholds at low frequencies compared to age matched controls. By 6 months of age (C-D), thresholds were indistinguishable from control. $Kv3.3^{-/-}$ (1 month) n = 7, $Kv3.3^{-/-}$ (6 month) n = 6, CBA (1 month) n = 5, CBA (6 month) = 10.

: KV3 in the Auditory Pathway

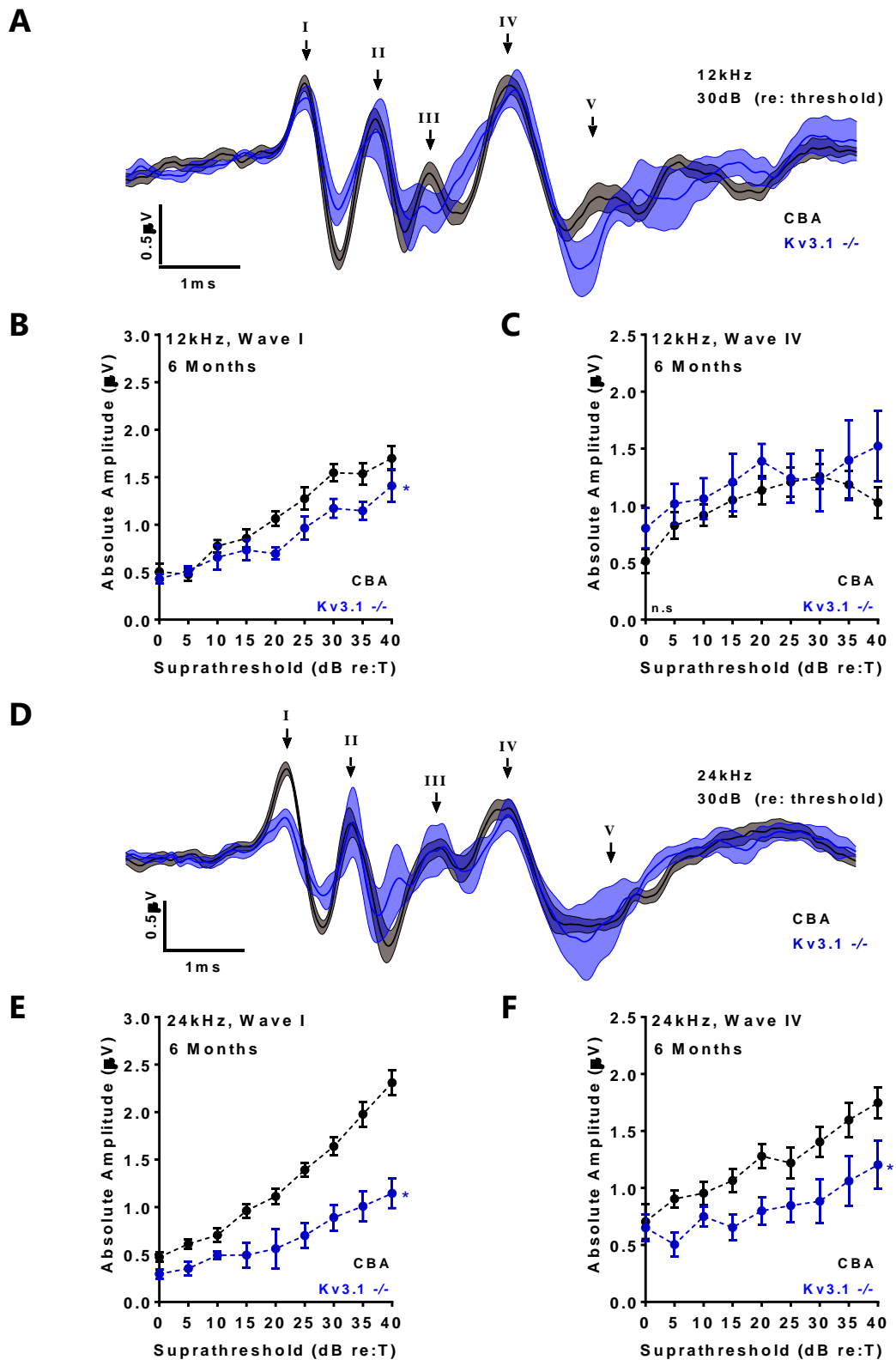


Figure A1.14: The ABR waveform in six month old *Kv3.1*^{-/-} mice. The ABR waveform for stimuli at 12 kHz (A-C) and 24 kHz (D-F). Minor deficits in wave I amplitude are seen at 12 kHz (B), while wave IV is indistinguishable from the age matched controls (C). However, at higher frequencies (24 kHz), significant deficits are seen in both wave I (E) and wave IV (F). *Kv3.1*^{-/-} n = 5, CBA n = 10. Asterisk (*) on plot denotes significant difference in trend when compared with a 2-way ANOVA.

: KV3 in the Auditory Pathway

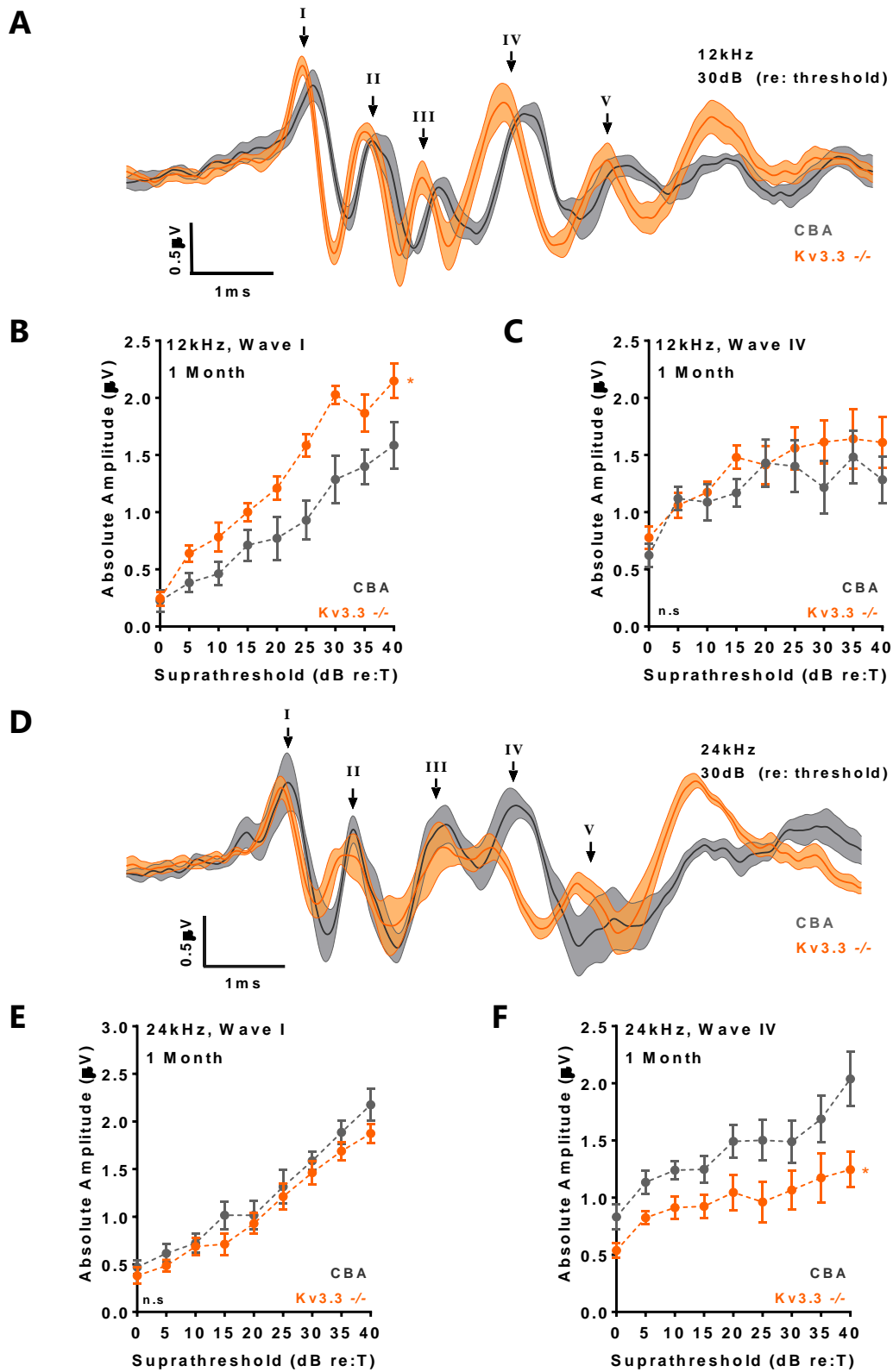


Figure A1.15: The ABR waveform in 1 month *Kv3.3*^{-/-} mice. The ABR waveform for stimuli at 12 kHz (A-C) and 24 kHz (D-F). At 12 kHz, wave I amplitude is increased in the *Kv3.3*^{-/-} mouse (B), a difference which is not carried through to wave IV (C). This increase is not seen at 24 kHz (E), and deficits can be seen in wave IV (F). *Kv3.3*^{-/-} n = 7, CBA n = 5. Asterisk (*) on plot denotes significant difference in trend when compared with a 2-way ANOVA.

: KV3 in the Auditory Pathway

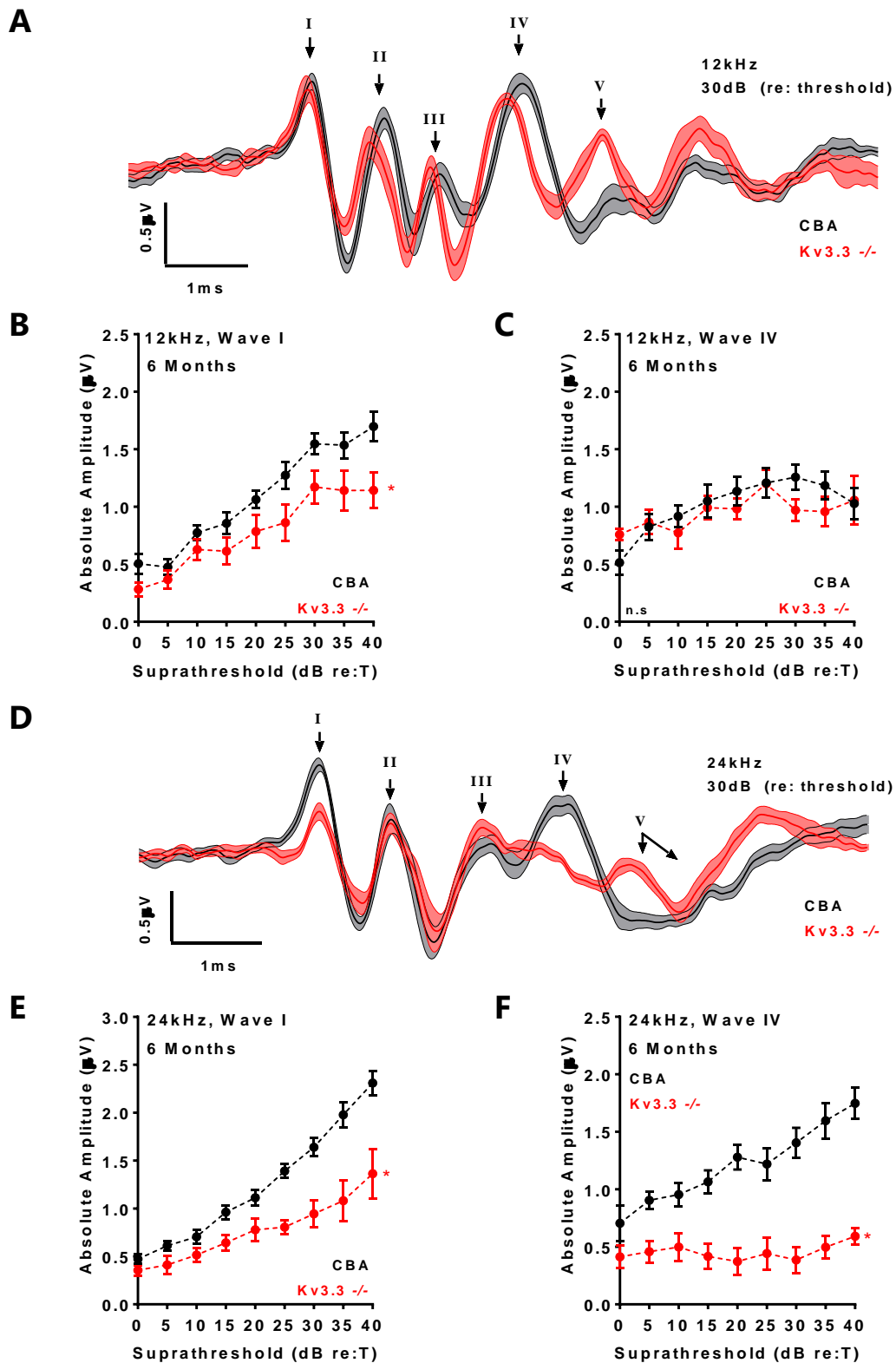


Figure A1.16: The ABR waveform in 6 month old $Kv3.3^{-/-}$ mice. The ABR waveform for stimuli at 12 kHz (A-C) and 24 kHz (D-F). Hyper-acusis of 12 kHz wave I at one month of age is lost by six months (B). At higher frequencies (24 kHz), major deficits in wave I (E) and a complete loss of wave IV (F) can be seen, despite the fact that wave IV is unchanged at 12 kHz (B). $Kv3.3^{-/-}$ n = 6, CBA n = 10. Asterisk (*) on plot denotes significant difference in trend when compared with a 2-way ANOVA.

A1.4 Summary

In summary, this chapter demonstrates that:

- 1) K_v3.1, K_v3.3, and K_v3.4 is expressed in spiral ganglion neurons.
- 2) All K_v3 subunits are present in the cochlear nucleus, however only K_v3.1 and K_v3.3 are membrane associated.
- 3) It is likely that K_v3.1 and K_v3.3 are the only subunits contributing to a K_v3 current in the superior olivary complex.
- 4) Whole brainstem expression levels of K_v3.1 and K_v3.3 increases between the ages of 1 and 6 months of age; and the increase in K_v3.1 occurs even in the absence of K_v3.3.
- 5) The absence of K_v3.1 results in decreased ABR waveform amplitudes at 6 months of age, but produces variable results.
- 6) The absence of K_v3.3 removes wave IV from the ABR waveform and decreases wave I at 6 months of age; this effect is more severe at high frequencies, and occurs without an increase in hearing thresholds.

Appendix 2 : Exemplar Scripts

Script 2.1: Example of script used to generate list of GO terms using the R Goseq package. Overenriched GO terms were ranked and output as a text file of all GO terms with corrected $P < 0.05$.

```
source("https://bioconductor.org/biocLite.R") #requires installation of packages
#biocLite("biomaRt")
#biocLite("org.Mm.eg.db")
#biocLite("goseq")
###Load required libraries###
library(org.Mm.eg.db)
library(goseq)
library(GO.db)
library(biomaRt)

txtfile<- "upday1_GO.txt"          #Sets name of output file

de.genes<-scan("up1daysignificantgenes.txt", what="char")      #Sets list of DE genes
assayed.genes<-scan("assayed.day28.txt", what="char")  #Sets total assay genes tested

mart<-useMart(biomart="ENSEMBL_MART_ENSEMBL",host="grch37.ensembl.org",
              path="/biomart/martservice", dataset="mmusculus_gene_ensembl")
gene.vector=as.integer(assayed.genes%in%de.genes)  #creates gene vector for analysis
names(gene.vector)=assayed.genes
###fit the probability weighting function (PWF) (mm10 not available)
pwf=nullp(gene.vector, "mm9", "geneSymbol")
###using the wallenius approximation (requires org.Mm.eg.db package to be installed)
GO.wall=goseq(pwf,"mm9", "geneSymbol", test.cats="GO:BP")
enriched.GO.over=GO.wall$category[p.adjust(GO.wall$over_represented_pvalue,
                                           method="BH")<.05]
enriched.GO.under=GO.wall$category[p.adjust(GO.wall$under_represented_pvalue,
                                           method="BH")<.05]
###Adjust P value using Benjamin & Hochberg
pval<-p.adjust(GO.wall$over_represented_pvalue, method="BH")

###Output GOterms into defined .txt file
count<-1
sink(txtfile)
cat("OVER-REPRESENTED GO TERMS:\n")
for(go in enriched.GO.over){
  cat("=====\n")
  cat(count, "\n")
  print(GOTERM[[go]])
  cat("\n")
  cat("pvalue: ",pval[count], "\n")
  cat("=====\n")
  count<-count+1
}
sink()
```

: Exemplar Scripts

Script 2.2: R Script to read .BAM files and retrieve additional gene information.

```
### dir must point to a folder with .BAM files only ###
###Load in required libraries###
library(GenomicAlignments)
library(GenomicFeatures)
library(biomaRt)
###Bam file is read and compiled into count tables###
generateCountTable<-function(
  files,
  transcripts="TxDb.Mmusculus.UCSC.mm10.knownGene",
  overlpto="gene"){
  require(transcripts, character.only=T)
  require(GenomicRanges)
  require(Rsamtools)
  txdb<-transcriptsBy(get(transcripts, envir=.GlobalEnv),
    overlpto)
  l<-vector("list", length(files))

  for(i in 1:length(files)){
    aIns<-readGAlignments(files[i])
    strand(aIns)<-"*"
    hits<-countOverlaps(aIns,txdb)
    l[[i]]<-countOverlaps(txdb, aIns[hits==1])
    names(l)<-gsub("\\.bam","",files)
  }
  ct<-as.data.frame(l)
  ct
}
counttable<-generateCountTable(dir(pattern=".bam"))

###Retrieve and convert information calling from biomaRt###
idents<-row.names(counttable)
mart<-useDataset("mmusculus_gene_ensembl", useMart("ensembl"))
info<-getBM(filters="entrezgene", values=idents, mart=mart, attributes=c(
  "ensembl_gene_id","external_gene_name", "entrezgene", "illumina_moueref_8_v2"))
row.names(info)<-info$entrezgene

###Save output for analysis###
full.table<-merge(counttable, info, by.x="row.names", by.y="entrezgene")
write.table(full.table, sep=";", file="counttable.cnuc.pilot.withidents.csv")
```

Appendix 3 : ABR Line of Best Fit Equations

Line of best fit (LOBF) equations for control ABR waveform data presented in section 3.2.1, figure 3.2. A quadratic LOBF was preferred when compared with an extra sum-of-squares, full model test.

Amplitude LOBF: $y = Ax^2 + Bx + C$			
Wave	A ($\mu \pm \text{SEM}$)	B ($\mu \pm \text{SEM}$)	C ($\mu \pm \text{SEM}$)
I	-0.0016 \pm 0.0001	0.2142 \pm 0.1074	0.4095 \pm 0.1398
III	-0.0008 \pm 0.0001	0.1475 \pm 0.0074	0.1450 \pm 0.0958
IV	-0.0022 \pm 0.0001	0.1670 \pm 0.0080	1.0420 \pm 0.1035

Latency LOBF: $y = Ax^2 + Bx + C$			
Wave	A ($\mu \pm \text{SEM}$)	B ($\mu \pm \text{SEM}$)	C ($\mu \pm \text{SEM}$)
I	0.0001 \pm 0.0000	-0.0122 \pm 0.0005	1.9020 \pm 0.0072
III	0.0001 \pm 0.0000	-0.0129 \pm 0.0015	3.4360 \pm 0.0225
IV	0.0001 \pm 0.0000	-0.0139 \pm 0.0009	4.3650 \pm 0.0113

References

- ALVES, F. R. & DE, A. Q. R. F. 2005. Revision about hearing loss in the Alport's syndrome, analyzing the clinical, genetic and bio-molecular aspects. *Braz J Otorhinolaryngol*, 71, 813-9.
- AMBROSI, G., CERRI, S. & BLANDINI, F. 2014. A further update on the role of excitotoxicity in the pathogenesis of Parkinson's disease. *J Neural Transm (Vienna)*, 121, 849-59.
- ASHMORE, J. 2008. Cochlear outer hair cell motility. *Physiol Rev*, 88, 173-210.
- BAI, X., ZHANG, C., CHEN, A., LIU, W., LI, J., SUN, Q. & WANG, H. 2016. Protective Effect of Edaravone on Glutamate-Induced Neurotoxicity in Spiral Ganglion Neurons. *Neural Plast*, 2016, 4034218.
- BAL, R. & BAYDAS, G. 2009. Electrophysiological properties of octopus neurons of the cat cochlear nucleus: an in vitro study. *J Assoc Res Otolaryngol*, 10, 281-93.
- BAL, R., BAYDAS, G. & NAZIROGLU, M. 2009. Electrophysiological properties of ventral cochlear nucleus neurons of the dog. *Hear Res*, 256, 93-103.
- BENGA, G. 2012. The first discovered water channel protein, later called aquaporin 1: molecular characteristics, functions and medical implications. *Mol Aspects Med*, 33, 518-34.
- BENN, M. 2009. Apolipoprotein B levels, APOB alleles, and risk of ischemic cardiovascular disease in the general population, a review. *Atherosclerosis*, 206, 17-30.
- BERGER, J. I., COOMBER, B., WELLS, T. T., WALLACE, M. N. & PALMER, A. R. 2014. Changes in the response properties of inferior colliculus neurons relating to tinnitus. *Front Neurol*, 5, 203.
- BEURG, M., MICHALSKI, N., SAFIEDDINE, S., BOULEAU, Y., SCHNEGGENBURGER, R., CHAPMAN, E. R., PETIT, C. & DULON, D. 2010. Control of exocytosis by synaptotagmins and otoferlin in auditory hair cells. *J Neurosci*, 30, 13281-90.
- BOASSA, D., STAMER, W. D. & YOOL, A. J. 2006. Ion channel function of aquaporin-1 natively expressed in choroid plexus. *J Neurosci*, 26, 7811-9.

References

- BOYLES, J. K., ZOELLNER, C. D., ANDERSON, L. J., KOSIK, L. M., PITAS, R. E., WEISGRABER, K. H., HUI, D. Y., MAHLEY, R. W., GEBICKE-HAERTER, P. J., IGNATIUS, M. J. & ET AL. 1989. A role for apolipoprotein E, apolipoprotein A-I, and low density lipoprotein receptors in cholesterol transport during regeneration and remyelination of the rat sciatic nerve. *J Clin Invest*, 83, 1015-31.
- BOWL, M. R., et al 2017. A large scale hearing loss screen reveals an extensive unexplored genetic landscape for auditory dysfunction. *Nat Commun*, 8, 886.
- BRADBURY, E. J., BURNSTOCK, G. & MCMAHON, S. B. 1998. The expression of P2X3 purinoreceptors in sensory neurons: effects of axotomy and glial-derived neurotrophic factor. *Mol Cell Neurosci*, 12, 256-68.
- BROOKS, D. N., HALLAM, R. S. & MELLOR, P. A. 2001. The effects on significant others of providing a hearing aid to the hearing-impaired partner. *Br J Audiol*, 35, 165-71.
- BROWNELL, W. E., BADER, C. R., BERTRAND, D. & DE RIBAUPIERRE, Y. 1985. Evoked mechanical responses of isolated cochlear outer hair cells. *Science*, 227, 194-6.
- BROZOSKI, T. J., BAUER, C. A. & CASPARY, D. M. 2002. Elevated fusiform cell activity in the dorsal cochlear nucleus of chinchillas with psychophysical evidence of tinnitus. *J Neurosci*, 22, 2383-90.
- BULANKINA, A. V. & MOSER, T. 2012. Neural circuit development in the mammalian cochlea. *Physiology (Bethesda, Md.)*, 27, 100-12.
- CAMINOS, E., GARCIA-PINO, E., MARTINEZ-GALAN, J. R. & JUIZ, J. M. 2007. The potassium channel KCNQ5/Kv7.5 is localized in synaptic endings of auditory brainstem nuclei of the rat. *J Comp Neurol*, 505, 363-78.
- CAMINOS, E., VALE, C., LUJAN, R., MARTINEZ-GALAN, J. R. & JUIZ, J. M. 2005. Developmental regulation and adult maintenance of potassium channel proteins (Kv 1.1 and Kv 1.2) in the cochlear nucleus of the rat. *Brain Res*, 1056, 118-31.
- CARMEL, P. W. & STARR, A. 1963. Acoustic and nonacoustic factors modifying middle-ear muscle activity in waking cats. *J Neurophysiol*, 26, 598-616.
- CAULIN, C., WARE, C. F., MAGIN, T. M. & OSHIMA, R. G. 2000. Keratin-dependent, epithelial resistance to tumor necrosis factor-induced apoptosis. *J Cell Biol*, 149, 17-22.

References

- CHEN, K., SPRUNGER, L. K., MEISLER, M. H., WALLER, H. J. & GODFREY, D. A. 1999. Reduced spontaneous activity in the dorsal cochlear nucleus of Scn8a mutant mice. *Brain Res*, 847, 85-9.
- CHEN, W. C. & DAVIS, R. L. 2006. Voltage-gated and two-pore-domain potassium channels in murine spiral ganglion neurons. *Hear Res*, 222, 89-99.
- CHO, Y., GONG, T. W., KANICKI, A., ALTSCHULER, R. A. & LOMAX, M. I. 2004. Noise overstimulation induces immediate early genes in the rat cochlea. *Brain Res Mol Brain Res*, 130, 134-48.
- CHUNG, D. Y., GANNON, R. P. & MASON, K. 1984. Factors affecting the prevalence of tinnitus. *Audiology*, 23, 441-52.
- CHUNG, J. W., AHN, J. H., KIM, J. Y., LEE, H. J., KANG, H. H., LEE, Y. K., KIM, J. U. & KOO, S. W. 2007. The effect of isoflurane, halothane and pentobarbital on noise-induced hearing loss in mice. *Anesth Analg*, 104, 1404-8, table of contents.
- COLLO, G., NORTH, R. A., KAWASHIMA, E., MERLO-PICH, E., NEIDHART, S., SURPRENANT, A. & BUELL, G. 1996. Cloning OF P2X5 and P2X6 receptors and the distribution and properties of an extended family of ATP-gated ion channels. *J Neurosci*, 16, 2495-507.
- COOMBER, B., BERGER, J. I., KOWALKOWSKI, V. L., SHACKLETON, T. M., PALMER, A. R. & WALLACE, M. N. 2014. Neural changes accompanying tinnitus following unilateral acoustic trauma in the guinea pig. *Eur J Neurosci*, 40, 2427-41.
- CORWIN, J. T. & WARCHOL, M. E. 1991. Auditory hair cells: structure, function, development, and regeneration. *Annu Rev Neurosci*, 14, 301-33.
- CRAY, C., ZAIAS, J. & ALTMAN, N. H. 2009. Acute phase response in animals: a review. *Comp Med*, 59, 517-26.
- CRUZ, J. I., LOSTE, J. M. & BURZACO, O. H. 1998. Observations on the use of medetomidine/ketamine and its reversal with atipamezole for chemical restraint in the mouse. *Laboratory animals*, 32, 18-22.
- DARBY, W. G., GRACE, M. S., BARATCHI, S. & MCINTYRE, P. 2016. Modulation of TRPV4 by diverse mechanisms. *Int J Biochem Cell Biol*, 78, 217-28.
- DAVIS, R. L. 2003. Gradients of neurotrophins, ion channels, and tuning in the cochlea. *Neuroscientist*, 9, 311-6.

References

- DEHMEL, S., PRADHAN, S., KOEHLER, S., BLEDSOE, S. & SHORE, S. 2012. Noise overexposure alters long-term somatosensory-auditory processing in the dorsal cochlear nucleus--possible basis for tinnitus-related hyperactivity? *J Neurosci*, 32, 1660-71.
- DEHNERT, K., RAAB, U., PEREZ-ALVAREZ, C., STEFFENS, T., BOLTE, G., FROMME, H. & TWARDELLA, D. 2015. Total leisure noise exposure and its association with hearing loss among adolescents. *Int J Audiol*, 54, 665-73.
- DIB-HAJJ, S. D., BLACK, J. A., CUMMINS, T. R., KENNEY, A. M., KOCSIS, J. D. & WAXMAN, S. G. 1998a. Rescue of alpha-SNS sodium channel expression in small dorsal root ganglion neurons after axotomy by nerve growth factor in vivo. *J Neurophysiol*, 79, 2668-76.
- DIB-HAJJ, S. D., TYRRELL, L., BLACK, J. A. & WAXMAN, S. G. 1998b. NaN, a novel voltage-gated Na channel, is expressed preferentially in peripheral sensory neurons and down-regulated after axotomy. *Proc Natl Acad Sci U S A*, 95, 8963-8.
- DING, Z. J., CHEN, X., TANG, X. X., WANG, X., SONG, Y. L., CHEN, X. D., MI, W. J., WANG, J., LIN, Y., CHEN, F. Q. & QIU, J. H. 2015. Calpain inhibitor PD150606 attenuates glutamate induced spiral ganglion neuron apoptosis through apoptosis inducing factor pathway in vitro. *PLoS One*, 10, e0123130.
- DONG, S., MULDER, W. H., RODGER, J., WOO, S. & ROBERTSON, D. 2010. Acoustic trauma evokes hyperactivity and changes in gene expression in guinea-pig auditory brainstem. *Eur J Neurosci*, 31, 1616-28.
- DUDOIT, S., YANG, Y. H., CALLOW, M. J. & SPEED, T. P. 2002. Statistical methods for identifying differentially expressed genes in replicated cDNA microarray experiments. *Statistica Sinica*, 12, 111-139.
- ENDEWARD, V., MUSA-AZIZ, R., COOPER, G. J., CHEN, L. M., PELLETIER, M. F., VIRKKI, L. V., SUPURAN, C. T., KING, L. S., BORON, W. F. & GROS, G. 2006. Evidence that aquaporin 1 is a major pathway for CO₂ transport across the human erythrocyte membrane. *FASEB J*, 20, 1974-81.
- FERNANDEZ, K. A., JEFFERS, P. W., LALL, K., LIBERMAN, M. C. & KUJAWA, S. G. 2015. Aging after noise exposure: acceleration of cochlear synaptopathy in "recovered" ears. *J Neurosci*, 35, 7509-20.

References

- FILOSA, J. A., YAO, X. & RATH, G. 2013. TRPV4 and the regulation of vascular tone. *J Cardiovasc Pharmacol*, 61, 113-9.
- FOX, M. A. & SANES, J. R. 2007. Synaptotagmin I and II are present in distinct subsets of central synapses. *J Comp Neurol*, 503, 280-96.
- FRIEDLAND, D. R., EERNISSE, R. & POPPER, P. 2007. Potassium channel gene expression in the rat cochlear nucleus. *Hear Res*, 228, 31-43.
- FRYATT, A. G. 2010. *Investigating voltage-gated sodium channel expression in rat spiral ganglion neurons following noise induced hearing loss*.
- FRYATT, A. G., MULHERAN, M., EGERTON, J., GUNTHORPE, M. J. & GRUBB, B. D. 2011. Ototrauma induces sodium channel plasticity in auditory afferent neurons. *Mol Cell Neurosci*, 48, 51-61.
- FRYATT, A. G., VIAL, C., MULHERAN, M., GUNTHORPE, M. J. & GRUBB, B. D. 2009. Voltage-gated sodium channel expression in rat spiral ganglion neurons. *Mol Cell Neurosci*, 42, 399-407.
- FURMAN, A. C., KUJAWA, S. G. & LIBERMAN, M. C. 2013. Noise-induced cochlear neuropathy is selective for fibers with low spontaneous rates. *J Neurophysiol*, 110, 577-86.
- FURNESS, D. N. & LAWTON, D. M. 2003. Comparative distribution of glutamate transporters and receptors in relation to afferent innervation density in the mammalian cochlea. *J Neurosci*, 23, 11296-304.
- GANNOUNI, N., LENOIR, M., BEN RHOUMA, K., EL MAY, M., TEBOURBI, O., PUEL, J. L. & MHAMDI, A. 2015. Cochlear neuropathy in the rat exposed for a long period to moderate-intensity noises. *J Neurosci Res*, 93, 848-58.
- GAO, J., TAN, M., GU, M., MARSHALL, C., DING, J., HU, G. & XIAO, M. 2012. Cellular localization of aquaporin-1 in the human and mouse trigeminal systems. *PLoS One*, 7, e46379.
- GLOWATZKI, E. & FUCHS, P. A. 2002. Transmitter release at the hair cell ribbon synapse. *Nat Neurosci*, 5, 147-54.
- GUITTON, M. J. & DUDAI, Y. 2007. Blockade of cochlear NMDA receptors prevents long-term tinnitus during a brief consolidation window after acoustic trauma. *Neural Plast*, 2007, 80904.

References

- GURGEL, R. K., WARD, P. D., SCHWARTZ, S., NORTON, M. C., FOSTER, N. L. & TSCHANZ, J. T. 2014. Relationship of hearing loss and dementia: a prospective, population-based study. *Otol Neurotol*, 35, 775-81.
- HAFIDI, A., BEURG, M. & DULON, D. 2005. Localization and developmental expression of BK channels in mammalian cochlear hair cells. *Neuroscience*, 130, 475-84.
- HART, T., KOMORI, H. K., LAMERE, S., PODSHIVALOVA, K. & SALOMON, D. R. 2013. Finding the active genes in deep RNA-seq gene expression studies. *BMC Genomics*, 14, 778.
- HED, J., DAHLGREN, C. & RUNDQUIST, I. 1983. A simple fluorescence technique to stain the plasma membrane of human neutrophils. *Histochemistry*, 79, 105-10.
- HEFFNER, H. E. & HARRINGTON, I. A. 2002. Tinnitus in hamsters following exposure to intense sound. *Hear Res*, 170, 83-95.
- HEFFNER, H. E. & HEFFNER, R. S. 2003. Audition. In: DAVIS, S. F. (ed.) *Handbook of research methods in experimental psychology*. Malden: Blackwell.
- HEFFNER, H. E. & HEFFNER, R. S. 2007. Hearing ranges of laboratory animals. *J Am Assoc Lab Anim Sci*, 46, 20-2.
- HENRY, K. R. 1979. Auditory brainstem volume-conducted responses: origins in the laboratory mouse. *J Am Aud Soc*, 4, 173-8.
- HIYAMA, T. Y., WATANABE, E., ONO, K., INENAGA, K., TAMKUN, M. M., YOSHIDA, S. & NODA, M. 2002. Na(x) channel involved in CNS sodium-level sensing. *Nat Neurosci*, 5, 511-2.
- HOSHI, A., TSUNODA, A., YAMAMOTO, T., TADA, M., KAKITA, A. & UGAWA, Y. 2016. Increased neuronal and astroglial aquaporin-1 immunoreactivity in rat striatum by chemical preconditioning with 3-nitropropionic acid. *Neurosci Lett*, 626, 48-53.
- HOSSAIN, W. A., ANTIC, S. D., YANG, Y., RASBAND, M. N. & MOREST, D. K. 2005. Where is the spike generator of the cochlear nerve? Voltage-gated sodium channels in the mouse cochlea. *J Neurosci*, 25, 6857-68.
- HOUSLEY, G. D., MORTON-JONES, R., VLAJKOVIC, S. M., TELANG, R. S., PARAMANANTHASIVAM, V., TADROS, S. F., WONG, A. C., FROUD, K. E.,

References

- CEDERHOLM, J. M., SIVAKUMARAN, Y., SNGUANWONGCHAI, P., KHAKH, B. S., COCKAYNE, D. A., THORNE, P. R. & RYAN, A. F. 2013. ATP-gated ion channels mediate adaptation to elevated sound levels. *Proc Natl Acad Sci U S A*, 110, 7494-9.
- HU, B. H., CAI, Q., MANOHAR, S., JIANG, H., DING, D., COLING, D. E., ZHENG, G. & SALVI, R. 2009. Differential expression of apoptosis-related genes in the cochlea of noise-exposed rats. *Neuroscience*, 161, 915-25.
- HU, J., XI, D., ZHAO, J., LUO, T., LIU, J., LU, H., LI, M., XIONG, H. & GUO, Z. 2016. High-density Lipoprotein and Inflammation and Its Significance to Atherosclerosis. *Am J Med Sci*, 352, 408-415.
- HUANG, L. C., RYAN, A. F., COCKAYNE, D. A. & HOUSLEY, G. D. 2006. Developmentally regulated expression of the P2X3 receptor in the mouse cochlea. *Histochem Cell Biol*, 125, 681-92.
- IHLER, F., STRIETH, S., PIERI, N., GOHRING, P. & CANIS, M. 2012. Acute hyperfibrinogenemia impairs cochlear blood flow and hearing function in guinea pigs in vivo. *Int J Audiol*, 51, 210-5.
- INGHAM, N. J., PEARSON, S. & STEEL, K. P. 2011. Using the auditory brain stem response (ABR) to determine the sensitivity of hearing in mutant mice. *Current Protocols In Mouse Biology*, 1, 279-287.
- ITO, M., NAGASAWA, M., HARA, T., IDE, T. & MURAKAMI, K. 2010. Differential roles of CIDEA and CIDEC in insulin-induced anti-apoptosis and lipid droplet formation in human adipocytes. *J Lipid Res*, 51, 1676-84.
- JALABI, W., KOPP-SCHEINPFLUG, C., ALLEN, P. D., SCHIAVON, E., DIGIACOMO, R. R., FORSYTHE, I. D. & MARICICH, S. M. 2013. Sound localization ability and glycinergic innervation of the superior olivary complex persist after genetic deletion of the medial nucleus of the trapezoid body. *J Neurosci*, 33, 15044-9.
- JENSEN, J. B., LYSAGHT, A. C., LIBERMAN, M. C., QVORTRUP, K. & STANKOVIC, K. M. 2015. Immediate and delayed cochlear neuropathy after noise exposure in pubescent mice. *PLoS One*, 10, e0125160.
- JIN, Z., LIANG, G. H., COOPER, E. C. & JARLEBARK, L. 2009. Expression and localization of K channels KCNQ2 and KCNQ3 in the mammalian cochlea. *Audiol Neurootol*, 14, 98-105.

References

- JINNO, Y., NAKAKUKI, M., SATO, A., KAWANO, H., NOTSU, T., MIZUGUCHI, K. & SHIMANO, H. 2010. Cide-a and Cide-c are induced in the progression of hepatic steatosis and inhibited by eicosapentaenoic acid. *Prostaglandins Leukot Essent Fatty Acids*, 83, 75-81.
- JOHNSTON, J., FORSYTHE, I. D. & KOPP-SCHEINPFLUG, C. 2010. Going native: voltage-gated potassium channels controlling neuronal excitability. *J Physiol*, 588, 3187-200.
- JOHNSTONE, B. M., PATUZZI, R. & YATES, G. K. 1986. Basilar membrane measurements and the travelling wave. *Hear Res*, 22, 147-53.
- JOHNSTONE, B. M. & SELICK, P. M. 1972. The peripheral auditory apparatus. *Q Rev Biophys*, 5, 1-57.
- JOVANOVIC, S., RADULOVIC, T., CODDOU, C., DIETZ, B., NERLICH, J., STOJILKOVIC, S. S., RUBSAMEN, R. & MILENKOVIC, I. 2017. Tonotopic action potential tuning of maturing auditory neurons through endogenous ATP. *J Physiol*, 595, 1315-1337.
- JULIUS, D. & BASBAUM, A. I. 2001. Molecular mechanisms of nociception. *Nature*, 413, 203-10.
- JUNG, D. K., LEE, S. Y., KIM, D., JOO, K. M., CHA, C. I., YANG, H. S., LEE, W. B. & CHUNG, Y. H. 2005. Age-related changes in the distribution of Kv1.1 and Kv3.1 in rat cochlear nuclei. *Neurol Res*, 27, 436-40.
- KALTENBACH, J. A. & AFMAN, C. E. 2000. Hyperactivity in the dorsal cochlear nucleus after intense sound exposure and its resemblance to tone-evoked activity: a physiological model for tinnitus. *Hear Res*, 140, 165-72.
- KALTENBACH, J. A., ZACHAREK, M. A., ZHANG, J. & FREDERICK, S. 2004. Activity in the dorsal cochlear nucleus of hamsters previously tested for tinnitus following intense tone exposure. *Neurosci Lett*, 355, 121-5.
- KANE, K. L., LONGO-GUESS, C. M., GAGNON, L. H., DING, D., SALVI, R. J. & JOHNSON, K. R. 2012. Genetic background effects on age-related hearing loss associated with Cdh23 variants in mice. *Hear Res*, 283, 80-8.
- KAYA, Y., OZSOY, U., DEMIR, N., HIZAY, A., SUZEN, L. B., ANGELOV, D. N. & SARIKCIOGLU, L. 2014. Temporal and spatial distribution of the aquaporin 1 in spinal cord and dorsal root ganglia after traumatic injuries of the sciatic nerve. *Childs Nerv Syst*, 30, 1679-86.

References

- KIM, D., PERTEA, G., TRAPNELL, C., PIMENTEL, H., KELLEY, R. & SALZBERG, S. L. 2013. TopHat2: accurate alignment of transcriptomes in the presence of insertions, deletions and gene fusions. *Genome Biol*, 14, R36.
- KIM, K. X. & RUTHERFORD, M. A. 2016. Maturation of NaV and KV Channel Topographies in the Auditory Nerve Spike Initiator before and after Developmental Onset of Hearing Function. *J Neurosci*, 36, 2111-8.
- KIM, Y. & TRUSSELL, L. O. 2009. Negative shift in the glycine reversal potential mediated by a Ca²⁺- and pH-dependent mechanism in interneurons. *J Neurosci*, 29, 11495-510.
- KING, A. E., WOODHOUSE, A., KIRKCALDIE, M. T. & VICKERS, J. C. 2016. Excitotoxicity in ALS: Overstimulation, or overreaction? *Exp Neurol*, 275 Pt 1, 162-71.
- KIRKEGAARD, M., MURAI, N., RISLING, M., SUNESON, A., JARLEBARK, L. & ULFENDAHL, M. 2006. Differential gene expression in the rat cochlea after exposure to impulse noise. *Neuroscience*, 142, 425-35.
- KUANG, X., CHEN, Y. S., WANG, L. F., LI, Y. J., LIU, K., ZHANG, M. X., LI, L. J., CHEN, C., HE, Q., WANG, Y. & DU, J. R. 2014. Klotho upregulation contributes to the neuroprotection of ligustilide in an Alzheimer's disease mouse model. *Neurobiol Aging*, 35, 169-78.
- KUJAWA, S. G. & LIBERMAN, M. C. 2006. Acceleration of age-related hearing loss by early noise exposure: evidence of a misspent youth. *The Journal of neuroscience*, 26, 2115-23.
- KUJAWA, S. G. & LIBERMAN, M. C. 2009. Adding insult to injury: cochlear nerve degeneration after "temporary" noise-induced hearing loss. *The Journal of neuroscience*, 29, 14077-85.
- KUJAWA, S. G. & LIBERMAN, M. C. 2015. Synaptopathy in the noise-exposed and aging cochlea: Primary neural degeneration in acquired sensorineural hearing loss. *Hear Res*, 330, 191-9.
- KURIOKA, T., LEE, M. Y., HEERINGA, A. N., BEYER, L. A., SWIDERSKI, D. L., KANICKI, A. C., KABARA, L. L., DOLAN, D. F., SHORE, S. E. & RAPHAEL, Y. 2016. Selective hair cell ablation and noise exposure lead to different patterns of changes in the cochlea and the cochlear nucleus. *Neuroscience*, 332, 242-57.

References

- LAND, R., BURGHARD, A. & KRAL, A. 2016. The contribution of inferior colliculus activity to the auditory brainstem response (ABR) in mice. *Hear Res*, 341, 109-118.
- LETZEN, B. S., LIU, C., THAKOR, N. V., GEARHART, J. D., ALL, A. H. & KERR, C. L. 2010. MicroRNA expression profiling of oligodendrocyte differentiation from human embryonic stem cells. *PLoS One*, 5, e10480.
- LEWIS, A. H. & RAMAN, I. M. 2014. Resurgent current of voltage-gated Na(+) channels. *J Physiol*, 592, 4825-38.
- LI, S., KALAPPA, B. I. & TZOUNOPOULOS, T. 2015. Noise-induced plasticity of KCNQ2/3 and HCN channels underlies vulnerability and resilience to tinnitus. *Elife*, 4.
- LI, Y. H., LEI, T., CHEN, X. D., XIA, T., PENG, Y., LONG, Q. Q., ZHANG, J., FENG, S. Q., ZHOU, L. & YANG, Z. Q. 2009. Molecular cloning, chromosomal location and expression pattern of porcine CIDEa and CIDEc. *Mol Biol Rep*, 36, 575-82.
- LIBERMAN, L. D., SUZUKI, J. & LIBERMAN, M. C. 2015. Dynamics of cochlear synaptopathy after acoustic overexposure. *J Assoc Res Otolaryngol*, 16, 205-19.
- LIBERMAN, M. C. & OLIVER, M. E. 1984. Morphometry of intracellularly labeled neurons of the auditory nerve: correlations with functional properties. *J Comp Neurol*, 223, 163-76.
- LIM, D. J. & ANNIKO, M. 1985. Developmental morphology of the mouse inner ear. A scanning electron microscopic observation. *Acta oto-laryngologica. Supplementum*, 422, 1-69.
- LIN, F. R., METTER, E. J., O'BRIEN, R. J., RESNICK, S. M., ZONDERMAN, A. B. & FERRUCCI, L. 2011a. Hearing loss and incident dementia. *Arch Neurol*, 68, 214-20.
- LIN, H. W., FURMAN, A. C., KUJAWA, S. G. & LIBERMAN, M. C. 2011b. Primary neural degeneration in the Guinea pig cochlea after reversible noise-induced threshold shift. *Journal of the Association for Research in Otolaryngology*, 12, 605-16.
- LIN, L., WU, M. & ZHAO, J. 2017. The initiation and effects of plasma contact activation: an overview. *Int J Hematol*, 105, 235-243.
- LIU, C. C., LIU, C. C., KANEKIYO, T., XU, H. & BU, G. 2013a. Apolipoprotein E and Alzheimer disease: risk, mechanisms and therapy. *Nat Rev Neurol*, 9, 106-18.

References

- LIU, Y., FERGUSON, J. F., XUE, C., SILVERMAN, I. M., GREGORY, B., REILLY, M. P. & LI, M. 2013b. Evaluating the impact of sequencing depth on transcriptome profiling in human adipose. *PLoS One*, 8, e66883.
- LIU, Y., ZHOU, J. & WHITE, K. P. 2014. RNA-seq differential expression studies: more sequence or more replication? *Bioinformatics*, 30, 301-4.
- LOBARINAS, E., SPANKOVICH, C., LE PRELL, C. G. 2017. Evidence of "hidden hearing loss" following noise exposure that produce robust TTS and ABR wave-I amplitude reductions. *Hear Res*, 349, 155-163.
- LONGENECKER, R. J. & GALAZYUK, A. V. 2011. Development of tinnitus in CBA/CAJ mice following sound exposure. *J Assoc Res Otolaryngol*, 12, 647-58.
- LU, X., SHU, Y., TANG, M. & LI, H. 2016. Mammalian Cochlear Hair Cell Regeneration and Ribbon Synapse Reformation. *Neural Plast*, 2016, 2523458.
- LUO, H., PACE, E., ZHANG, X. & ZHANG, J. 2014. Blast-Induced tinnitus and spontaneous firing changes in the rat dorsal cochlear nucleus. *J Neurosci Res*, 92, 1466-77.
- LUO, L., BRUMM, D. & RYAN, A. F. 1995. Distribution of non-NMDA glutamate receptor mRNAs in the developing rat cochlea. *J Comp Neurol*, 361, 372-82.
- MANIS, P. B., MOLITOR, S. C. & WU, H. 2003. Subthreshold oscillations generated by TTX-sensitive sodium currents in dorsal cochlear nucleus pyramidal cells. *Exp Brain Res*, 153, 443-51.
- MANOHAR, S., DAHAR, K., ADLER, H. J., DALIAN, D. & SALVI, R. 2016. Noise-induced hearing loss: Neuropathic pain via Ntrk1 signaling. *Mol Cell Neurosci*, 75, 101-12.
- MARCOTTI, W., JOHNSON, S. L., HOLLEY, M. C. & KROS, C. J. 2003. Developmental changes in the expression of potassium currents of embryonic, neonatal and mature mouse inner hair cells. *The Journal of physiology*, 548, 383-400.
- MATSUBARA, A., TAKUMI, Y., NAKAGAWA, T., USAMI, S., SHINKAWA, H. & OTTERSEN, O. P. 1999. Immunoelectron microscopy of AMPA receptor subunits reveals three types of putative glutamatergic synapse in the rat vestibular end organs. *Brain Res*, 819, 58-64.

References

- MCCOY, E. & SONTHEIMER, H. 2010. MAPK induces AQP1 expression in astrocytes following injury. *Glia*, 58, 209-17.
- MELCHER, J. R. & KIANG, N. Y. 1996. Generators of the brainstem auditory evoked potential in cat. III: Identified cell populations. *Hear Res*, 93, 52-71.
- MELTSER, I., CEDERROTH, CHRISTOPHER R., BASINOU, V., SAVELYEV, S., LUNDKVIST, GABRIELLA S. & CANLON, B. 2014. TrkB-Mediated Protection against Circadian Sensitivity to Noise Trauma in the Murine Cochlea. *Current Biology*, 24, 658-663.
- MENARDO, J., TANG, Y., LADRECH, S., LENOIR, M., CASAS, F., MICHEL, C., BOURIEN, J., RUEL, J., REBILLARD, G., MAURICE, T., PUEL, J. L. & WANG, J. 2012. Oxidative stress, inflammation, and autophagic stress as the key mechanisms of premature age-related hearing loss in SAMP8 mouse Cochlea. *Antioxid Redox Signal*, 16, 263-74.
- MENNERICK, S. & MATTHEWS, G. 1996. Ultrafast exocytosis elicited by calcium current in synaptic terminals of retinal bipolar neurons. *Neuron*, 17, 1241-9.
- MIDDLEBROOKS, J. C., NICK, H. S., SUBRAMONY, S. H., ADVINCULA, J., ROSALES, R. L., LEE, L. V., ASHIZAWA, T. & WATERS, M. F. 2013. Mutation in the kv3.3 voltage-gated potassium channel causing spinocerebellar ataxia 13 disrupts sound-localization mechanisms. *PLoS One*, 8, e76749.
- MILLER, T. R., SERULLE, Y. & GANDHI, D. 2016. Arterial Abnormalities Leading to Tinnitus. *Neuroimaging Clin N Am*, 26, 227-36.
- MULLER, M., VON HUNERBEIN, K., HOIDIS, S. & SMOLDERS, J. W. 2005. A physiological place-frequency map of the cochlea in the CBA/J mouse. *Hear Res*, 202, 63-73.
- NAMADURAI, S., YEREDDI, N. R., CUSDIN, F. S., HUANG, C. L., CHIRGADZE, D. Y. & JACKSON, A. P. 2015. A new look at sodium channel beta subunits. *Open Biol*, 5, 140192.
- NASEER, M. I., ULLAH, I., NARASIMHAN, M. L., LEE, H. Y., BRESSAN, R. A., YOON, G. H., YUN, D. J. & KIM, M. O. 2014. Neuroprotective effect of osmotin against ethanol-induced apoptotic neurodegeneration in the developing rat brain. *Cell Death Dis*, 5, e1150.

References

- NEELY, S. T. & KIM, D. O. 1986. A model for active elements in cochlear biomechanics. *J Acoust Soc Am*, 79, 1472-80.
- NIEDZIELSKI, A. S. & WENTHOLD, R. J. 1995. Expression of AMPA, kainate, and NMDA receptor subunits in cochlear and vestibular ganglia. *J Neurosci*, 15, 2338-53.
- NISKAR, A. S., KIESZAK, S. M., HOLMES, A., ESTEBAN, E., RUBIN, C. & BRODY, D. J. 1998. Prevalence of hearing loss among children 6 to 19 years of age: the Third National Health and Nutrition Examination Survey. *JAMA*, 279, 1071-5.
- NIU, Y., KUMARAGURU, A., WANG, R. & SUN, W. 2013. Hyperexcitability of inferior colliculus neurons caused by acute noise exposure. *J Neurosci Res*, 91, 292-9.
- NORDANG, L., CESTREICHER, E., ARNOLD, W. & ANNIKO, M. 2000. Glutamate is the afferent neurotransmitter in the human cochlea. *Acta Otolaryngol*, 120, 359-62.
- NORMAN, M., TOMSCHA, K. & WEHR, M. 2012. Isoflurane blocks temporary tinnitus. *Hear Res*, 290, 64-71.
- NOUVIAN, R., BEUTNER, D., PARSONS, T. D. & MOSER, T. 2006. Structure and function of the hair cell ribbon synapse. *J Membr Biol*, 209, 153-65.
- NOUVIAN, R., NEEF, J., BULANKINA, A. V., REISINGER, E., PANGRSIC, T., FRANK, T., SIKORRA, S., BROSE, N., BINZ, T. & MOSER, T. 2011. Exocytosis at the hair cell ribbon synapse apparently operates without neuronal SNARE proteins. *Nat Neurosci*, 14, 411-3.
- PAL, B., POR, A., POCSAI, K., SZUCS, G. & RUSZNAK, Z. 2005. Voltage-gated and background K⁺ channel subunits expressed by the bushy cells of the rat cochlear nucleus. *Hear Res*, 199, 57-70.
- PASCHEN, W. 1996. Glutamate excitotoxicity in transient global cerebral ischemia. *Acta Neurobiol Exp (Wars)*, 56, 313-22.
- PAULA-LIMA, A. C., TRICERRI, M. A., BRITO-MOREIRA, J., BOMFIM, T. R., OLIVEIRA, F. F., MAGDESIAN, M. H., GRINBERG, L. T., PANIZZUTTI, R. & FERREIRA, S. T. 2009. Human apolipoprotein A-I binds amyloid-beta and prevents Abeta-induced neurotoxicity. *Int J Biochem Cell Biol*, 41, 1361-70.

References

- PEPPI, M., LANDA, M. & SEWELL, W. F. 2012. Cochlear kainate receptors. *J Assoc Res Otolaryngol*, 13, 199-208.
- PEREZ-OTANO, I., LARSEN, R. S. & WESSELING, J. F. 2016. Emerging roles of GluN3-containing NMDA receptors in the CNS. *Nat Rev Neurosci*, 17, 623-35.
- PETRALIA, R. S., RUBIO, M. E., WANG, Y. X. & WENTHOLD, R. J. 2000. Differential distribution of glutamate receptors in the cochlear nuclei. *Hear Res*, 147, 59-69.
- PETRALIA, R. S., WANG, Y. X., MAYAT, E. & WENTHOLD, R. J. 1997. Glutamate receptor subunit 2-selective antibody shows a differential distribution of calcium-impermeable AMPA receptors among populations of neurons. *J Comp Neurol*, 385, 456-76.
- PETRALIA, R. S., WANG, Y. X., ZHAO, H. M. & WENTHOLD, R. J. 1996. Ionotropic and metabotropic glutamate receptors show unique postsynaptic, presynaptic, and glial localizations in the dorsal cochlear nucleus. *J Comp Neurol*, 372, 356-83.
- PETRUSKA, J. C., COOPER, B. Y., GU, J. G., RAU, K. K. & JOHNSON, R. D. 2000. Distribution of P2X1, P2X2, and P2X3 receptor subunits in rat primary afferents: relation to population markers and specific cell types. *J Chem Neuroanat*, 20, 141-62.
- PILATI, N., ISON, M. J., BARKER, M., MULHERAN, M., LARGE, C. H., FORSYTHE, I. D., MATTHIAS, J. & HAMANN, M. 2012a. Mechanisms contributing to central excitability changes during hearing loss. *Proc Natl Acad Sci U S A*, 109, 8292-7.
- PILATI, N., LARGE, C., FORSYTHE, I. D. & HAMANN, M. 2012b. Acoustic over-exposure triggers burst firing in dorsal cochlear nucleus fusiform cells. *Hear Res*, 283, 98-106.
- PILATI, N., LINLEY, D. M., SELVASKANDAN, H., UCHITEL, O., HENNIG, M. H., KOPPSCHHEINPFLUG, C. & FORSYTHE, I. D. 2016. Acoustic trauma slows AMPA receptor-mediated EPSCs in the auditory brainstem, reducing GluA4 subunit expression as a mechanism to rescue binaural function. *J Physiol*, 594, 3683-703.
- PUEL, J. L., RUEL, J., GERVAIS D'ALDIN, C. & PUJOL, R. 1998. Excitotoxicity and repair of cochlear synapses after noise-trauma induced hearing loss. *Neuroreport*, 9, 2109-14.

References

- PUJOL, R. & PUEL, J. L. 1999. Excitotoxicity, synaptic repair, and functional recovery in the mammalian cochlea: a review of recent findings. *Ann N Y Acad Sci*, 884, 249-54.
- PUJOL, R., PUEL, J. L., GERVAIS D'ALDIN, C. & EYBALIN, M. 1993. Pathophysiology of the glutamatergic synapses in the cochlea. *Acta oto-laryngologica*, 113, 330-4.
- QIU, G., WAN, R., HU, J., MATTSON, M. P., SPANGLER, E., LIU, S., YAU, S. Y., LEE, T. M., GLEICHMANN, M., INGRAM, D. K., SO, K. F. & ZOU, S. 2011. Adiponectin protects rat hippocampal neurons against excitotoxicity. *Age (Dordr)*, 33, 155-65.
- QU, J., LIAO, Y. H., KOU, Z. Z., WEI, Y. Y., HUANG, J., CHEN, J., YANAGAWA, Y., WU, S. X., SHI, M. & LI, Y. Q. 2015. Puerarin alleviates noise-induced hearing loss via affecting PKCgamma and GABAB receptor expression. *J Neurol Sci*, 349, 110-6.
- REIF, R., ZHI, Z., DZIENNIS, S., NUTTALL, A. L. & WANG, R. K. 2013. Changes in cochlear blood flow in mice due to loud sound exposure measured with Doppler optical microangiography and laser Doppler flowmetry. *Quant Imaging Med Surg*, 3, 235-42.
- REISINGER, E., BRESEE, C., NEEF, J., NAIR, R., REUTER, K., BULANKINA, A., NOUVIAN, R., KOCH, M., BUCKERS, J., KASTRUP, L., ROUX, I., PETIT, C., HELL, S. W., BROSE, N., RHEE, J. S., KUGLER, S., BRIGANDE, J. V. & MOSER, T. 2011. Probing the functional equivalence of otoferlin and synaptotagmin 1 in exocytosis. *J Neurosci*, 31, 4886-95.
- REVES, J. G., FRAGEN, R. J., VINIK, H. R. & GREENBLATT, D. J. 1985. Midazolam: pharmacology and uses. *Anesthesiology*, 62, 310-24.
- ROBERTSON, D. 1983. Functional significance of dendritic swelling after loud sounds in the guinea pig cochlea. *Hear Res*, 9, 263-78.
- ROBIN, N. H., MORAN, R. T. & ALA-KOKKO, L. 1993. Stickler Syndrome. In: PAGON, R. A., ADAM, M. P., ARDINGER, H. H., WALLACE, S. E., AMEMIYA, A., BEAN, L. J. H., BIRD, T. D., LEDBETTER, N., MEFFORD, H. C., SMITH, R. J. H. & STEPHENS, K. (eds.) *GeneReviews(R)*. Seattle (WA).
- ROPP, T. J., TIEDEMANN, K. L., YOUNG, E. D. & MAY, B. J. 2014. Effects of unilateral acoustic trauma on tinnitus-related spontaneous activity in the inferior colliculus. *J Assoc Res Otolaryngol*, 15, 1007-22.

References

- RUDY, B. & MCBAIN, C. J. 2001. Kv3 channels: voltage-gated K⁺ channels designed for high-frequency repetitive firing. *Trends Neurosci*, 24, 517-26.
- RUEL, J., BOBBIN, R. P., VIDAL, D., PUJOL, R. & PUEL, J. L. 2000. The selective AMPA receptor antagonist GYKI 53784 blocks action potential generation and excitotoxicity in the guinea pig cochlea. *Neuropharmacology*, 39, 1959-1973.
- RUEL, J., WANG, J., REBILLARD, G., EYBALIN, M., LLOYD, R., PUJOL, R. & PUEL, J. L. 2007. Physiology, pharmacology and plasticity at the inner hair cell synaptic complex. *Hear Res*, 227, 19-27.
- RUSSELL, I. J. & NILSEN, K. E. 1997. The location of the cochlear amplifier: spatial representation of a single tone on the guinea pig basilar membrane. *Proc Natl Acad Sci U S A*, 94, 2660-4.
- RUSZNAK, Z., BAKONDI, G., POCSAI, K., POR, A., KOSZTKA, L., PAL, B., NAGY, D. & SZUCS, G. 2008. Voltage-gated potassium channel (Kv) subunits expressed in the rat cochlear nucleus. *J Histochem Cytochem*, 56, 443-65.
- SAFIEDDINE, S. & EYBALIN, M. 1992. Co-expression of NMDA and AMPA/kainate receptor mRNAs in cochlear neurones. *Neuroreport*, 3, 1145-8.
- SAITO, H., NISHIWAKI, Y., MICHIKAWA, T., KIKUCHI, Y., MIZUTARI, K., TAKEBAYASHI, T. & OGAWA, K. 2010. Hearing handicap predicts the development of depressive symptoms after 3 years in older community-dwelling Japanese. *J Am Geriatr Soc*, 58, 93-7.
- SAKHARKAR, M. K., PERUMAL, B. S., SAKHARKAR, K. R. & KANGUEANE, P. 2005. An analysis on gene architecture in human and mouse genomes. *In Silico Biol*, 5, 347-65.
- SALIH, S. G., JAGGER, D. J. & HOUSLEY, G. D. 2002. ATP-gated currents in rat primary auditory neurones in situ arise from a heteromultimeric P2X receptor subunit assembly. *Neuropharmacology*, 42, 386-95.
- SAMBROOK, J. R., D. W. 2001. Molecular cloning: a laboratory manual. 3rd ed.: Cold Spring Harbour, N.Y.
- SAUNDERS, J. C., DEAR, S. P. & SCHNEIDER, M. E. 1985. The anatomical consequences of acoustic injury: A review and tutorial. *The Journal of the Acoustical Society of America*, 78, 833-60.

References

- SCHENA, M., SHALON, D., DAVIS, R. W. & BROWN, P. O. 1995. Quantitative monitoring of gene expression patterns with a complementary DNA microarray. *Science*, 270, 467-70.
- SCHRIJVER, I. 2004. Hereditary Non-Syndromic Sensorineural Hearing Loss: Transforming Silence to Sound. *J Mol Diagn*, 6, 275-284.
- SEAMAN, M. A., LEVIN, J. R. & SERLIN, R. C. 1991. New Developments in Pairwise Multiple Comparisons - Some Powerful and Practicable Procedures. *Psychological Bulletin*, 110, 577-586.
- SENDIN, G., BOURIEN, J., RASSENDREN, F., PUEL, J. L. & NOUVIAN, R. 2014. Spatiotemporal pattern of action potential firing in developing inner hair cells of the mouse cochlea. *Proc Natl Acad Sci U S A*, 111, 1999-2004.
- SHEILD, B. 2006. Evaluation of the social and economic costs of hearing impairment. *A report for Hear-It AISBL*.
- SHEN, J., SCHEFFER, D. I., KWAN, K. Y. & COREY, D. P. 2015. SHIELD: an integrative gene expression database for inner ear research. *Database (Oxford)*, 2015, bav071.
- SHI, L., CHANG, Y., LI, X., AIKEN, S., LIU, L. & WANG, J. 2016a. Cochlear Synaptopathy and Noise-Induced Hidden Hearing Loss. *Neural Plast*, 2016, 6143164.
- SHI, L., CHANG, Y., LI, X., AIKEN, S. J., LIU, L. & WANG, J. 2016b. Coding Deficits in Noise-Induced Hidden Hearing Loss May Stem from Incomplete Repair of Ribbon Synapses in the Cochlea. *Front Neurosci*, 10, 231.
- SHI, M., DU, F., LIU, Y., LI, L., CAI, J., ZHANG, G. F., XU, X. F., LIN, T., CHENG, H. R., LIU, X. D., XIONG, L. Z. & ZHAO, G. 2013. Glial cell-expressed mechanosensitive channel TRPV4 mediates infrasound-induced neuronal impairment. *Acta Neuropathol*, 126, 725-39.
- SHIBASAKI, K., SUGIO, S., TAKAO, K., YAMANAKA, A., MIYAKAWA, T., TOMINAGA, M. & ISHIZAKI, Y. 2015. TRPV4 activation at the physiological temperature is a critical determinant of neuronal excitability and behavior. *Pflugers Arch*, 467, 2495-507.
- SLEPECKY, N. B., SAVAGE, J. E. & YOO, T. J. 1992. Localization of type II, IX and V collagen in the inner ear. *Acta Otolaryngol*, 112, 611-7.

References

- SMITH, D. I. & MILLS, J. H. 1989. Anesthesia effects: auditory brain-stem response. *Electroencephalogr Clin Neurophysiol*, 72, 422-8.
- SONG, Q., SHEN, P., LI, X., SHI, L., LIU, L., WANG, J., YU, Z., STEPHEN, K., AIKEN, S., YIN, S. & WANG, J. 2016. Coding deficits in hidden hearing loss induced by noise: the nature and impacts. *Sci Rep*, 6, 25200.
- STERKERS, O., FERRARY, E. & AMIEL, C. 1984. Inter- and intracompartmental osmotic gradients within the rat cochlea. *Am J Physiol*, 247, F602-6.
- SUFFREDINI, A. F., FANTUZZI, G., BADOLATO, R., OPPENHEIM, J. J. & O'GRADY, N. P. 1999. New insights into the biology of the acute phase response. *J Clin Immunol*, 19, 203-14.
- SZYDLOWSKA, K. & TYMIANSKI, M. 2010. Calcium, ischemia and excitotoxicity. *Cell Calcium*, 47, 122-9.
- TAGOE, T., BARKER M., JONES, A., ALLCOCK, N., HAMANN, M. 2014 Auditory nerve perinodal dysmyelination in noise-induced hearing loss. *J Neurosci*, 34, 2684-8.
- TAN, W. J., THORNE, P. R. & VLAJKOVIC, S. M. 2016. Characterisation of cochlear inflammation in mice following acute and chronic noise exposure. *Histochem Cell Biol*, 146, 219-30.
- THAL, S. C. & PLESNILA, N. 2007. Non-invasive intraoperative monitoring of blood pressure and arterial pCO₂ during surgical anesthesia in mice. *Journal of neuroscience methods*, 159, 261-7.
- THALMANN, R., MARCUS, D. C. & THALMANN, I. 1981. Physiological chemistry of cochlear duct. *Acta Otolaryngol*, 91, 535-40.
- THUNDYIL, J., PAVLOVSKI, D., SOBEY, C. G. & ARUMUGAM, T. V. 2012. Adiponectin receptor signalling in the brain. *Br J Pharmacol*, 165, 313-27.
- TOLEDO-ARAL, J. J., MOSS, B. L., HE, Z. J., KOSZOWSKI, A. G., WHISENAND, T., LEVINSON, S. R., WOLF, J. J., SILOS-SANTIAGO, I., HALEGOUA, S. & MANDEL, G. 1997. Identification of PN1, a predominant voltage-dependent sodium channel expressed principally in peripheral neurons. *Proc Natl Acad Sci U S A*, 94, 1527-32.

References

- TONG, B., HORNAK, A. J., MAISON, S. F., OHLEMILLER, K. K., LIBERMAN, M. C. & SIMMONS, D. D. 2016. Oncomodulin, an EF-Hand Ca²⁺ Buffer, Is Critical for Maintaining Cochlear Function in Mice. *J Neurosci*, 36, 1631-5.
- TORNABENE, S. V., SATO, K., PHAM, L., BILLINGS, P. & KEITHLEY, E. M. 2006. Immune cell recruitment following acoustic trauma. *Hear Res*, 222, 115-24.
- TRAPNELL, C., HENDRICKSON, D. G., SAUVAGEAU, M., GOFF, L., RINN, J. L. & PACHTER, L. 2013. Differential analysis of gene regulation at transcript resolution with RNA-seq. *Nat Biotechnol*, 31, 46-53.
- TURNER, J. G., BROZOSKI, T. J., BAUER, C. A., PARRISH, J. L., MYERS, K., HUGHES, L. F. & CASPARY, D. M. 2006. Gap detection deficits in rats with tinnitus: a potential novel screening tool. *Behav Neurosci*, 120, 188-95.
- TURNER, J. G., PARRISH, J. L., HUGHES, L. F., TOTH, L. A. & CASPARY, D. M. 2005. Hearing in laboratory animals: strain differences and nonauditory effects of noise. *Comp Med*, 55, 12-23.
- VALOUSKOVA, E., SMOLKOVA, K., SANTOROVA, J., JEZEK, P. & MODRIANSKY, M. 2008. Redistribution of cell death-inducing DNA fragmentation factor-like effector-a (CIDEa) from mitochondria to nucleus is associated with apoptosis in HeLa cells. *Gen Physiol Biophys*, 27, 92-100.
- VULCHANOVA, L., RIEDL, M. S., SHUSTER, S. J., STONE, L. S., HARGREAVES, K. M., BUELL, G., SURPRENANT, A., NORTH, R. A. & ELDE, R. 1998. P2X3 is expressed by DRG neurons that terminate in inner lamina II. *Eur J Neurosci*, 10, 3470-8.
- WANG, Y., HIROSE, K. & LIBERMAN, M. C. 2002. Dynamics of noise-induced cellular injury and repair in the mouse cochlea. *Journal of the Association for Research in Otolaryngology*, 3, 248-68.
- WANG, Y. X., WENTHOLD, R. J., OTTERSEN, O. P. & PETRALIA, R. S. 1998. Endbulb synapses in the anteroventral cochlear nucleus express a specific subset of AMPA-type glutamate receptor subunits. *J Neurosci*, 18, 1148-60.
- WATANABE, E., HIYAMA, T. Y., KODAMA, R. & NODA, M. 2002. NaX sodium channel is expressed in non-myelinating Schwann cells and alveolar type II cells in mice. *Neurosci Lett*, 330, 109-13.

References

- WATANABE, M., MISHINA, M. & INOUE, Y. 1994. Distinct distributions of five NMDA receptor channel subunit mRNAs in the brainstem. *J Comp Neurol*, 343, 520-31.
- WEISS, B. G., BERTLICH, M., BETTAG, S. A., DESINGER, H., IHLER, F. & CANIS, M. 2017. Drug-induced Defibrinogenation as New Treatment Approach of Acute Hearing Loss in an Animal Model for Inner Ear Vascular Impairment. *Otol Neurotol*, 38, 648-654.
- WEN, J., DUAN, N., WANG, Q., JING, G. X. & XIAO, Y. 2017. Protective effect of propofol on noise-induced hearing loss. *Brain Res*, 1657, 95-100.
- WERSINGER, E. & FUCHS, P. A. 2011. Modulation of hair cell efferents. *Hear Res*, 279, 1-12.
- WHITAKER, W. R., FAULL, R. L., WALDVOGEL, H. J., PLUMPTON, C. J., EMSON, P. C. & CLARE, J. J. 2001. Comparative distribution of voltage-gated sodium channel proteins in human brain. *Brain Res Mol Brain Res*, 88, 37-53.
- WILLOTT, J. F. 2006. Measurement of the auditory brainstem response (ABR) to study auditory sensitivity in mice. *Curr Protoc Neurosci*, Chapter 8, Unit8 21B.
- WU, D., BACAJ, T., MORISHITA, W., GOSWAMI, D., ARENDT, K. L., XU, W., CHEN, L., MALENKA, R. C. & SUDHOF, T. C. 2017. Postsynaptic synaptotagmins mediate AMPA receptor exocytosis during LTP. *Nature*, 544, 316-321.
- WU, Y. X., ZHU, G. X., LIU, X. Q., SUN, F., ZHOU, K., WANG, S., WANG, C. M., JIA, J. W., SONG, J. T. & LU, L. J. 2014. Noise alters guinea pig's blood-labyrinth barrier ultrastructure and permeability along with a decrease of cochlear Claudin-5 and Occludin. *BMC Neurosci*, 15, 136.
- YAN, Z., XU, Y., LIANG, M. & REN, X. 2015. Expression and functional role of Nav1.9 sodium channel in cartwheel cells of the dorsal cochlear nucleus. *Mol Med Rep*, 11, 1833-6.
- YANG, S., CAI, Q., VETHANAYAGAM, R. R., WANG, J., YANG, W. & HU, B. H. 2016. Immune defense is the primary function associated with the differentially expressed genes in the cochlea following acoustic trauma. *Hear Res*, 333, 283-94.
- YAUNDONG, L., DONGYAN, W., LIJUN, H. & ZHIBO, X. 2014. Effects of downregulation of S100A8 protein expression on cell cycle and apoptosis of fibroblasts derived from hypertrophic scars. *Aesthet Surg J*, 34, 160-7.

References

- YOUNG, M. D., WAKEFIELD, M. J., SMYTH, G. K. & OSHLACK, A. 2010. Gene ontology analysis for RNA-seq: accounting for selection bias. *Genome Biol*, 11, R14.
- ZADORI, D., VERES, G., SZALARDY, L., KLIVENYI, P., TOLDI, J. & VECSEI, L. 2014. Glutamatergic dysfunctioning in Alzheimer's disease and related therapeutic targets. *J Alzheimers Dis*, 42 Suppl 3, S177-87.
- ZAMUDIO-BULCOCK, P. A., EVERETT, J., HARTENECK, C. & VALENZUELA, C. F. 2011. Activation of steroid-sensitive TRPM3 channels potentiates glutamatergic transmission at cerebellar Purkinje neurons from developing rats. *J Neurochem*, 119, 474-85.
- ZARATE, R., EL JABER-VAZDEKIS, N., TEJERA, N., PEREZ, J. A., RODRIGUEZ, C. 2017. Significance of long chain polyunsaturated fatty acids in human health. *Clin Transl Med*, 6, 25.
- ZHANG, H. & VERKMAN, A. S. 2015. Aquaporin-1 water permeability as a novel determinant of axonal regeneration in dorsal root ganglion neurons. *Exp Neurol*, 265, 152-9.
- ZHANG, K. D. & COATE, T. M. 2016. Recent advances in the development and function of type II spiral ganglion neurons in the mammalian inner ear. *Semin Cell Dev Biol*.
- ZHAO, X. S., WU, Q., PENG, J., PAN, L. H., REN, Z., LIU, H. T., JIANG, Z. S., WANG, G. X., TANG, Z. H. & LIU, L. S. 2017. Hyperlipidemia-induced apoptosis of hippocampal neurons in apoE(-/-) mice may be associated with increased PCSK9 expression. *Mol Med Rep*, 15, 712-718.
- ZHOU, X., JEN, P. H. S., SEBURN, K. L., FRANKEL, W. N. & ZHENG, Q. Y. 2006. Auditory brainstem responses in 10 inbred strains of mice. *Brain research*, 1091, 16-26.
- ZILBERSTEIN, Y., LIBERMAN, M. C. & CORFAS, G. 2012a. Inner hair cells are not required for survival of spiral ganglion neurons in the adult cochlea. *The Journal of neuroscience*, 32, 405-10.
- ZILBERSTEIN, Y., LIBERMAN, M. C. & CORFAS, G. 2012b. Inner hair cells are not required for survival of spiral ganglion neurons in the adult cochlea. *J Neurosci*, 32, 405-10.